UNIVERSITY OF OKLAHOMA

GRADUATTE COLLEGE

PRESSUREMETER AND CONE PENETROMETER TESTING IN A CALIBRATION CHAMBER WITH UNSATURATED MINCO SILT

A Dissertation

Submitted to graduate college faculty

In partial fulfillment of the requirements for the

degree of

Doctor of Philosophy

By

NORMAN K. TAN
Norman, Oklahoma
2005

PRESSUREMETER AND CONE PENETROMETER TESTING
IN A CALIBRATION CHAMBER
WITH UNSATURATED MINCO SILT

A DISSERTATION APPROVED FOR THE
SCHOOL OF CIVIL ENGINEERING AND ENVIRONMENTAL SCIENCE

BY

Gerald A. Miller

Kanthasamy K. Muraleetharan

Tohren C. G.Kibbey

Younane N. Abousleiman

Andy R. Magid

Amy B. Cerato

Dedicated to my parent and my wife.

ACKNOWLEDGEMENTS

I am thankful to God for everything I have accomplished. I would like to express my greatest gratitude to Dr. Miller, my research advisor and committee chairman for his valuable and inspiring academic instruction and indispensable mental support throughout my education at the University of Oklahoma. I am also thankful to him for the financial support he arranged for me during my study at University of Oklahoma.

I would like to thank my other committee members; Dr. Muraleetharan, Dr. Kibbey, Dr. Abousleiman, Dr. Magid and Dr. Cerato for serving on my committee and spending their valuable time in reviewing my dissertation. I also appreciate their valuable feedback, guidance and support throughout my research study for this dissertation.

I am grateful to Mr. Mike Schmitz for his valuable assistance in the laboratory. Sincere thanks to all my friends and colleagues: P.J Ananthanathan, Elie Cleomene, Francois Cazenove, Tariq Hamid, Charbel Khoury and Thulasi Vinayagam for their help and friendship.

Last but not least I am also grateful to my wife, parents and sisters for their understanding, moral support, and constant inspiration during the course of this research.

This research was supported by a grant (CMS-9813137) from the National Science Foundation (NSF).

TABLE OF CONTENTS

TABLE OF FIGURES

TABLE OF TABLES

ABSTARCT

The pressuremeter test (PMT) and cone penetrometer test (CPT) are becoming popular instruments for subsurface exploration. The PMT is an excellent test to determine the mechanical behavior of the soil and is one of the few geotechnical in situ investigation methods that gives a stress-strain relationship of soil, while the CPT is an excellent in situ test that gives a continuous subsurface profile rapidly. It is common for geotechnical engineers to encounter a zone of unsaturated soil prior to saturated soils below the groundwater table. In the arid regions of the world, the ground water table can be at substantial depth. However, many of the theories and methods of analysis of PMT and CPT are largely based on assumptions appropriate for saturated and dry soils. Over the last couple of decade it has been well accepted that the behavior of unsaturated soil is different from the completely saturated or dry soil. Therefore, there exists a need for methods to interpret PMT and CPT data from unsaturated soil.

The focus of this study is to investigate the influence of matric suction (ψ) on PMT and CPT results by conducting miniature pressuremeter (MPMT) and miniature cone penetrometer (MCPT) testing in a calibration chamber with unsaturated Minco Silt soil beds at the University of Oklahoma. Test beds were built to encompass a range of matric suction ranging from 15 kPa to 75 kPa in order to study the influence of ψ on the MPMT and MCPT results. The ψ was determined directly via tensiometers and indirectly by using the soil-water characteristic curve and water content (w) of samples. In addition to ψ, the influence of dry unit weight (γ_d) of the soil beds on the MPMT and MCPT results were studied. The γ_d and w of the soil beds were determine by collecting small

tube samples throughout the soil beds. The influence of net normal stress (σ_n) on MPMT results was also examined in this study by compressing the soil beds at three different σ_n. The MPMT and MCPT results were evaluated using the statistical analysis and cavity expansion equations for unsaturated soils developed by Muraleetharan et al. (1998). The statistical analysis of the test data reveals that the influence of soil processing methods, γ_d, w, ψ, volumetric water content (θ) and σ_n on MPMT and MCPT results are significant. Empirical correlations that correlate the parameters with MPMT and MCPT results were also developed. The analysis of the test data with cavity expansion equations for unsaturated soil shows that the volumetric strain of the soil in the zone of influence decreases as matric suction increases. In this study, the cavity expansion analysis revealed that during the expansion of the cavity, the soil within the plastic zone of influence for pre-bored MPMT underwent compression; meanwhile for MCPT the soil underwent dilation.

Chapter 1: Introduction

1.1 Introduction

During subsurface exploration geotechnical engineers often encounter unsaturated soil layers before hitting the ground water table. This unsaturated soil zone can sometimes extend to considerable depth especially in the arid and semi-arid regions. It is important to note that behavior of unsaturated soil is not consistent with many of the principles and concepts of traditional soil mechanics that assume the soil are either completely saturated or dry. Fredlund and Rahradjo (1993) stated that saturated or completely dry soils are special cases for unsaturated soil. The behavioral differences of unsaturated soil in terms of their nature and engineering properties from the two extreme cases (i.e. dry or saturated) have been a concern in geotechnical engineering. Over the last couple of decades, much research has been done in this field and many theories, concepts and principles have been developed in this field.

Cone Penetrometer tests (CPT) and Pre-bored Pressuremeter tests (PMT) have become increasingly popular methods for subsurface exploration. The PMT is an excellent test to determine the in situ mechanical behavior of the soil. It is one of few geotechnical in situ investigation methods that give a stress-strain relationship of soil. Meanwhile, the CPT is an excellent in situ test that rapidly gives a continuous profile of soil stratigraphy. Many of the theories and methods of analysis for PMT and CPT have been developed around saturated soil or dry soil mechanics. This is a concern to geotechnical engineers since unsaturated soil is frequently encountered during subsurface exploration as stated earlier. Currently, it is common in practice for geotechnical

engineers to assume saturated-undrained or drained soil behavior even though the behavior of the unsaturated and saturated soil differs significantly. Thus, there exist a need for methods to interpret both the PMT and CPT test data from unsaturated soil. Some experimental and theoretical modeling has been done for PMT testing in unsaturated soil and very little has been done for CPT testing in unsaturated soil.

In developing a method of interpretation for PMT and CPT tests in unsaturated soil, a set of test data are required. Even though in situ tests are in some ways preferred, there are not practical because the field boundary conditions can not be well defined and controlled; the soil is heterogeneous, the stress history is unknown and magnitude and stress state of soil is unknown. While much research has been conducted to obtain all these from the samples collected in field, it is almost impossible to collect a truly undisturbed sample. One alternative to overcome these uncertainties and problems is by using a calibration chamber. The primary role of a calibration chamber is mainly for calibrating the field instruments in a controlled environment. With all the advantages of testing in a calibration chamber, the data collected can be used to develop empirical correlations and also be used to study behavior of in situ test instruments as related to soil properties and initial stress conditions.

1.2 Hypotheses and Objectives

Hypotheses of the research are:

1. The limit pressure (P_L) and moduli (E_P and E_R) from a PMT test are influenced by matric suction and the behavior is predictable.

2. The tip resistance (q_c) from a CPT test is influenced by matric suction and the behavior is predictable.
3. The cavity expansion theory for unsaturated soil can be used as a basis for interpreting PMT and CPT results from unsaturated soil.

The objectives of this study are:

1. Produce a set of data from PMT and CPT tests conducted in a calibration chamber containing unsaturated Minco Silt beds.
2. Study the influence of various testing parameters on PMT and CPT tests results, including matric suction, dry unit weight, and net normal stress.
3. Examine the possibility of developing a new method to interpret PMT and CPT tests results in unsaturated soil by utilizing the cavity expansion theory for unsaturated soil.

1.3 Dissertation Layout

This dissertation is divided into seven chapters. Chapter two contains literature review discussing the basic concepts of unsaturated soil mechanics including the stress state variables, soil suction and shear strength theory of unsaturated soil. It also contains literature review discussing the general concepts behind PMT and CPT testing, relevant research done on PMT and CPT involving calibration chamber or unsaturated soil, and also the cavity expansion theory and its application to PMT and CPT. Chapter Three provides brief descriptions of the University of Oklahoma Calibration Chamber (OUCC). This chapter also reviews some of the published studies of previous research on soil bed preparation, followed by a discussion on the design of the University of Oklahoma Static

Compactor. The fourth chapter presents the details regarding the soil, PMT and CPT used in this research study.

Chapter Five comprises descriptions of the test bed preparation method, miniature pressuremeter testing method, miniature cone penetrometer testing method and test bed evaluation method. It includes the discussion of the challenges involved in each procedure and the solution or steps taken in this study to resolve problems. The results and discussion are presented in Chapter Six. The summary and conclusions from this study are summarized in Chapter Seven. Chapter Seven also includes the recommendation for future study involving PMT and CPT testing in unsaturated soil. References and Appendices follow Chapter Seven.

Chapter 2: Literature Review

2.1 Unsaturated Soil Mechanics

Traditionally, studies in soil mechanics have focused on saturated soil, which mainly involves positive pore water pressure, u_w. In the analysis of mechanical properties of the soil, the soil is often assumed saturated. In some instances the soil is assumed completely dry. This approach typically leads to analysis of two phase media; water and solids for saturated soil or air and solids for dry soil. However, there has been a lack of knowledge on the behavior of soil in between these two extreme conditions, which is known as partially saturated or unsaturated soil. Within the last couple of decades considerable advances have been made in the study of unsaturated soil mechanics. It has also revolutionized the idea of soil mechanics itself where saturated soil or completely dry soil are now considered as a special case of unsaturated soil.

Unlike saturated soil, unsaturated soil is a four phase material, which includes soil skeleton, pore air, pore water and the air water interface, also known as the contractile skin (Fredlund and Rahardjo, 1993). Thus, the analysis involved with unsaturated soil is typically more complex due to the compressibility of the air phase and the interface between air and water. Fredlund and Rahardjo (1993) suggested that the air-water interface is to be considered as an independent phase in the analysis of unsaturated soil except for volume-mass analysis where it should be considered as part of water phase since it is only a of couple molecules thick. The interaction between the contractile skin and soil particles influences the mechanical behavior of unsaturated soils. The stress state variable related to the contractile skin is referred to soil suction or matric suction.

2.1.1 Stress State Variables in Unsaturated Soil

Much research has been performed to find the appropriate stress state variables for unsaturated soils. Many attempts have been made to extend the use of the effective stress concept of saturated soil to unsaturated soil. The effective stress concept for saturated soil has been well accepted in geotechnical engineering practice. The effective stress as expressed in Equation 2-1 is assumed to represent a unique stress state variable.

$$\sigma' = \sigma - u_w \qquad \text{(Eq.2-1)}$$

Many researchers have attempted to incorporate or modify the effective stress concept to describe the stress state of unsaturated soil. However, experimental evidence shows that the single stress state variable concept is insufficient in describing the stress state of unsaturated soil. Some researchers have tried to incorporate soil properties in determining the stress state of unsaturated soil; this also leads to many difficulties. Thus, a stress-state represented by a combination of non-material properties is preferred. Based on the multiphase continuum mechanics and four phase system of unsaturated soil, Fredlund and Morgenstern (1977) concluded that stress state variables for unsaturated soil can be described by any two of the three possible normal stress variables (i.e. total stress (σ), pore air pressure (u_a), and pore water pressure (u_w)). The three valid combinations of stress state variables are tabulated in Table 2-1 (Fredlund and Rahardjo 1993).

Table 2-1: Combination of Stress State Variables for Unsaturated Soil

Reference Pressure	Stress State Variables
Air, u_a	$(\sigma-u_a)$ and (u_a-u_w)
Water, u_w	$(\sigma-u_w)$ and (u_a-u_w)
Total Stress, σ	$(\sigma-u_a)$ and $(\sigma-u_w)$

The combination that uses pore air pressure as the reference pressure is the best for use in most engineering applications (Fredlund and Rahardjo 1993) because the change in the total normal stress and change in pore water pressure can be treated independently. Fredlund and Rahardjo (1993) also stated that it is the simplest and most reasonable combination. The combination had been widely used in unsaturated soil mechanics in describing the stress state of unsaturated soil where the two stress state variables, $(\sigma-u_a)$ and (u_a-u_w), are known as net normal stress and matric suction, respectively. The combination is also valid for saturated and dry soil. Additionally, the transition between stress states from unsaturated soil to saturated or dry soil is smooth (Fredlund and Rahardjo 1993).

2.1.2 Soil Suction

Soil suction or total suction, ψ is a measure of free energy state of pore water (Fredlund and Rahardjo 1993). Richards (1965) via Fredlund and Rahardjo (1993) had expressed soil suction in terms of partial pressure of pore water vapor as follows:

$$\psi = \frac{RT}{v_{w0} w_v} \ln\left(\frac{u_v}{u_{v0}}\right) \qquad \text{(Eq.2-2)}$$

where:

ψ = soil suction or total suction,

R = universal gas constant,

T = absolute temperature,

v_{w0} = specific volume of water or inverse density of water,

w_v = molecular mass of water vapor,

u_v = partial pressure of pore-water vapor, and

u_{v0} = saturation pressure of water vapor over a flat surface of pure water at the same temperature.

Furthermore, total suction is made up of two components, matric suction (u_a-u_w) and osmotic suction (π) and can be written as follows:

$$\psi = (u_a - u_w) + \pi \quad \text{(Eq.2-3)}$$

2.1.2.1 Osmotic Suction

Osmotic suction is commonly associated with the solute or salt content in the pore water of soil. Therefore, it is very sensitive to the changes in the chemistry of the pore fluid in the soil. Typically the role of osmotic suction is not taken into account in most common geotechnical problems. However, there are some exceptions when the solute content of the pore fluid is significantly altered. In such case, it would usually lead to significant changes of osmotic suction and cause a notable effect on the mechanical behavior of the soil. However, in common geotechnical engineering problems, the changes in osmotic suction are almost insignificant compared to changes in matric suction. Therefore, for most geotechnical problems involving unsaturated soil, the change in matric suction is assumed to be equivalent to the change in total suction (i.e. $\Delta\psi$ =

$\Delta(u_a-u_w)$. Therefore, through this dissertation matric suction ($u_a - u_w$) is presented as ψ instead.

2.1.2.2 Matric Suction

Matric suction is associated with the contractile skin at the air-water interface. The interaction between the soil particles and the pore water forms a thin layer of contractile skin. Due to the difference in pressure in the pore water and air above the contractile skin, along with surface tension of water, the contractile skin will curve forming a meniscus. Under atmospheric conditions the pore water pressure (u_w) is negative relative to the pore air pressure (u_a). The difference between the pore air pressure (u_a) and pore water pressure (u_w) is known as matric suction (u_a-u_w). It is this quantity that is often measured and/or controlled while determining unsaturated soil behavior.

2.1.2.2.1 Measuring Matric Suction

Currently many techniques and devices have been developed for matric suction measurement. Among them are psycrometers, filter papers, high air entry porous disks, tensiometers, miniature pore pressure transducers, porous plate method, and pressure membranes. Illustrations of most of the techniques can be found in Fredlund and Rahardjo (1993). However only one of the techniques (i.e. tensiometer) is further illustrated and documented in the literature review of this dissertation as it is relevant to the research performed.

A tensiometer measures the negative pore-water pressure of the soil directly via a high air-entry porous cup. It is commonly used in the field for the measurement of pore-

water pressure. As for laboratory uses where relatively small soil specimens are used, a small tip tensiometer with flexible coaxial tubing is a preferred choice. However, the basic concept of the tensiometers remains the same. When the porous cups of the tensiometer is installed in a pre-cored hole, water in the tensiometer can flow in or out through the porous cup. As the water flows out from the tensiometer, a vacuum is created in the tensiometer and the pressure gauge on the tensiometer provides a direct readout of the negative pressure. The process will continue until equilibrium is achieved where the pore water pressure in the soil is equivalent to the water pressure in the tensiometer. It is common in practice that the measured negative pore-water pressure is taken as matric suction assuming the pore air pressure is at atmospheric (i.e. zero gauge pressure). Although the technique is relatively simple compared to other available techniques, it is limited for measurement of pore water down to -100 kPa due to cavitation in the water phase.

2.1.2.2.2 Soil-Water Characteristic Curve

The relationship of the amount of water in soil and soil suction of soil is expressed by the soil-water characteristic curve. The amount of water in the soil can be expressed in terms of volumetric water content (θ), gravimetric water content (w) or degree of saturation (S). It is common in practice to express the soil suction in terms of matric suction as opposed to total suction. Figure 2-1 shows the typical soil-water characteristic curve for drying and wetting of soil. The soil-water characteristic curve shows the matric suction has an inverse relationship with amount of water in soil. For instance as the water content in the soil increases, the matric suction decreases and vice versa. It is important to note that the soil-water characteristic curve exhibits hysteresis; at

given water content during the wetting and drying process, the matric suction is different. There are several factors that contribute to the soil-water characteristic curve hyteresis. Listed below are a few of the factors that have been cited in literature:

- Entrapped air in unsaturated soil (Fredlund and Rahardjo 1993),
- Non-uniform pore size distribution in soil (Fredlund and Rahardjo 1993),
- Variation of contact angles between water and solid during wetting and drying processes (Bear, 1979 via Fredlund and Rahardjo 1993).

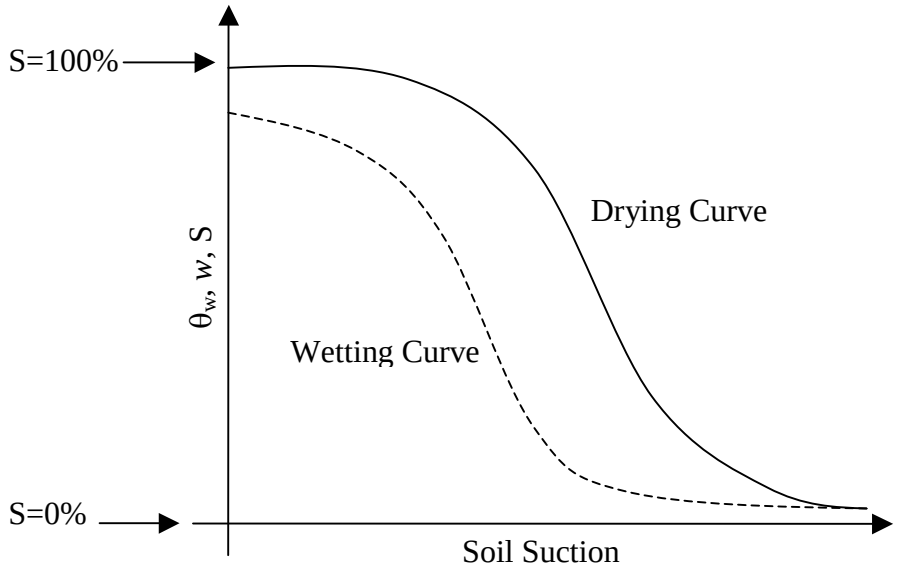

Figure 2-1: Typical Soil-Water Characteristic Curve; Wetting and Drying Curves (after Fredlund and Rahardjo 1993)

2.1.3 Shear Strength Theory

In traditional soil mechanics, the Mohr-Coulomb shear strength equation is typically used to describe the shear strength of soil. It is based on the effective stress concept where the stress state of the soil mass can be described by a single effective

stress variable. Effective stress (σ') is defined as total normal stress (σ_n) minus the pore water pressure (u_w). Below is the shear strength equation for saturated soil.

$$\tau = c' + (\sigma_n - u_w) \tan\phi' \qquad \text{(Eq.2-4)}$$

where:

τ = shear stress on shear plane at failure,

c' = effective cohesion intercept,

σ_n = total normal stress on shear plane at failure,

u_w = pore water pressure on shear plane at failure, and

ϕ' = effective angle of internal friction associated with σ_n.

However, the equation above is not applicable for unsaturated soil since more than one stress state variable is needed to describe the stress state of unsaturated soil. As discussed in Section 2.1.1, the two commonly used and widely accepted stress state variables are the net normal stress ($\sigma - u_a$) and matric suction ($u_a - u_w$). Fredlund et al. (1978) formulated the shear strength equation for unsaturated soil as follows:

$$\tau = c' + (\sigma_n - u_a) \tan\phi' + (u_a - u_w) \tan\phi^b \qquad \text{(Eq.2-5)}$$

where:

τ = shear stress on shear plane at failure,

c' = effective cohesion intercept,

σ_n = total normal stress on shear plane at failure,

u_a = pore air pressure on shear plane at failure,

u_w = pore water pressure on shear plane at failure,

ϕ' = effective angle of internal friction associated with $\sigma_n - u_a$, and

ϕ^b = angle indicating the rate of increase in shear strength relative to u_a-u_w.

The unsaturated soil shear strength equation is also applicable for saturated soil as there is a smooth transition from unsaturated shear strength equation to saturated soil shear strength equation. Fredlund and Rahardjo (1993) stated that as soil approaches saturation, the pore water pressure (u_w) approaches the pore air pressure (u_a) and the matric suction (u_a-u_w) approaches zero. This reduces the unsaturated soil shear strength equation to the saturated soil shear strength equation. Thus, it is acceptable to consider saturated soil as a special case for unsaturated soil. By comparing both of the equations, it is evident that matric suction plays an important role in determining the shear strength of unsaturated soil. Figure 2-2 shows the extended Mohr-Coulomb failure envelope corresponding to Eq. 2-5.

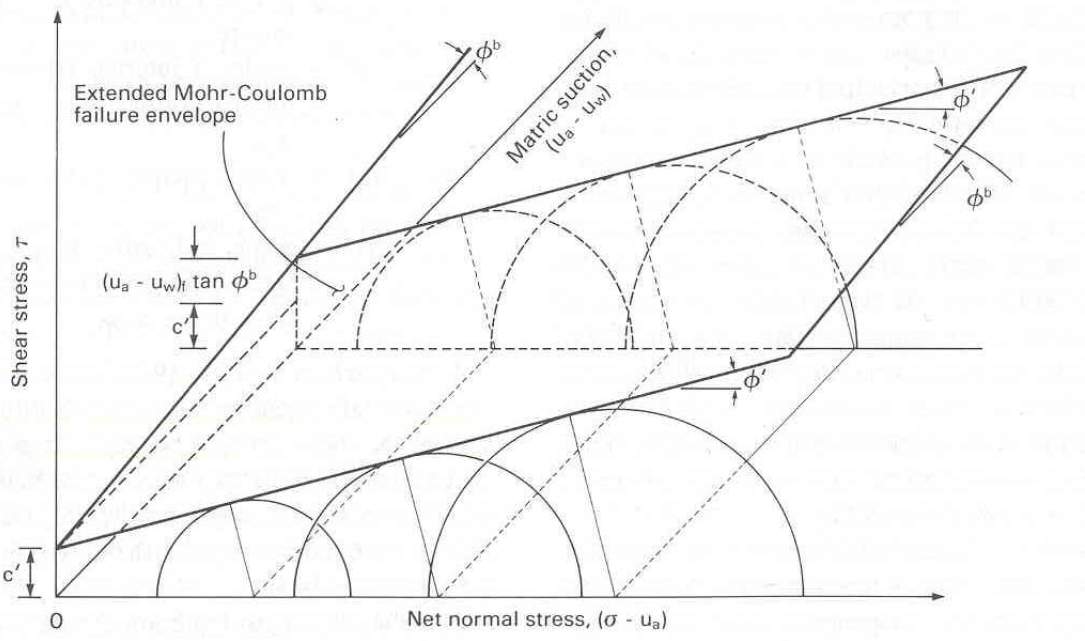

Figure 2-2: Extended Mohr-Coulomb Failure Envelope Defined by Equation 2.5 (Fredlund and Rahardjo 1993)

It has been noted that the matric suction is an inverse function of water content while the shear strength of unsaturated soil is function of net normal stress and matric suction. Thus, water content plays a very important role in the shear strength of unsaturated soil. It is anticipated that as water content decreases, the matric suction increases and so does the shear strength of the soil. Thus, any in situ tests that are used to determine the shear strength of unsaturated soil must be able to take matric suction or water content into account. Pressuremeter and cone penetrometer are among of the many in situ instruments that have been increasingly popular and frequently used by the geotechnical engineer for subsurface exploration that involves an unsaturated soil zone. Equation 2-5 and Figure 2-2 show that the shear strength of unsaturated soil increases with matric suction. Therefore, it is anticipated that the limit pressure and tip resistance measured from a pressuremeter and cone penetrometer test might be affected by change in matric suction.

2.2 Pressuremeter Testing

The pressuremeter test (PMT) is excellent for determining the in situ mechanical behavior of soil and it is one of few in situ tests that gives a stress-strain relationship of soil. The PMT was originally developed in France by Menard in 1954. The basic idea of the PMT is the expansion of a long cylindrical cavity in the ground by applying uniform pressure to the borehole walls via a probe with a flexible membrane. Briaud (1992) has recommended a minimal value of 6.5 for height to diameter ratio in order to ensure a good approximation of the plane strain cylindrical expansion. The probe is normally installed vertically at various depths in the ground and is connected to the control panel unit via tubing. The test can be either pressure controlled or volume controlled. Figure 2-

3 shows the basic principles of the pressuremeter test. The deformation and strain of the soil can be determined from the volume of fluid injected into the probe while the stress corresponds to the applied pressure. Figure 2-4 shows a pressure-volume curve from a pre-bored pressuremeter test. The PMT pressure-volume curve can be used to evaluate in situ stress, compressibility and strength of the soil.

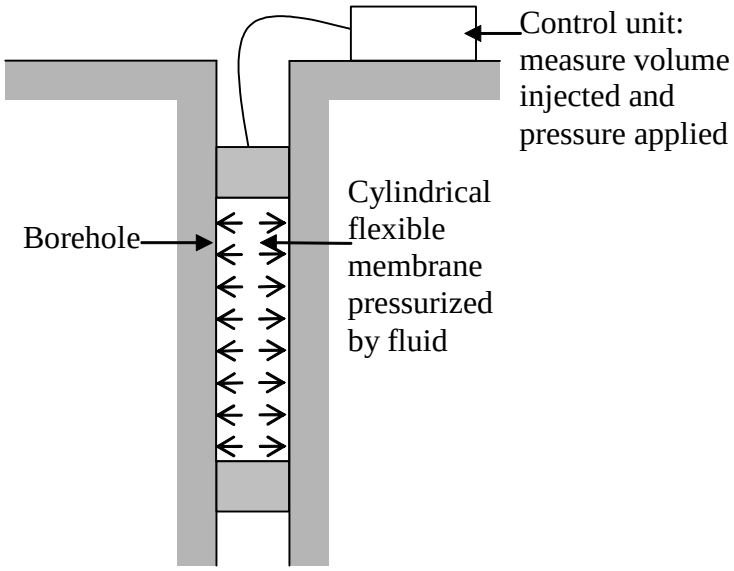

Figure 2-3: Basic Principles of Pressuremeter Test (after Mair and Wood 1987)

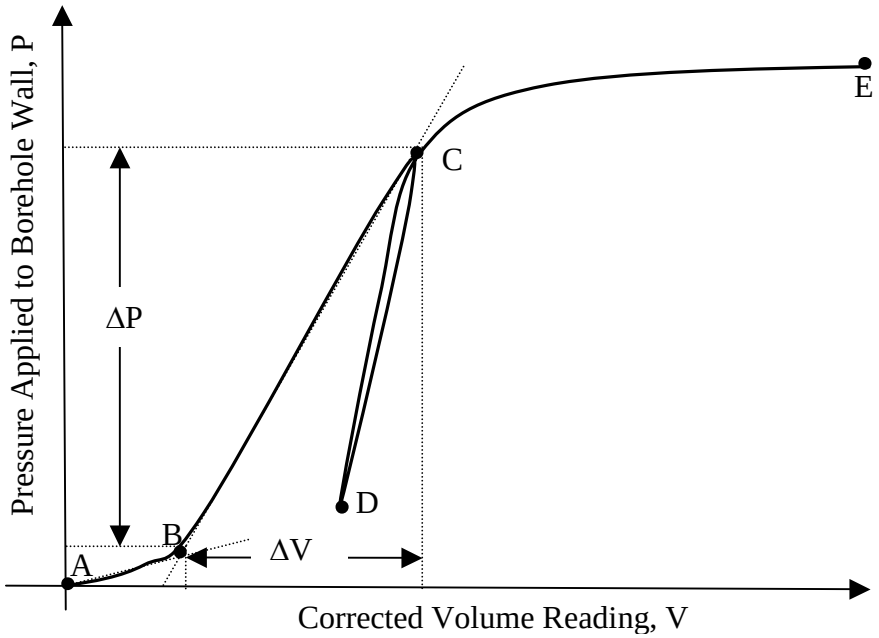

Figure 2-4: Typical In Situ Pressure-Volume Curve from Pre-bored Pressuremeter Testing

Limit pressure (P_L) and pressuremeter modulus (E_P) can be determined from the plot in Figure 2-4. Practically speaking, P_L is defined as the pressure at which the cavity reaches twice the initial volume of the cavity. The volume is defined as $2(V_0 + V_i)$ where V_0 is the volume of the measuring portion of the un-inflated probe at ground level and V_i is the corrected volume reading at the pressure where the probe made contact with borehole (point "B" as depicted in Figure 2-4). During a PMT limit pressure is generally not attainable, but is determined by extrapolating the pressure-volume curve beyond Point "E" in Figure 2-4, or by extrapolating from a P vs. 1/P plot as shown in Figure 2-5. In general practice the latter method is commonly used. The pressuremeter modulus (E_P) is calculated by using the straight line portion of the PMT curve, depicted as line BC in Figure 2-4. E_P is defined as follows:

$$E_p = 2(1+\nu)(V_0 + V_m)\frac{\Delta P}{\Delta V} \qquad \text{(Eq.2-6)}$$

where:

E_p = Pressuremeter modulus,

ν = Poisson's ratio,

V_o = Volume of measuring portion of un-inflated probe at ground surface,

V_m = Corrected volume reading at center point of ΔV volume increase (see Figure 2-4),

ΔP = Corrected pressure increase in the straight line portion of pressure-volume curve (see Figure 2-4), and

ΔV = Corrected volume increase in the straight line portion of pressure-volume curve (see Figure 2-4).

In this study the modulus obtained from the first straight line portion of the PMT curve (Line "BC" in Figure 2-4) is defined as the pressuremeter modulus (E_P) and the modulus obtained from the unload-reload straight line portion of the PMT curve (Line "DC" in Figure 2-4) is defined as the reload pressuremeter modulus (E_R). The equation used to determine the E_R is similar as Equation 2-6.

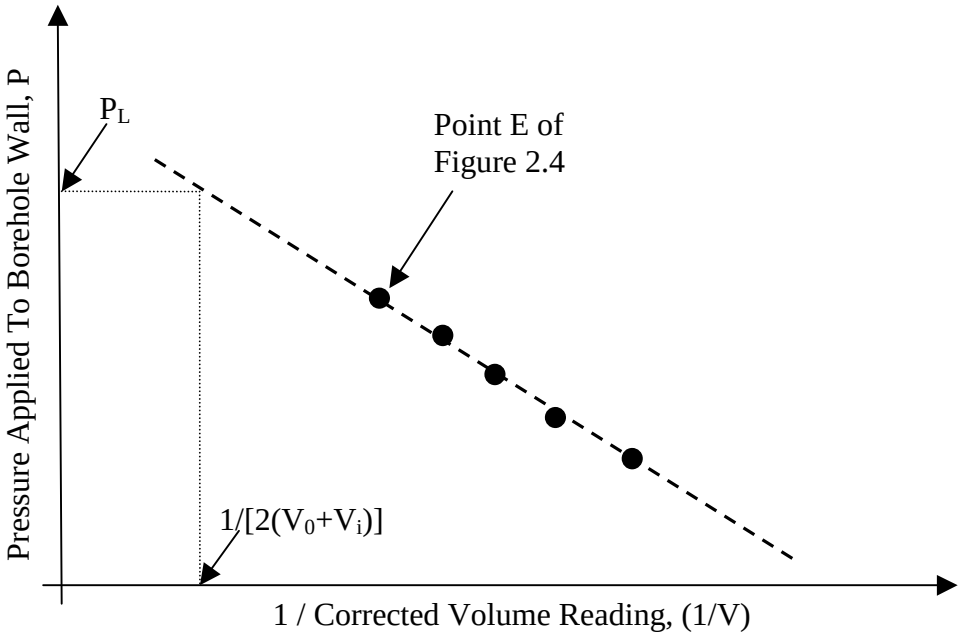

Figure 2-5: Determination of Limit Pressure (P_L) Using the Inverse Volume Method

As stated earlier the expansion of the pressuremeter cavity is assumed to be an expansion of an infinitely long cylinder in an infinite soil mass. Thus, the soil in assumed to deform under plain strain condition where the vertical strain of the soil is assumed to be zero ($\varepsilon_z=0$) (Wood and Wroth 1977). Figure 2-6 shows the diagram of the deformation of an element during the expansion of the cavity. Due to the axial symmetry condition, the principal stresses acting on the soil elements are σ_r, σ_θ and σ_z with σ_r as the major principal stress (Hughes et al. 1977). For given soil element at a distance r from the cavity wall, initially σ_r is equal to σ_θ. As the cavity expands, σ_r increases and σ_θ decreases. The soil element experiences circumferential extension, or negative circumferential strain (ε_θ) and radial compression, positive radial strain (ε_r). Hughes et al. (1977) stated that during the PMT probe expansion all the soil elements are subjected to

the same stress path. However the at any particular instant the soil elements would have reached different stages along the stress paths depending on the radial distance of the elements from the center of the probe.

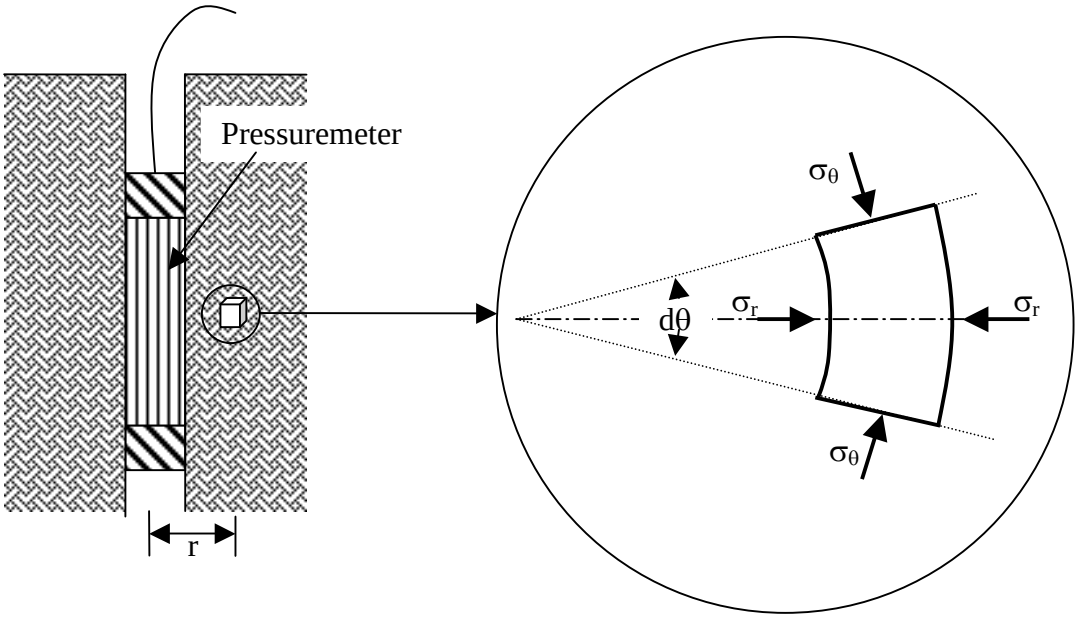

Figure 2-6: Stresses on Deformed Element

Much research has been performed with the pressuremeter to investigate strain-rate effects (Penumadu et al. 1998), and influence of pressuremeter geometry on pressuremeter test results (Ajalloeian and Yu 1998). Aside from experimental work, many researchers have also tried to model the pressuremeter and back predict the results. Hsieh et al. (2002) conducted a numerical study of drained pressuremeter tests in sand using the MIT-S1 model and finite element method. From the study it was concluded that there is a strong correlation between gradient of PMT expansion curve and initial state parameter of the test soil. Pye (1995) conducted a study for interpreting self-boring pressuremeter tests (SBP). In the study Pye (1995) utilized the computer-aided modeling

(CAM) technique to match the theoretical curve to SBP tests in clay. It was concluded from the study that both the elastic-perfectly plastic (EPP) and hyperbolic (HB) models along with CAM can be used to interpret SBP tests with reliable repeatability.

Although much research has been done on the pressuremeter, most of the research has been focused on either saturated or dry soil. Pereira et al. (2003) attempted some numerical modeling of pressuremeter testing in unsaturated soil and concluded that through the use of equivalent pore pressure and suction hardening function it is possible to correlate the stress-strain behavior of pressuremeter testing in unsaturated soil with suction. Although, the prediction made in the study is consistent with the knowledge of soil mechanics, there is still lack of experimental data to validate the predictions. Miller and Muraleetharan (2000) did some studies of PMT in unsaturated soil and showed that matric suction has a significant influence on limit pressure (P_L) and pressuremeter modulus (E_P). A study using a miniature PMT had been conducted in a calibration chamber with unsaturated soil at University of Oklahoma by Miller et al. (2002) as part of this dissertation research.

Schnaid et al. (2004) combined the cylindrical cavity expansion theory with the Cam clay critical state model along with the framework of unsaturated soil behavior for the interpretation of pressuremeter tests performed in unsaturated soil. The study showed that the expansion of a pressuremeter probe did not result in significant changes in matric suction. Muraleetharan et al. (2003) had conducted a fully coupled analysis of pressuremeter tests in unsaturated soil using a finite element computer code, U_DYSAC2. Muraleetharan et al. (2003) attempted to track the changes in matric suction during the expansion of the PMT probe via U-DYSAC2 and the soil-water characteristics

of the test soil. The study showed that even though the pore air (u_a) and pore water (u_w) pressure in the soil within the zone of influence increased during the expansion of the PMT probe, the net increase of matric suction is insignificant. Both Muraleetharan et al. (2003) and Schnaid et al. (2004) came to the same conclusion where the effects of cavity expansion on matric suction within the influence zone are insignificant. This observation is later used in this study as an assumption to simplify the cavity expansion in unsaturated soil equations.

2.3 Cone Penetrometer Testing

Basically, the Cone Penetration Test (CPT) involves advancing a cylindrical rod with a conical tip vertically into the soil at a constant rate and making nearly continuous measurements of the forces (i.e. tip resistance (q_c) and sleeve friction (f_s)). Some cones (i.e. peizocone penetrometers) are capable of measuring the pore water pressure (u_w). The CPT is an excellent tool for subsurface exploration in that it rapidly gives a continuous profile of soil stratigraphy. The CPT was originally developed in the Netherlands in the early 1930's (Lunne et al. 1997). The early cone was very simple and only measured the thrust required to push the cone through the ground. However, over the years there has been a rapid development of the technology. In addition to tip resistance (q_c) measurements, the CPT available in the market today is also capable of measuring sleeve friction (f_s) and pore water pressure (u_w). The tip resistance (q_c) is defined as the total force acting on the cone (Q_c) divided by the total projected area of the cone (A_c) and sleeve friction (f_s) is defined as total force acting on the sleeve (F_s) divided by the surface area of the sleeve. The friction ratio (i.e. ratio of f_s to q_c) helps to identify the soil types. The introduction of the electrical cone is a great leap in the development of the CPT. It

allows the continuous measurement of cone tip resistance and sleeve friction. Figure 2-7 shows a schematic diagram of a modern electrical friction cone. The current accepted standard for CPT according to ASTM D 3441 is a cone with projected cross sectional of area 10 cm^2, an apex angle of 60^o, and pushed into the ground at 2 cm/sec.

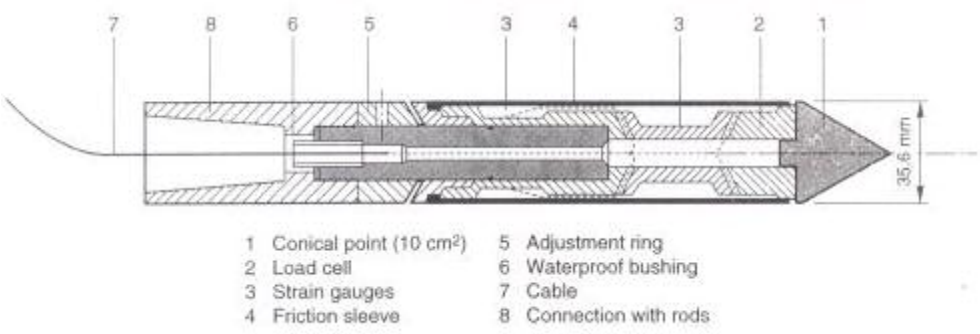

Figure 2-7: Schematic of Modern Electrical Friction Cone (from Lunne et al. 1997)

Much research has been done on the CPT in saturated soils and dry sand. Robertson and Campanella (1983) have compiled and present a summary work guide for interpreting the CPT data both in sand and clay. Edelman and Holguin (1996) had used CPT for subsurface characterization of materials as a cheaper alternative that provides higher quality data rapidly along with minimal health and safety concerns compared to the traditional drilling method. Peterson (1991) had conducted a study on CPT in a calibration chamber with fine sand beds. The study included the investigation of the effects of soil bed density, particle size, penetration rate, and induced pore water pressure on the CPT penetration resistance ($q_{c)}$. Peterson (1991) concluded that the density of the soil bed and the effective stress conditions at the time of penetration affects the penetration resistance. In the study Peterson (1991) also investigated the effects of

penetration rate and particle size on the penetration resistance by using a range of glass bead sizes (0.425-0.300-mm, 0.212-0.150-mm, 0.106-0.075-mm and 0.053-0.038-mm) and penetration rates ranging from 0.04-cm/s to 8.0-cm/s. The study showed that the effects of penetration rate and particle size on the penetration resistance were insignificant for cohesionless sand and silt size particles.

Although much research has been done on the pressuremeter, very little research has been done on cone penetration testing in unsaturated soil. Hryciw and Dowding (1987) conducted a laboratory study of CPT in unsaturated sand at low suction and concluded that tip resistance (q_c) tended to be greater in unsaturated soil than dry or saturated soil. Tan et al. (2003) conducted miniature CPT testing in a calibration chamber with unsaturated soil as part of this dissertation research, and observed that tip resistance increases with matric suction.

2.4 Cavity Expansion Theory

It has always been an interest of geotechnical engineers to assess the state variables of soils such as but not limited to the stresses and density of the soil from in situ tests results. In addition, geotechnical engineers are interested to be able to predict the test results if the state variables change. Many attempts have been made either directly or indirectly to find the correlation between the measured quantities from in situ tests and the state variables of soil. One of the approaches is through experimental work where the empirical relations between the measured quantities and the state variables are determined by conducting a series of tests in a well controlled environment. Robertson and Campanella (1983) and Lunne and Christoffersen (1983) conducted some studies to find the correlations between relative density and the measured quantities from CPT

results. Another alternative is through the theoretical approaches, which incorporate a mechanical model to simulate the deformation of the soil elements around the test probe and constitutive theory to describe the soil behavior. Among them are the bearing capacity theory and cavity expansion theory. The cavity expansion theory is described herein considering its importance and relevance to the research reported in this dissertation.

The original cavity expansion equations for the expansion of spherical and cylindrical cavities in an isotropic, linear elastic medium were developed by Vesic (1972). Since then, cavity expansion theories have been used quite often for the interpretation of both PMT and CPT data (e.g. Palmer 1972, Mitchell and Keaveny 1986, Silvestri 1998, Mantaras and Schnaid 2002, Russell and Khalili 2002, Tan et al 2003, and Salgado and Randolpf 2001).

Many of the theories and methods of interpretation are based on either completely dry sand or saturated cohesive soils. Very little has been done on unsaturated soil. Muraleetharan et al. (1998) and Russell and Khalili (2002) are among few that had looked into cavity expansion in unsaturated soil. Russell and Khalili (2002) developed a numerical procedure and solution for cavity expansion in unsaturated soil within the effective stress based framework, where a Modified Cam-Clay model was used to describe the behavior of unsaturated soil. The input parameters used for the study were back calculated using experimental data of other researchers. The study showed that matric suction significantly increased the limit pressure of a spherical cavity. The trend is more significant when the void ratio of the soil is high. Although the results from this

study seem to be convincing there is a lack of experimental data that can be used for validating existing theories.

Muraleetharan et al. (1998) developed equations for cavity expansion of spherical and cylindrical cavities in an infinite unsaturated soil mass by extending the Vesic's (1972) original cavity expansion equations. All the assumptions involved for the equations are listed in Section 6.5. Figure 2-8 shows cross-section through the cavity and surrounding soil. The equations take the following form:

1) For cylindrical cavity expansion in unsaturated soil

$$p_u = F'_q\left[p - u_a - \frac{E}{H(1-2v)}\Delta(u_a - u_w)\right] + F'_c + u_a \qquad \text{(Eq.2-7)}$$

where:

p_u = ultimate pressure,

F'_q, F'_c = dimensionless cylindrical cavity expansion factors,

$$F'_q = (1+\sin\phi')I'^{\,\sin\phi'/(1+\sin\phi')}_{rr} \qquad \text{(Eq.2-8)}$$

$$F'_c = (F'_q - 1)\cot\phi' \qquad \text{(Eq.2-9)}$$

I'_{rr} = reduced rigidity index,

$$I'_{rr} = \frac{1+\varepsilon_v^*}{\frac{f_2}{I_r} - \frac{2(1+v)\Delta(u_a-u_w)}{H(1-2v)} + \frac{2(1+v)\Delta u_a \sin\phi'}{E} + \varepsilon_v} \qquad \text{(Eq.2-10)}$$

$$f_2 = \cos\phi' \qquad \text{(Eq.2-11)}$$

I'_r = rigidity index,

$$I'_r = \frac{E}{2(1+v)[(p-u_a)\tan\phi' + c]} \quad \text{(Eq.2-12)}$$

p = mean net normal stress,

$$c = c' + (u_a - u_w)\tan\phi^b, \quad \text{(Eq.2-13)}$$

c' = effective cohesion,

$\Delta(u_a - u_w)$ = change in matric suction during cavity expansion,

u_a = pore air pressure,

u_w = pore water pressure,

ϕ' = angle of internal friction associated with net normal stress,

ϕ^b = angle of internal friction associated with the matric suction,

ε^*_v = volumetric strain in plastic zone at the ultimate condition,

H = Elastic modulus with respect to matric suction,

E = Young's Modulus, and

v = Poisson's ratio.

2) For spherical cavity expansion in unsaturated soil

$$p_u = F'_q\left[p - u_a - \frac{E}{H(1+2v)}\Delta(u_a - u_w)\right] + F'_c\, c + u_a \quad \text{(Eq.2-14)}$$

where:

F'_q, F'_c = dimensionless spherical cavity expansion factors,

$$F'_q = \frac{3(1+\sin\phi')}{3-\sin\phi'} I'^{\,4\sin\phi'/3(1+\sin\phi')}_{rr} \qquad \text{(Eq.2-15)}$$

$$F'_c = (F'_q - 1)\cot\phi' \qquad \text{(Eq.2-16)}$$

$$I'_{rr} = \frac{1+\varepsilon_v^*}{\frac{f_1}{I_r} - \frac{6(1+v)\sin\phi'\Delta(u_a-u_w)}{(1-2v)(3-\sin\phi')H} + \frac{6(1+v)\Delta u_a \sin\phi'}{E(3-\sin\phi')} + \varepsilon_v} \qquad \text{(Eq.2-17)}$$

$$f_1 = \frac{3\cos\phi'}{3-\sin\phi'} \qquad \text{(Eq.2-18)}$$

$$I'_r = \frac{E}{2(1+v)[(p-u_a)\tan\phi' + c]} \qquad \text{(Eq.2-19)}$$

The definitions of other terms are the same as for the cylindrical cavity expansion equation.

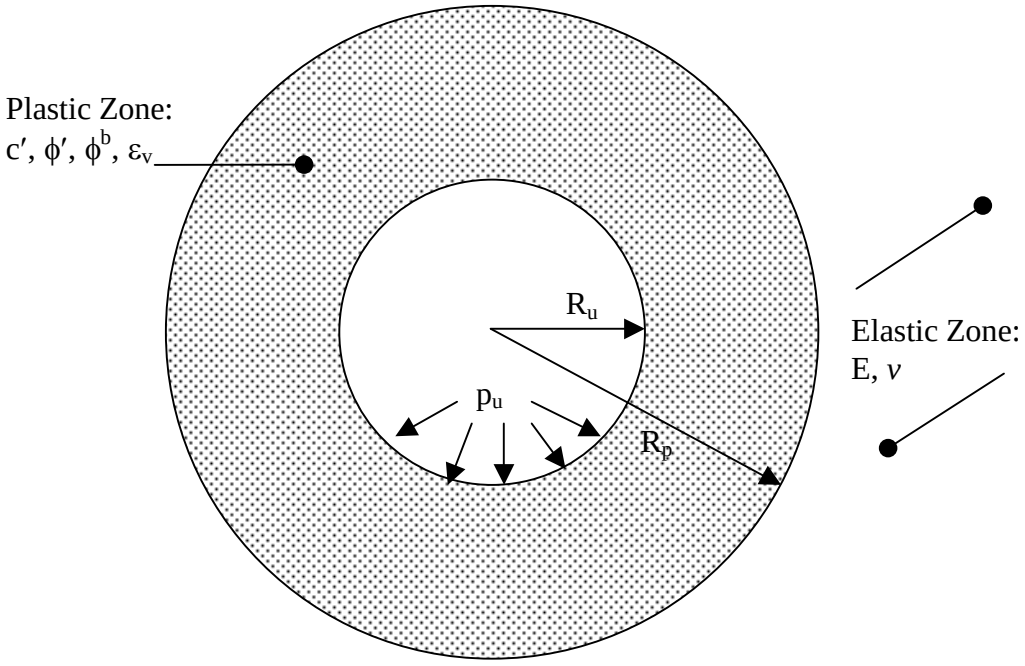

Figure 2-8: Expansion of Cylindrical Cavity (After Vesic 1972)

The expansion of prebored pressuremeter probe can be depicted by the expansion of the cylindrical cavity provided the length of the probe is sufficient such that the deformation of the soil along the probe is mainly radial soil displacement in a cylindrical coordinate system with zero vertical displacement. Therefore many researchers had used cylindrical cavity expansion in connection with the pressuremeter test (e.g. Palmer 1972, Hughes et al. 1977, Worth and Windle 1975, Yu and Carter 2002, Vesic 1972, Osinov and Cudmani 2001). Hence, in this study the cylindrical cavity expansion in unsaturated soil equation developed by Muraleetharan et al. (1998) is used to interpret the pressuremeter data.

However, for the cone penetrometer test the modeling of soil deformation during the cone penetration is much more complicated than the modeling of the pressuremeter. This is because the deformation of the soil around the cone tip does not resemble the expansion of a spherical or cylindrical cavity and is spatially two-dimensional (Osinov and Cudmani 2001). Osinov and Cudmani (2001) had introduced the use of shape factor into their solution for cavity expansion problems. However, Mitchell and Keaveny (1986) via Hryciw and Dowding (1987) stated that between cylindrical and spherical cavity expansion theories, spherical cavity expansion theory is better in prediction of penetration resistance of cone penetrometer in most cases except for overly consolidated or incompressible sand where the cylindrical cavity expansion theory is better. Based on the soil type and dry unit weight used in the study for this dissertation, it is safe to assume the soil is compressible. Therefore, the spherical cavity expansion in unsaturated soil

equation developed by Muraleetharan et al. (1998) is used to interpret the cone penetrometer data.

Although many studies were performed on cavity expansion for interpretation of the PMT and CPT, most of them have been oriented around saturated or dry soil. Only a handfull of published papers were found regarding cavity expansion in unsaturated soil. There is still lack of information on the influence of matric suction on limit pressure (P_L) from PMT, and tip resistance (q_c) from CPT conducted in unsaturated soil. One of the objectives of this dissertation research is to provide a data set to show the influence of suction on P_L and q_c. Along with equations for cavity expansion in unsaturated soil developed by Muraleetharan et al. (1998) and the data collected from this study, a framework for interpretation of PMT and CPT in unsaturated soil can be developed.

Chapter 3: Calibration Chamber

Calibration chambers have been used for many years to perform studies on in situ instruments such as the cone penetrometer (e.g., Schnaid and Houlsby 1991, Puppala et al. 1991, Lunne 1991, Kulhawy and Mayne 1991, Rix and Stokoe 1991, Peterson 1991, Hryciw and Dowding 1987), pressuremeter (e.g., Anderson et al. 1991, Penumadu and Chameau 1998, Pyrah and Anderson 1990), dilatometer (e.g., Baldi 1986, Borden 1991, and Bellotti et al. 1986), etc., under controlled conditions. Holden (1991) stated that the first large scale calibration chambers started in 1969 at the Materials Research Division, County Roads Board (CRB) in Melbourne, Australia when CRB tried to calibrate their friction-cone penetrometer in the laboratory mimicking the field conditions. The first CRB calibration chamber was designed to hold a 76.2-cm (30-inch) diameter and 91.4-cm (36-inch) high soil bed. During the early years of calibration chambers, rigid-walled cylinders were frequently used. Sweeney and Clough (1990) classified the rigid wall chambers as passive vessels since it is only used as a container for the soil mass. However, over the years, the flexible wall calibration chamber has gained popularity as it helps to reduce the boundary effects and also gives the operators a greater control over the stress state of the soil bed. It is also more economical and practical compared to a rigid wall chamber since a smaller soil bed can be used to minimize the boundary effects. There are four types of boundary conditions available for calibration chamber: 1) constant radial and vertical stress (BC1), 2) constant volume (BC2), 3) constant vertical stress and zero radial displacement (BC3), and 4) constant radial stress and zero vertical displacement (BC4) (Voyiadjis et al. 1993, Lauder 2000). In addition to boundary type, the test probe size also affects the results obtained from calibration chamber tests.

Extensive research has been done in this area and various probe to soil bed diameter ratios have been recommended for different types of soils and boundary conditions (e.g. Schnaid and Houlsby 1991, Sweeney and Clough 1990, Salgado et al. 1998, Mayne and Kulhawy 1991). Most of the calibration chambers utilized cylindrical specimens given that it is relatively easier to prepare and test, and the data obtained are easier to analyze compared to cubical specimens (Peterson and Arulmoli 1991). The details of University of Oklahoma calibration chamber will be discussed later in this chapter.

3.1 Reasons for Calibration Chamber Testing

Analysis of in situ test data obtained in the field is not practical for developing a method for interpreting PMT and CPT tests in unsaturated soil because field boundary conditions can not be well defined or controlled. Many limitations and uncertainties associated with heterogeneity of soil, unknown stress history, and stress state of soil complicate analyses. Although these uncertainties can be examined using laboratory tests on “undisturbed” samples collected from the field, it is almost impossible to obtain truly undisturbed samples. One alternative to overcome these uncertainties and problems is by using a calibration chamber. In the past, calibration chambers were used for calibrating field instruments in a controlled environment where the data collected can then be used to develop empirical correlations. It has also been used to validate some geotechnical theoretical models for some field instruments such as CPT and PMT.

There are several advantages of calibration chamber testing over field testing. One of the main advantages is it allows the user or researcher to have full control of the stress and strain history, boundary conditions, density, and water content of the test beds. The capability to prepare reproducible, homogeneous test beds with similar properties is

another added advantage. This helps to eliminate the uncertainties due to soil inhomogeneity and uncertainties regarding the magnitude of stresses and the in-situ stress history.

3.2 University of Oklahoma Calibration Chamber

As discussed earlier in Chapter 2, almost all of the calibration chambers were designed to accommodate either dry/saturated sand or saturated clay. Lauder (2000) used the available information in literature as an aid in the design of a calibration chamber for unsaturated soil testing. Additionally, Lauder (2000) had used the following criteria as a guideline when designing the University of Oklahoma Calibration Chamber (OUCC):

1. The chamber was designed as simple as possible and yet capable to perform the following tasks on the soil bed prepared:
    - measure and control pore water pressure,
    - measure and control pore air pressure,
    - measure and control pore water volume change,
    - measure total volume change, and
    - control the radial and axial stress applied to the soil beds independently.
2. The test bed and chamber should be large enough to minimize boundary effects.
3. The chamber should be able to accommodate other future tests with higher working pressure.

Figures 3-1 and 3-2 show the schematic diagram and a picture of the complete assembly of the OUCC. In general, the chamber is similar to a large unsaturated triaxial device. It is a self reacting, flexible wall chamber with BC1 type boundary conditions and

design working pressure up to 1380 kPa. The research conducted in this study utilized confining pressure not greater than 207 kPa. Thus, the high design working pressure helped to ensure there is no noticeable deformation of the chamber wall during the testing. This is important since Linear Variable Differential Transformers (LVDTs) are mounted on the chamber walls.

The OUCC consist of 10 main components or modules: 1) chamber shell (Figure 3-3), 2) top cap and top plate (Figure 3-4 and 3-5), 3) piston (Figure 3-6), 4) support flange and base plate (Figure 3-6), 5) stress application and control system, 6) pore water pressure control and monitoring system (Figure 3-7 and 3-8), 7) pore air pressure control and monitoring system (Figure 3-8), 8) total volume change measuring system, 9) pore water volume change measuring system (Figure 3-8), and 10) diffused air indicator (DAVI) (Figure 3-9). Details regarding the chamber design can be found in Lauder (2000). A brief illustrated description of each component is follows

3.2.1 Chamber Shell

The chamber shell (Figure 3-3) consists of three identical rigid metal segments. Thus, the height of the chamber can be varied using one, two or three segments to accommodate various in situ devices. This allows the chamber to accommodate soil beds with 610-mm diameter and various heights, ranging from 450-mm to 1420-mm depending on number of segments used. Each segment was made from a steel pipe with 737-mm inner diameter, 508-mm height, 25-mm wall thickness, and a 51-mm thick flange welded around the outer wall of the pipe on both ends. The segments are connected via twenty-four bolts placed around the flanges. O-rings between flanges prevent leakage of confining fluid or gas.

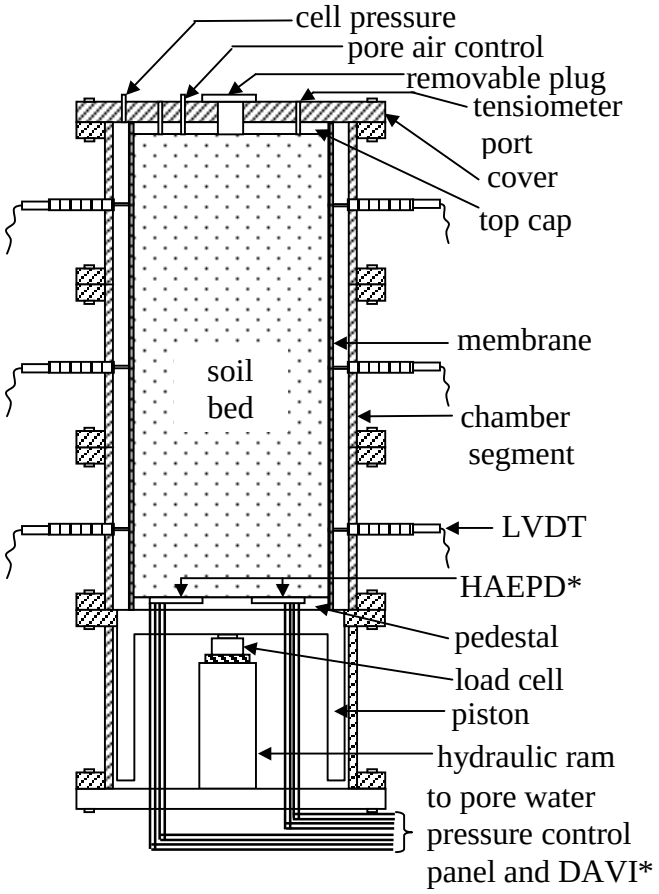

*HAEPD – High Air Entry Porous Disc
*DAVI – Diffuse Air Volume Indicator

Figure 3-1: Schematic Diagram of University of Oklahoma Calibration Chamber (OUCC) (after Miller et. al 2002)

Figure 3-2: Picture of University of Oklahoma Calibration Chamber

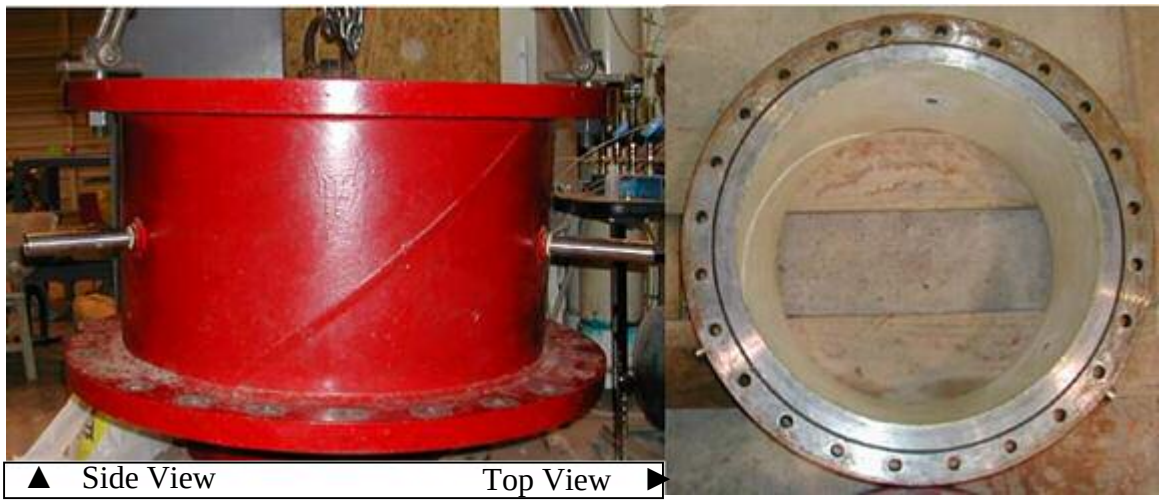

Figure 3-3: Picture of Chamber Section

3.2.2 Top Cap and Top Plate

The top cap as shown in Figure 3-4 is a 963-mm diameter steel plate with 64-mm thickness. The top plate as shown in Figure 3-5 is a 610-mm diameter aluminum plate with 38-mm thickness. Nine ports were made passing through the top cap and top plate for miniature tensiometer access. The top cap and top plate have a 79-mm diameter hole in the center for insertion of scaled down in-situ test devices and yet is large enough to accommodate a full size CPT and PMT. However, in this research scaled down devices are being used to minimize boundary effects. Two additional ports were made for the pore air pressure and cell pressure. Some minor modifications were made on the top cap and top plate from the original design. Three additional 20-mm diameter holes were made through the top cap and top plate, spaced 120^{o} apart and 127-mm from the center. These holes allow for additional testing with scaled down in-situ devices in the same soil bed. It also allows for the study of boundary effects.

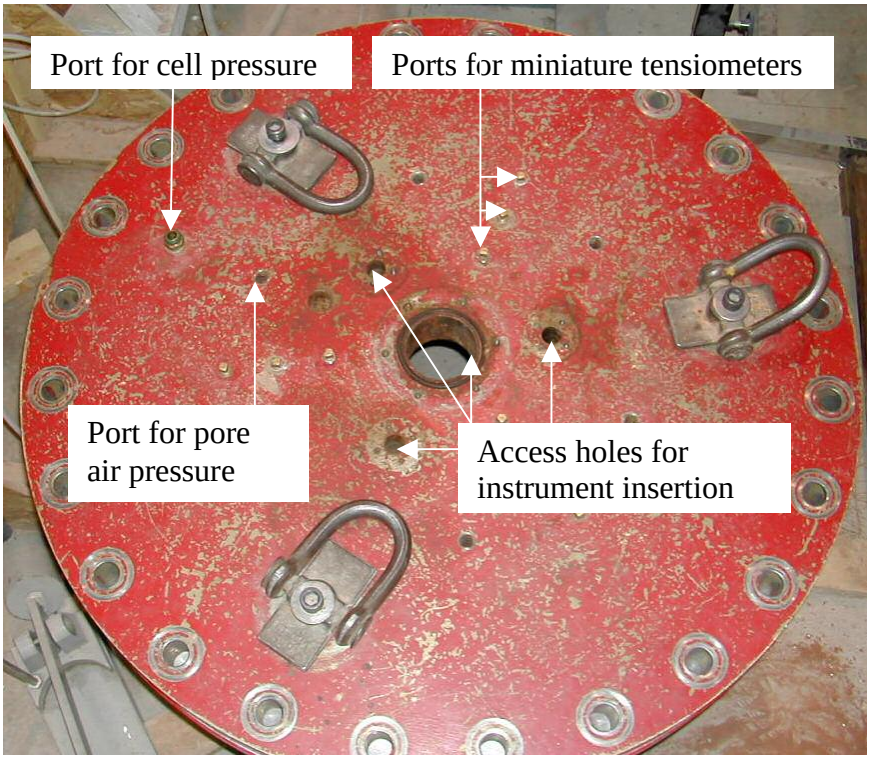

Figure 3-4: Picture of Top Cap

Figure 3-5: Picture of Top Plate

3.2.3 Piston

The piston is a 711-mm diameter by 76-mm thick steel plate with a 533-mm long skirt around its perimeter. It is held in place by the support flange. A hydraulic jack placed underneath the piston is used to apply axial load.

3.2.4 Support Flange and Base Plate

The support flange serves to hold the piston, load cell and hydraulic jack in place during testing. The dimensions of the support flange are the same as the dimension of the chamber shell segments. The support flange sits on a base, which has similar dimensions as the top plate. Lauder (2000) suggested that an additional plate with similar dimensions could be sandwiched together with the existing plate to reduce deflection if the deflection of the base plate is critical or intolerable in future research. In this study, the deflection is minimal since the pressure used in this study is less than 20% of the design working pressure. In Figure 3-2 and 3-6 the support flange and the base plate can be seen.

3.2.5 Stress Application and Control System

As stated earlier, the OUCC allows for application of BC1 type boundary conditions, where constant radial and vertical stresses are applied independently to the soil bed. Either air or water can be used as the pressurizing fluid in the annulus between the soil bed and the chamber wall. Air was used for the current research due to concern that water would diffuse across the membrane and change the soil water content. While radial stress is controlled via fluid pressure in the annulus, axial stress is controlled via the chamber's piston. A load cell placed between the piston and the hydraulic jack measures the total axial force. The load cell was calibrated to determine the magnitude of

axial force required to achieve desired axial stress while accounting for piston friction and soil weight. During testing the output from the load cell is recorded by a data acquisition system.

Figure 3-6: Picture of Support Flange and Base Plate

3.2.6 Pore Water Pressure Control and Monitoring System

The pore water pressure of the soil beds can be regulated via six high air-entry porous stones attached to the bottom plate (Figure 3-7). The pressure underneath the porous disks is controlled by regulating the pressure applied to the water in the burette system and monitored through a pressure gage (Figure 3-8). In order to achieve good

control or measurement, the porous disks are first saturated prior to the compaction of soil bed by passing water through the disks and leaving the disks under pressurized water. Each disk has a separate control valve so that it can be turned off in the event it does not function properly.

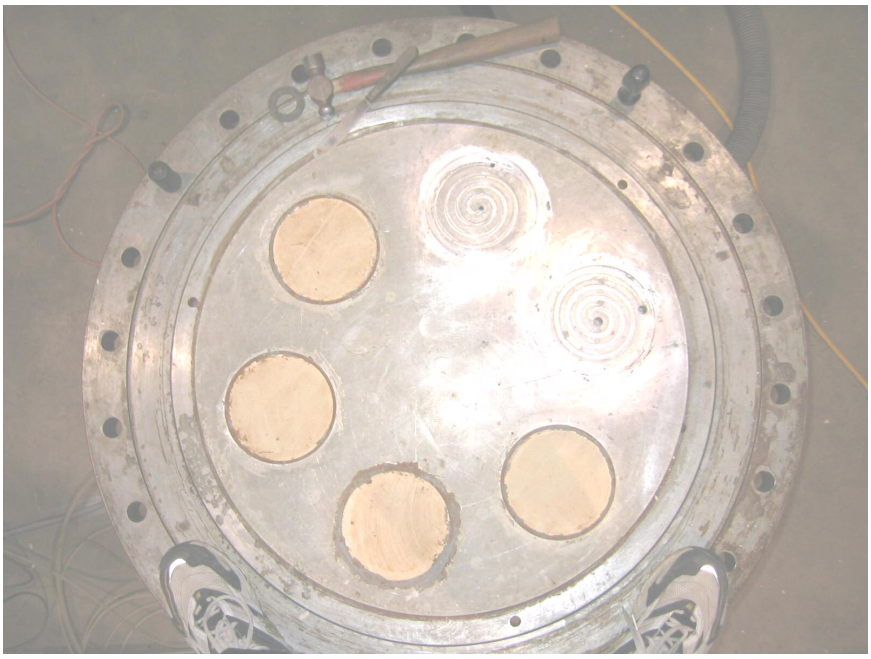

Figure 3-7: Picture of High Air-Entry Porous Stone and Grooves on Bottom Plate

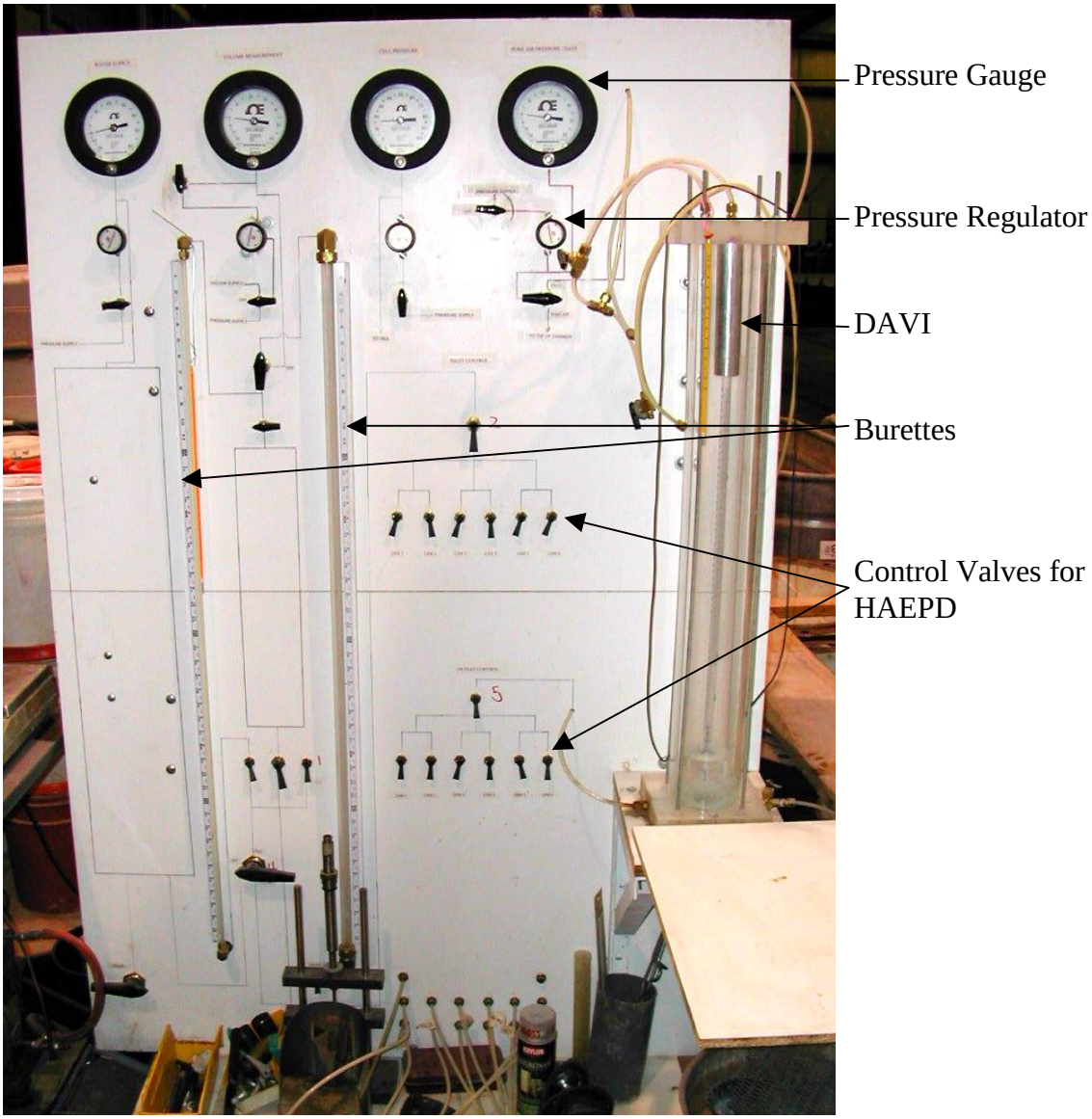

Figure 3-8: Picture of Pore Air, Pore Water and Cell Pressure Control Panel and DAVI

3.2.7 Pore Air Pressure Control and Monitoring System

An air compressor is used as the pressure source for the pore air pressure control system (Figure 3-8). Pore air pressure is regulated and monitored via a pressure gage and regulator. Fiberglass cloth is placed between top plate and top of soil bed to distribute the air pressure evenly and efficiently across the top surface of the soil beds.

3.2.8 Total Volume Change Measuring System

The total volume change of the soil bed is measured via Linear Variable Differential Transformers (LVDTs). The LVDTs are placed at 120^{o} intervals at mid height of each segments for measurements of radial deformation, and two at the bottom of the piston for measurements of axial deformations. The LVDTs used for radial deformation measurements are spring loaded, submersible, capable to withstand high pressure and have ± 25-mm range. The LVDTs used for axial deformation measurements are spring loaded, and have ± 51-mm range. The output from all the LVDTs is recorded by a data acquisition system.

3.2.9 Pore Water Volume Change Measuring System

Measuring water volume change for unsaturated soil is more complex compared to saturated soil due to the presence of air, a compressible pore fluid. The tendency for the air to migrate across the high entry disk further complicates the process. Water volume change is measured via a burette system; burettes respond to the change of water volume plus the volume of diffused air moving into the compartment below the porous disk. To obtain the exact water volume change in the soil bed, the volume of diffused air must be subtracted from the total water volume change. The volume of diffused air is measured by a Diffused Air Volume Indicator (DAVI) connected to the groove below the porous disks. The OUCC volume change measuring system consists of three burettes with different diameter. This allows for different volume measurement resolution. The burettes have inner diameters of 4.8-mm, 12.7-mm and 101.6-mm, with 0.03-cm^3, 0.20-cm^3 and 12.88-cm^3 resolutions respectively (Figure 3-8). Different burettes can be used at

different times during the test depending on the magnitude of water volume change anticipated.

3.2.10 Diffused Air Volume Indicator (DAVI)

The OU DAVI (Figure 3-9) is similar to the DAVI described by Fredlund and Rahardjo (1993). The OU DAVI consists of a 50-cm^3 glass burette and an acrylic plastic exit tube placed inside a larger acrylic plastic tube. The burette bushing and end tube are made from stainless steel. O-rings are used as sealers. The diffused air trapped underneath the porous disks is flushed by setting the water pressure below the disks slightly higher than the air pressure inside the DAVI. Once the air is pushed out into DAVI, it displaces the water in the DAVI burette. The water flows out from the burette through an exit tube into the DAVI chamber. With the initial and final burette readings, the volume of diffused air is calculated using the ideal gas law. At anytime, if the water in the burette is completely replaced by air, the burette can be refilled with water by opening the top vent. The plumbing systems were set up such that any combination of the six porous disks can be flushed at any time.

Figure 3-9: Picture of OU DAVI

3.3 Soil Bed Preparation Method

The preparation of the soil bed is a crucial part of calibration chamber testing. There are several methods available to prepare a soil bed for the calibration chamber. Most of them are used to prepare dry soil beds for sand or saturated soil beds for clay. Very little research has been attempted on silty soil, let alone unsaturated silty soil. The two most common methods for soil bed preparation developed in the past are pluviation for sandy material and slurry consolidation for clayey material. The potential of each method for preparation of an unsaturated soil bed containing Minco silt has been studied by Tan (2000) OU. The soil used by Tan (2000) is the same soil used in this study. The goal of Tan (2000) study was to develop a reliable method for producing unsaturated Minco Silt test beds with consistent properties. The preparation method needs to be repeatable and capable of producing a homogeneous soil bed.

Several methods for preparation of unsaturated soil beds using Minco Silt in bench scale models (1/4 scale) were studied by Tan (2000). The first method involved pluviating soil into the bench scale mold in lifts, followed by adding a predetermined volume of water on top of each lift. The second method involved mixing the soil to predetermined moisture content, then compacting in layers into the mold. Several methods were used to compact the soil-water mixture, including: impact compaction, static compaction and tamping. In all tests, sub-specimens were collected to check for homogeneity within soil beds with regard to variation in moisture content and dry unit weight (see Appendix B for distribution of moisture content and dry unit weight over depth for the soil beds used in this study and Appendix D for homogeneity of the of the soil beds with regard to CPT soundings). Among all of the methods studied, Tan (2000)

concluded that for Minco silt, static compaction was the most feasible for producing a homogeneous unsaturated soil bed. It is also more repeatable compared to the other methods that have been studied. Tan (2000) found that the upper limit of water content to produce a macroscopically homogeneous Minco silt–water mixture was about 12%. Above 12% excessive clods were formed and this would lead to nonuniform soil fabric. Tan (2000) concluded that molding water content between 8% and 12% would give satisfactory of fabric throughout the entire soil bed.

The subsections (Section 3.3.1-3.3.3) that follow give a brief literature review of some available methods for soil bed preparation that had been considered by Tan (2000).

3.3.1 Pluviation

The pluviation method involves raining of cohesionless soil particles into a mold either in water or air. This method is frequently used for the preparation of sand specimens. The density of the specimen formed by this method depends on the porosity (diameter and number of holes) of the rainer plate, number of sieves used, impact velocities and falling distance of soil particles during pluviation (Lo Presti et al. 1992, Vaid et al 1984). The advantage of this method is that it mimics the natural process of alluvial deposition of soils (Rad et al. 1987). Tan (2000) had utilized this method in his bench scale studies. In the study, the specimens were dry pluviated in five lifts, followed by misting predetermined volume of water on top of each lift. From the study, Tan (2000) concluded that the pluviation method did not give satisfactory homogeneity in the soil beds produced, required an impractical amount of time to achieve equilibrium for change in moisture content, and produced very loose soil beds.

3.3.2 Consolidation

The slurry consolidation method works well for producing saturated cohesive soil beds for calibration chamber testing (Voyiadjis et al. 1993). The process involves mixing the soil with water up to 1.5 to 2.0 times the liquid limit of the soil and consolidating the slurries under at rest earth pressure (K_o) conditions (Anderson et al. 1991). The advantage of this method is that it appeared to depict the natural process of soil sediments. This method involves considerable amount of time, considerable volume changes and complex instrumentation to monitor and maintain the pore pressure (Voyiadjis et al 1993). Therefore, Tan (2000) did not attempt this method for the preparation of unsaturated soil beds for calibration chamber testing. Tan (2000) also stated that another disadvantage of this technique is the specimen prepared is initially saturated and a vast amount of time is required to desaturate the soil bed to the desired matric suction range.

3.3.3 Compaction

The use of compaction to prepare soil beds for the calibration chamber is not well documented in the literature. However, it has been used to prepare other geotechnical test models. Deshpande (1997) used the impact compaction method to prepare Minco silt embankment models for centrifuge tests. Akanda (1998) used another compaction method known as “moist tamping” to prepare his test specimens. Akanda concluded that “moist tamping” method is capable of producing identical and uniform specimens. In the bench scale studies, Tan (2000) had tried several compaction methods; impact compaction, tamping and static compaction. From the study, Tan (2000) recommended static compaction method for the preparation of unsaturated soil beds for calibration

chamber testing as the most feasible and promising for producing homogeneous unsaturated soil beds.

3.4 University of Oklahoma Static Compactor

From the bench scale studies conducted by Tan (2000), the static compaction method was selected as the method to prepare the larger soil beds for calibration chamber testing. A large static compactor was built for the preparation of the unsaturated soil beds for calibration chamber testing. Figure 3-11 shows a picture of the OU static compactor. The compactor consists of compactor frame, a piston and a compacting plate. The compactor frame was designed such that it can be attached to the chamber shell making the compactor a self-reacting compactor. The compactor frame is 1.1-m in height and 0.7-m in width and length. Attached to the frame is a 13.8 MPa piston with a compactor plate attached to it. The steel compactor plate has diameter of 596.9-mm and thickness of 25.4-mm. Stiffeners were welded to the plate to reduce the deflection of the compacting plate during compaction. The sample former is made of a piece of stainless steel sheet metal rolled into 609.6-mm cylinder. The stainless steel sheet metal is fastened together with a hinge that runs the full height of the former. Three sample formers with different heights (508.0-mm, 762.0-mm and 1524.0-mm) were made for this study for the preparation of soil beds with different height. Figure 3-10 shows the picture of one of the sample formers used in this study.

Figure 3-10: Pictures of University of Oklahoma Static Compactor: a) Static Compactor Assembly Sitting on Calibration Chambers Segments, b) Close up View of Static Compactor Frame and Sample Former Lined with Rubber Gum Membrane, C) Top View of Compactor Plate with Stiffeners and D) Spacers

Figure 3-11: Picture of Sample Former with Stiffeners

Chapter 4: Material and Testing Equipment

4.1 Test Soil: Minco Silt

The soil used in this study is a silty soil known locally as Minco silt. This soil is found in central Oklahoma. Much research has been done at the University of Oklahoma (OU) using Minco silt. Therefore, a substantial database of the mechanical and physical properties of this soil is available. Additionally, it is ideal for unsaturated soil research because it is slightly cohesive and has lower matric suction compared to other more plastic clayey soils. Clayey soil develops high matric suction and it is difficult to achieve direct measurements of high matric suction. Since the Minco silt is slightly cohesive, it is easy to compact, trim and capable to support it own weight as long as the gravimetric water content is not greater than 12%. The soil also permits the use of tensiometers to determine the matric suction since the range of matric suction of interest is lower than 100 kPa. Minco Silt is classified as a CL (borderline CL-ML) soil according to the Unified Soil Classification System (USCS). The physical properties, textural composition and engineering properties of the soil are shown in Table 4-1.

4.2 University of Oklahoma Miniature Pressuremeter

In order to minimize boundary effects, a miniature pressuremeter (MPMT) with diameter of 15.2-mm and inflatable length of 130-mm was used. This gives a height to diameter ratio of 8.5, which exceeds the recommended value of 6.5 needed (Briaud 1992) to simulate plane strain cylindrical cavity expansion. Based on work of other researchers (Penumadu and Chameau 1998, Anderson et al. 1987) the soil bed to probe diameter ratio

of 40 was considered sufficient to minimize the radial boundary effects for the test soil used in this research.

Figure 4-1 shows a picture of the OU MPMT. The probe was machined from a solid stainless steel rod. Rubber tubing was used for the miniature pressuremeter membrane. The inner diameter and thickness of the tubing was 12.7-mm and 0.8-mm respectively. The membrane is clamped to the probe by tightening sleeves on both ends. O-rings placed between the steel rod and membrane form a leak proof seal. The assembly of the probe was completed by attaching a connector head to the top end of probe. The connector head allows the probe to be attached to a threaded rod, that is used to maneuver the probe in the borehole.

Table 4-1: Table 1: Physical Properties, Textural Composition and Engineering Properties of Minco Silt Used in the Test Program

Liquid Limit, %	28
Plastic Limit, %	20
Plasticity Index, %	8
Specific Gravity	2.68
Gravel, %	0
Sand, %	27
Fines, %	73
Clay Size Fraction, %	22
USCS Classification	CL
Maximum Dry Unit Weight, kN/m^3	18.1
Optimum Moisture Content, %	13.5

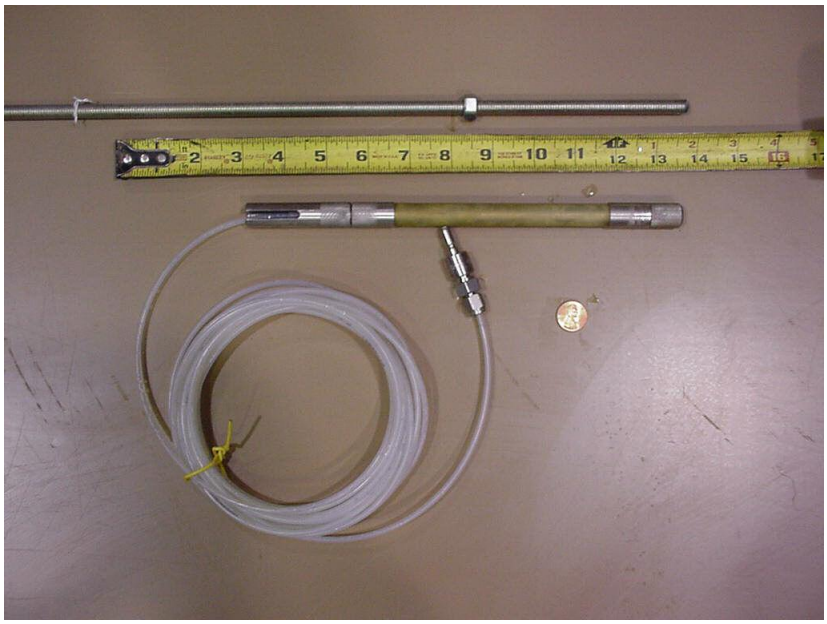

Figure 4-1: Picture of University of Oklahoma Miniature Pressuremeter (OU MPMT)

4.3 University of Oklahoma Miniature Cone Penetrometer

The miniature cone penetrometer (MCPT) used for this research is smaller than a standard cone. Again, for the same reason as stated earlier, a miniature cone was used in order to minimize the boundary effects. The cone used has a diameter of 1.78-cm, which gives a projected tip area of 2.49 cm^2. The soil bed to probe diameter ratio is 34, which is considered sufficient to minimize the radial boundary effects for the test soil type (Kurup et al. 1994, Schnaid and Houlsby 1991) and flexible wall calibration chamber test. A higher ratio would be anticipated if a rigid wall calibration chamber are to be used. The apex angle at the tip of the cone is 60^o, which is the same as the standard cone. The penetrometer is equipped to measure tip resistance with maximum load capacity of 8.9-kN. A cable-extension position transducer is used for the measurement of penetration

depth. The output from all the instruments is collected by a data acquisition system. Figure 4-2 shows a picture of OU MCPT.

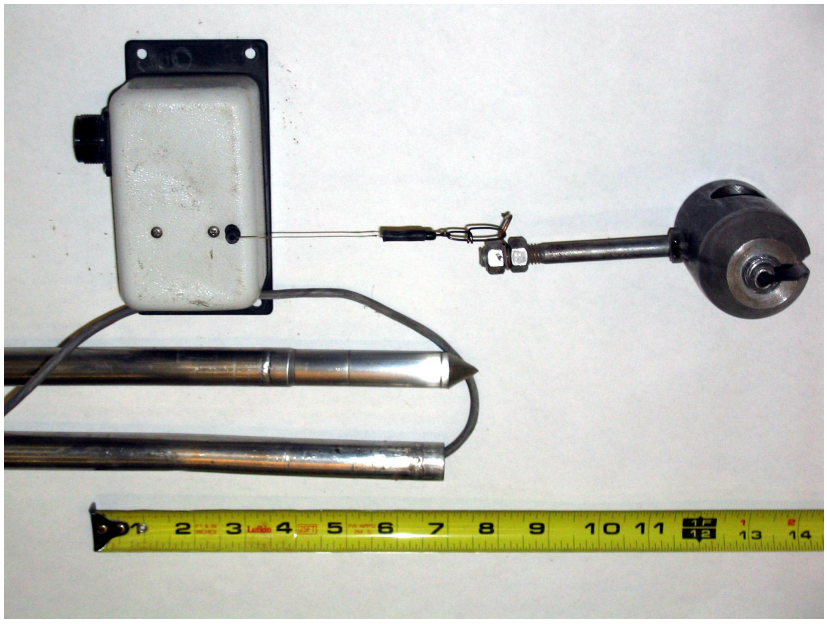

Figure 4-2: Picture of University of Oklahoma Miniature Cone Penetrometer (OU MCPT)

Chapter 5: Experimental Methodology and Testing

5.1 Test Bed Preparation Method

5.1.1 Soil Processing

The preparation of the soil for the test beds used in this research is similar to the process used by Tan (2000) for the bench scale study. The soil was first oven-dried at 110±5^{o}C, pulverized, passed through a #10 (2-mm) sieve and kept in airtight container. The processed soil was then mixed together with water in a 2.29-m^3 (3-yard^3) concrete mixer for at least 10 minutes to ensure homogeneity in the mixture. The soil-water mixture was then transferred to airtight 5-gallon containers and stored for at least one day to allow the moisture in the mixture to further equilibrate. Multiple samples were collected for water content determination prior to compaction. Figure 5-1 shows pictures taken during the test bed preparation.

5.1.2 Compacting Test Bed Soil

From the bench scale studies conducted by Tan (2000), the static compaction method was selected as the method to prepare the larger calibration chamber soil beds. Prior to compaction, the sample former was lined with a 1.6-mm thick pure gum rubber membrane. Then, the assembly of sample former and membrane was fixed to sit concentrically on the bottom plate (see Figure 5-1 bottom left picture). The soil-water mixture was statically compacted in the assembly by the compactor as describe in Section 3.4. However, some unforeseen obstacles were encountered. The piston on the compactor was not capable to produce sufficient force to achieve the desired soil bed density as

recommended by Tan (2000). Thus, the chamber's piston was used to help in the compaction. In order to use the chamber's piston in the compaction process, four equal length steel columns were used as braces between the compactor plate and the frame. First the compactor plate was lowered to the top of the soil-water mixture surface and was further advanced to compact the soil until the piston reached its maximum capacity. The compactor piston was then locked in its position and the vertical braces were placed between the frame and the compactor plate. The chamber piston was then raised to further compact the soil until it reached the desired density or the limit of the sample former, which will be discussed in next paragraph.

There were several problems encountered when proceeding from bench scale to calibration chamber scale. During compaction of the full-scale soil bed, it was observed that the sample former expanded radially. This was not observed during the bench scale studies since the mold used in the bench scale studies is relatively more rigid. Switching to a heavier wall sample former was considered but was not implemented, as it would be impractical. In order to minimize the deformation, stiffeners (metal straps) were wrapped around the sample former at 102-mm vertical spacing. At full-scale, it is harder to achieve high densities in the soil bed due to the large vertical forces required. Instead of targeting a soil dry unit weight of 15.7-kN/m^3 as recommended by Tan (2000) from the bench scale studies, the large soil bed was compacted with a lower target dry unit weight. Instead of 15.7-kN/m^3 the target dry unit weight was reduced to 13.5-kN/m^3. The reduction in the target density also helped to further reduce the sample former deformation during compaction.

Figure 5-1: Pictures Taken During Test Bed Preparation: a) 2.29-m^3 Concrete Mixer Used for Mixing Soil-Water Mixture, b) Storing Soil-Water Mixture in 5-gallons Containers, c) Soil-Water Mixture Inside the Sample Former Lined with Pure Gum Rubber Membrane Prior to Compaction, d) Exterior of 1.5-m Sample Former Sitting Concentrically on the Bottom Plate, e) Prepared Test Bed with Pure Gum Rubber Membrane and Top Plate and f) Side view of Prepared Test Bed.

Early in the study the prepared soil beds were isotropically compressed (consolidated) to 104-kPa in 34.5 kPa increments. This stress was chosen to stimulate stress conditions at about 2-m below ground. Later in the study, seven of the test beds were isotropically compressed to three different net normal stresses (104, 152 and 207-kPa) to allow the investigation of the influence of net normal stress on pressuremeter

results. For each stress increment, the deformations of the test bed were monitored over time. Each increment was maintained until the observed deformation was relatively small or insignificant. The volumetric strain over time was determined by using the average radial and axial deformations.

5.1.3 Controlling/Determining Matric Suction of Test Beds

As stated Section 3.2, the OUCC allows the pore air and pore water pressure to be controlled independently. Thus, matric suction in the soil bed can be controlled or regulated by maintaining the difference between pore water and pore air pressure. This is known as an active control approach. It was considered as a preferred approach early in the study. The author was interested in preparing all the test beds at same initial matric suction (or water content) followed by increasing or decreasing the matric suction via the pore water pressure control system. However, preliminary testing revealed that this approach was not practical as it requires a tremendous amount of time to induce a small change in matric suction due to the low permeability of the unsaturated soil and the large soil bed dimensions. Therefore, a more time-efficient approach was utilized. The soil beds were compacted at prescribed moisture content with reference to a target matric suction based on soil water characteristic curves (SWCC, Figure 5-2). Then, passive measurement approaches were utilized to determine the matric suction: 1) small tip tensiometers were installed in the soil bed, 2) water content samples were collected throughout the soil bed and were used with the soil water characteristic curve to determine the matric suction, and 3) several small thin-walled tube samples were collected from soil beds and matric suction of samples were determined via small tip tensiometers.

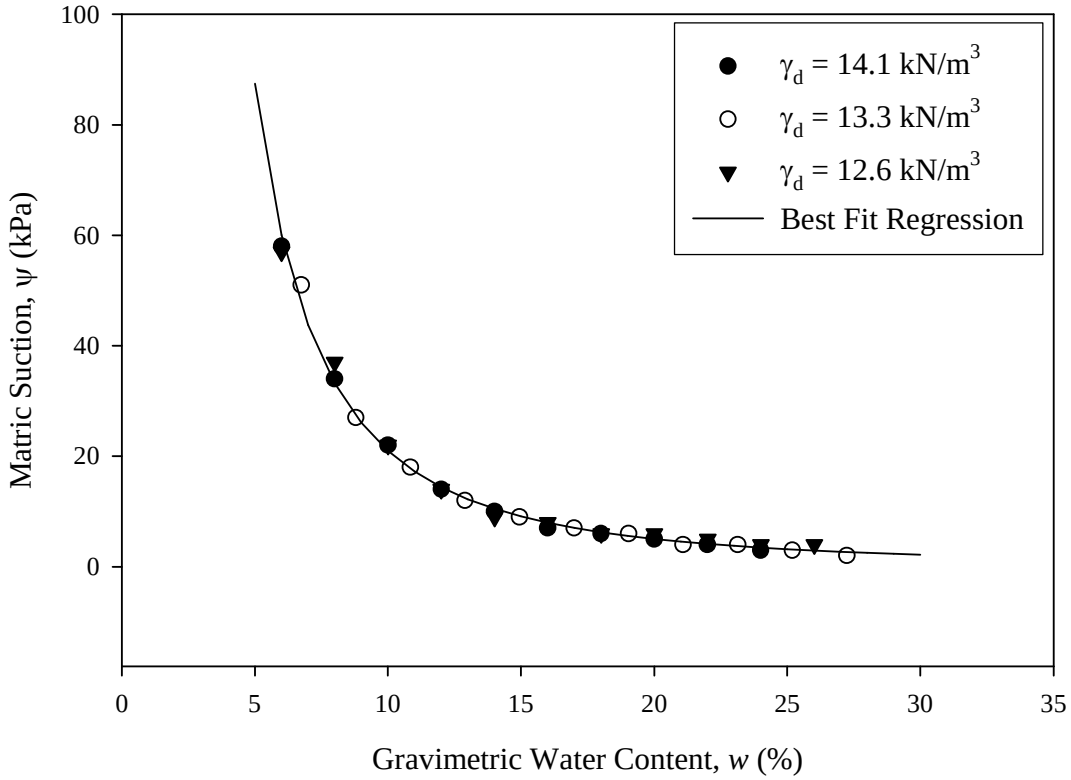

Figure 5-2: Soil-water characteristic curve for Minco Silt at various dry unit weights (after Ananthanathan, 2002)

5.2 Miniature Pressuremeter Testing

The miniature pressuremeter test (MPMT) was conducted using stress-control where constant pressure increments were maintained via a pressure regulator. The tests were conducted according to the standard method of practice, similar to the procedure described in ASTM Standard Test Method for Pressuremeter Testing in Soils (D 4718).

Upon completion of the soil bed compression phase and equalization of matric suction, the top plug was removed. A small cut was made on the fiber glass cloth exposing a small portion of top of the soil bed. Then, the drill cap was placed and tightened in the position where the top plug was previously located. The drill cap helped

to ensure the drill bit and its extensions remained in a vertical position. Since the diameter of the MPMT probe used is much smaller than the typical pressuremeter probe, a modified wood drill bit with extension was used to prepare the borehole in the soil bed. The drill bit has 304.8-mm flight length. Two rods, each at 609.6-mm were machined as extension rods for the drill bit. The diameter of the drill bit's cutting head is slightly larger than the flights. This helps to reduce friction from flights against the borehole wall. While advancing the drill bit into the soil bed, the vertical pressure was applied to the drill and the rotation rate of the drill bit was kept low to minimize disturbance on the soil around the borehole wall.

The pressure for the MPMT was supplied by a tank of compressed nitrogen gas. Volume of fluid injected into the MPMT was measured via a burette setup. All the fluid lines and the pressuremeter were first flushed with deaired water. For each calibration chamber test, the MPMT was calibrated to compensate for both volume and pressure losses. The calibration procedure will be discussed later in this section. The boreholes were drilled to the test depth; typically test were conducted at one or two different depths. The MPMT was then lowered into the borehole until the mid-section of the inflated portion reached the test depth. Initially, pressure was increased in small increments (approximately 2 to 3-kPa) until the membrane touched the borehole wall; then larger increments (approximately 5 to 6-kPa) were used. For practical purposes Briaud (1992) had recommended to obtain at least 7 to 14 pressure increments before the test reaches the limit pressure (P_L). However in this study a minimum of 15 stress increments were obtained before the test reached the P_L. Typically 18 ± 3 stress increments were used in each test. Volume readings were taken at 30-seconds and 1-minute after each pressure

increment. The test was conducted until the probe reached its limit volume. Figure 5-3 shows a typical MPMT pressure expansion curve.

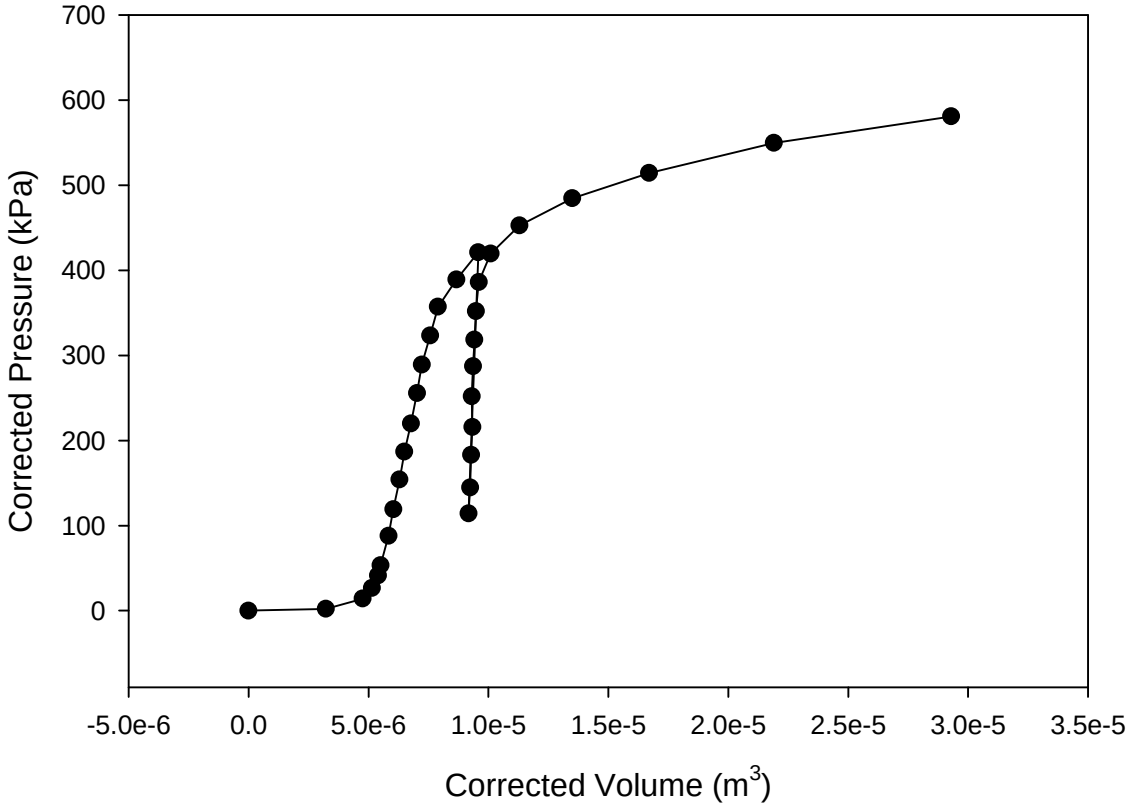

Figure 5-3: Typical MPMT Pressure Expansion Curve (from MPMT Test ID 27_15B)

In each test, when the pressure reached the end of the linear portion of the pressuremeter curve, one unload-reload cycle was conducted by reducing the pressure near the initial linear portion of the pressuremeter curve. In this study the end of the linear portion of the pressuremeter curve was estimated during testing by observing the creep volume between 30-second and 60-second readings for each stress increments. The creep volume stays relatively constant (typically zero for this study) during the linear portion of the pressuremeter curve. The creep volume increased when the soil started to

yield. When first significant creep volume was observed, the pressure was reduced for the unload-reload cycle. The pressure was maintained for about 10-minutes before reloading. During the test, the height of initial fluid level in the burette and height of pressuremeter from the datum were recorded for hydrostatic pressure correction. Table 5-1 shows the summary of the MPMT conducted in each test bed including the test depth with reference to the top of the test bed and confining stress during testing (net normal stress, σ_n).

Prior to each calibration chamber test, the MPMT was calibrated to compensate for both volume and pressure losses. The calibration for volume losses was done by inflating the MPMT probe in a heavy duty steel pipe. The pressure was increased in increments of 34.5-kPa and held for 60-seconds per pressure increment. Volume measurements were taken at 30-seconds and 60-seconds after each pressure increment. The pressure vs. volume plot obtained from this part of calibration is known as the volume calibration curve as shown in Figure 5-4. It shows the volume loss due to the system compressibility and expansion of tubing at a given pressure. Thus, for the volume correction, the volume loss at each given pressure was subtracted from the MPMT volume reading during a test. In addition, the volume loss calibration procedure also helped in checking for leaks in the system. As for the calibration for pressure losses due to membrane resistance, the MPMT probe was inflated in the air at ground level using pressure increments of approximately 6.9-kPa. Again, volume measurements were taken at 30-seconds and 60-seconds after each pressure increment. The probe was inflated until it reached its maximum volume, which is about twice the initial volume of the inflatable portion of the probe. Figure 5-5 shows an example of a pressure expansion curve for determination of membrane resistance. It shows the pressure losses in order to inflate the

probe for a given volume, which means the pressure exerted in the interior of the membrane is completely utilized to inflate the probe. Therefore, the pressure does not exist on the exterior of the membrane nor the borehole wall. Thus for the pressure loss due to membrane resistance correction, the pressure loss at each given volume was subtracted from the MPMT pressure reading during a test. Another correction was made for hydrostatic pressure exerted on the MPMT probe due to the fluid column in the system above the test depth. The correction was done by measuring the difference in the elevation of the center of probe and top of fluid level in the volume readout panel; this difference was multiplied by the unit weight of the fluid to obtain the hydrostatic pressure correction. The correction obtained was then added to the MPMT pressure reading during testing. Figure 5-6 shows the picture of MPMT during calibration.

Table 5-1: Summary of MPMT Conducted in OUCC

Soil Bed ID	Number of Test Conducted	σ_n (kPa)	Test Depth (mm)
CCT2	1	103	267
	1	103	495
CCT3	1	103	267
	1	103	495
CCT4	1	103	267
	1	103	495
CCT5	1	103	267
	1	103	495
CCT6	1	103	267
	1	103	495
CCT8	1	103	267
	1	103	495
CCT9	1	103	267
	1	103	495
CCT10	1	103	267
	1	103	495
CCT11	4	103	267
	4	103	495
CCT19	4	103	216
CCT20	2	103	267
	2	103	495
CCT21	1	103	267
	1	103	495
CCT22	1	103	267
	1	103	495
CCT23	1	103	267
	1	103	495
CCT24	1	103	216
	2	152	216
	1	207	216
CCT25	1	103	216
	2	152	216
	1	207	216
CCT26	1	103	216
	2	152	216
	1	207	216
CCT27	1	103	216
	2	152	216
	1	207	216
CCT28	1	103	216
	2	152	216
	1	207	216
CCT29	1	103	216
	2	152	216
	1	207	216
CCT30	1	103	216
	2	152	216
	1	207	216

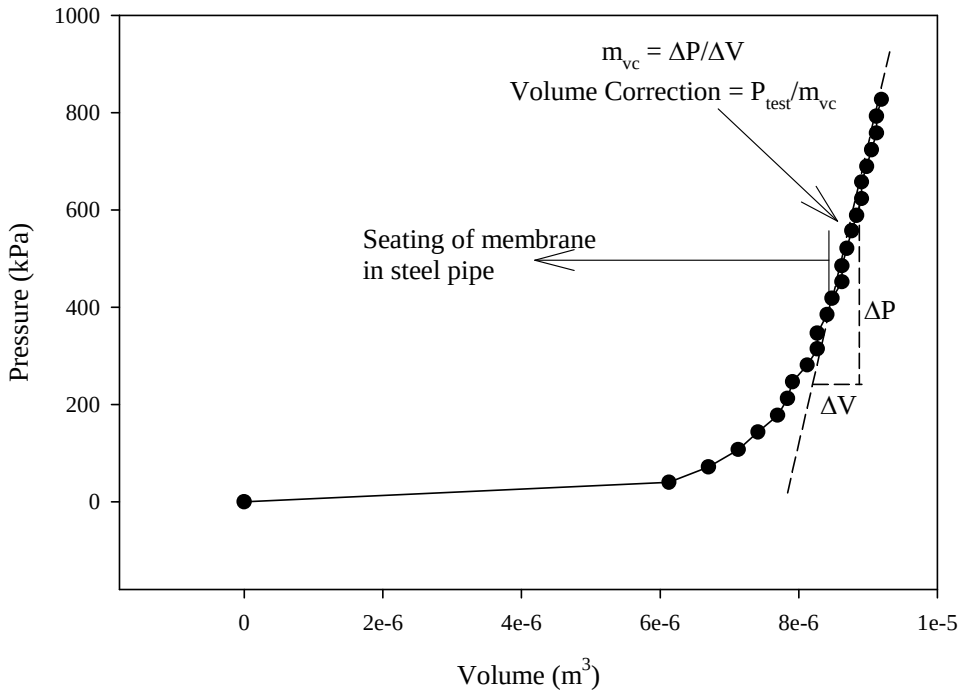

Figure 5-4: Calibration Curve for System Compressibility, Volume Losses (from MPMT Test ID 27_15B)

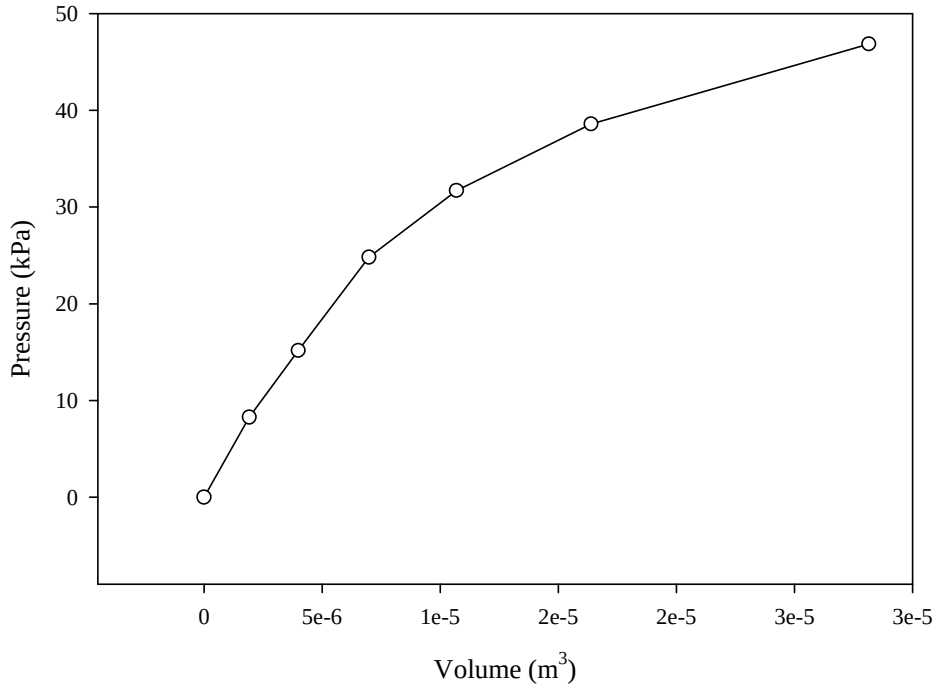

Figure 5-5: Calibration Curve for Membrane Resistance, Pressure Losses (from MPMT Test ID 27_15B

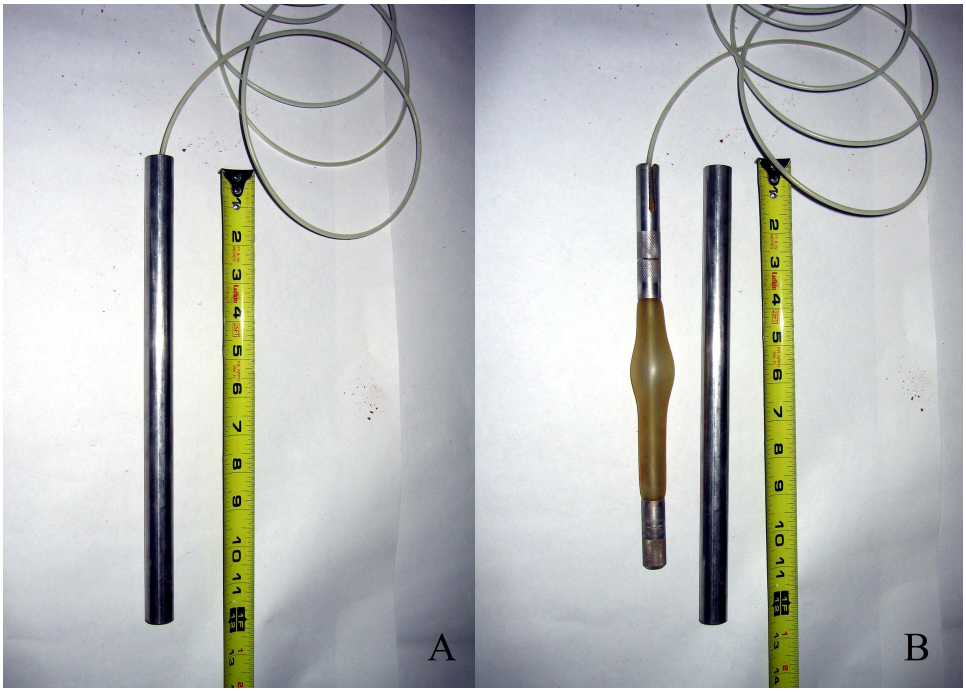

Figure 5-6: Picture of MPMT During Calibration for Volume (A) and Pressure (B) Losses

5.3 Miniature Cone Penetrometer Testing

The miniature cone penetrometer (MCPT) used in this research is only equipped to measure tip resistance with maximum load capacity of 8.9-kN. It is not equipped to measure sleeve friction and pore water pressure. For this initial work it was decided to focus on the tip resistance since the stress-strain fields around the sleeve are complex and difficult to model. Furthermore, accurate measurements of pore water pressure, such as with a piezocone, are not possible because of the large hydrodynamic time lag associated with unsaturated soil. As describe earlier in Section 4.3, the cone penetrometer used in this research is much smaller than the standard cone, so it was not necessary for the cone penetrometer to be pushed at the standard rate in this study since the dimension of the

cone penetrometer itself is not standard. The penetrometer was pushed into the soil bed at a rate of 0.5 cm/s as opposed to the standard rate of 2 cm/s. A slower rate was chosen to provide better control for the relatively short penetration in the chamber. The cable-extension position transducer was used to measure the depth of penetration.

The hydraulic system of the soil compactor (frame and piston) was used as the pushing system for the cone. Using a small connector, the end of the piston was connected to the pushing rods of the MCPT. Figure 5-7 shows a picture of the connecters. The female end sleeve was inserted into the piston rod and secured by a 25.4-mm (1-inch) bolt. The other end of the connector is a threaded stud that is connected to the pushing rods. The length of each pushing rod is 457-mm (18-inches).

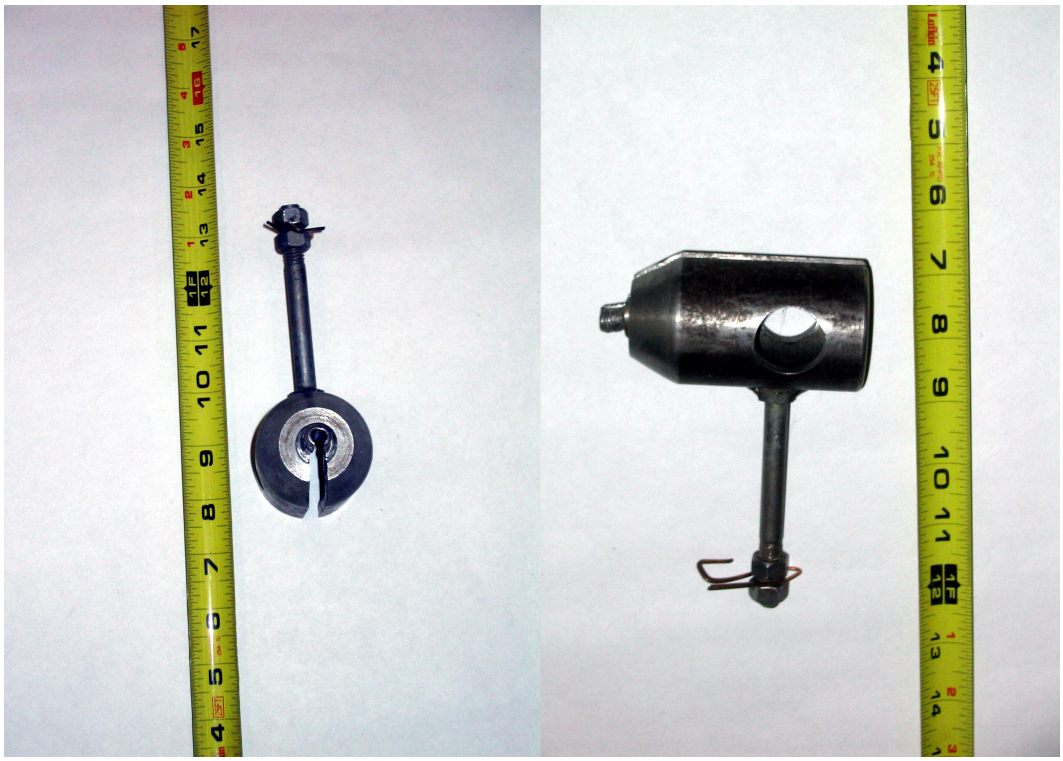

Figure 5-7: Picture of Connector Used for Connecting Piston to MCPT Pushing Rods

At the end of the soil bed compression stage (103.4-kPa), all the four plugs on the top cap and top plate were removed. Then the pushing frame was fixed to sit concentrically on top of the top cap and secured by eight 25.4-mm (1-inch) bolts (see Figure 5-8). During penetration, the penetration rate was monitored. The penetration rate of the cone can be regulated by a valve on the pushing piston. The rate of penetration was monitored and adjusted to 0.5-cm/sec as necessary. The outputs from the MCPT and cable-extension position transducer were recorded by a data acquisition system.

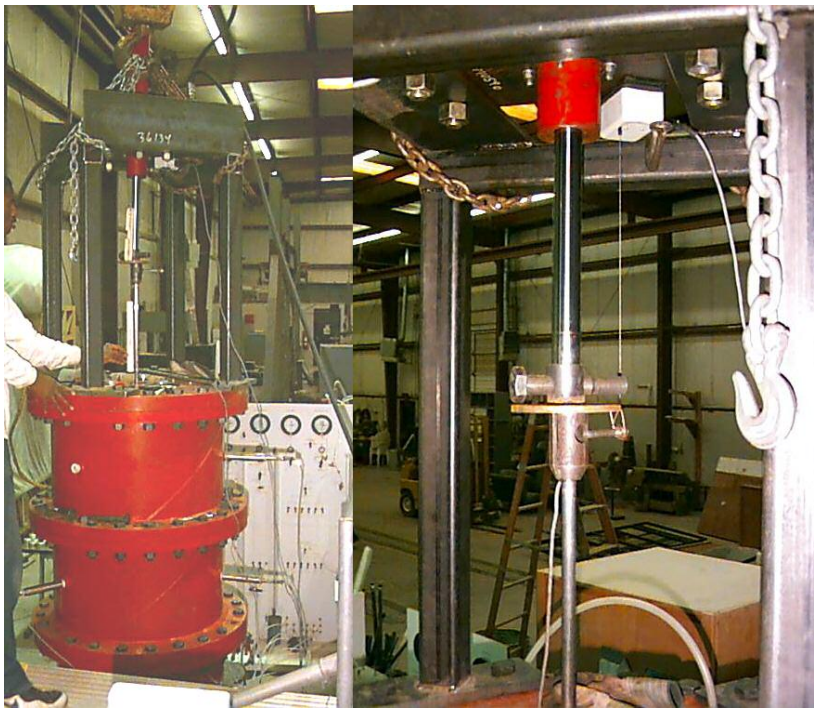

Figure 5-8: Pictures of the Pushing Frame for MCPT on top of OUCC

It is important to note that the height of the soil bed used for the miniature cone penetrometer testing (MCPT) was 1372-mm (56-inches) as opposed to the soil beds used for miniature pressuremeter testing (MPMT), which were 762-mm and 406-mm (30-inches and 16-inches). Higher soil beds were needed due to boundary effects at the top

and bottom of the soil beds. Four MCPTs were conducted in each soil bed, one (1) in the center of the soil bed cross section and three (3) others at 120^{o} apart from each other and 127-mm from the center. This allowed for investigation of edge boundary effects, uniformity of soil beds, and repeatability.

5.4 Test Bed Evaluation Methodology

Upon completion of the MPMT and MCPT testing, the soil beds were dissected and the uniformity of the soil beds were evaluated in terms of dry unit weight and water content distribution over depth.

5.4.1 Dry Unit Weight Assessment Technique

A small push tube was used for assessing the dry unit weight variation within soil beds by collecting small soil specimens from the soil beds. The sampling tube is a brass tube with 38.1-mm inner diameter, 76.2-mm height and 1.0-mm wall thickness and beveled on one end. The tube was pushed into the soil beds via an adapter, which was attached to the top of the tube. Figure 5-8 shows pictures of the sampler used in this research. A slight twist was applied before it was pulled out from the soil bed. The specimens recovered were then trimmed and weighted for unit weight determination. The water content of the specimens was determined in order to determine the dry unit weight. Specimens were collected at a minimum of 76.2-mm (3-inches) depth intervals. At each level, multiple specimens were collected in order to provide a clear picture of the uniformity of dry unit weight horizontally and vertically within each soil bed. This was verified by an alternative approach, which involved measuring the weight and moisture content of soil-water mixtures used for test bed preparation, dimensions of the test bed,

and the deformation of the test bed during compression under various net normal stresses (σ_n). The alternative approach is only capable to give an estimate of the overall average dry unit weight of the test bed at each stress level.

Figure 5-9: Pictures of Soil Sampler

5.4.2 Water Content Assessment Technique

The procedure used to investigate the uniformity of water content within each soil bed involved determining average water content within each plane from the specimens recovered for unit weight. The specimens were collected at minimum of 76.2-mm (3-inches) depth intervals around the locations where the MPMT probe was inflated or around the location where the MCPT was penetrated into the soil beds.

Chapter 6: Presentation and Discussion of Results

6.1 Soil Beds

The intent of Section 6.1 is to introduce and discuss the quality of the soil beds produced during calibration chamber testing in terms of dry unit weight (γ_d) and gravimetric water content (w) distribution. In this research, a total of 30 soil beds were been built. Table 6-1 shows a summary of the soil bed average properties, maximum compression stress applied and number and type of tests conducted on each soil bed. No test was conducted in the first soil bed (CCT1) as it was a trial bed. It allowed the author to be familiarized with the calibration chamber system and soil bed preparation method. It is also important to note that no tests were conducted in soil bed CCT7 and CCT16. The soil beds failed prior to testing. The target w for these two soil beds were between 13% and 14%. At higher w the soil failed to support its own weight.

It is observed that the average γ_d of the soil beds increased with w as shown in Figure 6-1. This did not occur in Tan's (2000) study with the bench scale soil beds. In the bench scale study the sample former used was relatively more rigid and there was also better control over the force applied during the static compaction. Another reason for obtaining higher γ_d as w increased was the limitation of the sample former and the compression forces provided by the pistons. As w decreased, more compaction energy was required to compact a given soil-water mixture to a specific γ_d. Since the magnitude of force provided by the compactor and chamber pistons were limited, the γ_d of the soil beds prepared was limited by the resulting maximum compaction stress that was applied to the soil bed. In addition, it was observed that the sample former tended to expand

radially during the compaction process especially at lower *w*. As stated earlier, at lower *w*, the compaction energy required to compact the soil-water mixture was relatively higher. Thus, more force was exerted on the sample former during compaction, which caused it to expand radially. Since only the layer thickness was measured during the compaction process, the expansion of the sample former led to more than expected layer volume, which then led to a reduction in the γ_d from its target values. The variation in γ_d was considered when analyzing the MPMT and MCPT results.

6.1.1 Soil Bed Compression

Test beds were isotropically compressed with 35-kPa stress increments. The maximum net normal stress (σ_n) experienced by each soil bed is listed in Table 6-1. Figure 6-2 shows a typical plot of volumetric strain of the soil bed as function of time (from CCT27). The plots for all the remaining soil beds can be found in Appendix A. It is observed that a major portion of the compression generally occurs within the first 30 minutes of a stress increment. Thus, in order to reduce the time required for the experimentation, later in the research (from CCT9 onwards) the first two loading stages were shortened to approximately one day as no tests were performed at the end of the first two stages. However, for the remaining stages, the soil beds were compressed for seven days followed by testing at the end of each stage.

6.1.2 Dry Unit Weight and Moisture Content Distribution

Upon completion of MPMT or MCPT testing, the net normal stress was released and the chamber was disassembled. The soil bed was then dissected for *w* and γ_d determination. Figure 6-3 shows the γ_d and *w* distribution within three soil beds (CCT2,

CCT10 and CCT27) as function of depth. Individual plots for γ_d and *w* distribution for all the soil beds are included in Appendix B. It is observed that the quality of the soil beds in terms of the distribution *w* and γ_d improved as the research progressed. For instance, Figure 6-3 shows that the *w* and γ_d distribution as function of depth within each soil bed became more uniform as the study progressed (e.g. CCT2 versus CCT27). This is because as the research progressed the author managed to overcome some of the difficulties in preparation of the soil beds and got more familiarized with the equipment and procedures involved. Generally, both the *w* and γ_d are reasonably consistent throughout the depth of each soil bed.

Table 6-1: Summary of Soil Bed Average Properties, Maximum Compression Stress Applied and Number and Type of Tests Conducted in Each Soil Bed

Soil Bed ID	Initial Height	Initial Diameter	Average [1]		$\sigma_{n,\,max}$	Test	
			γ_d	W			
	(mm)	(mm)	(kN/m^3)	(%)	(kPa)	MPMT	MCPT
CCT1	305	610	N/A	9.4	103	-	-
CCT2	762	610	13.7	10.6	103	2	-
CCT3	794	610	12.9	5.8	103	2	-
CCT4	762	610	14.3	12.7	103	2	-
CCT5	794	623	13.5	8.2	103	2	-
CCT6	794	630	14.1	9.0	103	2	-
CCT7	*	*	*	*	*	*	*
CCT8	762	630	12.8	7.4	103	2	-
CCT9	776	631	13.4	8.8	103	2	-
CCT10	781	630	13.5	8.1	103	2	-
CCT11	762	630	12.8	6.3	103	8	-
CCT12	1375	616	13.2	5.8	103	-	4
CCT13	1372	616	13.5	7.6	103	-	4
CCT14	1372	616	14.0	9.7	103	-	4
CCT15	1372	616	14.2	10.9	103	-	4
CCT16	*	*	*	*	*	*	*
CCT17	1372	616	13.6	8.6	103	-	4
CCT18	1372	616	13.2	6.8	103	-	4
CCT19	406	616	13.3	8.2	103	4	-
CCT20	762	616	13.2	8.1	103	4	-
CCT21	762	616	14.6	11.9	206	2	-
CCT22	762	616	13.3	5.6	206	2	-
CCT23	762	616	13.2	7.6	206	2	-
CCT24	406	610	13.4	6.7	206	4	-
CCT25	380	614	14.7	11.9	206	4	-
CCT26	404	614	13.6	8.8	206	4	-
CCT27	398	613	14.4	12.1	206	4	-
CCT28	420	606	13.1	6.9	206	4	-
CCT29	405	607	13.8	7.7	206	4	-
CCT30	406	611	14.7	12.0	206	4	-

* Soil bed failed prior to testing

[1] The average dry unit weight (γ_d) and average gravimetric water content (w) were obtained from the post mortem sampling process

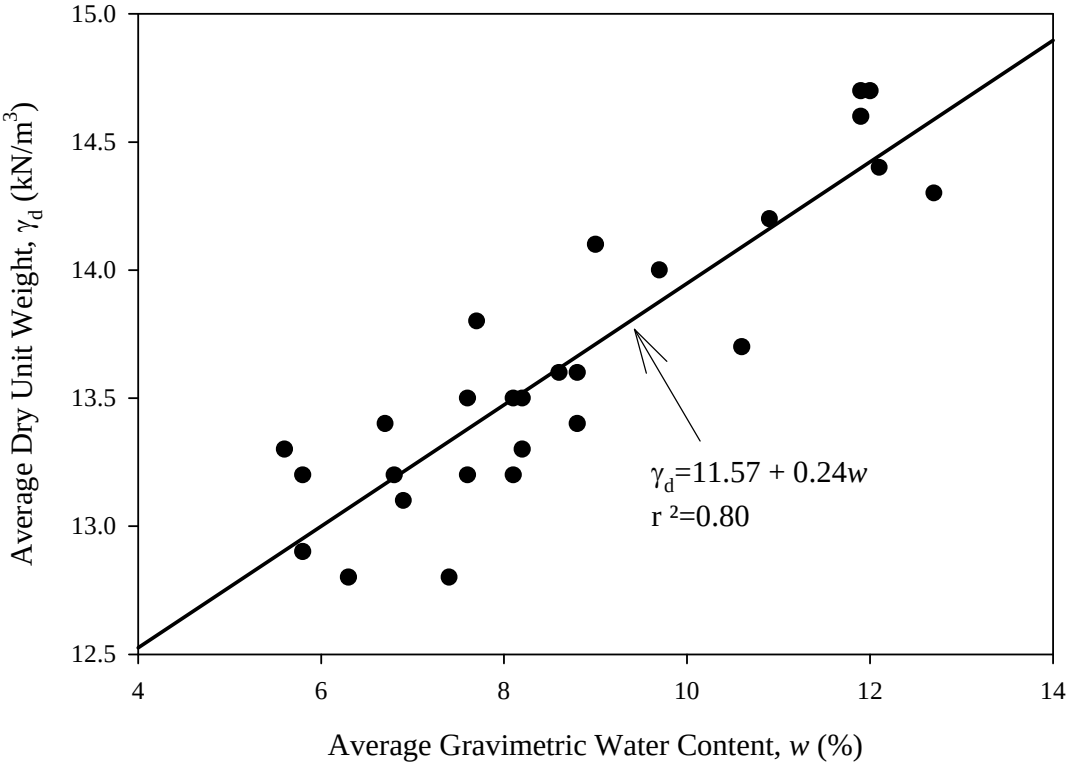

Figure 6-1: Average γ_d vs. *w* of Soil Beds

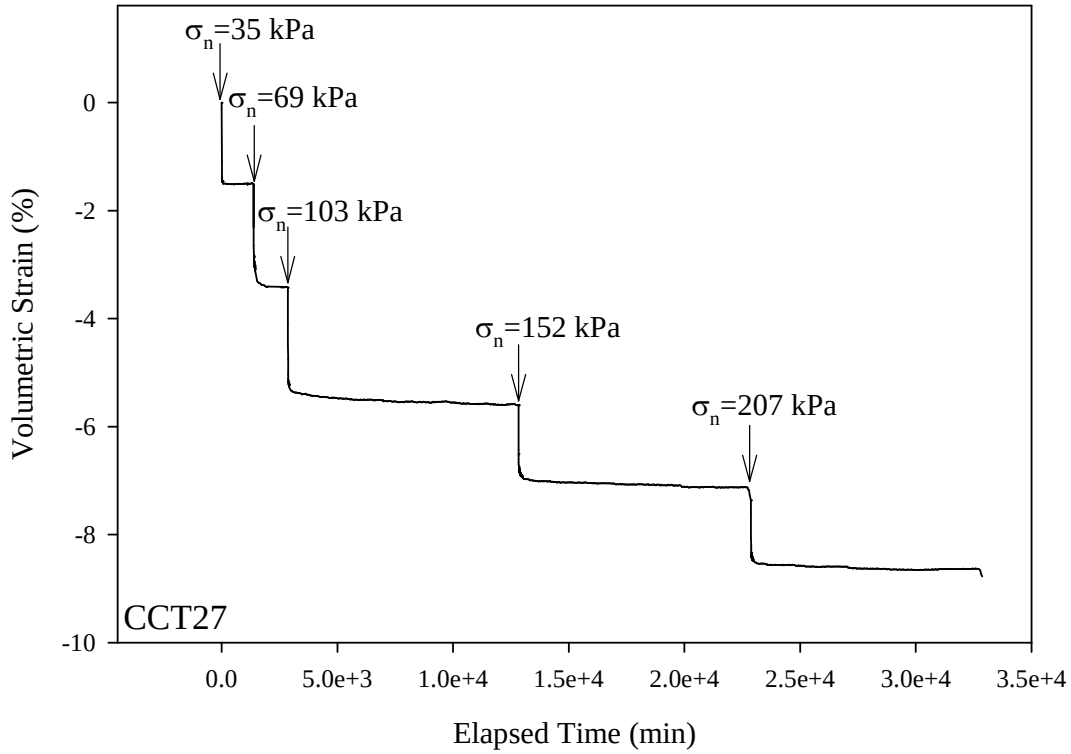

Figure 6-2: Volumetric Strain during Compression of Soil Bed (CCT27)

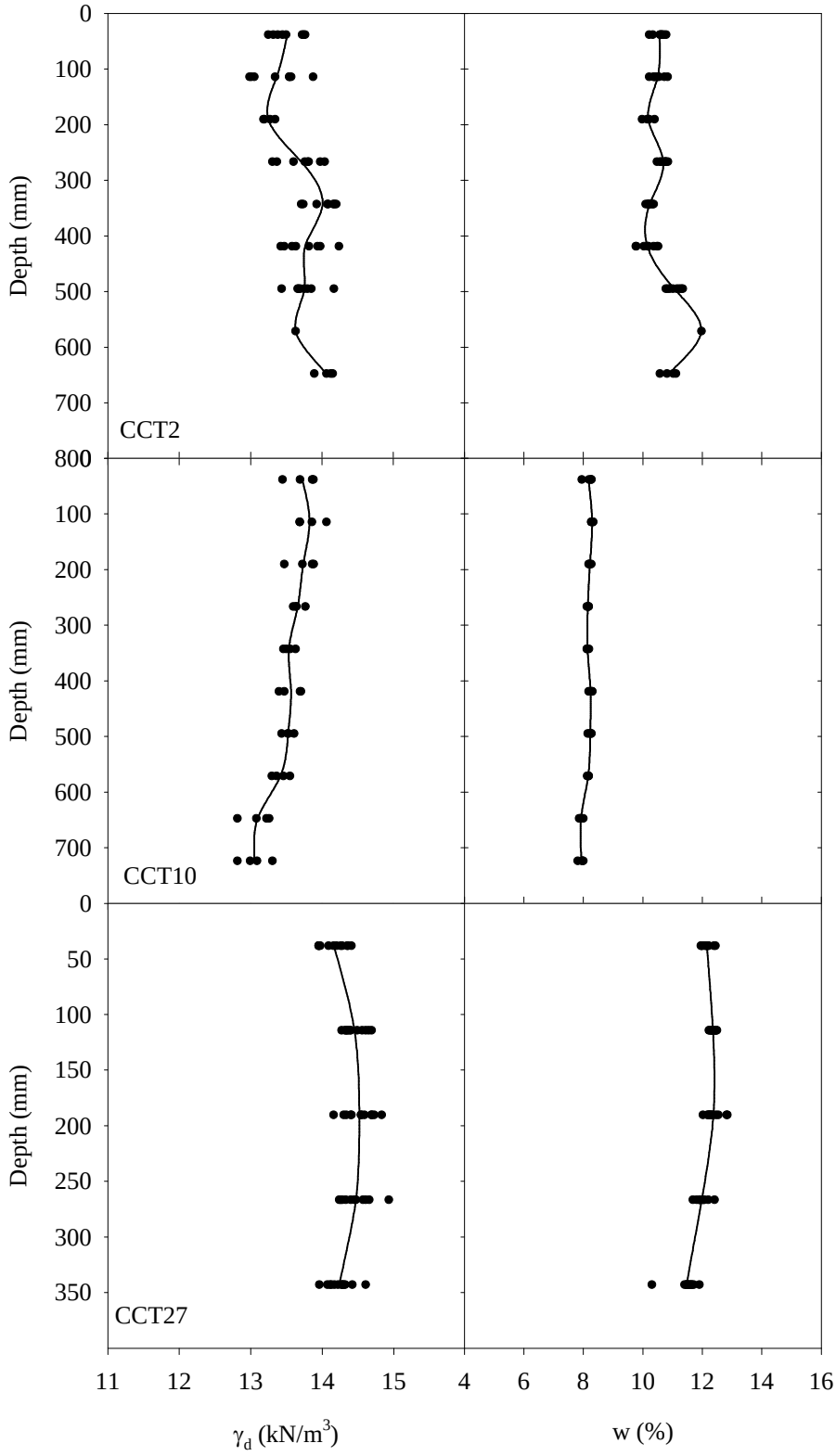

Figure 6-3: Gravimetric Moisture Content and Dry Unit Weight Sampling Results from CCT10, CCT19 and CCT27

6.2 Miniature Pressuremeter Testing

The pressuremeter testing is divided into two parts. The first part involved MPMT testing at constant net normal stress (σ_n) while varying the matric suction (ψ). Two chamber segments were used for this part of testing to accommodate the nominal soil bed height of 762 mm (30-inches). Fourteen soil beds were prepared for this part of testing (CCT2-CCT11, CCT20-CCT23). The results are discussed in Section 6.2.2. Later in the research the author was interested in the effects of net normal stress (σ_n) on the pressuremeter results in addition to the effects of matric suction (ψ). Seven chamber beds were prepared (CCT24-CCT30) for this part of testing and the results are discussed in Section 6.2.3. The soil beds used were shorter; the nominal height of the soil beds used was 406 mm (16-inches). A shorter soil bed was preferred because it can be reproduced more rapidly than the taller soil beds. However, there was concern with using a shorter soil bed, as the height-to-average diameter ratio of the soil bed was only 0.67, which could possibly result in boundary effects. The results from soil bed CCT19 and CCT20 were used to investigate the effects of using a shorter soil bed as discussed in Section 6.2.1. Section 6.2.1 also discusses the influence of the lateral soil bed boundary on MPMT results.

6.2.1 Boundary Effects

Much research has been done on potential influence of soil bed boundary conditions on results of pressuremeter testing in a calibration chamber. It is typically described in terms of ratios of soil bed diameter to the diameter of the pressuremeter probe. In this research the study of lateral boundary effects was carried out by conducting

four MPMTs within the same plane in the soil bed. One in the center of the cross section of the soil bed and three others spaced 120^o apart and 127 mm (5 inches) from the center. This allowed for investigation of the influence of the lateral boundary on MPMT results. Figure 6-4 shows the layout of the MPMT test locations.

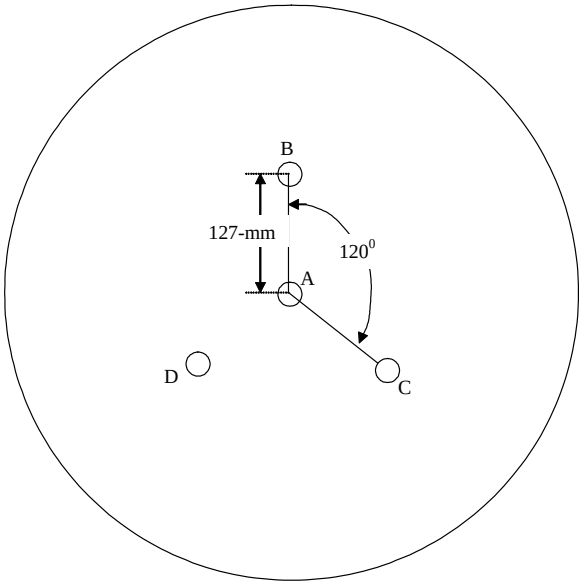

Figure 6-4: Layout of MPMT Test Locations on a Cross Section of the Soil Bed

Table 6-2 shows the summary of MPMT results from CCT11 along with the average *w* and γ_d of the soil samples recovered around the locations where the MPMT probe was inflated. A total of eight tests were conducted in CCT11. The σ_n applied to the soil bed was 103 kPa. It is observed that the γ_d and *w* around all eight test locations in CCT11 stay relatively consistent. The limit pressure (P_L) varies from 485 kPa to 580 kPa with an average of 518 kPa. The standard deviation is 31 kPa and coefficient of variation (C.O.V) is 5.9%. Since the C.O.V value is relatively small (<10%), it indicates that the dispersion of P_L about the average or expected value is relatively small (Mendenhall and

Sincich 2003). Thus, it appears that the lateral boundary effects on P_L values are insignificant.

Table 6-2: Summary of MPMT Results from CCT11

Test ID	Test Depth [1] (mm)	Average γ_d (kN/m^3)	Average *w* (%)	P_L (kPa)
11A-1	267	12.9	6.1	502
11A-2	495	12.8	5.9	532
11C-1	267	13.1	6.0	485
11C-2	495	12.9	6.0	523
11B-1	267	12.7	6.1	487
11B-2	495	12.7	5.9	580
11D-1	267	12.8	6.2	528
11D-2	495	12.6	5.9	506
Average (kPa)				518
Standard Deviation (kPa)				31
Coefficient of Variance (%)				5.9

[1] Depth is measured from top of soil bed to midpoint of inflated portion of probe

As stated earlier there was concern in using a shorter test bed for some of the MPMT testing. Thus, two soil beds with similar properties in terms of γ_d and *w* but different height were prepared. Both soil beds were compressed up to 103 kPa. Four MPMT tests were conducted in each soil bed. The MPMT tests results are summarized in Table 6-3. It is observed that the mean difference in P_L is about -60 kPa. Two t-tests for equality of means were conducted on the data set: 1) assuming the variances are equal, and 2) without assuming the variances are equal. The 99% confidence intervals of lower and upper differences from both of the analyses are -126 kPa and 6 kPa, respectively. The mean difference of P_L is within this range. Thus, statistically there is insufficient evidence (at α of 0.01) of difference between the true mean of P_L from both test beds (tall versus

short soil beds). If there was some effect in switching from a taller soil bed to a shorter soil bed, the mean difference in P_L would have fallen outside the upper and lower limit of the 99% confidence intervals. Therefore, the effect of switching from a taller soil bed to a shorter soil bed on PMT results is considered relatively insignificant.

Table 6-3: MPMT Results from CCT19 and CCT20

Test Bed ID	Test ID	Test Depth (mm)	Height of Soil Bed (mm)	$\gamma_{d,\,avg.}$ (kN/m^3)	$w_{avg.}$ (%)	P_L (kPa)	$P_{L,avg.}$ (kPa)
CCT19	19A	216	406	13.4	8.3	406	413
CCT19	19B	216	406	13.3	8.3	413	
CCT19	19C	216	406	13.4	8.2	448	
CCT19	19D	216	406	13.4	8.3	386	
CCT20	20A-1	267	762	13.3	8.3	468	474
CCT20	20A-2	495	762	13.5	8.2	501	
CCT20	20B-1	267	762	13.3	8.3	443	
CCT20	20B-2	495	762	13.3	8.2	482	

6.2.2 Test Conducted at a Net Normal Stress of 103 kPa

Table 6-4 shows the summary of the MPMT test results where all the soil beds were only compressed up to 103 kPa at various ψ. Presented along with the MPMT test data (Limit Pressure (P_L), Pressuremeter Modulus (E_P) and Unload-Reload Modulus (E_R)) are the properties of the soil bed (i.e. gravimetric water content (w), dry unit weight (γ_d) and matric suction (ψ)) around the inflated portion of the MPMT probe. It is also important to note that there were two soil processing methods involved. The soil for test beds CCT1 to CCT 10 were pulverized by a crusher, while the soil for the remaining soil beds (CCT 11 – CCT23) were pulverized by a soil grinder.

Table 6-4: Summary of MPMT Results from Soil Beds with $\sigma_{n,\,max}$ of 103 kPa

Test ID	P_L (kPa)	E_P (kPa)	E_R (kPa)	w (%)	γ_d (kN/m^3)	ψ (kPa)	SPM[1]
2-1	833	16009	30400	10.1	13.7	20	Crusher
2-2	765	14847	42962	11.0	13.7	17	Crusher
3-1	1308	12919	18364	5.9	13.0	63	Crusher
3-2	1578	20202	31058	5.4	13.3	74	Crusher
4-1	635	7175	9417	12.5	14.2	13	Crusher
4-2	606	7140	10674	12.8	14.3	13	Crusher
5-1	782	10317	12100	7.8	13.5	35	Crusher
5-2	793	15966	31324	8.1	13.5	32	Crusher
6-1	1024	28950	92081	8.7	13.9	28	Crusher
6-2	978	25457	262927	8.6	14.3	29	Crusher
8-1	525	9798	15554	7.3	12.8	40	Crusher
8-2	549	9564	13810	7.2	12.8	41	Crusher
9-1	774	16128	23054	8.8	13.5	28	Crusher
9-2	741	14478	23368	8.7	13.5	28	Crusher
10-1	863	15704	35418	8.0	13.5	33	Crusher
10-2	776	18797	44293	8.2	13.5	32	Crusher
11A-1	502	10847	23555	6.1	12.9	58	Grinder
11A-2	532	14764	41269	5.9	12.8	62	Grinder
11C-1	485	7798	17243	6.0	13.1	60	Grinder
11C-2	523	12116	24108	6.0	12.9	60	Grinder
11B-1	487	11663	26270	6.1	12.7	59	Grinder
11B-2	580	10930	23992	5.9	12.7	63	Grinder
11D-1	528	10870	20299	6.2	12.8	56	Grinder
11D-2	506	9453	18547	5.9	12.6	63	Grinder
19A	406	9112	19150	8.3	13.4	31	Grinder
19B	413	9123	18925	8.3	13.3	31	Grinder
19C	448	17268	32234	8.2	13.4	32	Grinder
19D	386	8383	16490	8.3	13.4	30	Grinder
20A-1	468	6308	11508	8.3	13.3	31	Grinder
20A-2	501	7454	13086	8.2	13.5	32	Grinder
20B-1	443	5559	9501	8.3	13.3	31	Grinder
20B-2	482	8606	10252	8.2	13.3	32	Grinder
21A-1	429	7935	18408	12.1	14.2	14	Grinder
21A-2	466	8720	21978	11.9	14.3	15	Grinder
22A-1	547	14485	50569	5.4	12.9	74	Grinder
22A-2	629	23271	38458	5.6	13.2	70	Grinder
23A-1	606	6331	9606	7.6	13.0	37	Grinder
23A-2	658	7448	13465	7.8	12.9	35	Grinder

[1] Soil Processing Method

Figure 6-5 depicts typical pressuremeter test results from one of the soil beds. Individual pressure expansion curves for all the MPMT tests are included in Appendix C. The MPMT pressure expansion curve presented in Figure 6-5 is expressed in terms of corrected pressure and corrected volume of fluid injected into the probe. It is observed that very small pressure increments (approximately between 14 to 21 kPa) were applied initially until point “A” as depicted in the Figure 6-5. Point “A” can be interpreted as the point at which the membrane had made full contact with the borehole wall and recompression of the disturbed soil around the borehole had taken place. It is typically considered as the point where the soil is brought back to its original condition prior to drilling the borehole (Baguelin et al. 1978). Beyond point “A”, the pressure increment used was approximately 35 kPa. Between point “A” and point “B” is considered the elastic range for the soil, where the creep volume for each pressure increment was relatively constant. At point “B” the soil yields and starts to transform into the plastic range. In this study, typically one or two pressure increments were applied to the MPMT beyond the beginning of the plastic range (until point “C” as in Figure 6-5) before being reduced to point “D” for an unload-reload cycle. The pressure was maintained for approximately 10 minutes at point “D” prior to reloading. The pressure was then increased in approximately 35-kPa increments from point “D” until the MPMT probe reached its maximum allowable volume or maximum allowable injected volume (point “E” as shown in Figure 6-5).

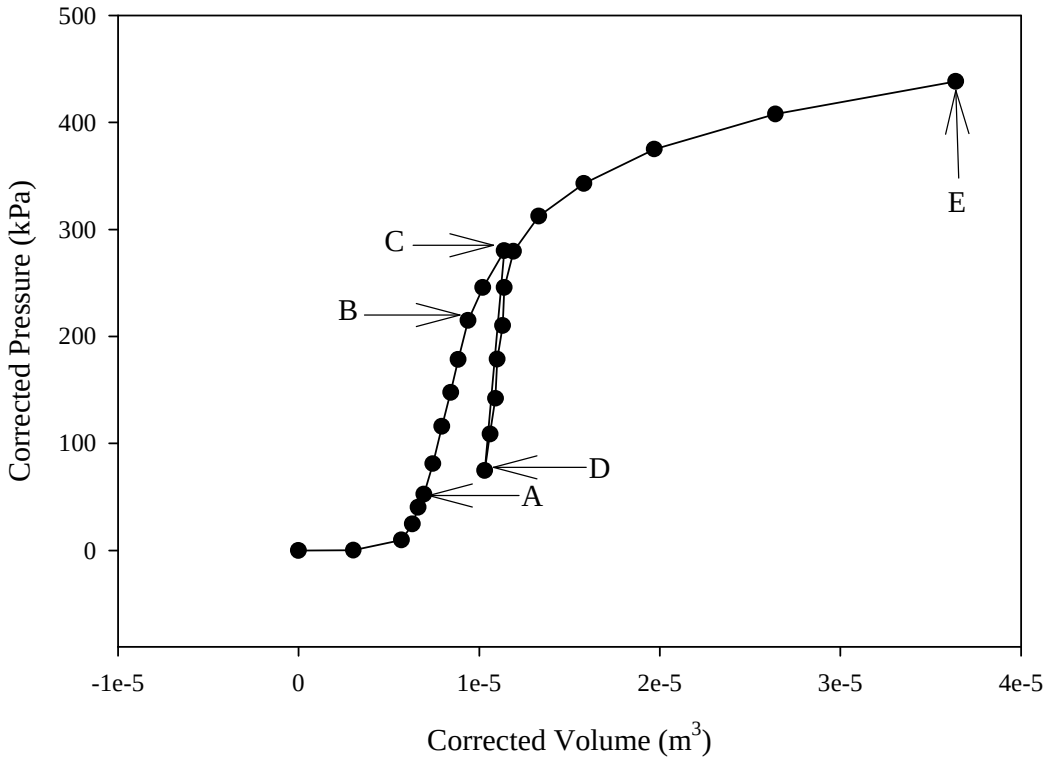

Figure 6-5: MPMT Pressure Expansion Curve (from MPMT Test ID 27_15B)

As discussed earlier in Section 6.1 it was observed that the γ_d tended to be higher in soil beds with lower ψ, and vice versa. Therefore, the variation in γ_d was taken into account in analyzing the MPMT results. In order to include the effects of γ_d into the data analysis, the data was further divided into groups based on the range of γ_d of the soil beds where the test was conducted as shown in Figures 6-6, 6-7 and 6-8. Figure 6-6 show plots of $P_{L,}$ E_P and E_R versus ψ for tests conducted at σ_n of 103 kPa on soil beds processed by crusher and grinder. The "solid" symbols represent tests conducted in soil beds processed by crusher while the "open" symbols represent tests conducted in soil beds processed by grinder. The shape of the symbols represents the γ_d range of the soil beds where the test was conducted. Figure 6-6 shows that ψ, γ_d and soil processing methods have a

significant influence on P_L. It is observed that generally P_L is relatively insensitive to ψ at γ_d less than 13.5 kN/m^3 and P_L tends to increases with increasing ψ for γ_d greater than 13.5 kN/m^3 regardless of the soil processing methods. Another prominent observation is for a given range of γ_d, the P_L from the soil beds processed by crusher tends to be higher than those processed by grinder. Thus, it is obvious that soil processing methods for the soil beds have a significant influence on the MPMT results. For this reason the test data for MPMT conducted at σ_n of 103 kPa was divided into 2 groups based on the soil processing methods used. The plots for MPMT results for tests conducted in soil beds prepared by crusher and grinder are presented in Figures 6-7 and 6-8 respectively.

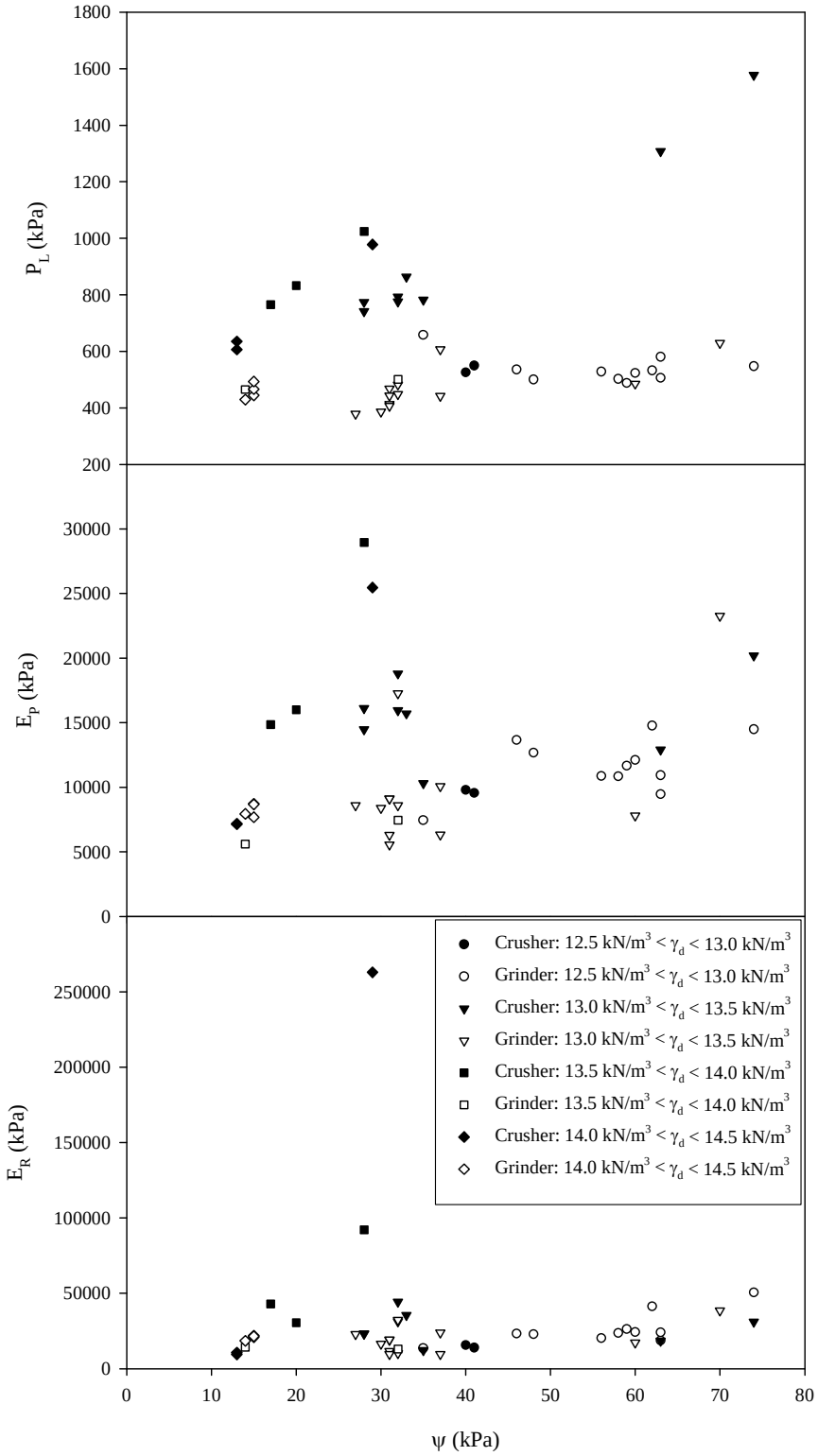

Figure 6-6: P_L, E_P and E_R vs. ψ at σ_n of 103 kPa for Soil Beds Processed by Crusher and Grinder

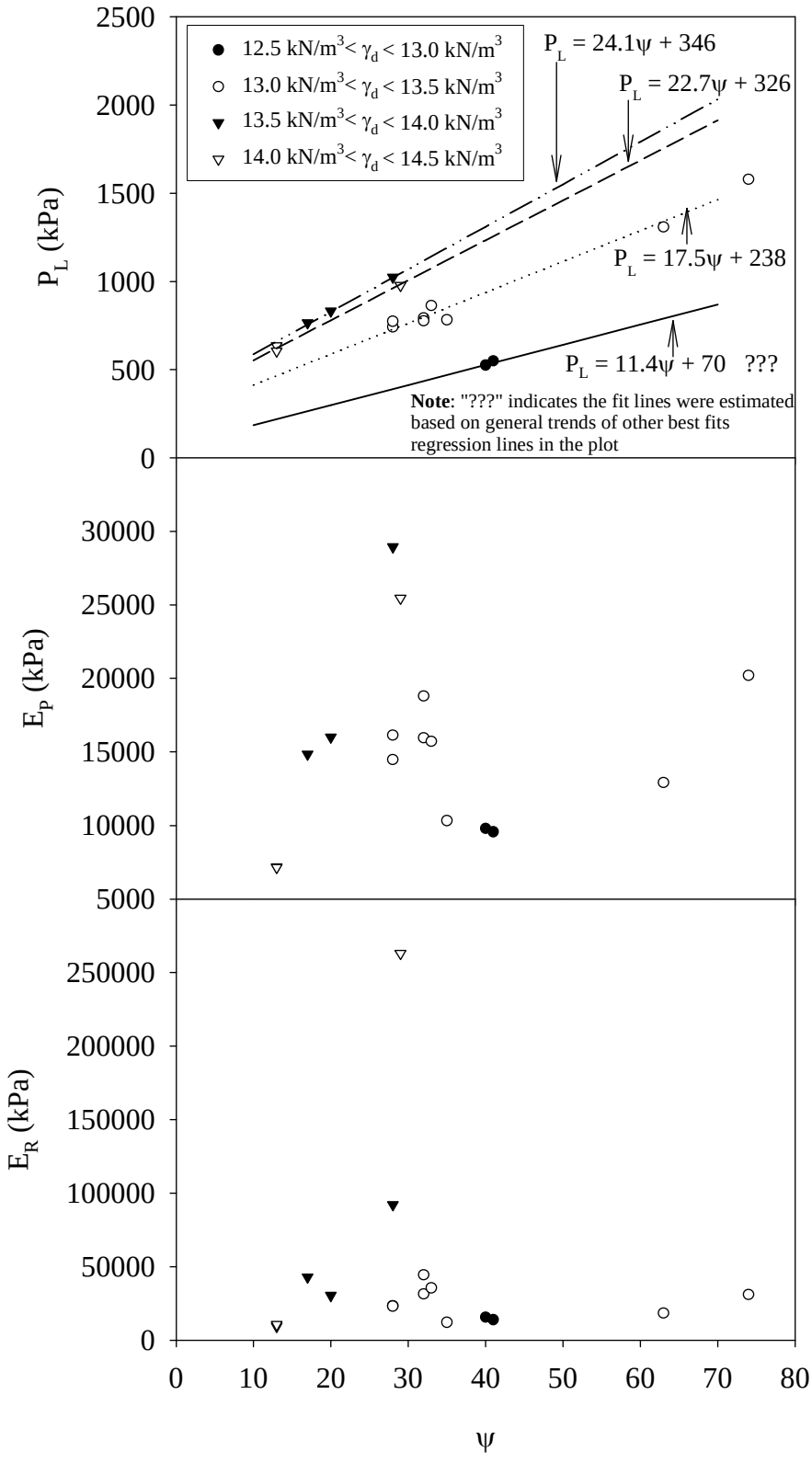

Figure 6-7: P_L, E_P and E_R vs. ψ at σ_n of 103 kPa for Soil Beds Processed by Crusher

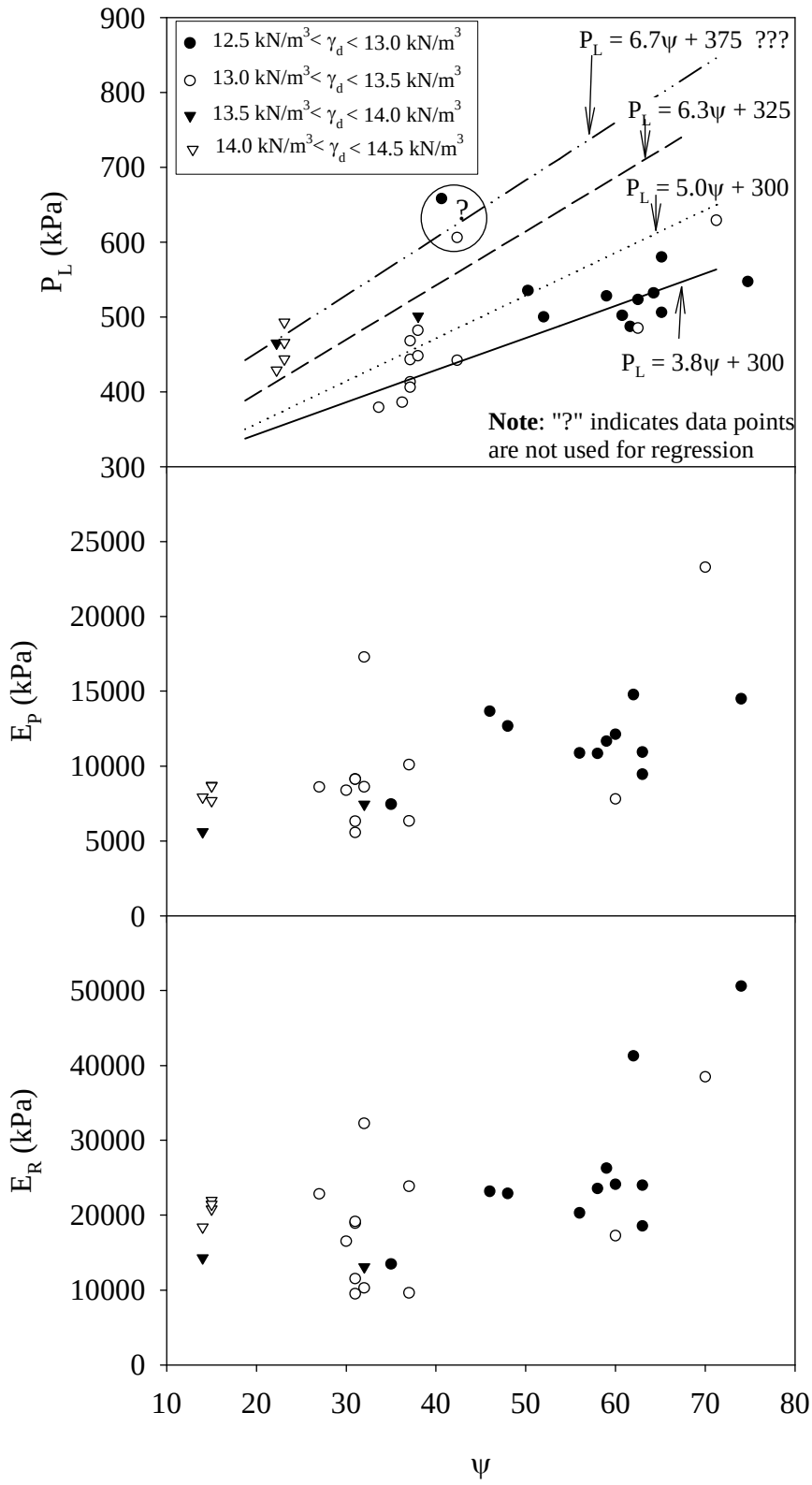

Figure 6-8: P_L, E_P and E_R vs. ψ at σ_n of 103 kPa for Soil Beds Processed by Grinder

Figures 6-7 and 6-8 show that generally for a given range of γ_d, P_L increased with increasing ψ. This observation is consistent with the unsaturated soil shear strength theory where the shear strength of unsaturated soil increases with increasing suction. The plots also show that P_L increases with increasing γ_d for a given ψ. Again, this observation is consistent with the soil mechanics theory where at higher γ_d the contact area between soil particles increases, thus increasing the shearing resistance. Best fit regression lines were presented in the P_L versus ψ plots in both Figures 6-7 and 6-8 where possible. Due to limited amount of data, some of the best fit lines were estimated based on general trends of other best fits regression lines in the plot. These line are presented with a "???" at the end of the equation in the plots. The plots suggest that generally the slopes of the P_L versus ψ curves increase with increasing γ_d and the importance of ψ increases as γ_d increases. This is consistent with theoretical expectations and can be explained by using the capillary model for spherical particles as discussed in the following paragraphs.

Figure 6-9 shows a physical model of the capillary menisci for two smooth spherical particles under unsaturated conditions. The assumptions made for this simple model are: 1) water only exists in vertical particle contacts, 2) the spherical particles are weightless, 3) the gravitational force of the water is negligible, and 4) contact angle between the meniscus and spherical particle is zero. The pressure difference across the three dimensional membrane can be represented by the Equation 6-1.

$$(u_a - u_w) = T_s\left(\frac{1}{R_{m1}} + \frac{1}{R_{m2}}\right) \qquad \text{(Eq. 6-1)}$$

where:

(u_a-u_w) = ψ = matric suction,

T_s = surface tension of contractile skin,

R_{m1} and R_{m2} = radius of curvature of meniscus in 2 orthogonal planes and are defined as:

$$R_{m1} = \frac{R_p + z_0}{\cos\beta} - R_p, \quad \text{(Eq. 6-2)}$$

$$R_{m2} = (R_p + R_{m1})\sin\beta - R_{m1}, \quad \text{(Eq. 6-3)}$$

R_p = radius of spherical particle,

$r = 2\,R_p \cos(90-\beta)$, (Eq. 6-4)

$z = R_{m1}\cos(\beta)$, and (Eq. 6-5)

z_0 = half of the vertical distance between 2 spherical particles.

Therefore, β can be back calculated for a given (u_a-u_w) and z_0 by assuming T_s and R_p values, In the analysis for this study, T_s was assumed to be 73-mN/m^2, which is a reasonable value for pure water at a temperature between 15 to 20^{o}C (Fredlund and Rahardjo 1993) and R_P is assumed to be 0.01 mm corresponding to the d_{20} of the soil used in this study. With these assumptions, the interfacial area between the meniscus water can also be determined for a given (u_a-u_w) and z_0. Figure 6-10 shows the plots of interfacial area and interfacial force due to ψ as function of ψ at various z_0. Larger z_0 values represent greater distance between the spherical particles, which can also be interpreted as lower γ_d. The γ_d of the spherical particles arrangements can be estimated as follows:

$$\gamma_d = \frac{W_{spheres}}{V_{total}} \quad \text{(Eq. 6-6)}$$

where:

$$W_{spheres} = V_{spheres}\,\gamma_{spheres}, \quad \text{(Eq. 6-7)}$$

$\gamma_{spheres}$ = $G_s \gamma_{water}$, (Eq. 6-8)

γ_{water} = unit weight of water (assumed to be equal to 9.81 kN/m^3),

G_s = specific gravity of the sphere = specific gravity of Minco Silt = 2.68,

$$V_{spheres} = 2\left(\frac{4}{3}\pi R_p^3\right), \text{ and} \quad \text{(Eq. 6-9)}$$

$$V_{total} = (2R_P)^2(4R_P + 4z_0) \quad \text{(Eq. 6-10)}$$

In comparing Figure 6-10 to the trends observed in Figures 6-7 and 6-8, the following rationale is applied.

1. As the γ_d in soil decreases, the size of the capillary pores increases; thus, water must recede further into the particle contacts (or pores) for a given matric suction. It follows that the interfacial area between the water and solid phases will decrease for a given value of matric suction as γ_d decreases. In the simple model described above, the increase of the interparticle spacing, $2z_0$ is used to model the effect of decreasing γ_d and increasing pore size.
2. The shear strength of soil is directly a function of interparticle force. Limit pressure (P_L) is measure of soil shear strength and thus, is directly a function of interparticle force. Thus, the variation of the interparticle force with matric suction should mimic the trend of P_L with matric suction.

It is observed that at low ψ, the inter-particle force due to matric suction converges for the range of z_0 (or γ_d) used in the analysis as shown in Figure 6-10. The same trend is observed in Figures 6-7 and 6-8 for P_L versus ψ plots where P_L tends to converge at low ψ for γ_d ranging between 12.5 kN/m^3 to 14.5 kN/m^3. Figure 6-10 also shows that the inter-particle force due to matric suction tends to increase with increasing

ψ. However, at low γ_d the inter-particle force due to matric suction will reach a peak value and then decrease slightly as ψ continues to increase. As γ_d increases, this trend becomes less apparent. Instead of decreasing, the inter-particle force due to matric suction continues to increase and plateau with increasing ψ, for the range of ψ investigated. This is mainly due to the effect of change in interfacial area, which decreases more rapidly at low γ_d for a given increase in ψ. Therefore, based on these observations it is speculated that the importance of ψ on the strength of unsaturated soil increases with increasing γ_d, which is consistent with the observations made in Figures 6-7 and 6-8 for P_L. It also shows that at lower γ_d, the role of ψ in strength of unsaturated soil is relatively minor which, again supports the significance of observations made in Figures 6-7 and 6-8 for P_L. Nevertheless, it is important to note that this observation is only based on a limited amount of data with ψ ranging between 15 to 75 kPa and γ_d ranging between 12.5 and 14.5 kN/m^3.

As for E_P and E_R there is a slight trend that E_P and E_R increase with increasing ψ and are relatively insensitive to variation of γ_d. This might be due to the fact that while the determination of P_L involves large strain (plastic) behavior of soil, the moduli (e.g. E_P and $E_{R)}$ involve primarily small strain (elastic) behavior of soil. It is speculated that for small strain behavior the effect of variation in γ_d is not as important compared to large strain behavior. All these observations were later analyzed by statistical analysis as discussed in Section 6.4.

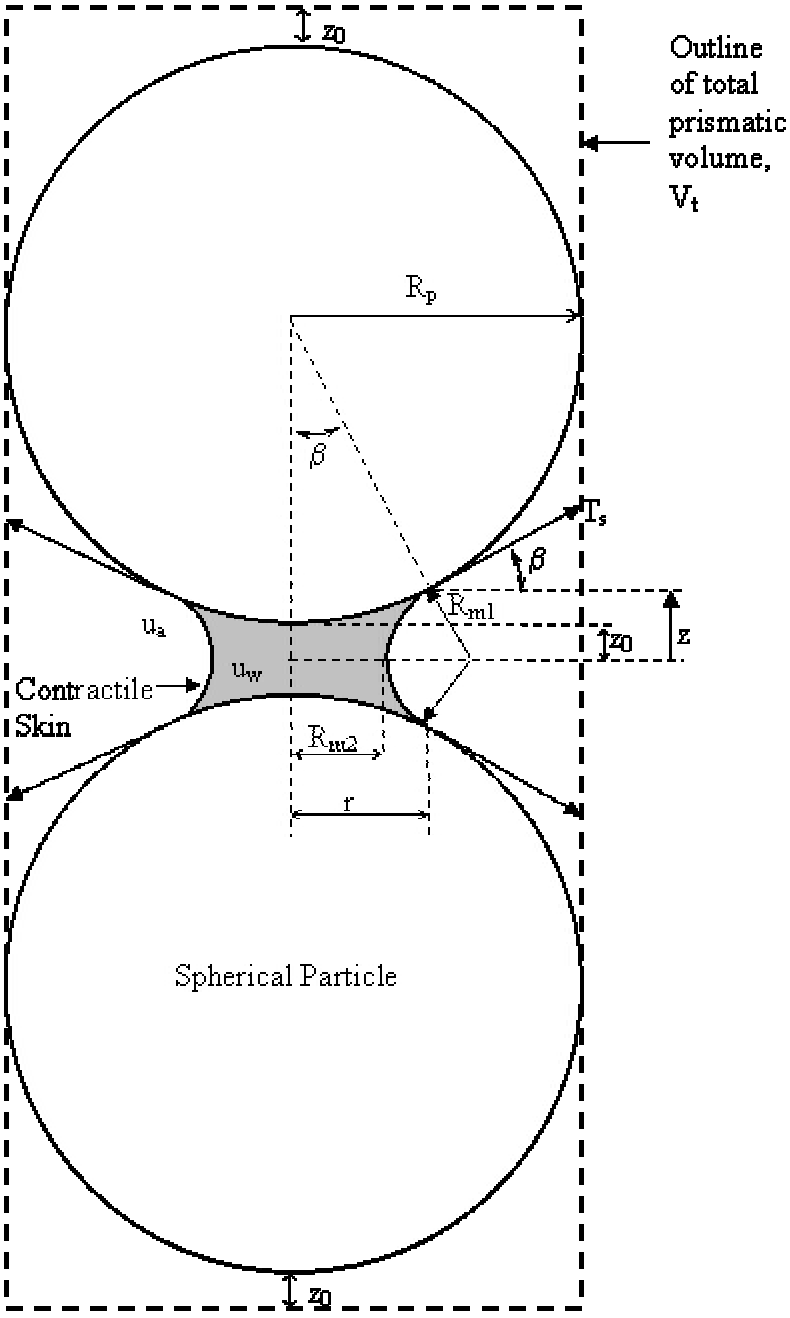

Figure 6-9: Schematic Diagram of 3-D Capillary Model for Spherical Particles

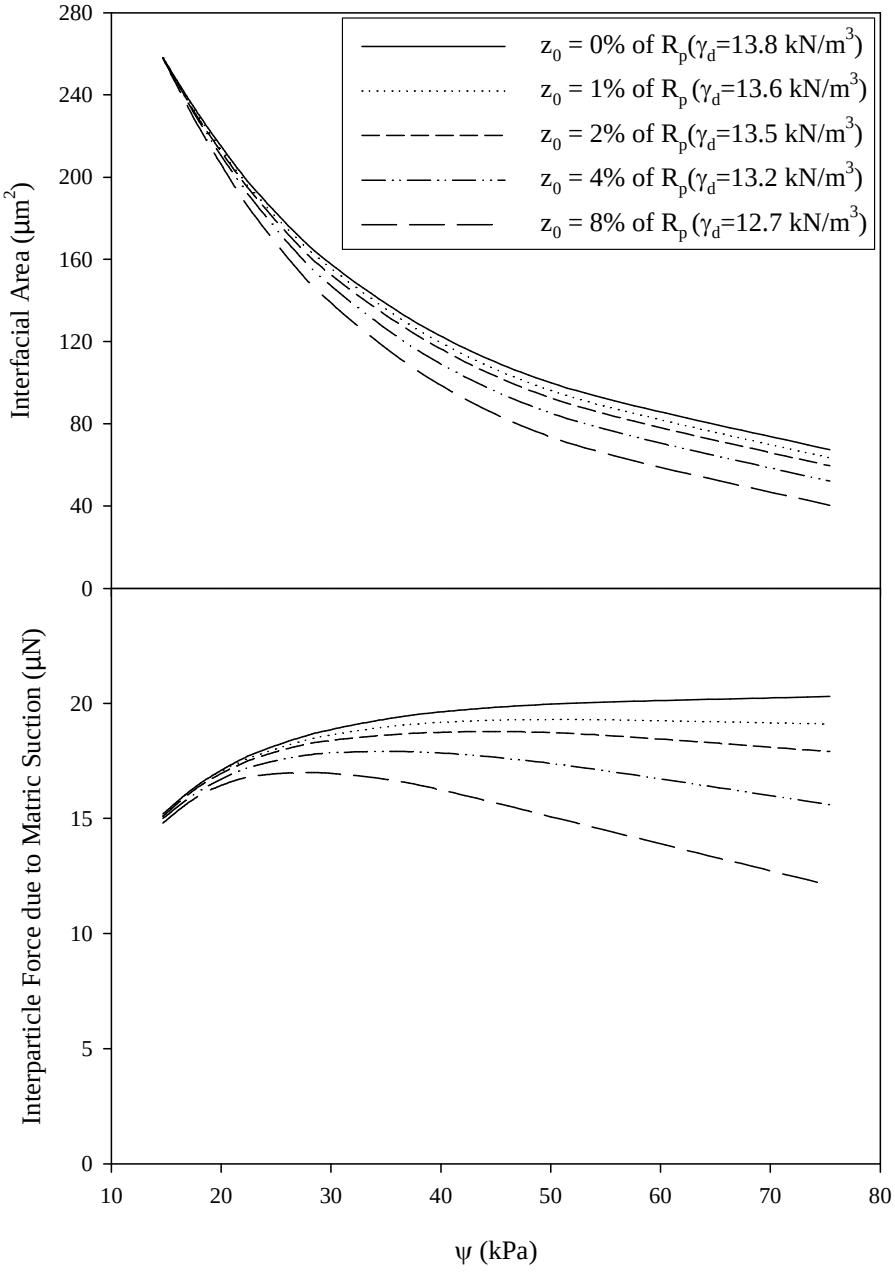

Figure 6-10: Back-Calculated Interfacial Area and Interfacial Forces due to Matric Suction from Capillary Model for Spherical Particles

6.2.3 Test Conducted at Various Net Normal Stress

Seven soil beds were prepared for MPMT testing at three different σ_n (i.e. 103, 152 and 207 kPa). Table 6-5 shows the summary of the MPMT test results. Presented along with the MPMT test data (P_L, E_P and E_R) are the properties of the soil bed (i.e. *w*, γ_d and ψ). The *w* and γ_d were determined from the soil specimens collected around the inflated portion of the MPMT probe. The ψ is determined by using the average *w* of soil samples around a test location and the soil water characteristic curve. Only one soil processing method was involved in this part of testing. All the soil beds for this part of testing (CCT24 to CCT 30) were prepared with soil that was first pulverized using the soil grinder.

Figure 6-11 shows P_L, E_P and E_R as a function of ψ at various σ_n. The corresponding γ_d of the soil beds are also shown in the plot. For ψ greater than 20 kPa, it is evident that ψ has a strong influence on P_L, where P_L increases with increasing ψ for a given σ_n. The influence of γ_d on P_L can be observed in Figure 6-11; for a given σ_n, at ψ greater than 20 kPa, P_L increases with increasing ψ and at ψ less than 20 kPa, the P_L does not fit the same trend. However, it is observed that generally the γ_d for ψ less than 20 kPa is considerably higher than γ_d for ψ greater than 20 kPa. Therefore, it is speculated that relatively higher P_L values at ψ less than 20 kPa are probably due to the variation in γ_d. The empirical equations for P_L as a function of ψ as presented in Figure 6-11 are based on data for ψ greater than 20 kPa, where generally γ_d falls around 13.25 ± 0.50 kN/m^3. It is expected that the same equations are also applicable for ψ ranges between 10 and 20 kPa for soil beds with γ_d of 13.25 ± 0.50 kN/m^3. Different empirical equations that

correlate P_L and ψ are expected for γ_d greater than 13.75 kN/m^3. Due to the limited amount of data, no empirical equations that correlate P_L and ψ at γ_d greater than 13.75 kN/m^3 were developed. As for E_P and E_R it is observed that E_P and E_R generally increase with increasing ψ for a given σ_n. It is also observed that E_P and E_R are relatively insensitive to variation of γ_d. Best fit regression lines were also presented in the E_P and E_R versus ψ plots in Figure 6-11.

Although the influence of σ_n is observable in Figure 6-11 where P_L, E_P and E_R increase with increasing σ_n, it is clearer when presented as in Figures 6-12, 6-13 and 6-14 where P_L, E_P and E_R are plotted against σ_n. The data points are grouped in terms of the range of γ_d and ψ. Although the amount of data is limited, it is observed that generally for a given range of γ_d the P_L, E_P and E_R increase with σ_n. This is consistent with unsaturated soil mechanics theory where the strength and modulus of unsaturated soil increases as σ_n increases. Based on the data set depicted in Figures 6-11, 6-12, 6-13, and 6-14 the following observations are noted:

a) There are fairly strong relationships between P_L, E_P, E_R and ψ for a given σ_n and γ_d.

b) There are fairly strong relationships between P_L, E_P, E_R and σ_n for a given ψ and γ_d.

These observations were further analyzed by conducting a statistical analysis as discussed in Section 6.4.

Table 6-5: Summary of MPMT Results tested at σ_n of 103, 152 and 207 kPa

Test ID	σ_n (kPa)	P_L (kPa)	E_P (kPa)	E_R (kPa)	W (%)	γ_d (kN/m3)	ψ (kPa)	SPM[1]
24_15B	103	500	12671	22887	6.7	12.9	48	Grinder
25_15B	103	493	8674	21476	12.0	14.4	15	Grinder
26_15B	103	379	8596	22830	8.9	13.2	27	Grinder
27_15B	103	465	5608	14284	12.3	13.6	14	Grinder
28_15B	103	535	13659	19672	6.8	12.7	46	Grinder
29_15B	103	442	10087	23839	7.6	13.4	37	Grinder
30_15B	103	444	7684	28474	11.9	14.2	15	Grinder
24_22A	152	613	21156	48900	6.7	13.2	47	Grinder
24_22C	152	637	18843	44463	6.5	13.2	50	Grinder
25_22A	152	565	8891	29131	12.0	14.5	14	Grinder
25_22C	152	546	11439	32139	11.9	14.5	15	Grinder
26_22A	152	481	11525	22759	8.9	13.4	26	Grinder
26_22C	152	521	12054	20640	9.0	13.4	26	Grinder
27_22A	152	617	10590	55591	12.3	13.8	14	Grinder
27_22C	152	612	8564	22177	12.1	13.8	14	Grinder
28_22A	152	664	22299	46922	6.9	13.0	45	Grinder
28_22C	152	653	18714	47444	6.9	13.0	45	Grinder
29_22A	152	528	11212	26487	7.5	13.6	38	Grinder
29_22C	152	591	14477	32711	7.7	13.6	36	Grinder
30_22A	152	570	9304	31261	12.2	14.5	14	Grinder
30_22C	152	543	7708	19366	12.2	14.5	14	Grinder
24_30D	207	752	18004	54227	6.7	13.4	48	Grinder
25_30D	207	808	12443	35994	11.9	14.7	15	Grinder
26_30D	207	686	15697	28818	8.5	13.6	29	Grinder
27_30D	207	846	11193	28642	12.0	14.1	14	Grinder
28_30D	207	840	20423	44381	7.0	13.1	44	Grinder
29_30D	207	765	14578	26884	7.4	13.8	39	Grinder
30_30D	207	756	9361	33945	12.5	14.7	13	Grinder

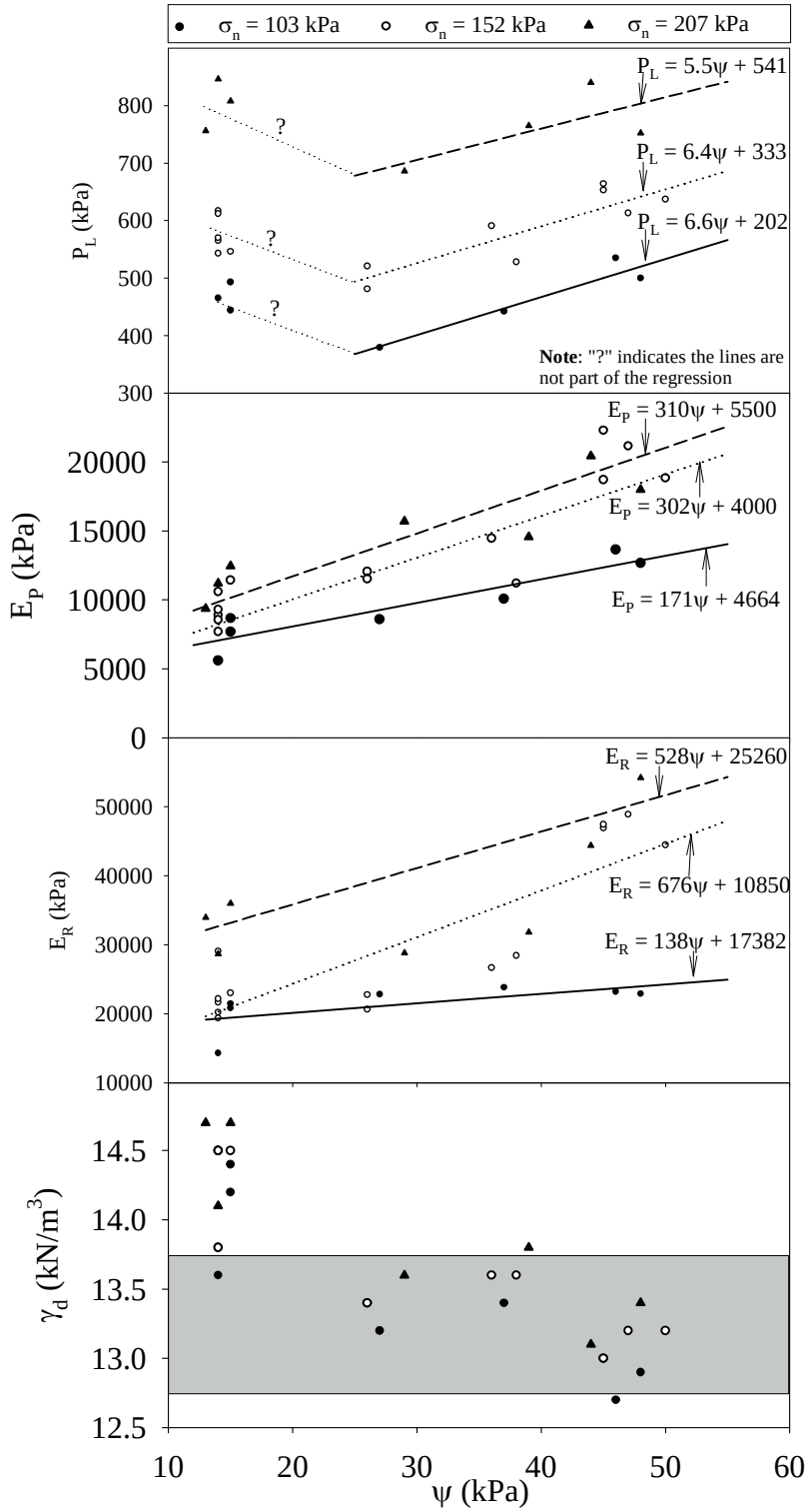

Figure 6-11: P_L, E_P, E_R and γ_d vs. ψ at σ_n of 103, 152 and 207 kPa for Soil Beds Processed by Grinder

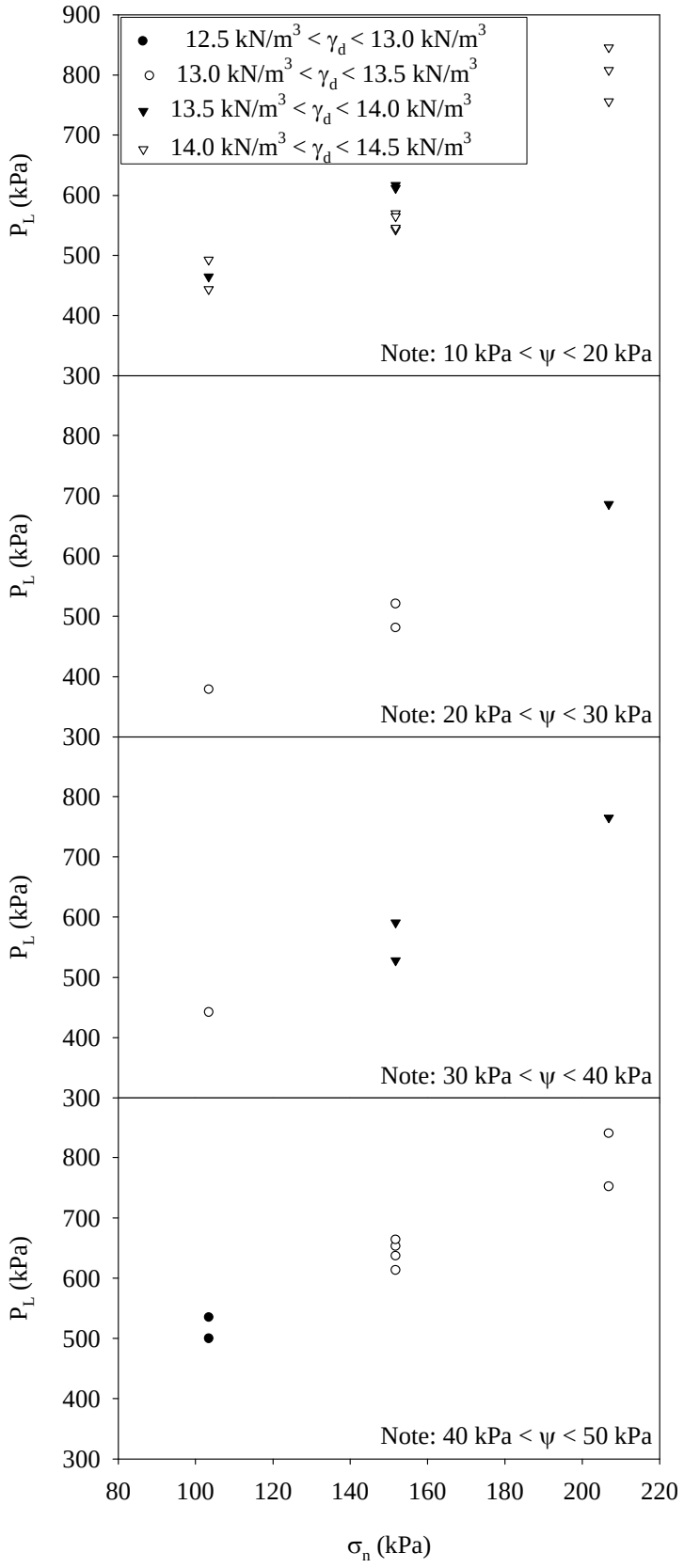

Figure 6-12: P_L vs. σ_n at various range of ψ for Soil Beds Processed by Grinder

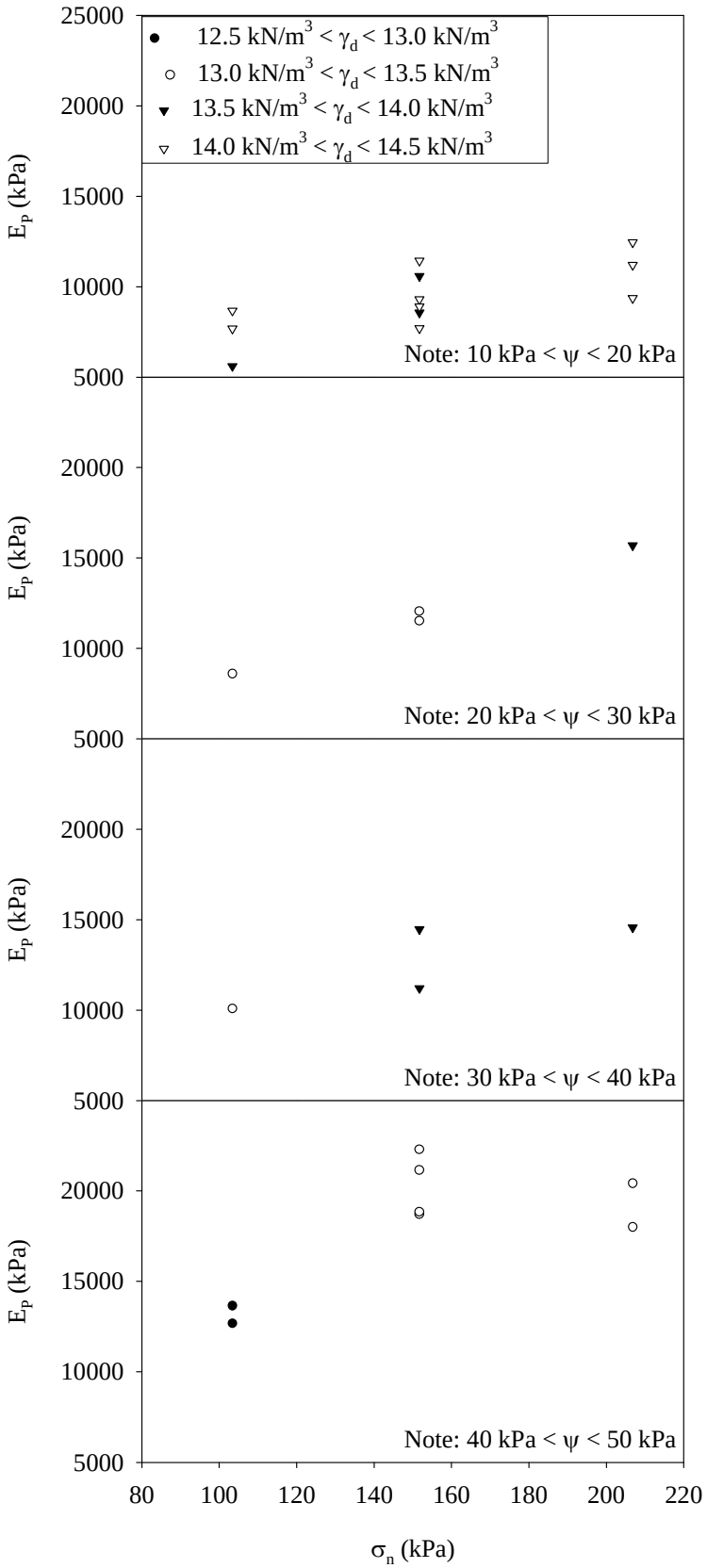

Figure 6-13: E_P vs. σ_n at various range of ψ for Soil Beds Processed by Grinder

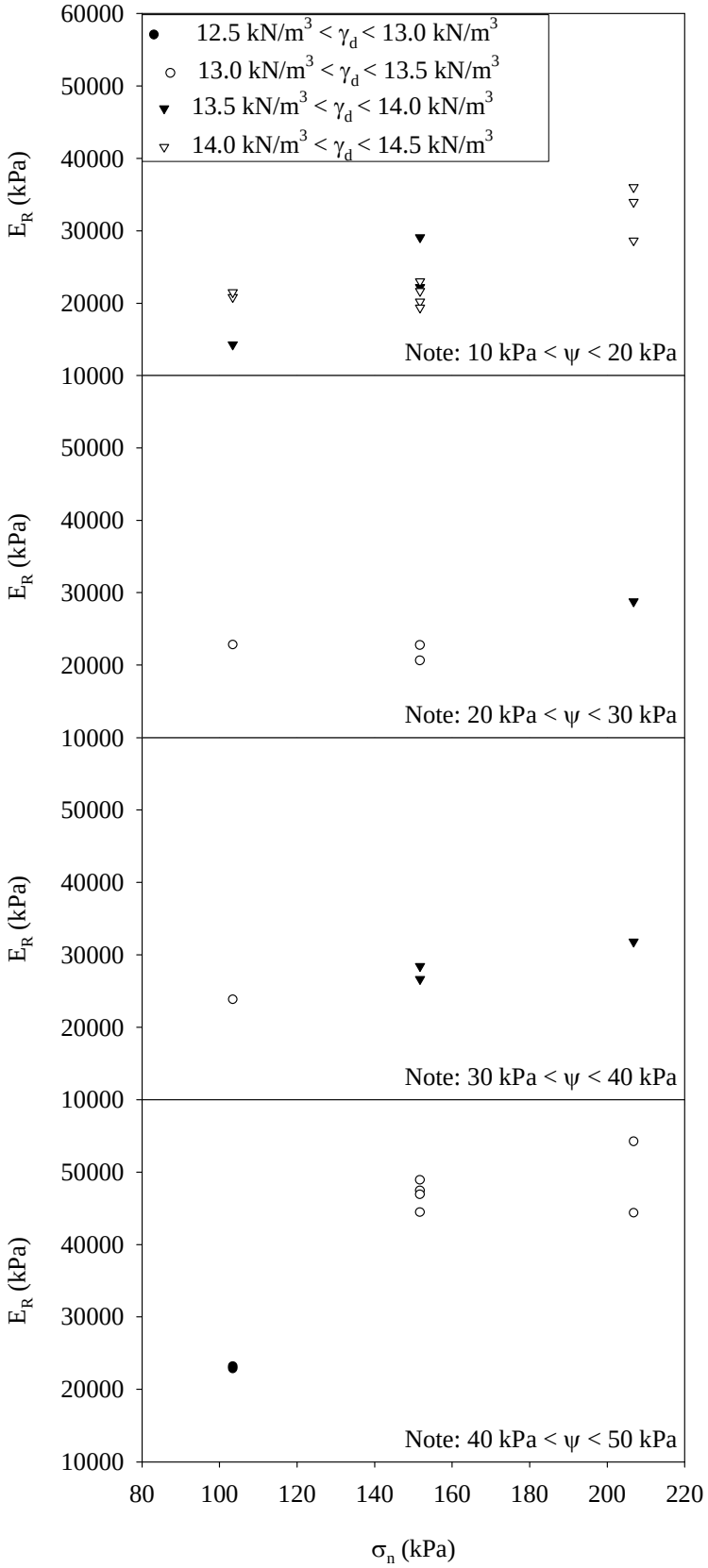

Figure 6-14: E_R vs. σ_n at various range of ψ for Soil Beds Processed by Grinder

6.3 Cone Penetrometer Testing

In this research, six test beds were prepared at different *w* giving ψ ranging from 15 kPa to 60 kPa for MCPT testing. Only σ_n of 103 kPa was used in this part of testing. All three segments of the calibration chamber were used. Four CPT soundings were conducted in each soil bed; one in the center and three others spaced 120^o apart and 127 mm from the center. This allowed for investigation of boundary effects, uniformity of soil beds, and repeatability. After testing, the chamber was disassembled and the soil bed was dissected for *w* and γ_d determination.

Figure 6-15 shows typical MCPT results from one of the soil beds (CCT12). The plots for all of the remaining MCPT results are included in Appendix D. It is observed that the cone tip resistance (q_c) varies within each layer but the amplitude of the variations is similar from layer to layer and from test to test. This indicates that within each layer the soil beds are heterogeneous with depth but are relatively homogeneous horizontally. It is also observed that q_c tends to peak at layer interfaces and is minimum somewhere near the mid-depth of layers. Table 6-6 presents the mean values of q_c for each CPT profile along with the average properties of the soil beds (i.e. *w*, γ_d, and ψ). The matric suction was determined by using the average water content around the MCPT test location and soil-water characteristic curve. These ψ values agreed with the values measured using tensiometers. The coefficient of variation (C.O.V) of the q_c within each soil bed is also listed in Table 6-6. Since the C.O.V values are relatively small (<10%) (Mendenhall and Sincich, 2003), this indicates that the dispersion of q_c about the average or expected value is relatively small. The q_c versus depth plots for all four test locations

within each soil bed tend to overlap one another as shown in Figure 6-15. Thus, it is evident that the lateral boundary effects on q_c values are insignificant.

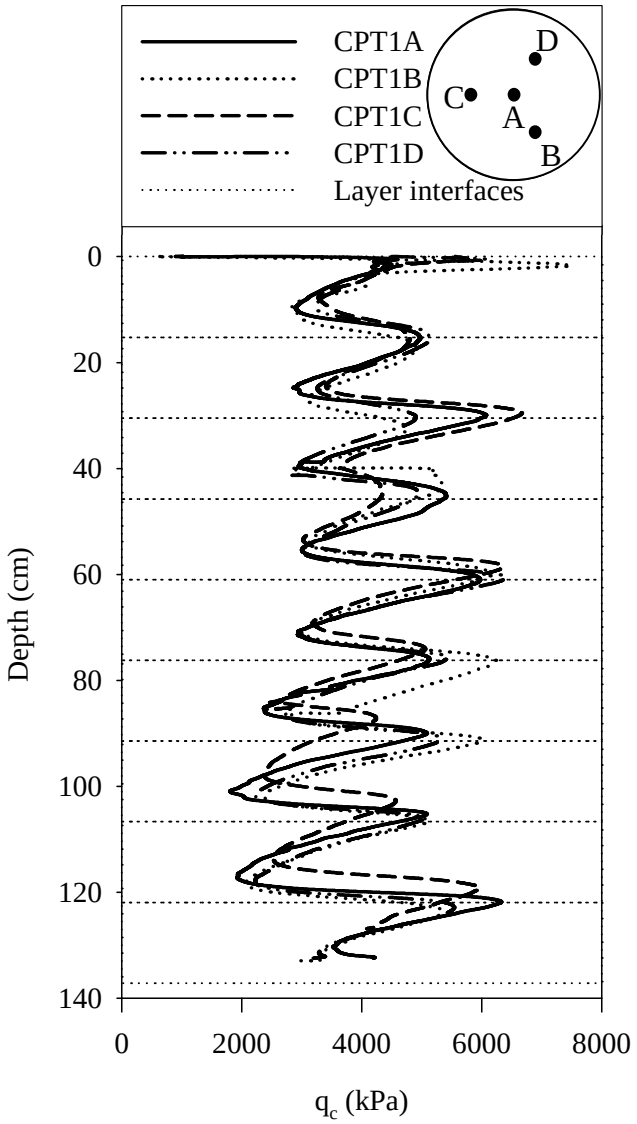

Figure 6-15: MCPT Results from Soil Bed CCT12

Table 6-6: Mean Values of q_c and Average Properties of Soil Beds Around Vicinity of Test Location

Test ID		w	γ_d	ψ	q_c			
					q_c	Average	Stdev.[1]	C.O.V[2]
		(%)	(kN/m^3)	(kPa)	(kPa)	(kPa)	(kPa)	(kPa)
CPT1 (CCT12)	A	5.7	13.3	59	3888	3967	77	1.95
	B	5.9	13.0	59	4055			
	C	5.9	13.2	59	4006			
	D	5.9	13.2	59	3918			
CPT2 (CCT13)	A	7.6	13.5	43	2883	3043	142	4.66
	B	7.6	13.6	43	3208			
	C	7.6	13.3	44	2978			
	D	7.6	13.1	45	3101			
CPT3 (CCT14)	A	9.6	13.8	27	2979	2925	110	3.78
	B	9.9	14.4	22	2779			
	C	9.9	14.2	23	2908			
	D	9.6	13.4	28	3035			
CPT4 (CCT15)	A	11.0	14.0	18	2812	2628	176	6.70
	B	10.8	14.5	18	2507			
	C	10.9	14.5	18	2741			
	D	11.0	13.7	20	2450			
CPT5 (CCT17)	A	8.6	13.6	34	3433	3197	297	9.30
	B	8.5	13.6	35	2896			
	C	8.6	13.7	34	2988			
	D	8.6	13.4	35	3471			
CPT6 (CCT18)	A	6.9	13.0	52	3363	3396	61	1.80
	B	6.9	13.4	50	3439			
	C	6.8	13.4	50	3327			
	D	6.8	13.1	52	3455			

[1] Standard Deviation
[2] Coefficient of Variation

Figure 6-16 shows a plot of q_c versus ψ. The same approach applied to the MPMT data has been applied to the MCPT data to account for the variation of γ_d. Again, in order to include the effects of γ_d into the data analysis the data was further divided into several groups based on the range of the γ_d of the soil beds where the test was conducted. It is observed that q_c increases with increasing ψ, and as shown in Figure 6-16 q_c appears to increase with increasing γ_d. These observations suggest that q_c depends on ψ and γ_d; however, the trend q_c with γ_d is not so clear. As a first approximation of the effect of γ_d, best fit regression lines are presented in the q_c versus ψ plots in Figures 6-16. Some of the data points seem to fall out of the general trend observed; these data points are marked with a "??" in the plots and were not used for developing the empirical equations presented in the figure. Interestingly, the average values of q_c, ψ and γ_d from eact test bed, reprented by the large symbols in Figure 6-16, match the trend lines quite well.

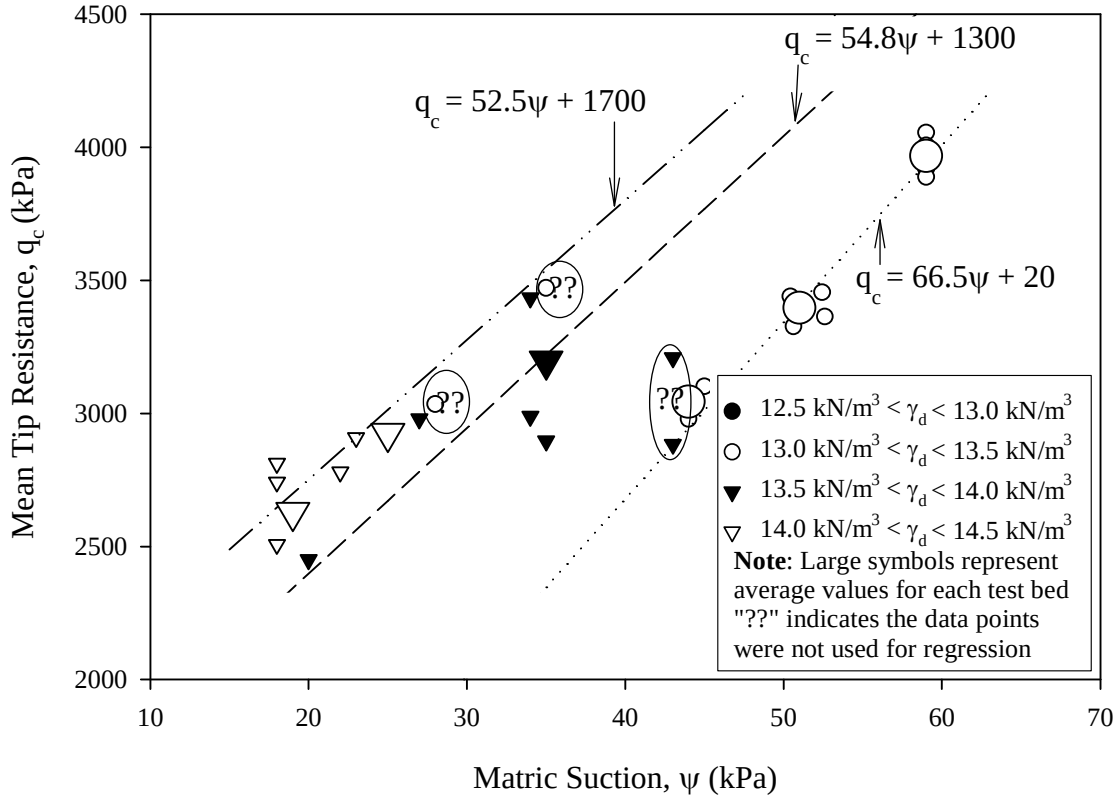

Figure 6-16: Mean Values of Tip Resistance (q_c) vs. Matric Suction (ψ)

It is important to note that main the purpose of the empirical equations presented in Section 6.2 and 6.3 are to show the correlation of MPMT and MCPT parameters to ψ, γ_d, and σ_n and not necessarily for predictions of a practical nature. Nevertheless, as more soil types are investigated, the current work will greatly benefit future development of empirical models for pressuremeter and cone penetrometer testing in unsaturated soil.

6.4 Statistical Analysis

The observations in Section 6.2 and Section 6.3 suggest that the MPMT and MCPT results depend primarily on the variables γ_d, ψ and σ_n. No investigation was conducted on the influence of σ_n on MCPT results in this study. This section discusses

the statistical analysis conducted on the results. Both the MPMT and MCPT data were analyzed statistically by utilizing the Statistical Analysis Software (SAS). First, the experimental data were keyed in as input into the SAS data set. Then the SAS procedures were used to analyze and process the data set. SAS procedures are the computer programs that read the SAS data set, perform various manipulations, and print the results of the computation. The capability of SAS to perform multivariate analysis was utilized in this process. It allows modeling data with multiple variables and also allows identifying relationships among several variables without designating particular variables as response or predictor variables. From the statistical point of view, there rarely is any deterministic relationship between the response or predictor variables. Most of the relationships involve many other unknown parameters, which sometime can not be fully accounted for or even modeled (Tamhane and Dunlop, 2000). Furthermore, from the statistical point of view, the actual relationships between parameters can never be exactly known. Therefore, probabilistic model regressions were also used in the analyses. A stepwise variable selection method was used in the analyses. The main idea behind the stepwise regression method is that the variables are entered or removed one at a time. "*This is done by taking into account the marginal contribution of each variable to the model controlling for the contribution of the other variables already present in the model*" (Tamhane and Dunlop, 2000). The marginal contributions were then evaluated based on a partial F-test. However, there are some limitations to stepwise regression methods in that they do not account for all of the other possible interactions of the various terms in the model. The stepwise methods are typically recommended to be used as variable screening methods as used in this study. In this study the stepwise regression

method was used to screen the variables, followed by selecting the appropriate variables for the model building. The same process and assumptions can be used for the model building but without the stepwise variable selection method. Figure 6-17 shows the summary of steps involved in the statistical analysis. All the results for the statistical analysis in this study can be reproduced using SAS procedures included in Appendix "E" (for MPMT) and "F" (for MCPT).

In this study the statistical analysis is broken into three sub-sections; as listed below:

1. Study the significance of soil processing methods on the MPMT results (i.e. P_L, E_P, E_R).
2. Statistical analyses on MPMT results: Study the influence of ψ, γ_d and σ_n on results of MPMT.
3. Statistical analyses on MCPT results: Study the influence of ψ and γ_d on q_c from MCPT.

As a first approximation, the effects of ψ, γ_d and σ_n on P_L, E_P, E_R and q_c were modeled using a first order regression. Several attempts were also made to incorporate higher order regression models but the results revealed that there was no improvement in the p-values. A "p-value" is defined as the probability the null hypotheses, which assume the influences of the independent variables on dependent variables are insignificant. Therefore, it is reasonable for simplicity purposes that the first order models were employed throughout this analysis.

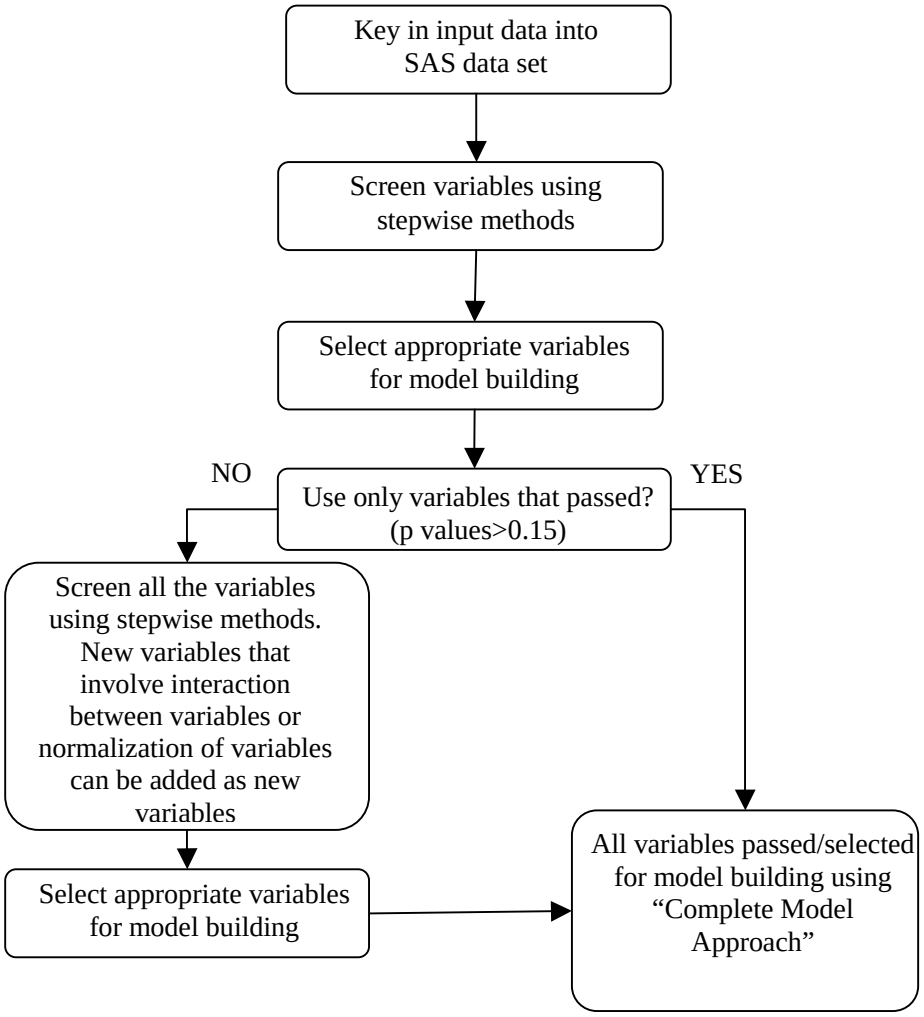

Figure 6-17: Summary of the Steps Involved in Statistical Analysis in This Study

6.4.1 Significance of Soil Processing Methods on MPMT Results

The MPMT data from soil beds CCT2 to CCT30, including all the MPMT testing in soil beds subjected to σ_n of 103 kPa, were used for this part of the study. Two soil bed processing methods were involved in the data sets as discussed and presented in Section 6.2.2. The data were analyzed statistically by SAS with P_L, E_P and E_R as dependent variables and ψ, γ_d and soil processing method as independent variables. As shown in

Table 6-7, the computed F-analysis probabilities (p-values) that the soil processing method has no influence on P_L and E_P are <0.0001 and 0.0014, respectively. In other words, the influence of soil processing method on P_L and E_P is significant to 99%. Therefore, the contribution of soil processing methods on P_L and E_P are significant in this study. However, when analyzing the variables that influence E_R using the stepwise method, the soil processing method was not selected as one of the predictor (i.e. independent) variables that determine E_R. This indicated that the affect of soil processing method on E_R was not as significant as on P_L and E_P. Overall, it is concluded that the influence of the soil processing method on the MPMT test results is significant. It is also important to note that in the analyses, ψ and γ_d have been consistently chosen as predictor variables throughout. Thus, it is evident that ψ and γ_d of the soil beds have significant influences on the MPMT results. The influences of ψ and γ_d are discussed in following sections. Table 6-30 shows the summary of p-values obtained for soil processing methods, ψ and γ_d by using the complete model approach. Note, the variables having p-values less than 0.15 are considered significant.

Table 6-7: Summary of p-Values from Screening Analysis of Soil Processing Method, ψ and γ_d as Predictor Variables for P_L, E_P and E_R.

Dependent Variable	p-Values			
	SPM[1]	ψ	γ_d	Model
P_L	<0.0001	0.0003	0.0027	<0.0001
E_P	0.0014	0.0081	0.0100	<0.0001
E_R	-	0.0595	0.0190	0.0107

[1] SPM = Soil Processing Method

6.4.2 Statistical Analyses on Miniature Pressuremeter Testing Results

Since the influence of the soil processing methods on the P_L and E_P are significant, in this section the data are separated into two groups according to the soil processing methods. Soil beds CCT2 to CCT10 were processed by the crusher and labeled as group "C" while soil beds CCT11 to CCT30 were processed by the soil grinder and labeled as group "G". The MPMT data conducted in soil beds CCT11 to CCT30 (group "G") were further separated into two (2) groups. The first group consists of data from soil beds CCT11 to CCT30, where all the MPMT testing was conducted when soil beds were subjected to σ_n of 103 kPa are labeled as group "G1". The second group consists of data from soil beds CCT24 to CCT30, where the MPMT tests were carried out when the soil beds were subjected to various σ_n (i.e. 103, 152 and 207 kPa) and are labeled as group "G2". Table 6-8 presents the summary of how the MPMT data from the calibration chamber testing were grouped for statistical analysis. The following sub-sections discuss the statistical analyses of the MPMT results.

Table 6-8: Grouping of MPMT Test Data

Group ID	Soil Beds Used	σ_n During MPMT Testing (kPa)
C	CCT2-CCT10	103
G1	CCT11, CCT19-CCT23, CCT24-CCT30[A]	103
G2	CCT24-CCT30	103, 152 and 207

[A] Only for MPMT at σ_n=103 kPa

Initially, when analyzing the MPMT data statistically with SAS, the P_L, E_P and E_R were assigned as dependent variables and ψ, γ_d and σ_n (influence of σ_n is only studied for Group "G2") as independent variables. The SAS procedures for these computations are contained in Appendix E. Table 6-9 shows the summary of the p-values from the

computed F-analysis. Table 6-10 shows the coefficient of each independent variable as function of the dependent variables and the r^2 values for the least squares fit based on the complete model.

Table 6-9: Summary of p-Values from the Analysis of ψ, γ_d and σ_n as Predictor Variables for P_L, E_P and E_R

Data Set Group ID	Dependent Variable	p–Values			
		γ_d	ψ	σ_n	Model
C	P_L	0.0006	0.0003	N/A	<0.0001
	E_P	0.0925	0.1129	N/A	0.1924
	E_R	0.0358	0.2195	N/A	0.0978
G1	P_L	0.9031	0.0837	N/A	0.0116
	E_P	0.0515	0.0004	N/A	0.0005
	E_R	0.0049	<0.0001	N/A	0.0001
G2	P_L	0.9617	0.4414	<0.0001	<0.0001
	E_P	0.7265	0.0006	0.0025	<0.0001
	E_R	0.4929	0.0026	0.0050	<0.0001
G2A*	P_L	0.0574	0.0015	<0.0001	<0.0001
	E_P	0.0648	0.0430	0.0022	0.0007
	E_R	0.4361	0.0143	0.0119	0.0017

*G2A: Used only data from G2 with ψ>20 kPa

Table 6-10: Coefficient Values for ψ, γ_d and σ_n as Predictor Variables for P_L, E_P and E_R and r^2 Value for the Empirical Model

Data Set Group ID	Dependent Variable	Coefficient Values for Independent Variables				r^2 of Model
		C	γ_d	ψ	σ_n	
C	P_L	-5.65E+03	4.29E+02	2.02E+01	N/A	0.8352
	E_P	-9.62E+04	7.72E+03	2.05E+02	N/A	0.2240
	E_R	-1.31E+06	9.61E+04	1.50E+03	N/A	0.3007
G1	P_L	4.79E+02	-4.75E+00	1.88E+00	N/A	0.2901
	E_P	-5.01E+04	3.90E+03	2.10E+02	N/A	0.4468
	E_R	-1.86E+05	1.38E+04	5.89E+02	N/A	0.4962
G2	P_L	1.56E+02	-2.18E+00	1.41E+00	2.80E+00	0.7456
	E_P	6.33E+03	-5.44E+02	2.41E+02	2.45E+01	0.7697
	E_R	-5.04E+04	3.18E+03	6.12E+02	1.21E+02	0.6438
G2A*	P_L	1.02E+03	-8.3E+01	4.48E+00	3.19E+00	0.9510
	E_P	7.66E+04	-6.15E+03	2.04E+02	7.98E+01	0.7450
	E_R	7.24E+04	-7.35E+03	7.79E+02	1.82E+02	0.7045

NOTE: General form of empirical equations: P_L, E_P $E_R = C + a\gamma_d + b\psi + c\sigma_n$
*G2A: Used only data from G2 with ψ>20 kPa

From Table 6-9 it is observed that the contribution of ψ on the P_L, E_P and E_R is significant ($p < 0.15$) in most of the cases, except for two: 1) E_R from data in Group C and 2) P_L from data in Group G2. In the case of the former, this might be due to the significant scatter in the E_R data or some other factors that are not included in the analysis but are discussed in following paragraphs. As for the latter, the influence of ψ appears to be masked by the data at low values of ψ, which destroys the increasing trend of P_L with ψ seen for data at ψ greater than 20 kPa (see Figure 6-11). As for γ_d, its contribution to P_L, E_P and E_R is generally significant with the exception Group G2, where the p-values are greater than 0.15 and where coefficients for γ_d are negative. One of the significant differences of this data set compared to the other data sets is that the MPMT tests were conducted at various σ_n (103, 152 and 207 kPa). It is recognized that for a soil with given

initial γ_d, the γ_d would increase with σ_n. Thus, it is not surprising that the p-values for γ_d in the models for this group are relatively large since σ_n has also been incorporated into the model as one on the predictor variables and appear to have influenced the MPMT results more significantly than γ_d. The p-values for σ_n in the model are relatively small. This observation can be interpreted that in this particular model the contribution of σ_n as a predictor for P_L, E_P and E_R is more significant compared to the contribution of γ_d. Also, γ_d does not vary much for ψ greater than 20 kPa. An additional run was conducted for data from Group G2 with ψ greater than 20 kPa. The data set is labeled as Group G2A as presented in Table 6-9 and 6-10. It appears that both the p-values and r^2 values improve significantly. It shows that σ_n, ψ and γ_d have a significant influence on P_L, E_P and E_R.

There are many possible reasons why the p-values for some of the models are relatively high. One of the main reasons might be due to the scatter in the data, which may be a consequence of measurement uncertainty in the testing procedure, disturbance in the borehole, and variation in fabric of soil beds involved in this study. Since the soil bed preparation methods involved controlling the target γ_d, the compaction effort used for the soil bed preparation varies from one soil bed to another depending on the *w* of the soil-water mixture. Therefore, it is anticipated the apparent overconsolidation ratio (OCR) of the soil beds might vary from one bed to another. It has been well documented in the literature that OCR has a significant impact on the modulus of a soil bed.

The burette used for the volume measurement during the MPMT testing is only capable to measure to an accuracy of 10^{-7} m^3. The pressure gauge used for the MPMT testing has an accuracy of 1.7 kPa. Thus, the cumulative error due to the precision of the burette and the pressure gauge reading could lead to an error in E_R values as large as 20%

and slightly less for E_P. Another possible source of data scatter is that the soil beds were prepared at different initial moisture content, which could cause variation in the fabric of the soil bed itself. Nevertheless, given these many uncertainties, from the statistical analysis, it is evident that the σ_n, ψ, and γ_d generally have a significant influence on P_L, E_P and E_R. Furthermore, high p-values may results partly from erroneous assumptions; independent variables were not truly independent and relationship between variables are not actually linear.

6.4.3 Statistical Analyses on Miniature Cone Penetrometer Testing Results

Six soil beds were prepared for the miniature cone penetrometer testing (MCPT). Four MCPTs were conducted in each soil bed with σ_n of 103 kPa. Similar to the process used in analyzing the MPMT data, the first step involved assigning q_c as the dependent variable and γ_d, and ψ as independent variables. The results of the computations can be reproduced using the SAS procedures contained in Appendix F. Table 6-11 shows the summary of p-values from the analyses and Table 6-12 shows the coefficients of the predictor variables for the model with corresponding r^2 values. It is observed that the p-value of ψ is 0.0002 while the p-value of γ_d is 0.6343. This shows that the influence of ψ on q_c is much more significant than γ_d. It also implies that the MCPT in unsaturated soil is highly dependent on ψ. However, looking back at the soil bed data it is observed that the γ_d of the soil beds did not remain constant for all the test beds used for conducting the MCPT. In order to be consistent with the basic principles of soil mechanics and for the sake of consistency with the analyses done for the MPMT results, the variable γ_d is retained in the analysis.

Table 6-11: Summary of p-Values from the Analysis of γ_d and ψ as Predictor Variables for q_c

Dependent Variable	p-values		
	γ_d	ψ	Model
q_c	0.6343	0.0002	<0.0001

Table 6-12: Coefficient Values for γ_d and ψ as Predictor Variables for q_c and r^2 Value for the Empirical Model

Dependent Variable	Coefficient Values of Independent Variables			r^2 Values
	C	γ_d	ψ	
q_c	6.99E+02	9.98E+01	2.94E+01	0.7485

NOTE: General form of empirical equations: $q_c = C + a\gamma_d + b\psi$

6.4.4 Summary of Statistical Analysis

The main purpose of the statistical analyses were to show the significance of soil processing methods, matric suction (ψ), dry unit weight (γ_d) and net normal stress (σ_n) on the MPMT and MCPT results. The statistical analyses shows that the soil processing method had a significant effect on the MPMT results. No study on effect of soil processing methods or σ_n was conducted for MCPT. It also shows that generally the influences of ψ, γ_d and σ_n on MPMT and MCPT results are significant. It is also important to note that the empirical equations developed in this section are only applicable to the range of ψ used in this study (i.e. 15 kPa< ψ < 70 kPa). Its applicability at fully saturated conditions (ψ = 0 kPa) or at completely dry conditions have not been

studied in the course of this research. As described earlier, the purpose of these empirical equations is to show the correlation of MPMT and MCPT parameters to γ_d, σ_n and ψ and not necessarily for predictions.

6.5 Cavity Expansion for Unsaturated Soil

Cavity expansion theory has been widely used for the interpretation the PMT and CPT testing. In this preliminary study, the MPMT and MCPT data were interpreted using the equations for expansion of cylindrical and spherical cavities in an infinite unsaturated soil mass developed by Muraleetharan et al. (1998) (see Figure 2-8 for schematic of the cross section through the cavity and surrounding soil). Listed below are several important assumptions applied during the current study:

- Beyond the plastic zone the soil behaves as a linear elastic solid and soil within the zone behaves as a compressible plastic solid. Therefore, when the internal pressure of the cavity reaches its ultimate value p_u, the radius of the cavity and plastic zone are R_u and R_p, respectively (Muraleetharan et al., 1998). Equation 6-11 was derived by Muraleetharan et al. (1998) to relate R_u and R_p based on this assumption.

$$\frac{R_p}{R_u} = \sqrt{I'_{rr}} \qquad \text{(Eq. 6-11)}$$

- The Young's Modulus, E was taken as the MPMT modulus, E_p,
- Poisson's ratio, $v = 0.333$,
- Gravimetric water content, w stays constant during the cavity expansion,
- Matric suction, ψ stays constant during cavity expansion, and

- Pore air pressure, u_a remains at atmospheric pressure (i.e. u_a = 0 kPa gage pressure) during the cavity expansion.

Ananthanathan (2002) developed a series of soil-water characteristic curves for Minco silt compacted statically with γ_d ranging from 12.6-kN/m^3 to 15.7-kN/m^3 as shown in Figure 6-18. It is observed that the curve is unique and independent of γ_d. Since the soil in the plastic zone is assumed to be in a closed system, the assumption that the gravimetric water content (*w*) and hence matric suction (ψ) remains constant during cavity expansion seems valid for Minco Silt. The assumption that ψ stays constant during cavity expansion for pressuremeter testing is consistent with the assumption made by Schnaid et al. (2004). Schnaid et al. (2004) stated that during cavity expansion, the mean net stress experienced by soil elements remains constant provided the soil element is still within the elastic phase. This is because during the elastic phase of cavity expansion the magnitude of change in circumferential stress is equal to the magnitude of change in radial stress but in the opposite direction. Therefore, Schnaid et al. (2004) concluded that the matric suction would remain constant around the pressuremeter during cavity expansion. The experimental work done by Schnaid et al. (2004) further proved that ψ remains constant during cavity expansion throughout both the elastic and plastic phase. Houlsby (1998) stated that the change in degree of saturation (S) of the soils within the region affected by the cavity expansion is generally insignificant except those that are very close to the cavity wall. Indirectly this supports the assumption that ψ remains constant during cavity expansion since alternative to gravimetric water content, the degree of saturation (S) is also typically used in soil-water characteristic curve to express the amount of water in the soil as discussed in Section 2.1.2.2.2. The assumption that

matric suction remains constant during cavity expansion is further supported by a study done by Muraleetharan et al. (2003). In the study Muraleetharan et al. (2003) used a fully coupled finite element computer code to predict the MPMT results. In the study, it was observed that the change in matric suction in the zone of influence during the expansion of the PMT probe was relatively small. Given that Minco Silt contains appreciable amount of sand and silt and considering the ψ and γ_d range used in this research, it is speculated that continuous air voids existed throughout the soil skeleton; the assumption that pore air pressure (u_a) remains constant during cavity expansion is therefore reasonable.

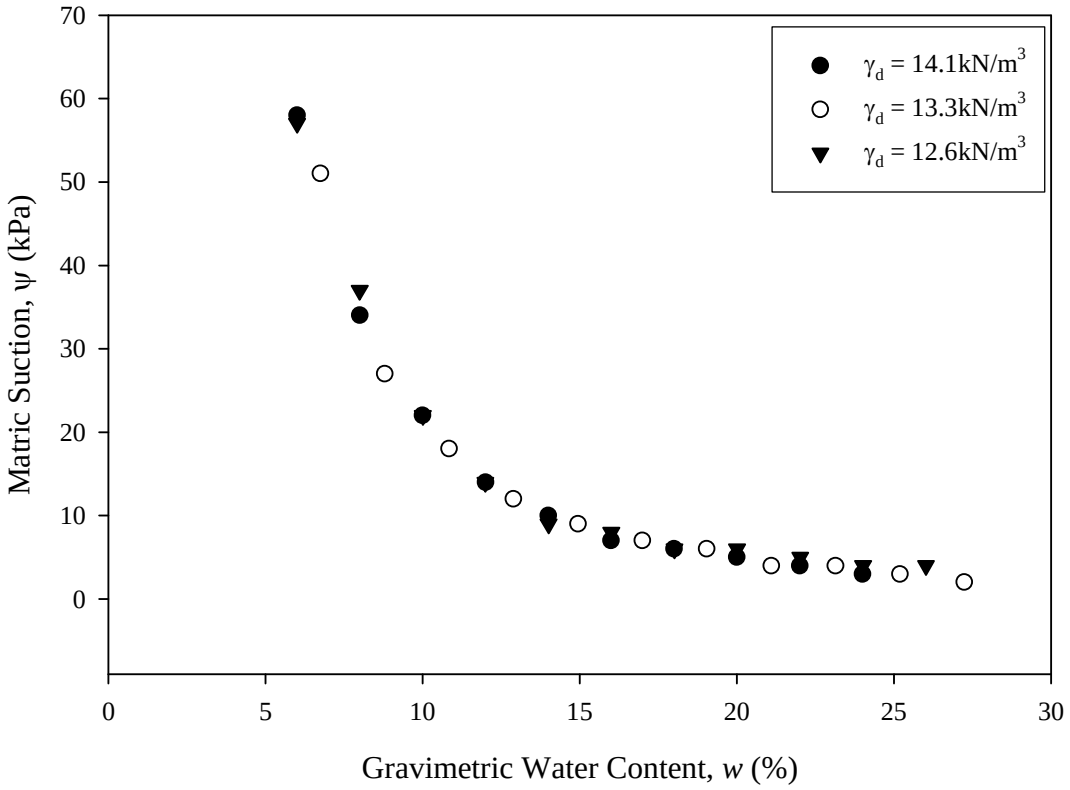

Figure 6-18: Soil-Water Characteristic Curve for Minco Silt at Various γ_d

The assumption that pore air pressure, u_a remains at atmospheric pressure (i.e. zero gage pressure) and matric suction, ψ stays constant during the cavity expansion reduces the cavity expansion equation in unsaturated soil, developed by Muraleetharan et al. (1998) as shown in Section 2.4, to the following forms:

1) Reduced form of cylindrical cavity expansion equation in unsaturated soil:

$$p_u = F'_q\, p + F'_c\, c \qquad \text{(Eq. 6-12)}$$

where:

p_u = ultimate pressure,

F'_q, F'_c = dimensionless cylindrical cavity expansion factors,

$$F'_q = (1+\sin\phi')I'^{\,\sin\phi'/(1+\sin\phi')}_{rr} \qquad \text{(Eq.6-13)}$$

$$F'_c = (F'_q - 1)\cot\phi' \qquad \text{(Eq.6-14)}$$

$$I'_{rr} = \frac{1+\varepsilon_v^*}{\frac{f_2}{I_r}+\varepsilon_v^*} \quad = \quad \text{reduced rigidity index,} \qquad \text{(Eq.6-15)}$$

$$f_2 = \cos\phi' \qquad \text{(Eq.6-16)}$$

$$I'_r = \frac{E}{2(1+v)[p\tan\phi'+c]} \quad = \quad \text{rigidity index} \qquad \text{(Eq.6-17)}$$

2) Reduced form of spherical cavity expansion equation in unsaturated soil:

$$p_u = F'_q\, p + F'_c\, c \qquad \text{(Eq. 6-18)}$$

where:

F'_q, F'_c = dimensionless spherical cavity expansion factor,

$$F'_q = \frac{3(1+\sin\phi')}{3-\sin\phi'} I'^{\,4\sin\phi'/3(1+\sin\phi')}_{rr} \quad \text{(Eq.6-19)}$$

$$F'_c = (F'_q - 1)\cot\phi' \quad \text{(Eq.6-20)}$$

$$I'_{rr} = \frac{1+\varepsilon_v^*}{\frac{f_1}{I_r}+\varepsilon_v^*} \quad = \quad \text{reduced rigidity index,} \quad \text{(Eq.6-21)}$$

$$f_1 = \frac{3\cos\phi'}{3-\sin\phi'} \quad \text{(Eq.6-22)}$$

$$I'_r = \frac{E}{2(1+\nu)[p\tan\phi' + c]} \quad = \quad \text{rigidity index} \quad \text{(Eq.6-23)}$$

The definitions of all other terms (i.e., p, c, c′, (u_a-u_w), ϕ', ϕ^b, ε_v, E and ν) remain unchanged. Five other parameters (c, c′, ϕ', $\phi^b$and ε_v) are required in order to be able to use the cavity expansion equation for unsaturated soil. Ananthanathan (2002) has conducted a series of laboratory triaxial tests on Minco silt at the University of Oklahoma. The results from the laboratory testing were used to estimate the soil bed properties, which were needed for use with the cavity expansion equations. Based on the work done by Ananthanathan (2002) c, c′, ϕ' and ϕ^b of the soil beds were estimated. However, ε_v is a parameter that is unknown and is not easily obtained from regular laboratory tests.

6.5.1 Purpose of Cavity Expansion Analyses of PMT and CPT in Unsaturated Soil

As discussed in a previous paragraph in Section 6.5, most of the parameters needed in order to use the reduced form equations can be estimated from a series of laboratory triaxial tests or typical values from the literature. However, the remaining unknown parameter, ε_v can not be obtained from laboratory tests. Thus, in this study ε_v was back calculated by using: 1) the laboratory data, 2) the assumptions made in Section 6.5, 3) the cavity expansion equations, and 4) assuming the limit pressure of the PMT is equal to the ultimate cylindrical cavity pressure (i.e. $P_L=p_u$) and the cone tip resistance (q_c) is equal to the ultimate spherical cavity pressure (i.e. $q_c=p_u$). Thus, one purpose for this part of the research is to provide curves that allow estimation of ε_v for a given set of soil conditions. This will allow one to estimate the limit pressure or tip resistance in unsaturated soil using the unsaturated soil cavity expansion equations. However, it is important to note that the curves obtained from this study are for a specific soil type, soil state and stress conditions used in this study. Nonetheless, it provides a framework for construction of families of curves that will allow the estimation of ε_v for various soil types under unsaturated conditions. The two sections that follow discuss the back-calculation of ε_v along with the analyses of the results.

6.5.2 Sensitivity Analysis

Sensitivity analyses were conducted on the reduced cavity expansion equations to determine the sensitivity of ε_v to some of the parameters such as E, c, ϕ', ν, p and ψ at various p_u. The range of each of the parameters used in the sensitivity analysis is based

on the range of typical values used in this study or based on the range of the data obtained from the calibration chamber testing. It is important to note that in the sensitivity analysis only the influence of one parameter was studied at a time and the remaining parameters were held constant, although in reality some of the parameters are dependent on each other.

6.5.2.1 Cylindrical Cavity Expansion

Figure 6-19 shows the influence of modulus (E) on ε_v at various p_u. It is observed that ε_v increases with increasing E for a given p_u. However, the sensitivity of ε_v to E diminishes as E increases, i.e., the rate of increase in ε_v decreases with increasing E at a given p_u. It is observed that for a given E, ε_v decreases at a diminishing rate as p_u increases. For instance, at E of 10000 kPa, the difference between the ε_v at p_u of 400 kPa and 500 kPa is 0.02577, while the difference between the ε_v at p_u of 900 kPa and 1000 kPa is 0.00095, although the increment of p_u in both cases is the same (i.e. 100 kPa). This shows that ε_v is relatively more sensitive to p_u at lower p_u, and the sensitivity decreases as p_u increases for a given E. It is also of interest to note that for large p_u values some curves show negative ε_v, which indicates volumetric expansion (i.e. dilation).

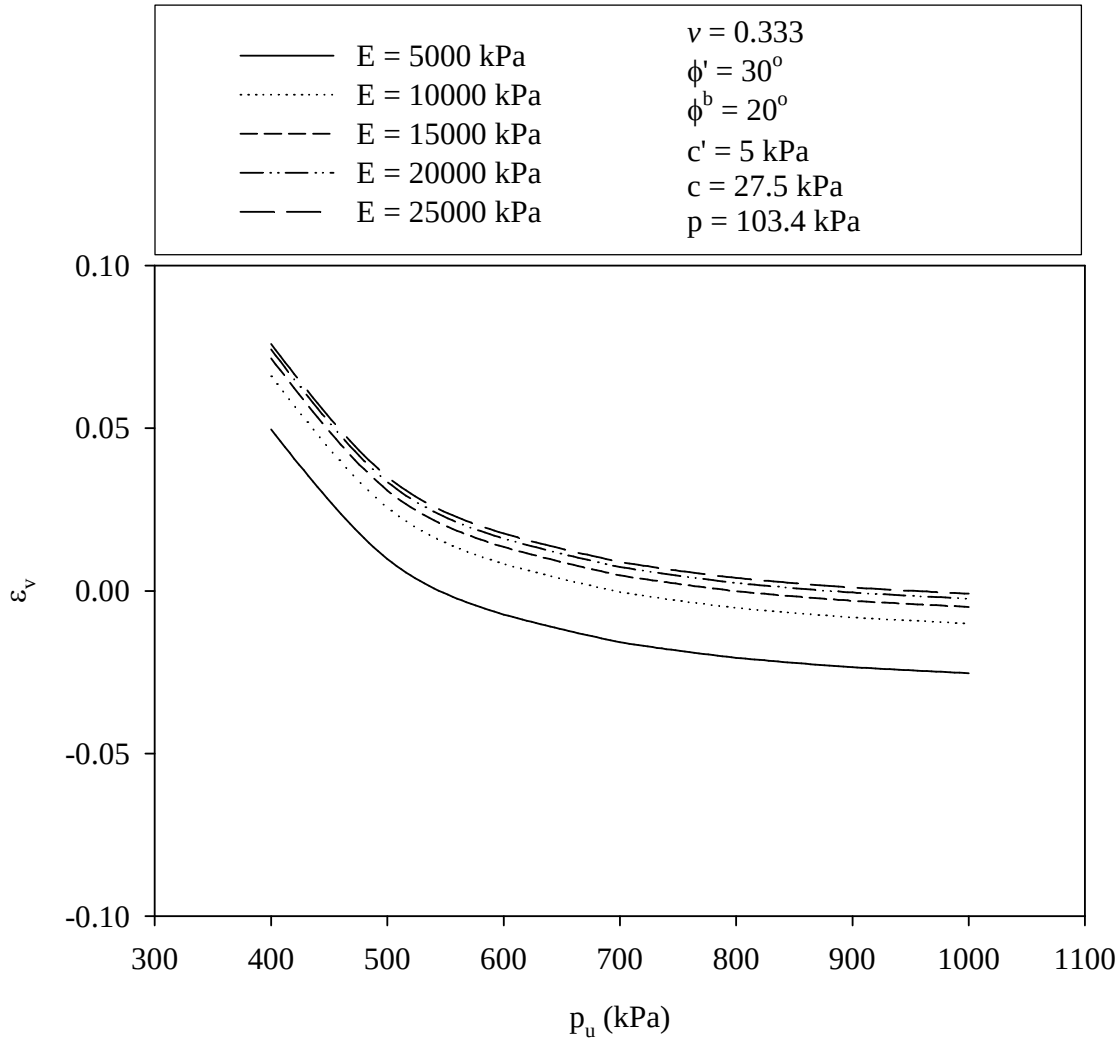

Figure 6-19: Sensitivity of ε_v of Cylindrical Cavity Expansion with Respect to E

Figure 6-20 shows the sensitivity of ε_v with respect to ϕ' at various p_u. It is observed that the influence of ϕ' on ε_v is relatively significant at lower p_u (e.g. p_u = 400 kPa). However, the sensitivity of ε_v with respect to ϕ' decreases with increasing p_u. At high p_u (e.g. p_u = 1000 kPa), ε_v is relatively insensitive to ϕ'. Another parameter of interest is c. Figure 6-21 shows the sensitivity of ε_v with respect to c at various p_u.

Generally, it shows that ε_v is relatively insensitive to the range of c used in this study although at low p_u (e.g. p_u = 400 kPa) it shows that there is a slight decrease in ε_v as c increases. The sensitivity analysis of ε_v to ν is presented in Figure 6-22; ε_v is relatively insensitive for the range of ν ($0.3 < \nu < 0.5$) typically used for soil (Coduto 1998). The sensitivity analysis of ε_v to p is presented in Figure 6-23; ε_v is relatively sensitive for the p typically used in this study (i.e. 103, 152 and 207 kPa). ε_v increases with p for a given p_u. Additional discussion for this behavior is presented in Section 6.5.3. The comparison of Figures 6-19, 6-20, 6-21, 6-22 and 6-23 show that ε_v is most sensitive to p followed by E, ϕ', c and ν in decreasing order of sensitivity. It is also important to note that p_u plays a significant role in the determination of ε_v where the sensitivity of all the parameters decreases rapidly as p_u increases.

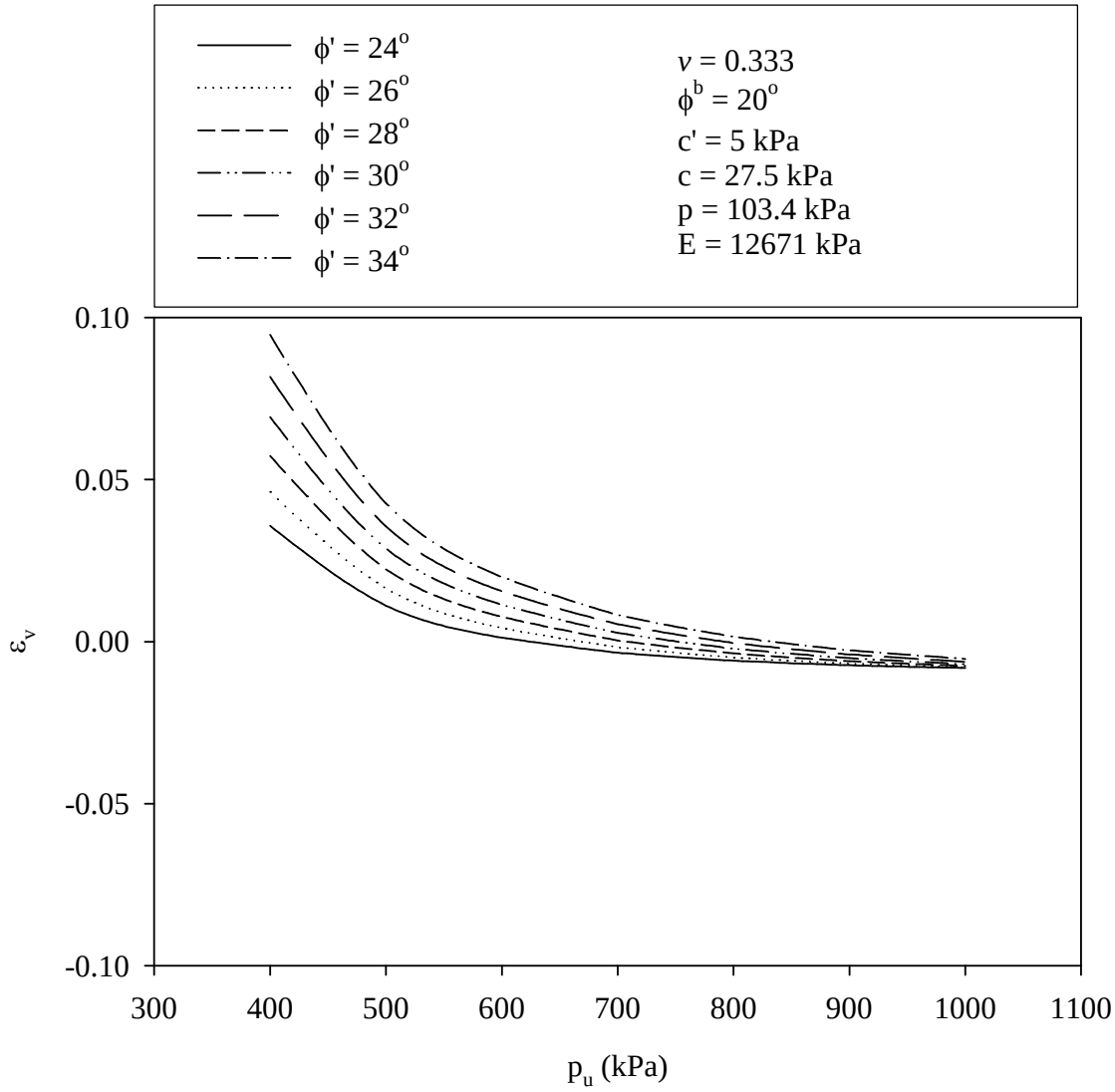

Figure 6-20: Sensitivity of ε_v of Cylindrical Cavity Expansion with Respect to ϕ'

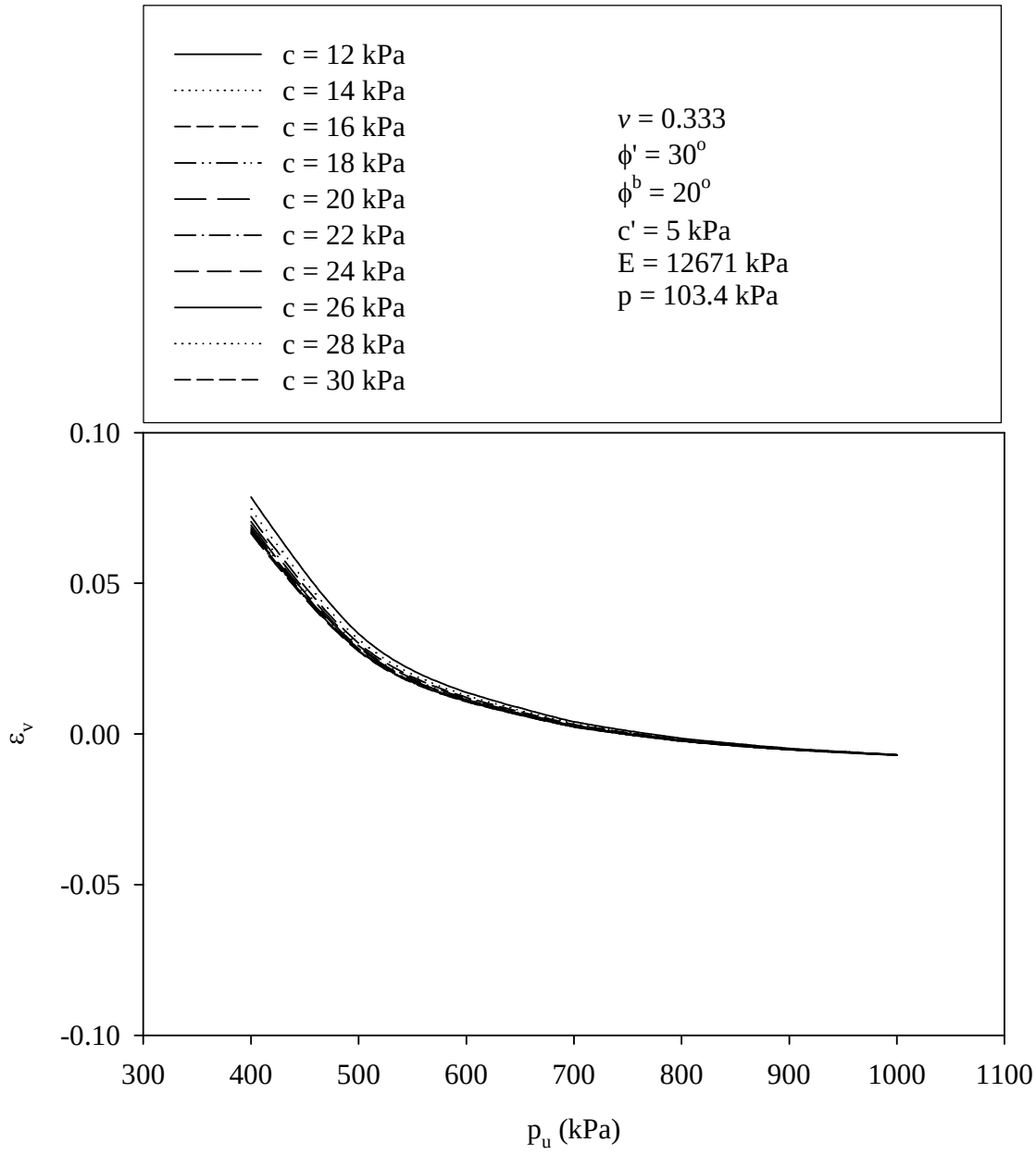

Figure 6-21: Sensitivity of ε_v of Cylindrical Cavity Expansion with Respect to c

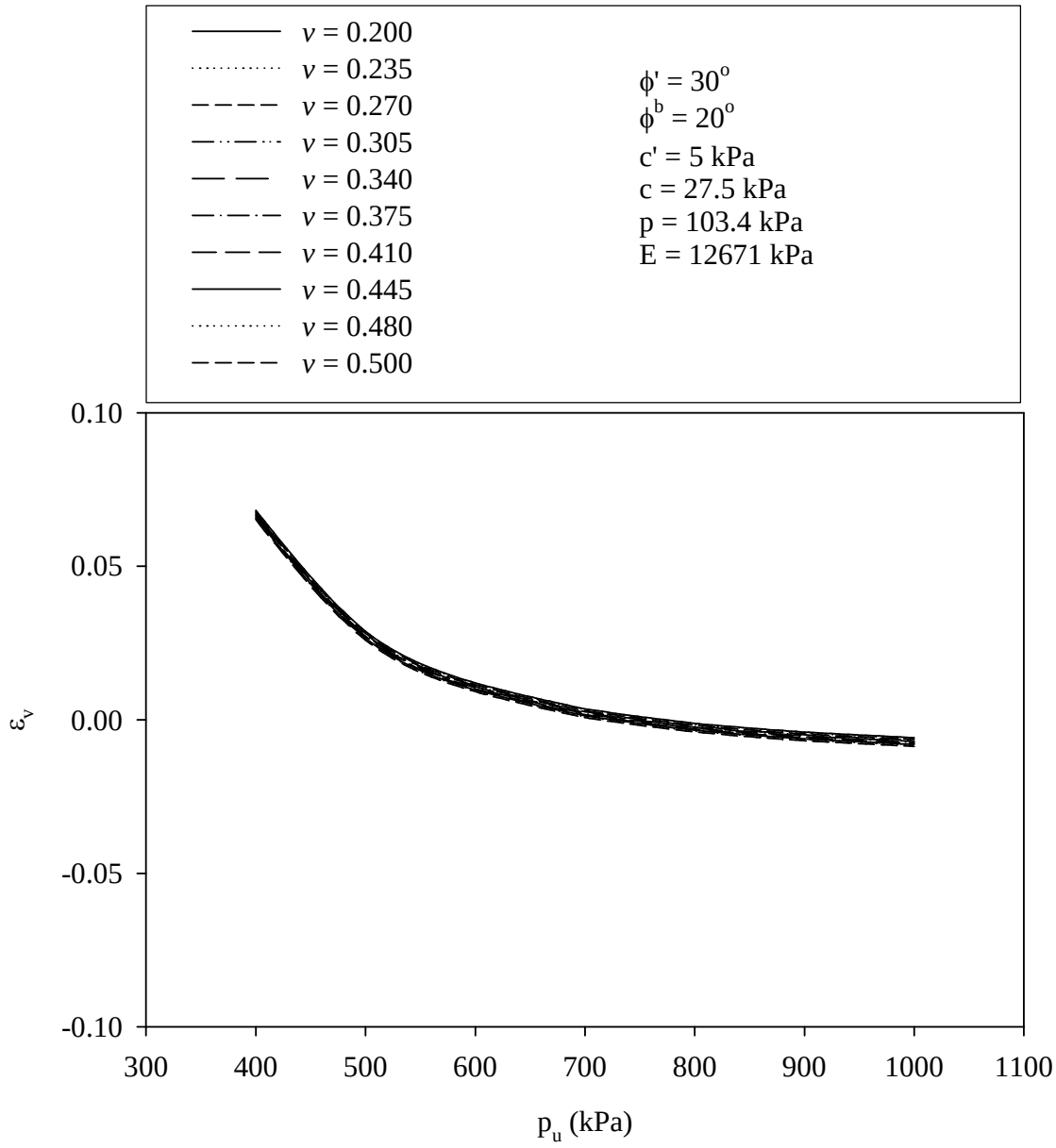

Figure 6-22: Sensitivity of ε_v of Cylindrical Cavity Expansion with Respect to *ν*

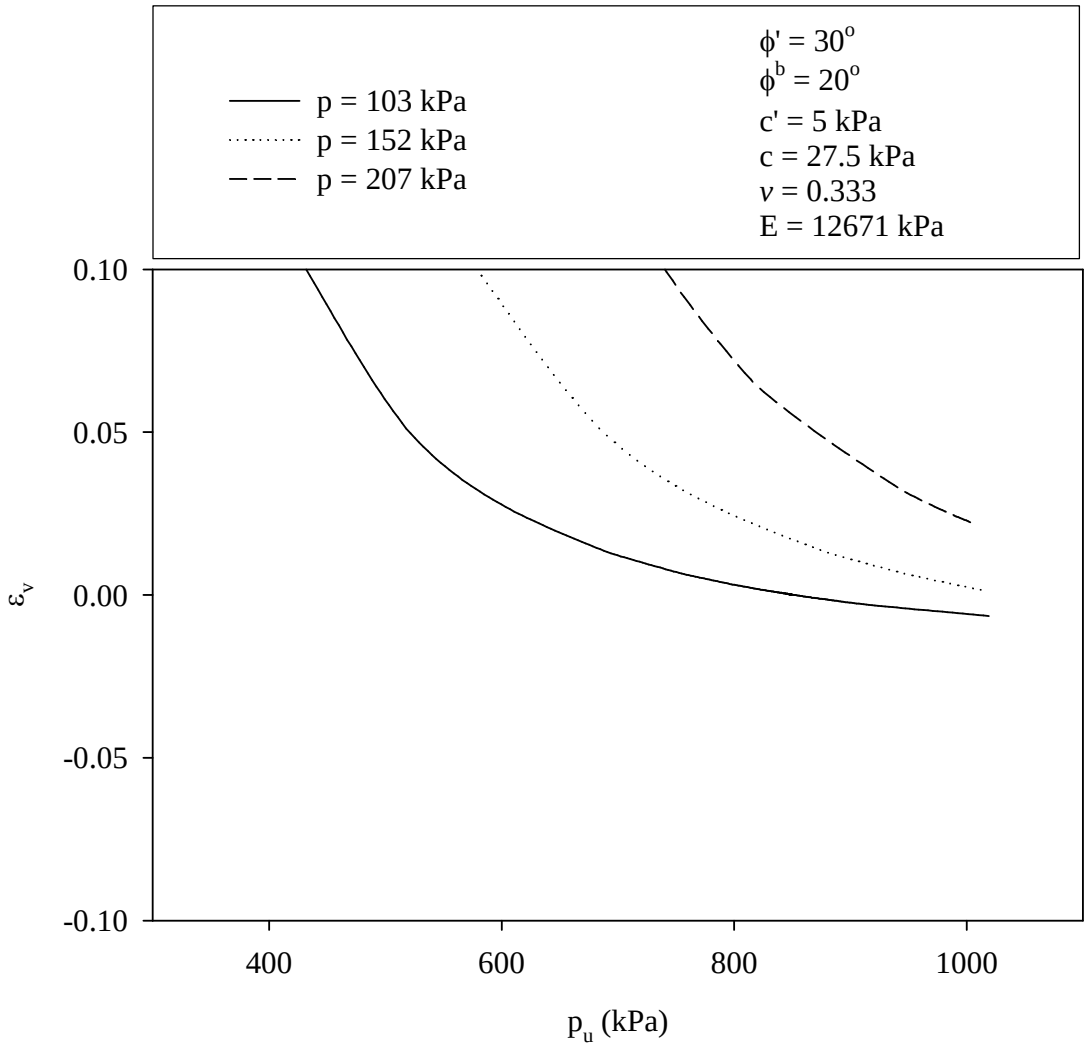

Figure 6-23: Sensitivity of ε_v of Cylindrical Cavity Expansion with Respect to p

Although, the term for matric suction ($(u_a - u_w)$ or ψ as used in the manuscript for this dissertation) was not observed in Equation 6-12 to Equation 6-17, it is a very important parameter in the prediction of p_u through its important role in the unsaturated soil shear strength. Many of the parameters used in Equation 6-12 to Equation 6-17 depend on ψ either directly or indirectly. Thus, the prediction of ε_v is much more complicated when the variation of ψ is taken into account. However, in the analyses some of the parameters were held constant. The influence of ψ on ε_v at various p_u is shown in Figure 6-24. It is observed that ε_v is relatively insensitive to ψ for a given p_u. It stays relatively constant throughout the range of ψ used in this study. The plot shows that for a given ψ, ε_v decreases with increasing p_u at a diminishing rate (i.e. for the same magnitude of increase in p_u, a greater decreases of ε_v is observed at low p_u compared to high p_u.) However, it is important to note that from the experimental data from MPMT, it is evident that p_u (i.e. P_L or q_c) increases with ψ. For that reason, ε_v will decrease as ψ increases, particularly for lower values of p_u.

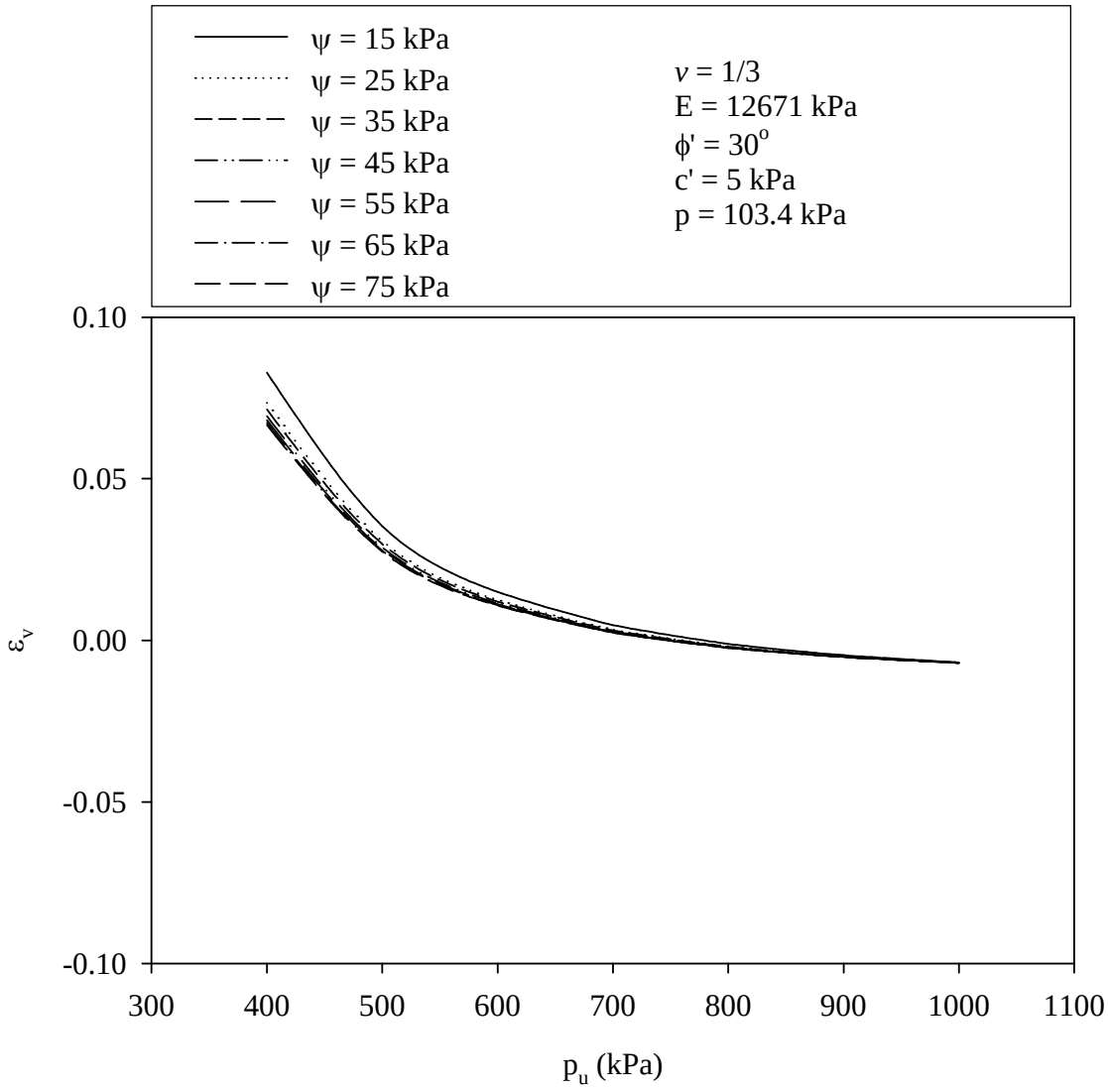

Figure 6-24: Sensitivity of ε_v of Cylindrical Cavity Expansion with Respect to ψ

Figure 6-25 shows a cross section through a cavity and surrounding soil with initial radius of cavity of R_i. At ultimate pressure (p_u) the plastic zone is defined by R_p, and ultimate radius of cavity is define by R_u, and u_p is the radial displacement of the outer plastic zone during the cavity expansion. For a cylindrical cavity the initial and ultimate volume of the plastic zone is defined as follow:

Initial volume of the plastic zone:

$$V_{p,i} = \pi h [(R_p - u_p)^2 - R_i^2] \quad \text{(Eq.6-24)}$$

Final volume of the plastic zone:

$$V_{p,f} = \pi h (R_p^2 - R_u^2) \quad \text{(Eq.6-25)}$$

where h is the length of the inflated portion of the probe.

Thus, the volumetric strain in the plastic zone (ε_v) can be expressed as:

$$\varepsilon_v = \frac{\Delta V}{V_{p,i}} = \frac{V_{p,f} - V_{p,i}}{V_{p,i}} = \frac{R_p^2 - R_u^2}{(R_p - u_p)^2 - R_i^2} - 1 \quad \text{(Eq.6-26)}$$

A sensitivity analysis of ε_v with respect to R_p/R_u at various values of u_p was conducted. In this part of study it was assumed that the ultimate radius of the cavity (R_u) is 1.52 cm, which is twice the MPMT probe radius. It is also assumed that the initial radius of the cavity (R_i) is equal to the radius of the MPMT probe, which is 0.76 cm. These values were selected because the P_L value is extrapolated from the MPMT pressure expansion curve when the volume of the cavity doubled its initial volume. Thus, the values are acceptable with the assumption that the radius of the borehole is equal to the radius of the MPMT probe. The parameter u_p used in the study is expressed in term of percentage of R_p (i.e. 0.1%, 0.2%, 0.4%, 0.8%, 1.6% and 3.2%). Figure 6-26 shows the

influence of R_p/R_u on ε_v at various u_p. Consistent with the sign convention used in soil mechanics, positive ε_v values represent compression and negative ε_v values represent dilation or expansion. It is observed that as the R_p/R_u ratio increases, the soil in the plastic zone experiences a transition from compression to dilation for larger values of u_p. It is also observed that the transition is more rapid as u_p increases. Therefore, it is possible for the soil to undergo either compression or dilation depending on the R_p/R_u ratio and the u_p values. The shaded regions in Figure 6-26 represents the range of back-calculated ε_v values for MPMT data subsequently presented in Section 6.5.3. It is observed that the soil in the plastic zone during the MPMT probe expansion undergoes mainly compression. Based on the range of back-calculated ε_v values for MPMT data and the plots in Figure 6-26, it appears that R_p/R_u and the radial displacement of the plastic zone (u_p) are relatively small. This is reasonable because the MPMT test used in this study is a pre-bored type; therefore, the radial displacement of soil in the plastic zone is relatively small due to the presence of a substantial existing cylindrical cavity prior to expansion.

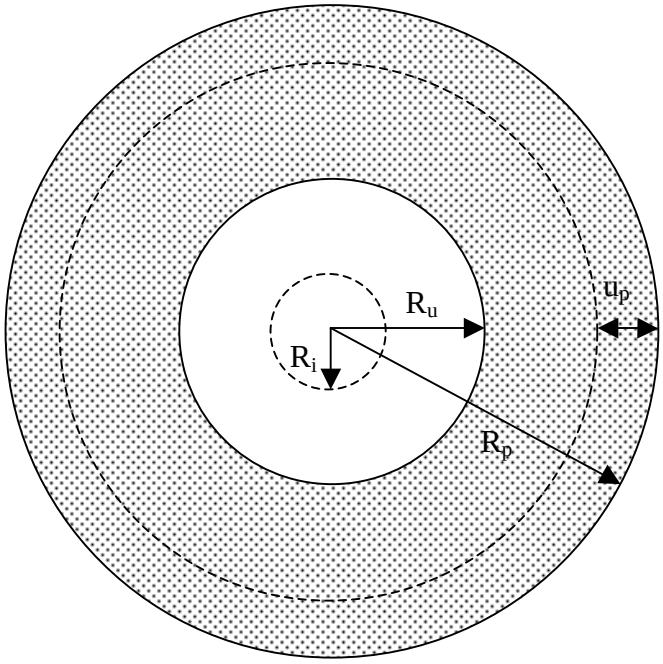

Figure 6-25: Expansion of Cavity (after Vesic 1972)

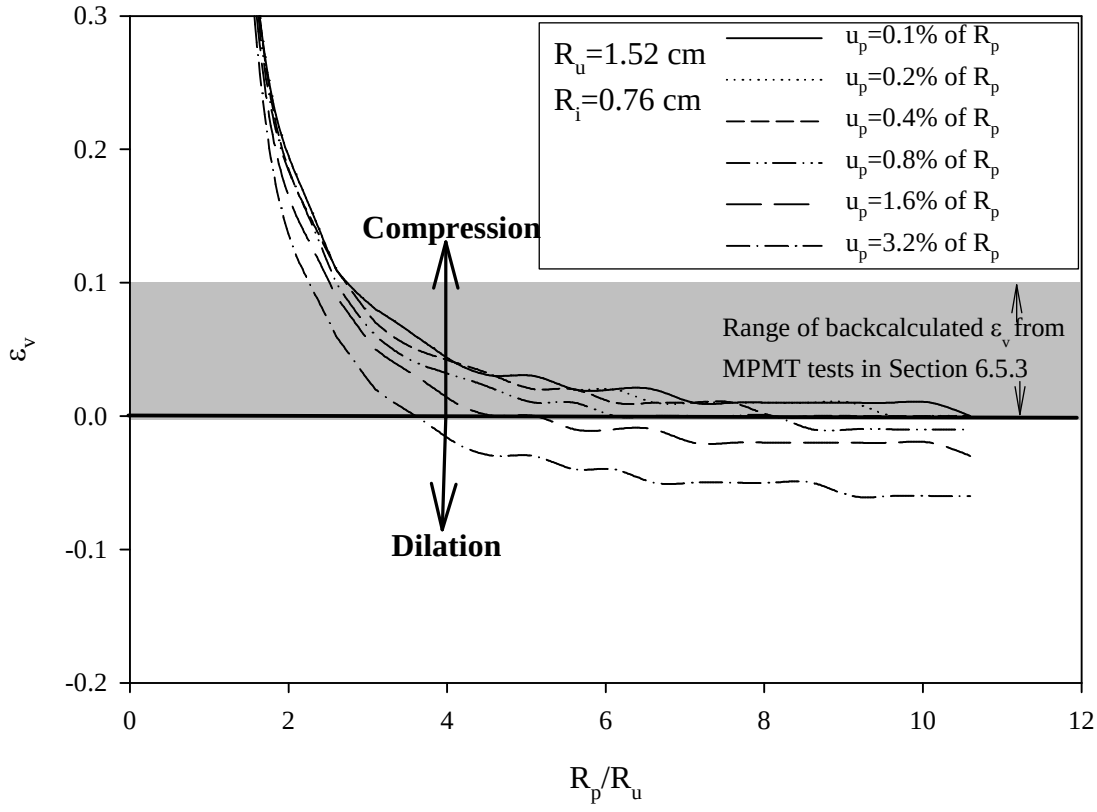

Figure 6-26: Sensitivity of ε_v to R_p/R_u Ratio of Cylindrical Cavity Expansion

6.5.2.2 Spherical Cavity Expansion

Similar sensitivity analyses were also done for the spherical cavity equation. Figures 6-27 to Figure 6-31 show the sensitivity of ε_v to E, ϕ', c, *v*, and ψ at various p_u, respectively. No sensitivity analysis was conducted on p since only one net normal stress (σ_n) were used in this study for MCPT testing. The range of each parameter used in the spherical cavity expansion sensitivity study is based on the range of values used in this study or based on the range of data obtained from the MCPT. Figure 6-27 shows the sensitivity of ε_v with respect to E. The main difference of this analysis from the cylindrical cavity expansion analysis is that for the given range of parameters used in this study, the soil generally is experiencing dilation (e.g., negative ε_v). It is observed that ε_v increases (i.e. decreasing in dilation) with increasing E. Similar to the observation made for cylindrical cavity expansion, for a given E, ε_v decreases rapidly as p_u increases. As for the sensitivity of ε_v to ϕ', c, *v* and p it is observed that generally the observations are similar to those made for cylindrical cavity expansion. However, due to scale differences in these plots (Figures 6-27 to 6-31) compared to the plots in Figures 6-19 to 6-24, the sensitivity of ε_v to ϕ', c, *v* and p is more apparent although the magnitudes are relatively small. It is observed that as ε_v increases with increasing ϕ' and p, and decreases with increasing c and *v*. Again by comparing Figures 6-27, 6-28, 6-29, and 6-30 it is observed that ε_v is most sensitive to p followed by E, ϕ', *v* and c. The influence of ψ on ε_v is shown in Figure 6-31. It is observed that ε_v increases towards zero with increasing ψ. This observation is justifiable since as ψ increases the unsaturated soils tend to be more rigid and thus would allow less deformation to occur. Similar to the observation made for cylindrical cavity expansion, ε_v is relatively sensitive to p_u and for a given ψ, ε_v

decreases with increasing p_u. Again from the MCPT experimental data, it is evident that p_u (i.e q_c) increases with ψ. Therefore, it is anticipated that ε_v will decrease with increasing ψ.

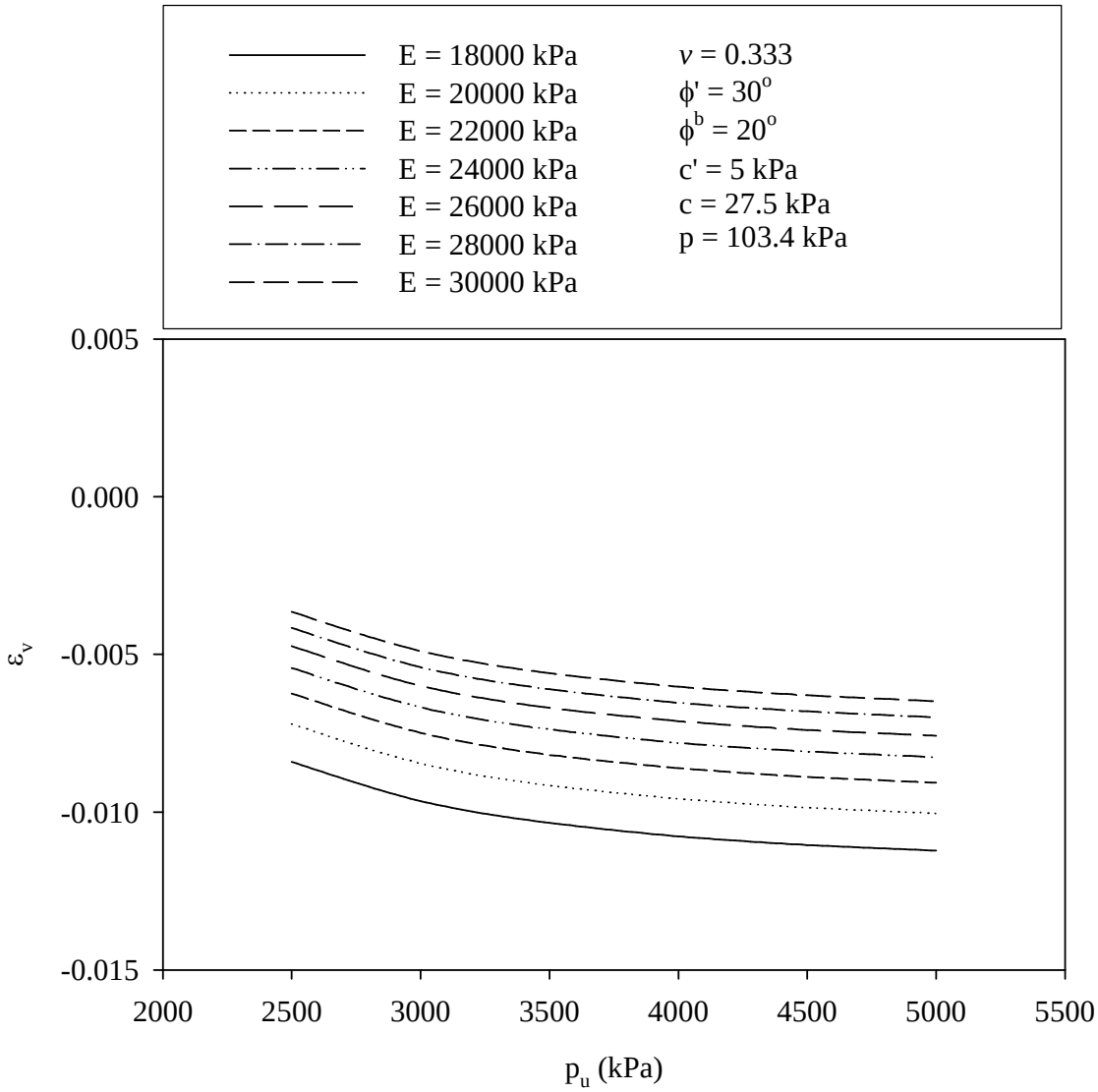

Figure 6-27: Sensitivity of ε_v of Spherical Cavity Expansion with Respect to E

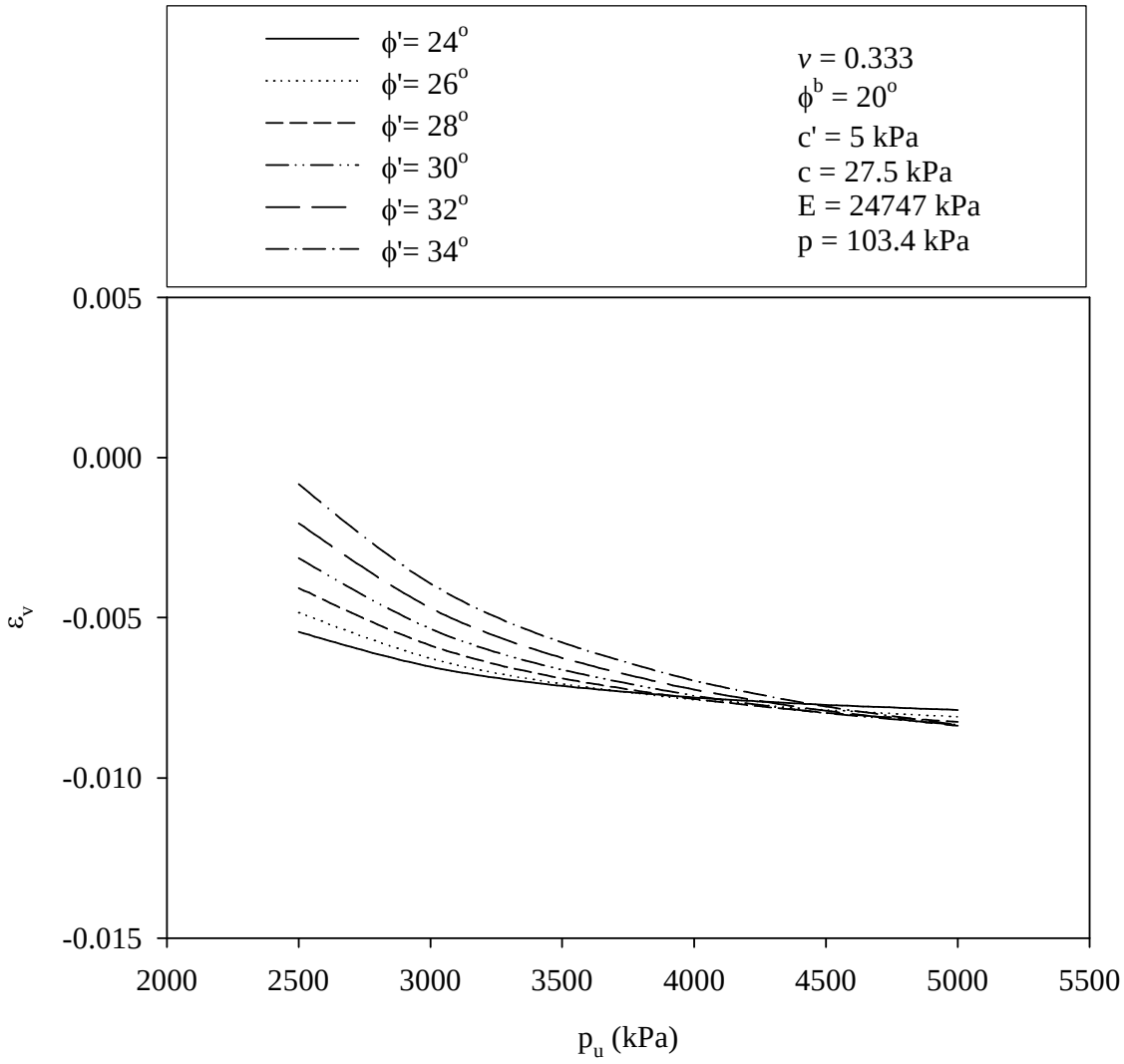

Figure 6-28: Sensitivity of ε_v of Spherical Cavity Expansion with Respect to ϕ'

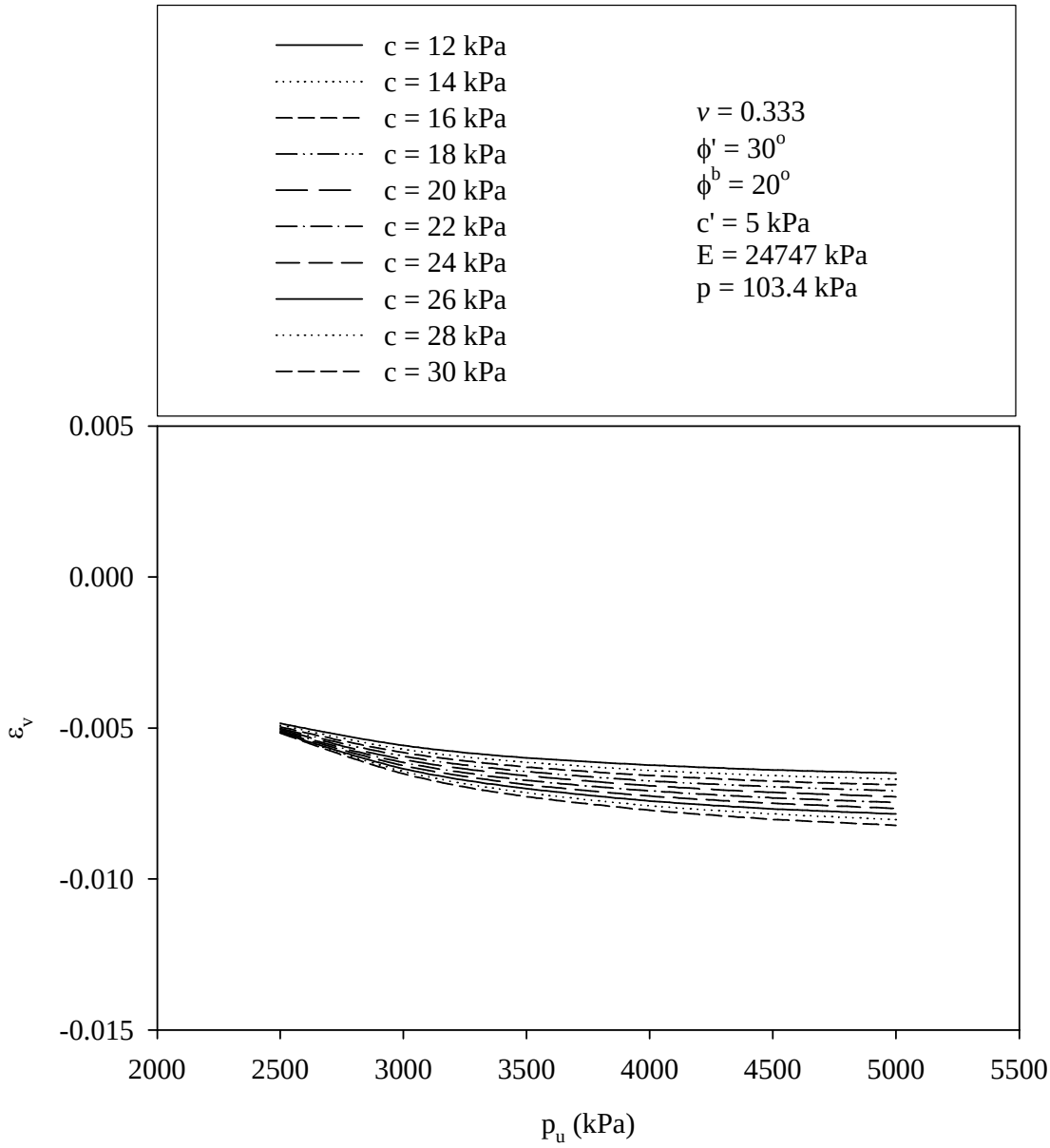

Figure 6-29: Sensitivity of ε_v of Spherical Cavity Expansion with Respect to c

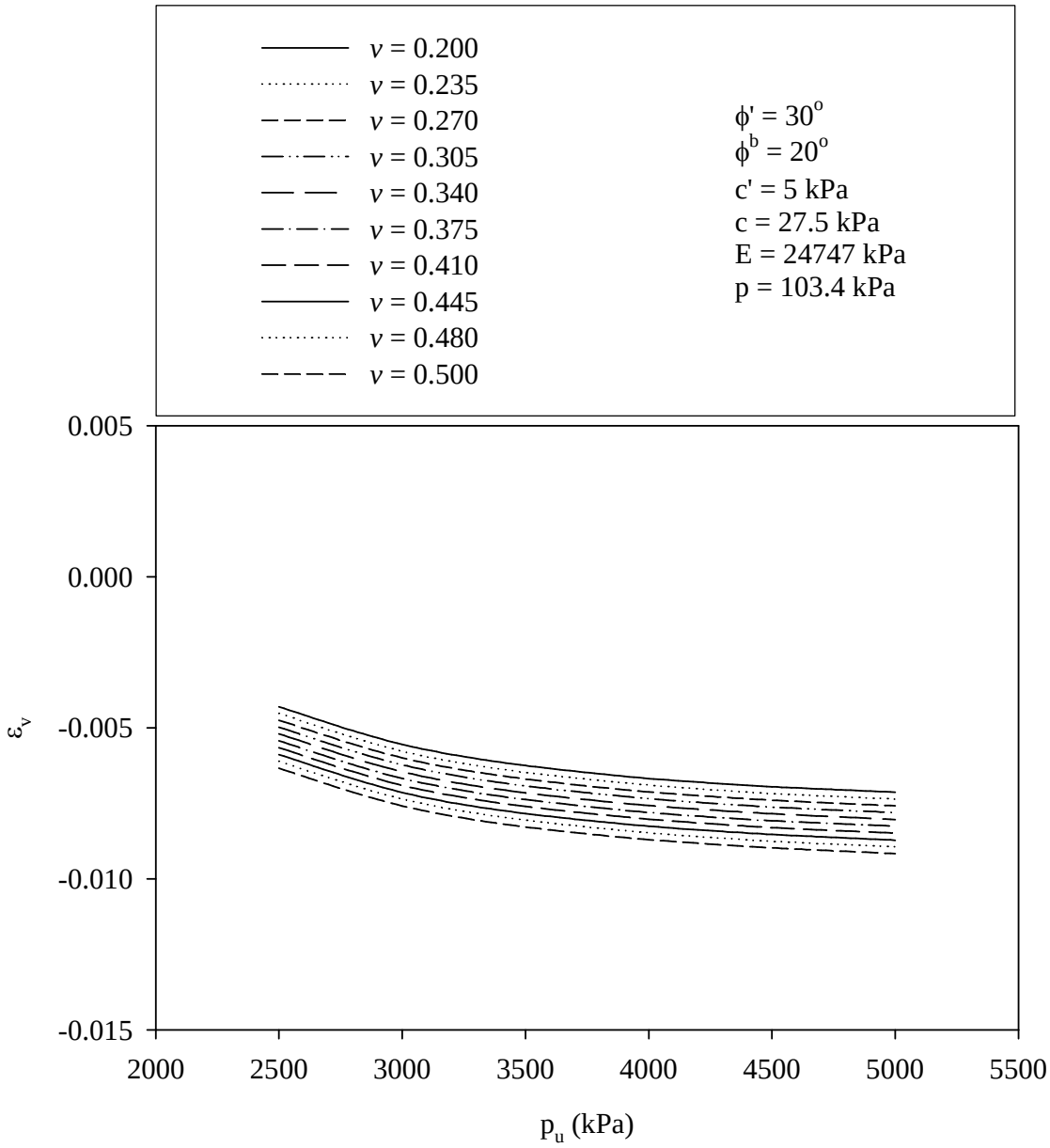

Figure 6-30: Sensitivity of ε_v of Spherical Cavity Expansion with Respect to *ν*

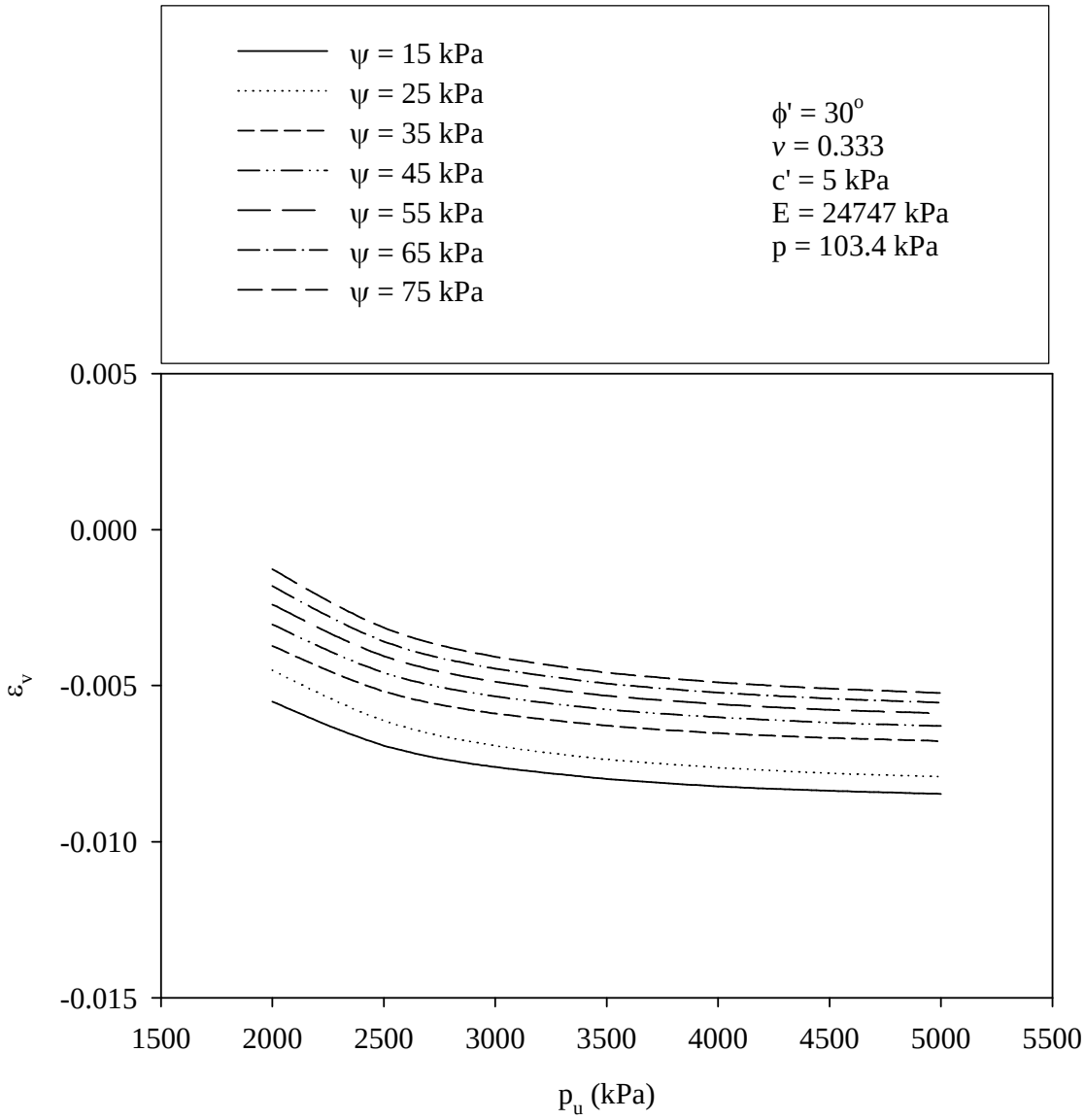

Figure 6-31: Sensitivity of ε_v of Spherical Cavity Expansion with Respect to ψ

Based on Figure 6-25, the spherical initial and ultimate volume of the plastic zone and the volumetric strain in the plastic zone (ε_v) can be expressed as follows:

Initial volume of the plastic zone = $V_{p,i} = 4/3\ \pi\ [(R_p - u_p)^3 - R_i^3]$ (Eq.6-27)

Final volume of the plastic zone = $V_{p,f} = 4/3\ \pi\ [(R_p^3 - R_u^3]$ (Eq.6-28)

Volumetric strain in the plastic zone:

$$\varepsilon_v = \frac{\Delta V}{V_{p,i}} = \frac{V_{p,f} - V_{p,i}}{V_{p,i}} = \frac{R_p^3 - R_u^3}{(R_p - u_p)^3 - R_i^3} - 1 \qquad \text{(Eq.6-29)}$$

A sensitivity analysis of ε_v with respect to R_p/R_u at various values of u_p was conducted. In this part of study it was assumed that the ultimate radius of the cavity (R_u) is 0.89 cm, which is the radius of the MCPT cone. It is also assumed that the initial radius of the cavity (R_i) is equal to the 0.00 cm since no prebored hole was made for the MCPT. Thus, the values selected are considered reasonable. The parameter u_p used in this part of the study is also expressed in terms of percentage of R_p (i.e. 0.1%, 0.2%, 0.4%, 0.8%, 1.6% and 3.2%). Figure 6-32 shows the influence of R_p/R_u on ε_v at various u_p. The sign conventions for ε_v remain the same as discussed earlier. It is observed that as the R_p/R_u ratio increases, the soil in the plastic zone experiences a transition from compression to dilation for a given u_p. It is also observed that the transition is more rapid as u_p increases. The shaded region in Figure 6-32 represents the range of back-calculated ε_v values for MCPT data presented subsequently in Section 6.5.4. It is observed that the soil in the plastic zone during the MCPT probe expansion undergoes mainly dilation. It is reasonable to conclude that R_p/R_u and the radial displacement of the plastic zone (u_p) are relatively large since the penetration of the MCPT probe involves full displacement of soil to create the ultimate cavity volume. Therefore, based on Figure 6-32 it is anticipated

that the soil in the plastic zone primarily undergoes dilation during the penetration of the MCPT probe.

The comparison of Figure 6-26 and Figure 6-32 reveals that for a given u_p, ε_v approaches a negative value more rapidly in the spherical cavity expansion than in the cylindrical cavity expansion as R_p/R_u increases. This is because for the same magnitude of radial displacement in the plastic zone, the magnitude of volume change in the plastic zone is larger for the spherical cavity relative to the cylindrical cavity.

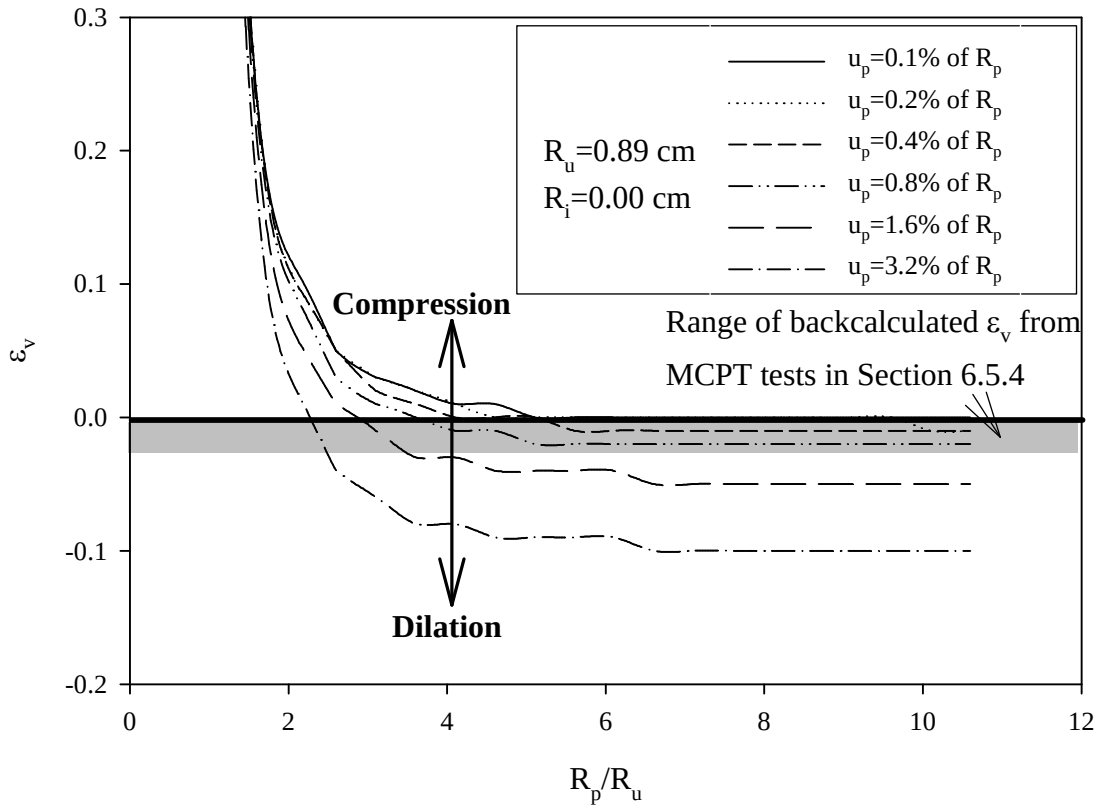

Figure 6-32 Sensitivity of ε_v to R_p/R_u Ratio of Spherical Cavity Expansion

6.5.3 Analyses of MPMT Data with Cylindrical Cavity Expansion Equations

It is generally accepted that cylindrical cavity expansion can be used for the interpretation of PMT data provided the length of the expanding portion of the probe is sufficiently long such that the soil deformation simulates plane strain conditions with zero vertical strain (Wood and Wroth 1977, Ladanyi 1972, Baguelin et al. 1972, Palmer 1972, and Coutinho 1990). The reduced form of the cylindrical cavity expansion equations developed by Muraleetharan et al. (1998) were used in this study for the analysis of MPMT test data along with the assumptions stated earlier in Section 6.5. Figure 6-33 shows back calculated ε_v for the MPMT data versus ψ for data group C and G1 and Figure 6-34 shows the back calculated ε_v for the MPMT data versus ψ for data group G2. Both figures show that ε_v decreases with increasing ψ. This is reasonable since at higher matric suction, the soil beds tend to be more rigid. It is also important to note that all the values obtained for ε_v are positive values, which indicates that the soil in the plastic zone undergoes compression during the expansion of the MPMT probe. The MPMTs were conducted in a prebored borehole; thus, the radial displacement in the plastic zone and the R_p/R_u ratio are anticipated to be relatively small. Based on the sensitivity analysis for the cylindrical cavity expansion equations in Section 6.5.2 it is reasonable to expect the soil in the plastic zone to compress during the expansion of the cavity, which is consistent with the results observed here.

Figure 6-33 shows that the effects of the soil processing method on ε_v are quite significant. The back calculated ε_v from MPMT tests conducted in soil beds where the soil was processed by the crusher (i.e. data set group C) tends to be significantly lower and insensitive to variations of matric suction. ε_v stays relatively constant at about 0.01

through the entire range of matric suction used in this study. This observation is reasonable since the P_L values obtained from data set group C are generally much higher than those from data set group G1 (i.e. MPMT tests conducted in soil beds where the soil was processed by the grinder). The sensitivity analysis shows that changes in ε_v are more significant at lower p_u (i.e. P_L) compared to higher p_u for similar change in p_u (i.e. Δp_u). The sensitivity analysis also shows that ε_v decreases as p_u increases. Since the P_L values obtained from data set group C are relatively greater than those from data set group G1, it is reasonable that the ε_v for data in group C to be relatively small and falling within a very small range. These observations are illustrated by Figure 6-35. Figure 6-35 shows the reproduction of Figure 6-23 along with the range of P_L values obtained from data set group C and G1 and the corresponding possible range of ε_v values. It is observed that the possible range of ε_v values for data set group G1 is relatively greater than data set group C.

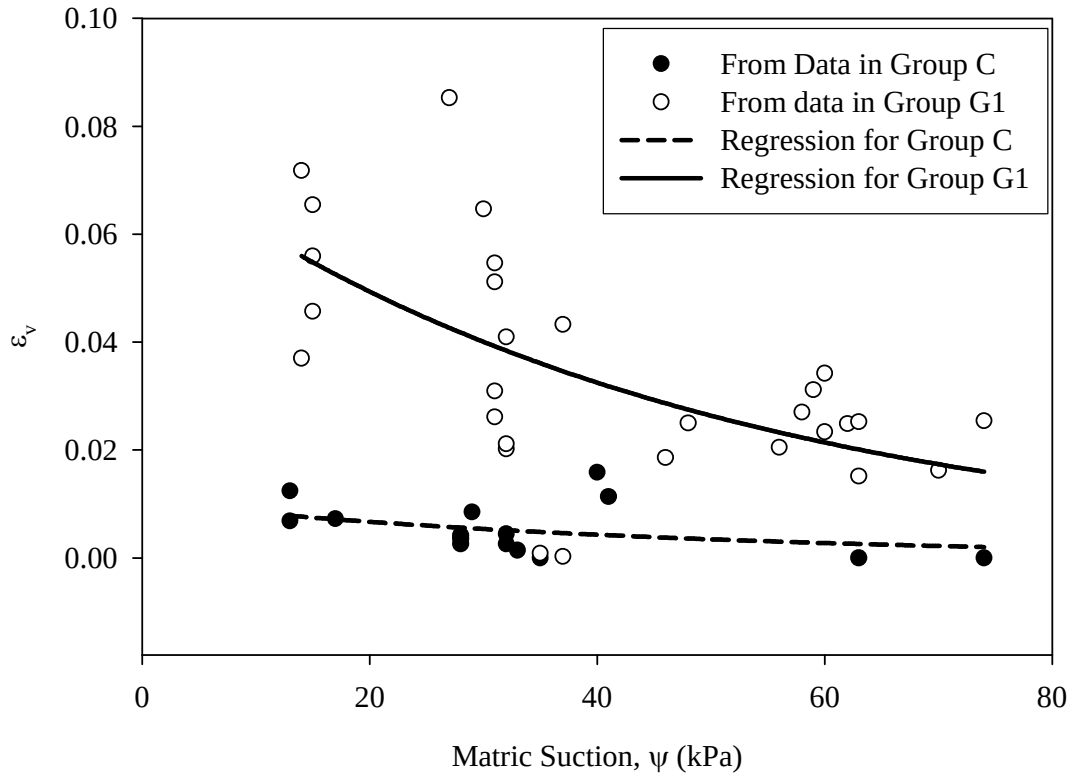

Figure 6-33: Back Calculated ε_v vs. ψ at σ_n of 103 kPa

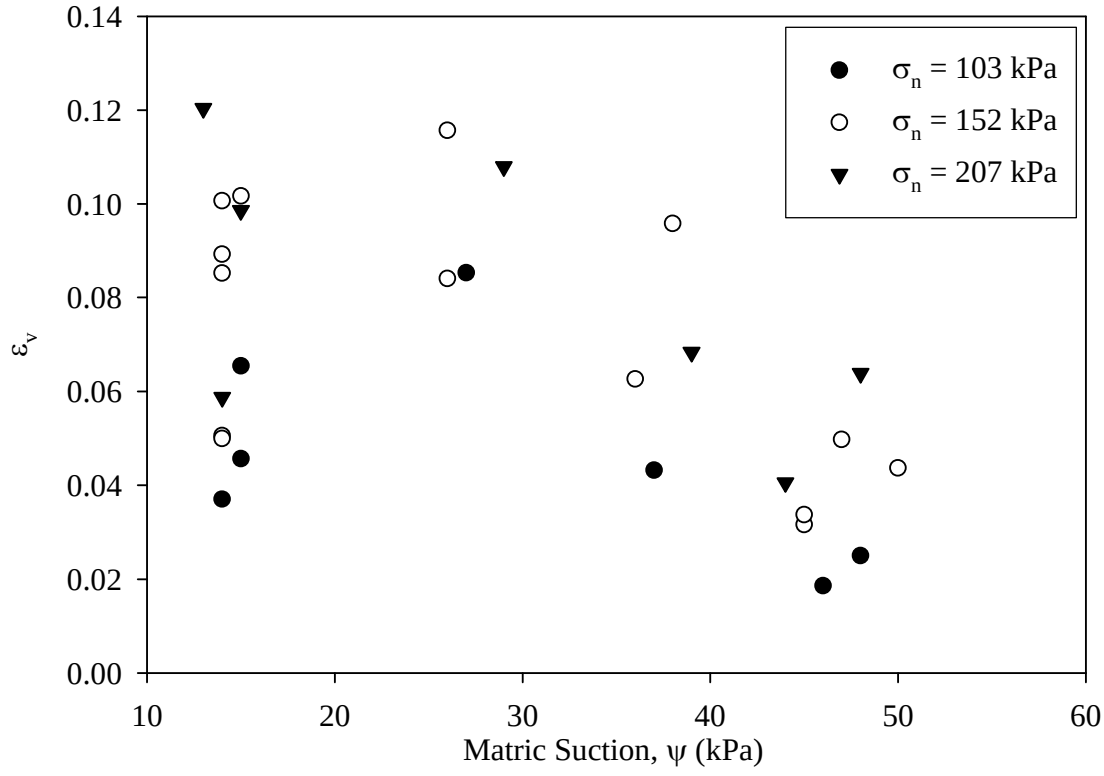

Figure 6-34: Back Calculated ε_v vs. ψ at various σ_n

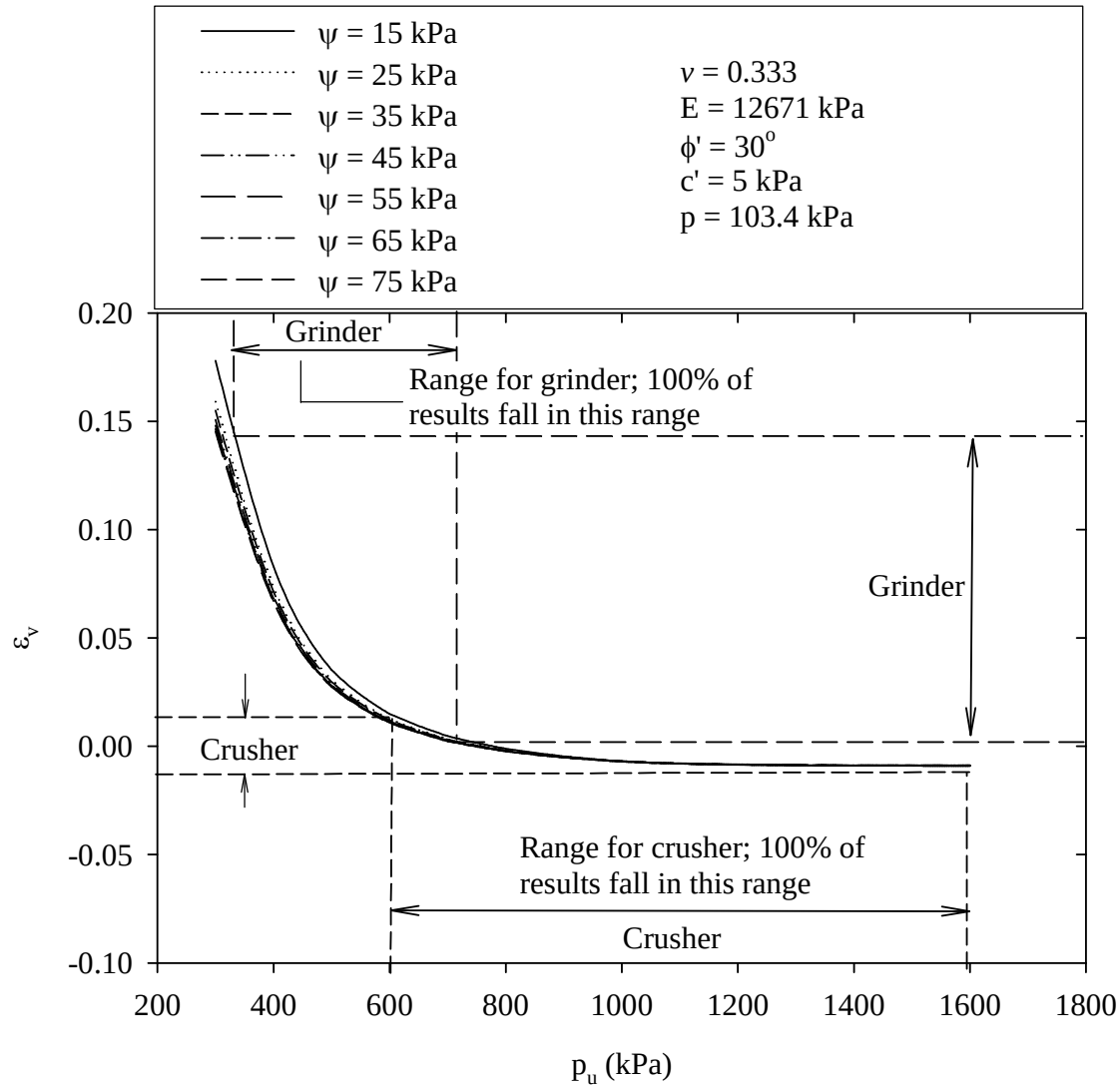

Figure 6-35: Sensitivity of ε_v of Cylindrical Cavity Expansion with Respect to ψ along with range of P_L values for data set groups C and G1

There are two possibilities that made the soil processing method an important factor in this study. One is the effect of soil processing method on the fabric of the soil beds prepared and the other is the significant difference in the γ_d of the soil beds prepared by the two methods. The paragraph that follows discusses both of these possibilities.

Although, in both of the soil processing methods the soil was pulverized and passed a #10 sieve (2 mm), the soil processed by the crusher tends to have more dry clumps in comparison to those processed by the grinder. It is speculated that within each clump of soil, there is already some bonding between the particles. The clumps also reduce the total surface area available when water is introduced into the mixture. Thus, during the soil-water mixing and curing process, the water may not fully penetrate into the clumps. Therefore, the soil particles in the middle of the clumps tend to be dryer yet the soil beds produced gave the same apparent matric suction as the soil beds with soil processed by the grinder. However, at the microscopic level the matric suction within each clump tends to be higher. As a result, it tends to be stronger and more rigid. So lower back calculated ε_v values for soil beds processed with crusher compared to those processed by grinder are reasonable. This also helps to explain the higher P_L values for MPMT tests conducted in soil beds where the soil was processed by the soil crusher. Another factor is the range of γ_d of the prepared soil beds. It is observed in Figure 6-6 that a majority of the soil beds where the soil was processed by crusher have higher γ_d. Therefore, again it is reasonable that the soil beds prepared tend to be more rigid and thus would result in lower ε_v.

Figure 6-34 shows the back calculated ε_v versus ψ at various σ_n. It is observed that generally ε_v decreases with increasing ψ for any given σ_n with the exception of ψ less than 20 kPa. Again, this inconsistency most likely be due to variation in γ_d of the soil beds, which affected P_L and the back-calculated ε_v (see Section 6.2.3). Figure 6-34 shows that for a given ψ, ε_v tends to increase with increasing σ_n. In the cavity expansion equations for unsaturated soil presented in Section 6.5, σ_n is represented by the notation p

which is the mean net normal stress. Mathematically, based on the cavity expansion equation for unsaturated soil, it is reasonable for ε_v to decrease with increasing p. This is because the rigidity index (I'_r), which is the ratio of shear modulus (G) of the soil to its initial shear strength (s), decreases with increasing p (see Equations 6-16 and 6-23 and Figure 6-23). The same observation has also been noted by Vesic (1977). As a result, a decrease in I'_r would lead to a decrease in the reduced rigidity index (I'_{rr}) for a given ultimate pressure (p_u), which would results in an increase of ε_v. Therefore, it is reasonable for ε_v to increase with increasing p (or σ_n).

From a physical point of view, one of the possibilities is that as p increases, the outer boundary (i.e. the elastic zone) becomes relatively more rigid and thus there is less give in that zone during the expansion of the cavity. Therefore, the soil in the plastic zone would then seem to be relatively less rigid. As a consequence more compression would occur within the plastic zone during the cavity expansion as p increases. Therefore, it is logical that ε_v increases as p (σ_n) increases.

There are several explanations for the scatter in the back-calculated ε_v. The modulus of elasticity is one of the input parameters required in the unsaturated soil cavity expansion equations. In this analysis it is assumed that it is equivalent to the pressuremeter modulus (E_P). As presented earlier in Figure 6-11 in Section 6.2.3 the plots for E_P are quite scattered.

6.5.4 Analyses of MCPT Data with Spherical Cavity Expansion Equations

As discussed in Chapter 2, spherical cavity expansion is more commonly used for the CPT data analysis. In this study the reduced form of the spherical cavity expansion equations developed by Muraleetharan et al. (1998) were used for the analysis of MPMT

test data along with assumptions stated earlier in Section 6.5. Figure 6-36 shows back calculated ε_v for the MCPT data versus ψ. It shows that ε_v decreases with ψ. Again, this is reasonable since at higher ψ, the soil beds tend to be more rigid. It is observed that all the values obtained for ε_v are negative, which indicates that the soil in the plastic zone undergoes dilation during the spherical cavity expansion. Since the cone was pushed into the soil bed directly, the displacement of soil involved is significant since the cavity expanded from zero initial radius to the radius of the cone tip itself. Thus, it is anticipated that the radius of the plastic zone, R_p/R_u and the radial displacement in the plastic zone (u_p) are relatively large. Hence, it reasonable for the soil in the plastic zone to dilate during the MCPT testing based on the sensitivity analysis for spherical cavity expansion discussed in Section 6.5.2. This also helps to explain why q_c is much greater than P_L in similar soil.

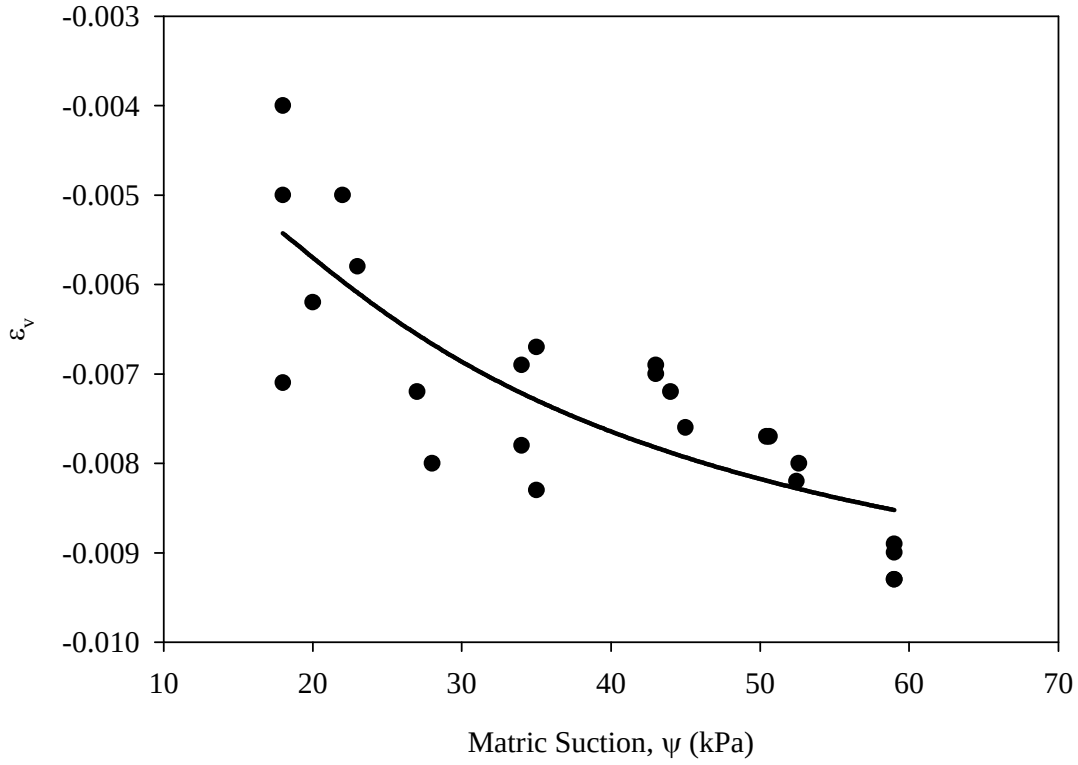

Figure 6-36: Back Calculated ε_v vs. ψ at σ_n of 103 kPa

6.5.5 Methods for Interpretation of in Situ Test in Unsaturated Soil

This section discusses a possible method for interpretation of in situ tests in unsaturated soil by utilizing the cavity expansion equations for unsaturated soil. For illustration purposes the PMT is used as the example to illustrate the method of interpretation. The same method is applicable to interpret both PMT and CPT data. As discussed in Section 6.5.3 it is evident that the back-calculated ε_v is strongly dependent on P_L. It is also observed that ε_v increases with increasing P_L. Hence, a series of model curves are included in the ε_v versus ψ plots obtained from this study based on the range of P_L values, and at σ_n of 103 kPa (see Figure 6-37). Only the curve for P_L equal to 400

kPa was developed by using a best fit regression method. The remaining curves were developed by using the same equation obtained from the regression and by adjusting the coefficients of the parameters involved. In developing the series of curves it is assumed that the soil processing method is not significant other than the influence of γ_d and P_L. Similar curves can also be developed for the CPT.

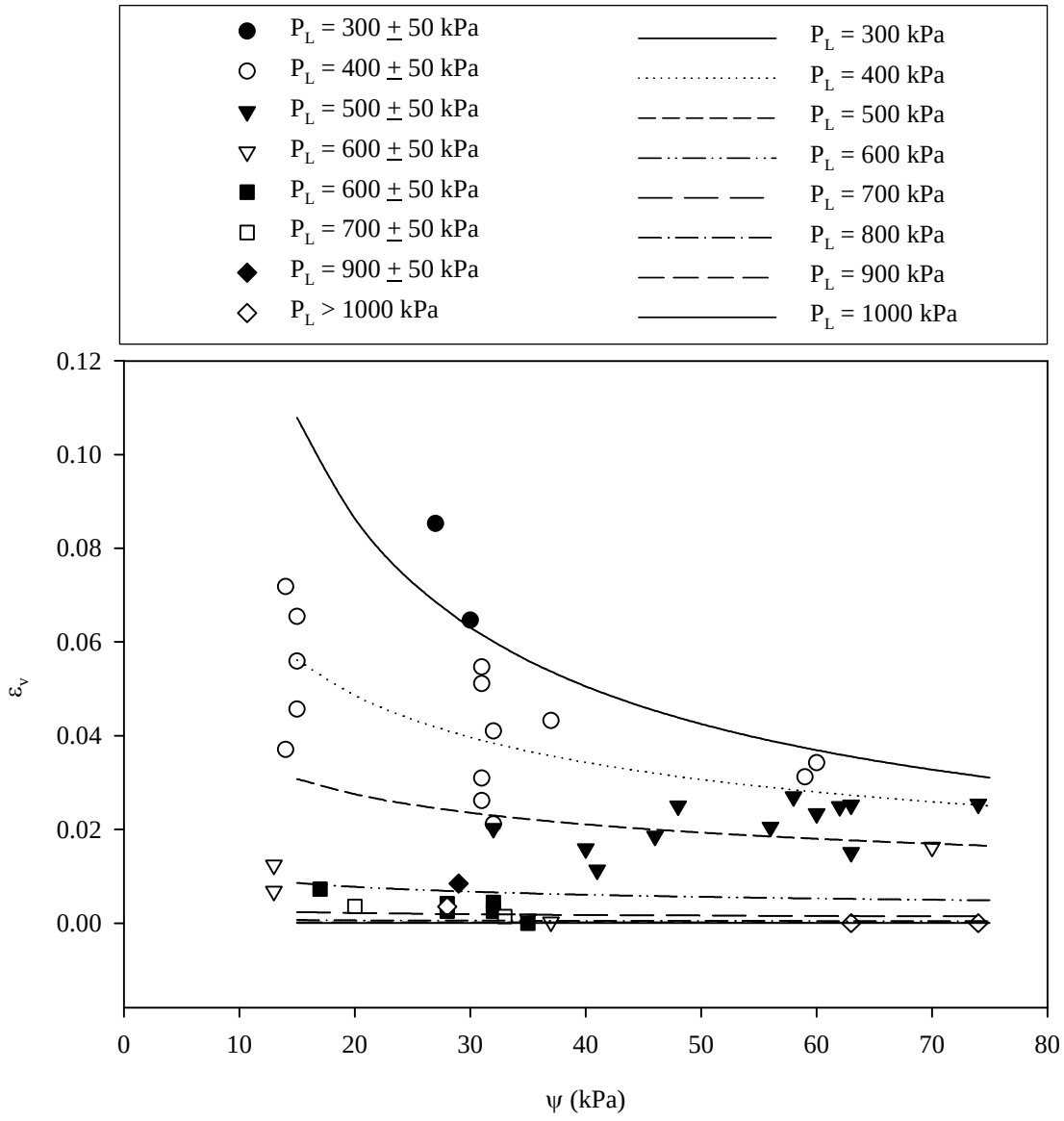

Figure 6-37: Series of ε_v versus ψ plots for given P_L and at σ_n of 103 kPa

Figure 6-38 shows pre-bored pressuremeter (PMT) field test results in unsaturated Minco Silts from Miller and Muraleetharan (2000). The field data shows similar trends as observed for MPMT tests in the calibration chamber where P_L generally increases with ψ. In this study, data from one (i.e. at ψ of 48 kPa) of the four tests were used to estimated the remaining three P_L at various ψ (i.e. at ψ of 16, 28 and 56 kPa) by using the cylindrical cavity expansion equations for unsaturated soil and the ε_v versus ψ curves in Figure 6-37 along with the corresponding correction factor from Figure 6-39.

Since the field test was conducted at approximately 1 m below the ground surface, it is estimated that the $\sigma_{n,field}$ is approximately 17 kPa. In contrast, the curves developed in Figure 6-37 were based on σ_n of 103 kPa. In addition, as discussed earlier in Section 6.5.2.1, ε_v is relatively sensitive to the variation of σ_n. Figure 6-23 shows that for a given p_u, ε_v increases with increasing p (i.e. σ_n). Therefore, a correction factor is needed for the ε_v obtained from Figure 6-37 if the $\sigma_{n,field}$ is estimated to be other than 103 kPa. Figure 6-39 shows the curves of correction factors at various σ_n for a given p_u. It is meant to be used together with Figure 6-37.

First, the ε_v value for the field pressuremeter test conducted at ψ of 48 kPa was determined by using the chart (Figure 6-37) and the ε_v obtained from the chart was multiplied by the appropriate correction factor from Figure 6-39. Assuming P_L equal to p_u, the cylindrical cavity expansion equations for unsaturated soils were then calibrated. The equations are calibrated by adjusting the parameters (i.e. ϕ', ϕ^b, E, ν, p and c) in the equations such that it will give an ε_v that agrees with the ε_v obtained from the chart. ϕ', ϕ^b, E and c can be estimated based on laboratory test results and p

can be estimated by multiplying the nominal total unit weight of the soil on the site by the test depth. Since the equations are relatively insensitive to *v*, *v* is assumed to be 0.333. It is also important to keep the magnitude for the parameter (i.e. ϕ', ϕ^b, E, *v*, p and c) within a reasonable range during the calibration process for a given soil type.

Then by using the calibrated cavity expansion equations for unsaturated soil, the P_L corresponding to various ψ were estimated. Table 6-13 gives the calibrated parameters used in the analysis. Figure 6-38 also shows the comparison between the $P_{L,field}$ and $P_{L,estimated}$. It is observed that $P_{L,estimated}$ was generally overestimated by roughly 10-25% compared to the $P_{L,field}$. Beside the many assumptions involved there are several reasons that might have contributed to this discrepancy such as the stress history and anisotropy of field conditions. However, this method has demonstrated a very promising approach for estimating P_L to due seasonal changes in suction (i.e change in ψ due to wetting and drying of soil).

Table 6-13: Summary of Calibrated Parameters Used in the Analysis of Interpretation of PMT Results in Unsaturated Soil

ε_v[1]	Correction Factor[2]	ε_v corrected	ϕ'	ϕ^b	E	*v*	p	c'
0.1026	0.0219	0.0022	35	30	12671	0.333	17	5
0.0666	0.0219	0.0015	35	30	12671	0.333	17	5
0.0313	0.0219	0.0007	35	20	12671	0.333	17	5
0.0290	0.0219	0.0006	35	20	12671	0.333	17	5

[1] From Figure 6-37
[2] From Figure 6-39

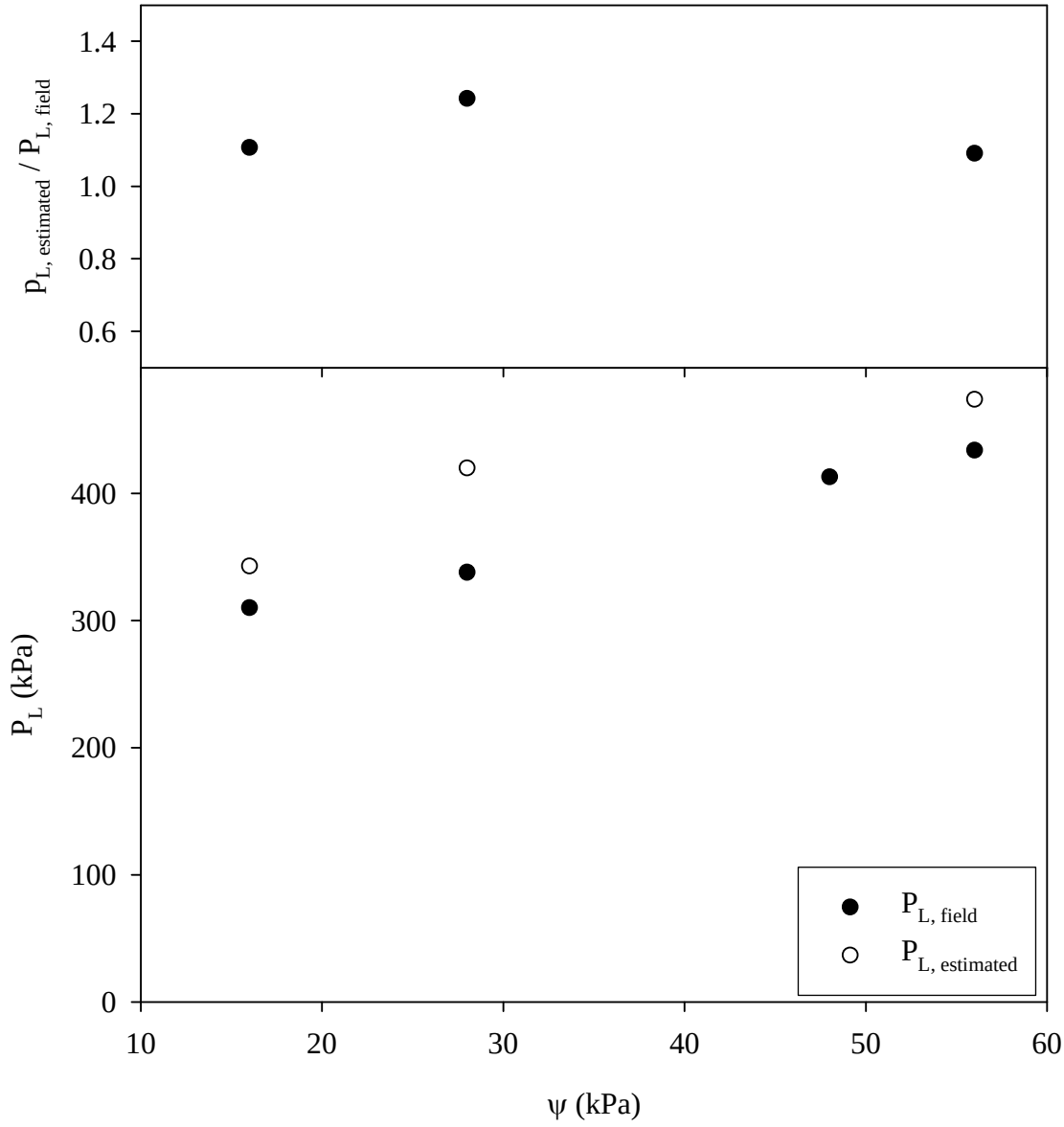

Figure 6-38: $P_{L,field}$, $P_{L\ estimated}$ and Ratio of $P_{L, estimated}$/ $P_{L, field}$ Versus ψ

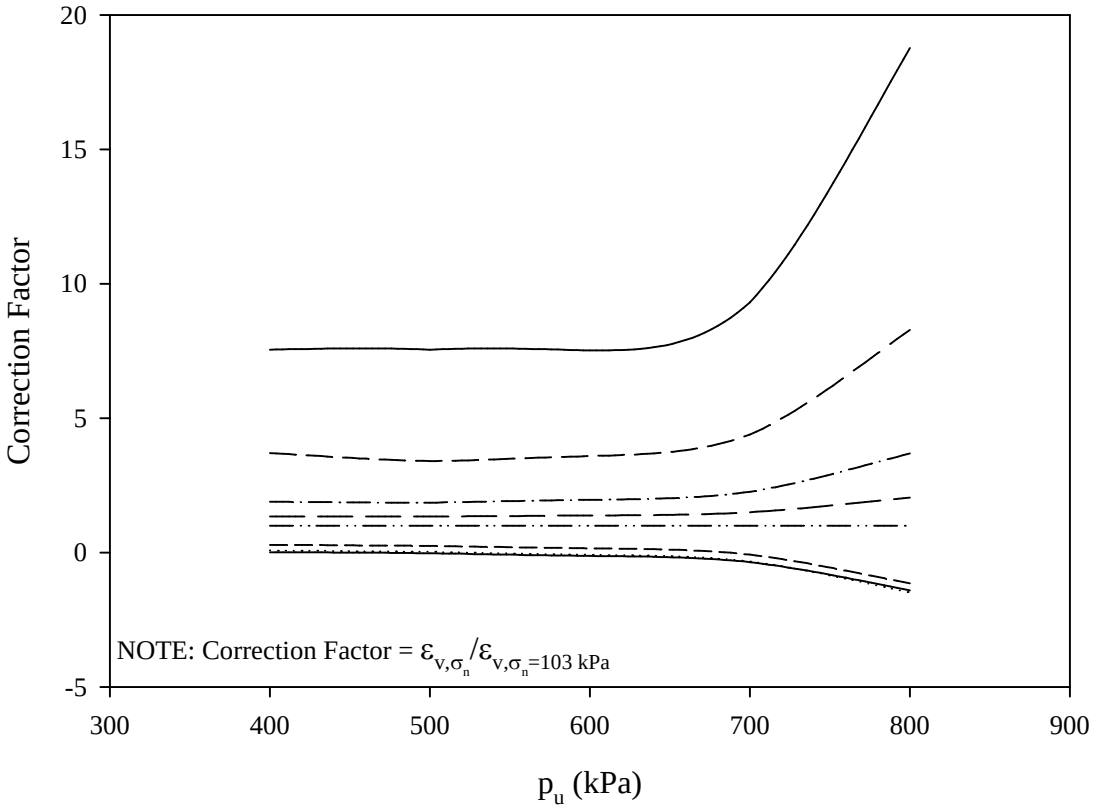

Figure 6-39: Correction Factors for ε_v (to be used together with chart on Figure 6-37)

Chapter 7: Conclusions and Recommendations

7.1 Major Contributions of the Research

In this study, the influence of matric suction (ψ) on the Pressuremeter Test (PMT) and Cone Penetrometer Test (CPT) in unsaturated soil was studied via calibration chamber testing with unsaturated Minco Silt. In addition, the effect of variation of dry unit weight (γ_d) was examined in the study. The data obtained from the calibration chamber were analyzed statistically and utilized together with cavity expansion equations for unsaturated soil to examine the volumetric strain of soil in the plastic zone surrounding the PMT and CPT. Following are the major contributions of this research.

1. Provided a data set showing the influence of matric suction (ψ) on pressuremeter test results, including the Limit Pressure (P_L), Pressuremeter Modulus (E_P) and Unload-Reload Modulus (E_R).
2. Provided a data set showing the influence of matric suction (ψ) on the tip resistance (q_c) of a cone penetrometer.
3. Demonstrated the significance of soil processing methods on pressuremeter test results.
4. Demonstrated the significance of matric suction (ψ), dry unit weight (γ_d) and net normal stress (σ_n) on P_L, E_P and E_R via statistical analyses.
5. Demonstrated the significance of matric suction (ψ) and dry unit weight (γ_d) on q_c via statistical analyses.

6. Provided empirical correlations for P_L, E_P and E_R as functions of ψ for a given γ_d, and σ_n.

7. Provided empirical correlations for q_c as a function of ψ for a given γ_d at σ_n of 103 kPa.

8. Developed relationships between volumetric strain (ε_v) in the plastic zone and ψ during cavity expansion in unsaturated soil by utilizing the calibration chamber test data and cavity expansion equations for unsaturated soils developed by Muraleetharan et al. (1998).

9. Developed a framework for a possible method of interpretation for PMT and CPT tests in unsaturated soil by utilizing the cavity expansion equations for unsaturated soil.

7.2 Conclusions Based on Experimental Observations

Following are the conclusions based on the experimental observations during calibration chamber testing with the miniature pressuremeter (MPMT) and miniature cone penetrometer (MCPT) in unsaturated Minco Silt beds.

1. For flexible wall calibration chamber testing, the following soil bed to test probe diameter ratio ($d_{soil\ bed}$ / $d_{test\ probe}$) was sufficient to minimize the boundary effects.
   a. MPMT: $d_{soil\ bed}$ / $d_{MPMT\ probe}$ = 48
   b. MCPT: $d_{soil\ bed}$ / $d_{MCPT\ probe}$ = 34

2. The unsaturated soil beds prepared in the calibration chamber were relatively homogeneous horizontally, heterogeneous with depth within each layer but similar from layer to layer.
3. Soil processing methods influenced the results of the MPMT, especially the P_L and E_P. Generally, the P_L and E_P for soil beds processed with a crusher tended to be higher than those processed by the soil grinder. While both methods produced dry soil that passed a #10 sieve (2 mm), the soil processed by the crusher tended to be coarser. The resulting differences in fabric and dry unit weight appeared to affect the PMT results. However, for E_R the effect of soil processing methods appeared less significant.
4. γ_d, σ_n, and ψ of soil beds had a significant influence on the MPMT results. P_L, E_P and E_R generally increased with increasing γ_d, σ_n and ψ, which is consistent with expectations based on unsaturated soil mechanics theory.
5. γ_d and ψ of soil beds had a significant influence on the MCPT results where q_c tended to increase with increasing γ_d and ψ, which is consistent with expectations based on unsaturated soil mechanics theory. However, the influence of γ_d appeared not so pronounced as for PMT (P_L) test results.

7.3 Conclusions Based on Statistical Analyses

1. Statistical analyses confirmed that the effects of soil processing methods on MPMT results are significant, especially for P_L and E_P.
2. Generally, the statistical analyses confirmed that the influence of ψ, γ_d, and σ_n on P_L, E_P and E_R are significant.

3. Statistical analysis confirmed that the influence of ψ on q_c was significant. Results were inconclusive regarding γ_d.

7.4 Conclusions Regarding Cavity Expansion Theory for Unsaturated Soils

1. The study of cylindrical cavity expansion equations for unsaturated soil using the MPMT data indicated that:
    a. soil in the plastic zone around the PMT probe most likely undergoes compression during the expansion,
    b. ε_v decreased with increasing ψ, and
    c. ε_v decreased with increasing P_L.
2. The study of spherical cavity expansion equations for unsaturated soil using the MCPT data indicated that:
    a. soil in the plastic zone around the CPT probe undergoes dilation during the probe penetration,
    b. ε_v decreased with increasing ψ, and
    c. ε_v decreased with increasing q_c
3. The method of interpretation of PMT and CPT tests in unsaturated soil presented in this study showed that the cavity expansion equations can be applied to interpretation of PMT and CPT tests in unsaturated soil. It also suggested that the approach presented is very promising since predictions are within 25% of actual field values.

7.5 Recommendations

1. Develop a more efficient method for soil bed preparation, which would give a better control over the γ_d of the soil beds.
2. Since the soil beds were prepared at various initial moisture contents, it is recommended to study the influence of soil bed fabric on the MPMT and MCPT results. The soil fabric can be studied by taking soil samples around the probe and observing the soil fabric via scanning electron microscopy (SEM).
3. Develop a method that is capable of monitoring stress changes and soil displacements in the soil bed during the expansion of the MPMT probe or penetration of MCPT probe. The stress can be monitored by using total stress cells and the soil displacements can be monitored by using lead fibers and x-ray techniques or by fiber optic strings. The data obtained can be used to verify the analysis done with the cavity expansion equations.
4. A more comprehensive experimental investigation should be performed to study the influence of ψ on pressuremeter and cone penetrometer testing results. It is suggested that tests be performed on different soil types at various γ_d, ψ, σ_n and OCR.
5. Conduct more laboratory tests to provide additional data to estimate the parameters needed for the cavity expansion equations for unsaturated soils.
6. Develop a series of ε_v vs. ψ curves for various soil types, γ_d, ψ, σ_n and OCR. By using the curves developed and in situ test data, try to predict the in situ results as a function of ψ. Conduct several insitu tests over period of time to monitor the

changes in ψ, P_L, E_P, E_R and q_c and compare the results with the results of the predictions.

7. Develop numerical modeling to predict both PMT and CPT data for other soil types under unsaturated conditions. The data obtained from this study can either be used to calibrate or validate the model.

References

Ajalloeian, R., and Yu, H. S., "Chamber Studies of the Effects of Pressuremeter Geometry on Test Results in Sand," Geotechnique, Vol. 48, No. 5, October 1998, pp. 621-636.

Akanda, A. S., "Effect of Moisture Content and Clay Fraction on the Cyclic Behavior of Soil During Compaction," Master of Science Thesis, University of Oklahoma, Norman, 1998.

Ananthanathan, P. J., "Laboratory Testing of Unsaturated Minco Silt," Master of Science Thesis, University of Oklahoma, Norman, 2002.

Anderson, W. F., Pyrah, I. C., and Fryer, S. J., "A Clay Calibration Chamber for Testing Field Devices," Geotechnical Testing Journal, Vol. 14, No. 4, Dec. 1991, pp. 440-450.

Baguelin, F., Jezequel, J. F., Mee, E. L., and Mehaute, A. L., "Expansion of Cylindrical Probes in Cohesive Soils," Journal of the Soil Mechanics and Foundations Division, Vol. 98, SM11, Nov. 1972, pp.1129-1142.

Baguelin, F., Jezequel, J. F., and Shields, D. H., The Pressuremeter and Foundation Engineering, 1st Ed., Trans Tech, Germany, 1978.

Bear, J., Hydraulic of Groundwater, McGraw-Hill, New York, 1979, pp. 567.

Borden, R. H., "Boundary Displacement Induced by DMT Penetration," Proceedings of the First International Symposium on Calibration Chamber Testing, An-Bin Huang, Ed., Clarkson University, Postdam, New York, 1991, pp. 101-118.

Briaud, J. L., The Pressuremeter, A. A. Balkema, Rotterdam, 1992.

Coutinho, A. G. F. D. S., "Radial Expansion of Cylindrical Cavities in Sandy Soils: Application to Pressuremeter Tests," Canadian Geotechnical Journal, Vol. 27, No. 6, Dec. 1990, pp. 737-748.

Deshpande, S. D., "Static and Dynamic Centrifuge Modelling of Unsaturated Soil Embankments, Master of Science Thesis, University of Oklahoma, Norman, 1997.

Edelman, S. H., and Holguin, A. R., "Cone Penetrometer Testing for Characterization and Sampling of Soil and Groundwater," Sampling Environmental Media, ASTM STP 1282, James Howard Morgan, Ed., American Society for Testing Material, 1996, pp. 192-206.

Fredlund, D. G., and Morgenstern, N. R., "Stress State Variables for Unsaturated Soils," ASCE Journal Geotechnical Engineering Division GT5, Vol. 103, 1977, pp. 447-466.

Fredlund, D. G., and Rahardjo, H., Soil Mechanics for Unsaturated Soils, John Wiley and Sons, New York, 1993.

Fredlund, D. G., Morgenstern, N. R., and Widger, R. A., "The Shear Strength of Unsaturated Soils," Canadian Geotechnical Journal, Vol. 15, No. 3, 1978, pp. 313-321.

Holden, J. C., "History of First six CRB Calibration Chambers," Proceedings of the First International Symposium on Calibration Chamber Testing, An-Bin Huang, Ed., Clarkson University, Postdam, New York, 1991, pp. 1-12.

Hryciw, R. D., and Dowding, C.H., "Cone Penetration of Partially Saturated Sands," Geotechnical Testing Journal, Vol. 10, No. 3, September 1987, pp. 135-141.

Hsieh, Y. M., Whittle, A. J., and Yu, H. S., "Interpretation of Pressuremeter Test in Sand Using Advanced Soil Model," Journal of Geotechnical and Geoenvironmental Engineering, Vol. 128, No. 3, March 2002, pp. 274-278.

Hughes, J. M. O., Wroth, C. P., and Windle, D., "Pressuremeter Tests in Sand," Geotechnique, Vol. 27, 1977, pp. 455-477.

Kulhawy, F. H., and Mayne, P. W., "Relative Density, SPT and CPT Interrelationships," Proceedings of the First International Symposium on Calibration Chamber Testing, An-Bin Huang, Ed., Clarkson University, Postdam, New York, 1991, pp. 197-212.

Kurup, P. U. "Calibration Chamber Studies of Miniature Piezocone Penetration Tests in Cohesive Soil Specimens," Ph.D. Dissertation, Louisiana State University, 1993.

Ladanyi, B., "In-Situ Determination of Undrained Stress-Strain Behavior of Sensitive Clays with the Pressuremeter," Canadian Geotechnical Journal, Vol. 9, 1972, pp. 313-319.

Lauder, D. R., "The Design and Construction of a Calibration Chamber for Testing Unsaturated Soils," Master of Science Thesis, University of Oklahoma, Norman, 2000.

Lo Presti, D. C. F., Pedroni, S., and Crippa, V., "Maximum Dry Density of Cohesionless Soils by Pluviation and by ASTM D 4253-83: A Comparative Study," Geotechnical Testing Journal, Vol. 15, No. 2, June 1993, pp. 180-189.

Lunne, T., "Practical use of CPT Correlations in Sand Based on Calibration Chamber Tests," Proceedings of the First International Symposium on Calibration Chamber Testing, An-Bin Huang, Ed., Clarkson University, Postdam, New York, 1991, pp. 225-236.

Lunne, T., and Christoffersen, H. P., "Interpretation of Cone Penetrometer Data for Offshore Sands," Proceedings of 15th Offshore Technology Conference at Houston, Texas, Vol. 1, 1981, pp. 181-192.

Lunne, T., Robertson, P. K., and Powell J. J. M., Cone Penetration Testing in Geotechnical Practice, Spon press, Great Britain, 1997.

Mair, R. J., and Wood, D. M., Pressuremeter Testing Methods and Interpretation, CIRIA, Butterworths, 1987.

Mantaras, F. M., and Schnaid, F., "Cylindrical Cavity Expansion in Dilatant Cohesive-Frictional Materials," Geotechnique, Vol. 52, No. 5, June 2002, pp. 337-348.

Mayne, P. W., and Kulhawy, F. H., "Calibration Chamber Database and Boundary Effects Corrections for CPT Data," Proceedings of the First International Symposium on Calibration Chamber Testing, An-Bin Huang, Ed., Clarkson University, Postdam, New York, 1991, pp. 257-264.

Menard, L., "An Apparatus for Measuring the Strength of Soil in Place," Master of Science Thesis, University of Illinois, Urbana, Illinois.

Mendenhall, W. and Sincich, T., A Second Course in Statistics Regression Analysis, 6th Edition, Prentice Hall, Upper Saddle River, 2003.

Miller, G. A., and Muraleetharan, K. K., "Interpretation of Pressuremeter Tests in Unsaturated Soil," Geotechnical Special Publication No. 99: Proceedings of Sessions of Geo-Denver 2000, Geo-Institute of ASCE, Reston, 2000, pp. 40-53.

Miller, G. A., Muraleetharan, K. K., Tan, N. K., and Lauder,, D. R., "A Calibration Chamber for Unsaturated Soil Testing," Proceedings of the 3rd International

Conference on Unsaturated Soils, UNSAT 2002, Vol. 2, Balkema, Lisse, 2002, pp.453-457.

Mitchell, J. K., and Keaveny, J. M., "Determining Sand Strength by Cone Penetrometer," Geotechnical Special Publication No. 6: Use of In Situ Tests in Geotechnical Engineering, ASCE, 1986, pp. 823—839.

Muraleetharan, K. K., Ravichandran, N., Miller, G. A., and Tan N. K., "Fully Coupled Analyses of Pressuremeter Tests in Unsaturated Soils," Proceedings of the 2nd Asian Conference on Unsaturated Soils, UNSAT-ASIA 2003, UNSAT-ASIA 2003, 2003, pp. 313-318.

Muraleetharan, K. K., Yang, Y., Salehipour, S. A., and Dhavala, M. D., "Cavity Expansion Theories for Unsaturated Soils," Technical Report, school of Civil Engineering and Environmental Science, University of Oklahoma, Norman, 1998.

Osinov, V. A., and Cudmani, R., "Theoretical Investigation of the Cavity Expansion Problem Based on a Hypoplasticity Model," International Journal for Numerical and Analytical Methods in Geomechanics, Vol. 25, 2001, pp. 473-495.

Palmer, A. C., "Undrained Plane-Strain Expansion of Cylindrical Cavity in Clay: A Simple Interpretation of Pressuremeter Test," Geotechnique, Vol. 22, No. 3, 1972, pp. 451-457.

Penumadu, D. and Chameau, J. L., "Interpretation off Model Pressuremeter Test Using Automated Clay Calibration Chamber Data," Geotechnical Testing Journal, Vol. 21, No. 1, March 1998, pp. 18-30.

Penumadu, D., Skandarajah, A., and Chameau, J., "Strain-Rate Effects in Pressuremeter Testing Using a Cuboidal Shear Device: Experiments and Modeling," Canadian Geotechnical Journal, Vol. 35, 1998, pp. 27-42.

Pereira, J. M., Dubujet, P., and Wong, H., "Numerical Modeling of Unsaturated Soils in Pressuremeter test," 16th ASCE Engineering Mechanics Conference July 16-18, 2003, ASCE, 2003, pp. 1-9.

Peterson, R. W., "Penetration Resistance of Fine Cohesionless Materials," Proceedings of the First International Symposium on Calibration Chamber Testing, An-Bin Huang, Ed., Clarkson University, Postdam, New York, 1991, pp. 315-328.

Peterson, R. W., and Arulmoli, K., "Overview of a Large Stress Chamber System," Proceedings of the First International Symposium on Calibration Chamber Testing, An-Bin Huang, Ed., Clarkson University, Postdam, New York, 1991, pp. 329-338.

Puppala. A. J., Acar, Y. B., and Tumay, M. T., "Miniature CPT Tests in Dense Monterey No. 0/30 Sand in a Flexible Double-Walled Calibration Chamber," Proceedings of the First International Symposium on Calibration Chamber Testing, An-Bin Huang, Ed., Clarkson University, Postdam, New York, 1991, pp. 339-350.

Pye, C. N., "The Influence of Constitutive Models on Self-Boring Pressuremeter Interpretation in Clay," Canadian Geotechnical Journal, Vol. 32, 1995, pp. 420-427.

Pyrah, I. C., and Anderson, W. F., "Numerical Assessment of Self-Boring Pressuremeter Tests in a Clay Calibration Chamber," Pressuremeter, London, 1990, pp. 179-188.

Rad, N. S., and Tumay, M. T., "Factors Affecting Sand SpecimenPreparation by Raining," Geotechnical Testing Journal, Vol. 10, No. 1, March 1987, pp. 31-37.

Richards, B. G., :Measurements of the Free Energy of Soil Moisture by the Psychrometric Technique Using Thermistors," Moisture Equilibria and Moisture Changes in Soils Beneath Covered Areas, Australia: Butterworths, 1965, pp. 39-46.

Rix, G. J., and Stokoe, K. H., "Correlation of Initial Tangent Modulus and Cone Penetration Resistance," Proceedings of the First International Symposium on Calibration Chamber Testing, An-Bin Huang, Ed., Clarkson University, Postdam, New York, 1991, pp. 315-327.

Robertson, P. K., and Campanella, R. G., "Interpretation of Cone Penetration Tests, Part I: Sand," Canadian Geotechnical Journal, Vol. 20, No. 4, 1983, pp. 718-733.

Russell, A. R., and Khalili, N., "Cavity Expansion in Unsaturated Soils," Proceedings of the 3rd International Conference on Unsaturated Soils, UNSAT 2002, Vol. 1, Balkema, Lisse, 2002, pp.233-238.

Russell, A. R., and Khalili, N., "Drained Cavity Expansion in Sands Exhibiting Particle Crushing," International Journal for Numerical and Analytical Methods in Geomechanics, Vol. 26, 2002, pp. 323-340.

Salgado, R., Mitchell, J. K., and Jamiolkowski, M., "Calibration Chamber Size Effects on Penetration Resistance in Sand," Journal of Geotechnical and Geoenvironmental Engineering, Vol. 124, No. 9, Sept. 1998, pp.878-888.

Salgado, R., amd Randolph, M. F., "Analysis of Cavity Expansion in Sand," The International Journal of Geomechanics, Vol. 1, No. 2, 2001, pp. 175-192.

Schnaid, F., Oliveira, L. A. K., and Gehling, W. Y. Y., "Unsaturated Constitutive Surfaces from Pressuremeter Tests," Journal of Geotechnical and Geoenvironmental Engineering, Vol. 130, No. 2, Feb. 2004, pp. 174-185.

Schnaid, F., Houlsby, G. T., "An Assessment of Chamber Size Effects in the Calibration of In Situ Tests in Sand," Geotechnique, Vol. 41, No. 3, 1991, pp. 437-445.

Schnaid, F., Houlsby, G. T., "Discussion: Measurement of the Properties of Sand in Calibration Chamber by Cone Pressuremeter Test," Geotechnique, Vol. 44, No. 3, 1994, pp. 529-532.

Schnaid, F., Houlsby, G. T., "Measurement of the Properties of Sand in Calibration Chamber by Cone Pressuremeter Test," Geotechnique, Vol. 42, No. 4, 1992, pp. 587-601.

Silvestri, V., "On the Determination of the Stress-Strain Curve of Clay From the Undrained Plane-Strain Expansion of Hollow Cylinders: A long-Forgotten Method," Canadian Geotechnical Journal, Vol. 35, No. 2, April 1998, pp. 360-363.

Sweeney, B. P., and Clough, G. W., "Design of a Large Calibration Chamber," Geotechnical Testing Journal, Vol. 13, No. 1, March 1990, pp. 36-44.

Tan, N. K. "Preparation of Model Unsaturated Soil Beds for Calibration Chamber Testing," Master of Science Thesis, University of Oklahoma, Norman, 2000.

Tan, N. K. and Miller, G. A., "Pressuremeter Testing in a Calibration Chamber with Unsaturated Minco Silt," Proceedings of the 16th International Conference on Soil Mechanics and Geotechnical Engineering, Milpress Science, Rotterdam, 2005 (in print).

Tan, N. K., Miller, G. A., and Muraleetharan, K. K., " Preliminary Laboratory Calibration of Cone Penetration in Unsaturated Silt," Proceedings of Soil Rock America 2003: 12th Pan-American Conference on Soil Mechanics and Geotechnical Engineering, VGE, Germany, 2003, pp. 391-396.

Tamhane, A. C., and Dunlop, D. D., Statistics and Data Analysis From Elementary to Intermediate, Prentice Hall, Upper Saddle River, 2000.

Vaid, Y. P., and Negussey, D., "Preparation of Reconstituted Sand Specimens," Advanced Triaxial Testing of Soil and Rock, ASTM STP 977, American Society for Testing Materials, 1998, pp. 405-417.

Vesic, A. S., "Expansion of Cavities in Infinite Soil Mass," Journal of Soil Mechanics and Foundation Division, Vol. 98, No. SM3, March 1972, pp.265-291.

Vinayagam, T., "Understanding the Stress-Strain Behavior of Unsaturated Minco Silt Using Laboratory Testing and Constitutive Modeling," Master of Science Thesis, University of Oklahoma, Norman, 2004.

Voyiadjis, G. Z., Kurup, P. U., and Tumay, M. T., "Preparation of Large-Size Cohesive Specimens for Calibration Chamber Testing," Geotechnical testing Journal, Vol. 16, No. 3, Sept. 1993, pp. 339-349.

Wood, D. M. and Wroth, C. P., "Some Laboratory Experiments Related to the Results of Pressuremeter Tests," Geotechnique, Vol. 27, No. 2, June 1977, pp. 181-201.

Worth, C. P., and Windle, D., "Analysis of Pressuremeter Tests Allowing for Volume Change," Geotechnique, Vol. 25, 1975, pp. 173-183.

Yu, H. S., and Carter, J. P., "Rigorous Similarity Solutions for Cavity Expansion in Cohesive-Frictional Soils," The International Journal of Geomechanics, Vol. 2, No. 2, 2002, pp. 233-258.

Appendix A: Volumetric Strain During Soil Bed Compression

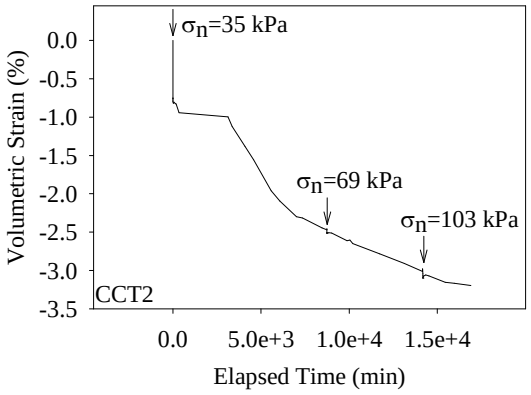

Figure A-1: Volumetric Strain during Compression for Soil Bed CCT2

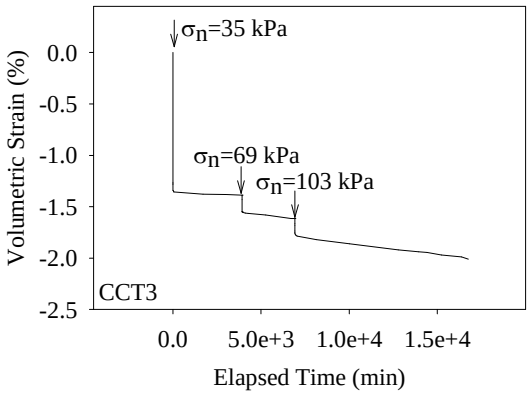

Figure A-2: Volumetric Strain during Compression for Soil Bed CCT3

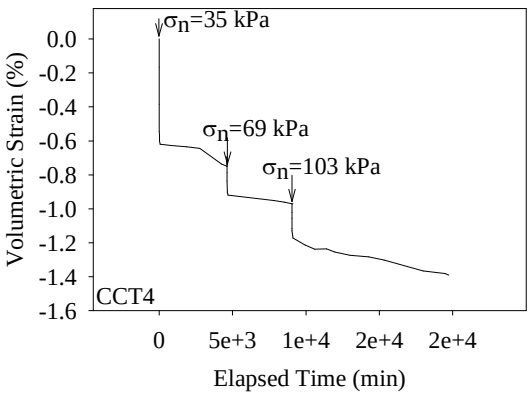

Figure A-3: Volumetric Strain during Compression for Soil Bed CCT4

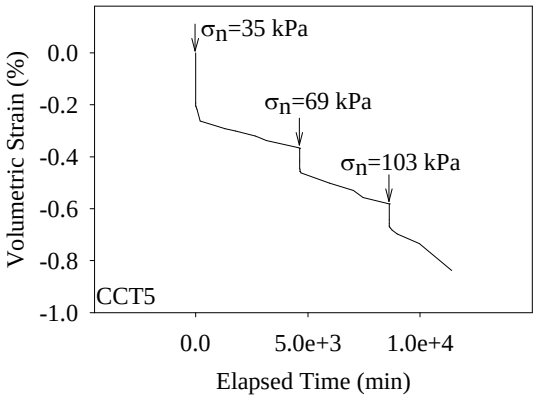

Figure A-4: Volumetric Strain during Compression for Soil Bed CCT5

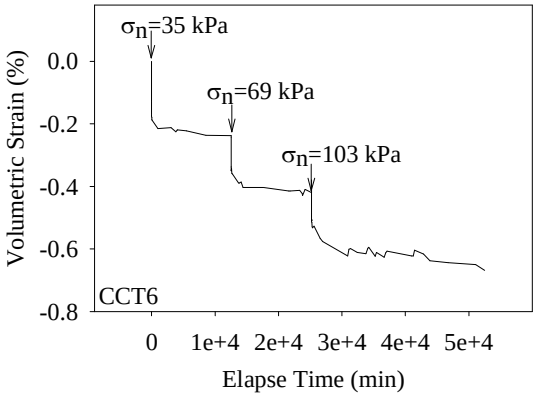

Figure A-5: Volumetric Strain during Compression for Soil Bed CCT6

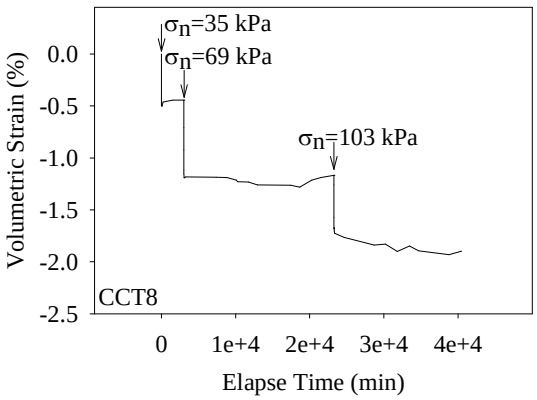

Figure A-6: Volumetric Strain during Compression for Soil Bed CCT8

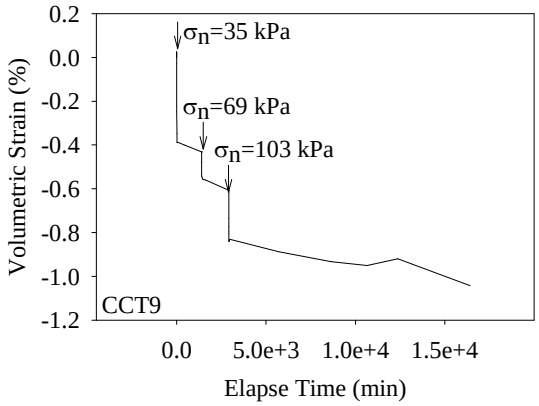

Figure A-7: Volumetric Strain during Compression for Soil Bed CCT9

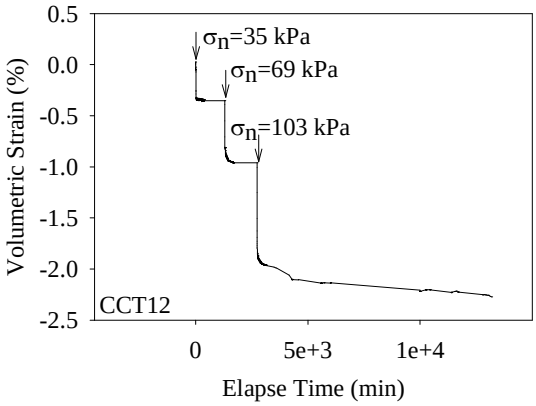

Figure A-10: Volumetric Strain during Compression for Soil Bed CCT12

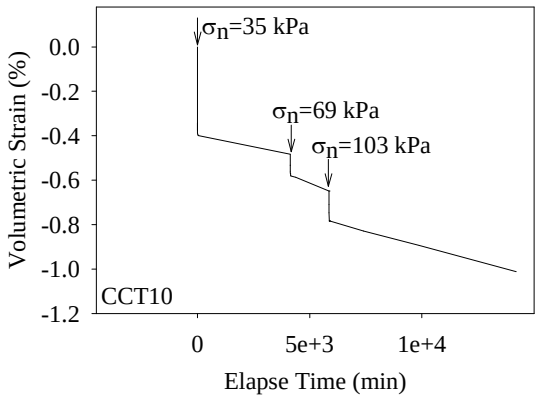

Figure A-8: Volumetric Strain during Compression for Soil Bed CCT10

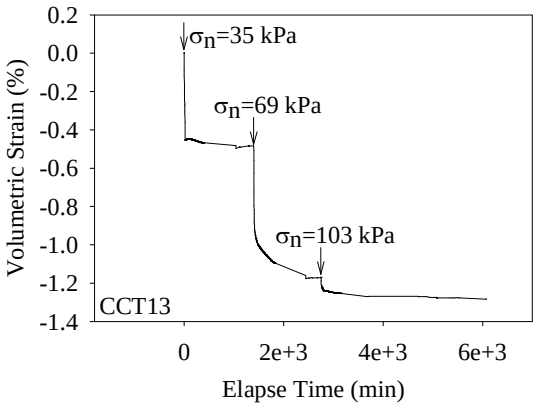

Figure A-11: Volumetric Strain during Compression for Bed CCT13

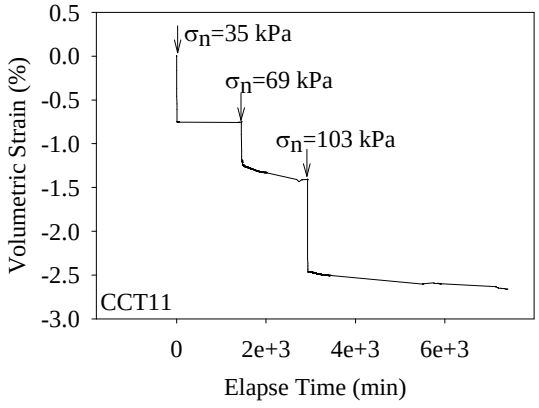

Figure A-9: Volumetric Strain during Compression for Soil Bed CCT11

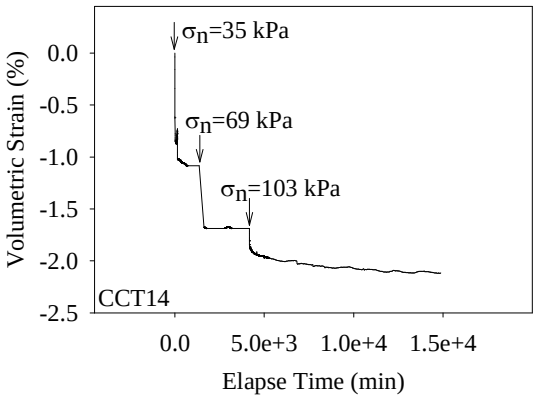

Figure A-12: Volumetric Strain during Compression for Soil Bed CCT14

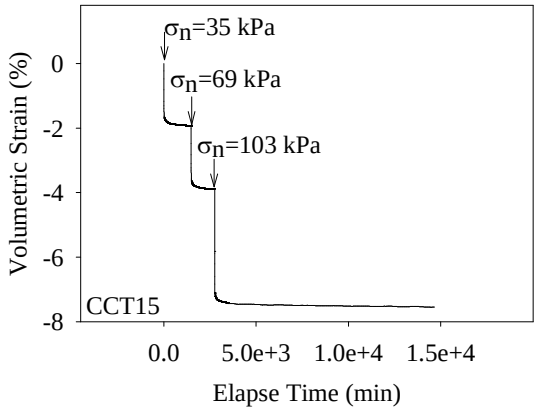

Figure A-13: Volumetric Strain during Compression for Soil Bed CCT15

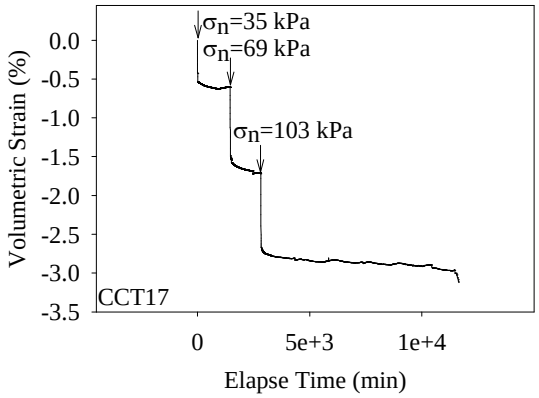

Figure A-14: Volumetric Strain during Compression for Soil Bed CCT17

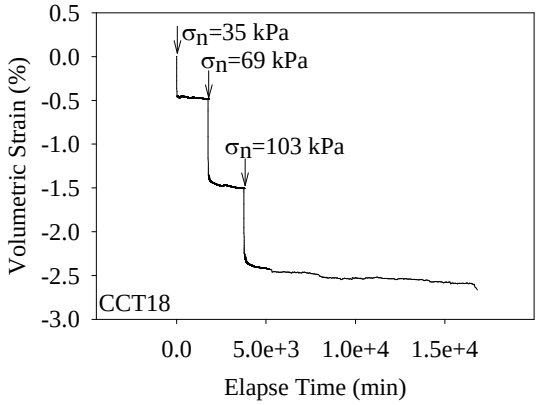

Figure A-15: Volumetric Strain during Compression for Soil Bed CCT18

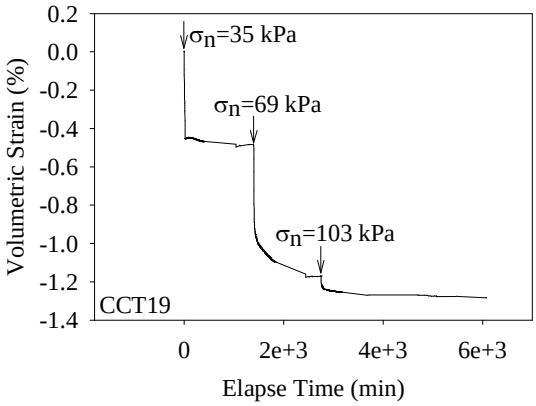

Figure A-16: Volumetric Strain during Compression for Soil Bed CCT19

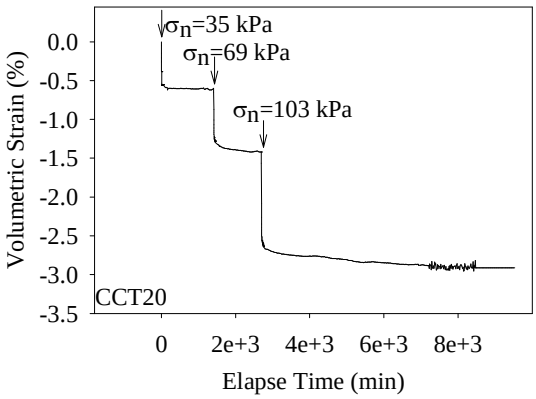

Figure A-17: Volumetric Strain during Compression for Soil Bed CCT20

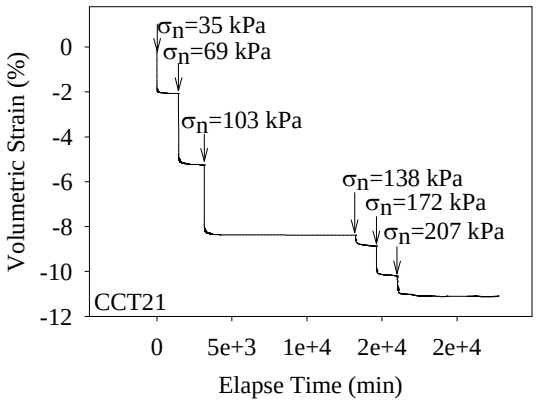

Figure A-18: Volumetric Strain during Compression for Soil Bed CCT21

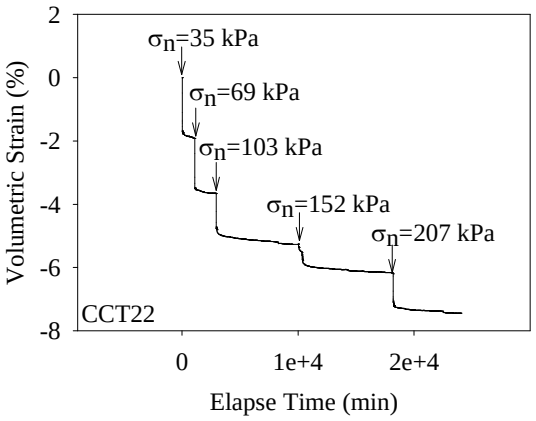

Figure A-19: Volumetric Strain during Compression for Soil Bed CCT22

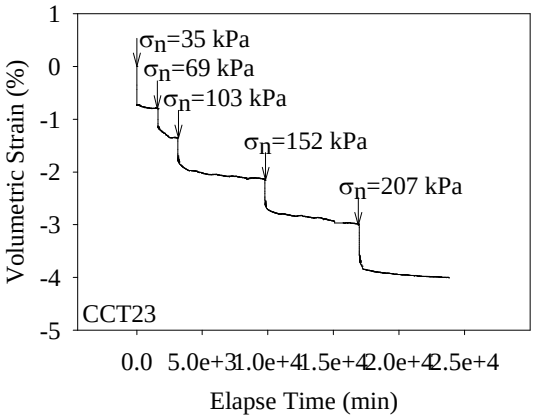

Figure A-20: Volumetric Strain during Compression for Soil Bed CCT23

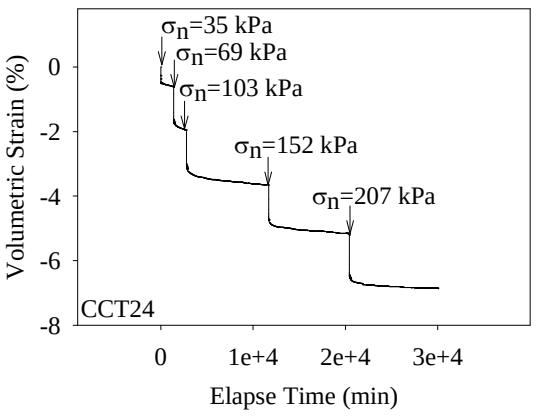

Figure A-21: Volumetric Strain during Compression for Soil Bed CCT24

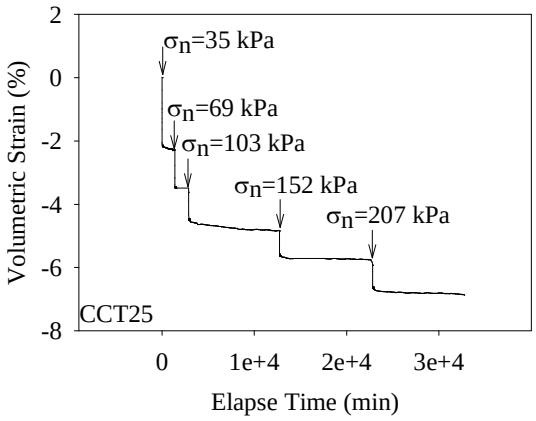

Figure A-22: Volumetric Strain during Compression for Soil Bed CCT25

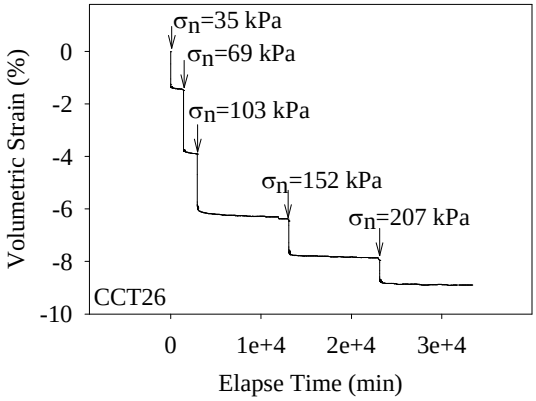

Figure A-23: Volumetric Strain during Compression for Soil Bed CCT26

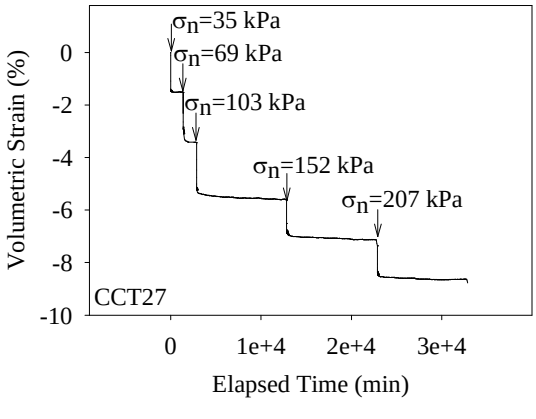

Figure A-24: Volumetric Strain during Compression for Soil Bed CCT27

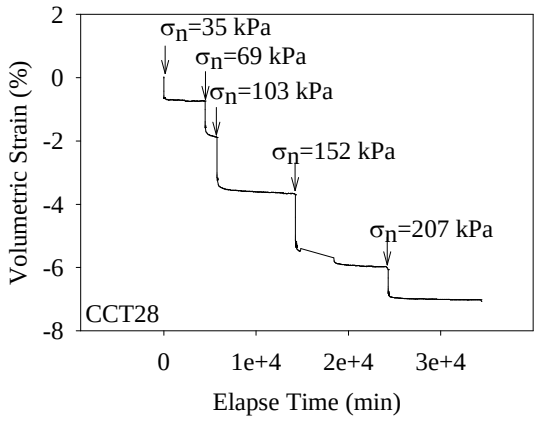

Figure A-25: Volumetric Strain during Compression for Soil Bed CCT28

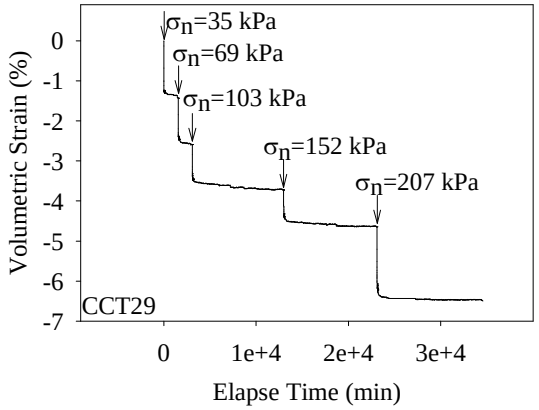

Figure A-:26: Volumetric Strain during Compression for Soil Bed CCT29

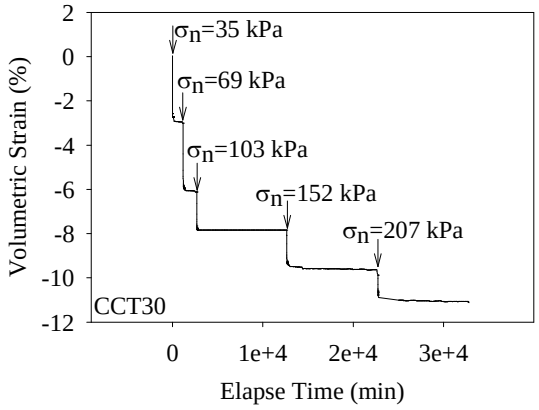

Figure A-27: Volumetric Strain during Compression for Soil Bed CCT30

Appendix B: γ_d and *w* Distribution in Soil Beds

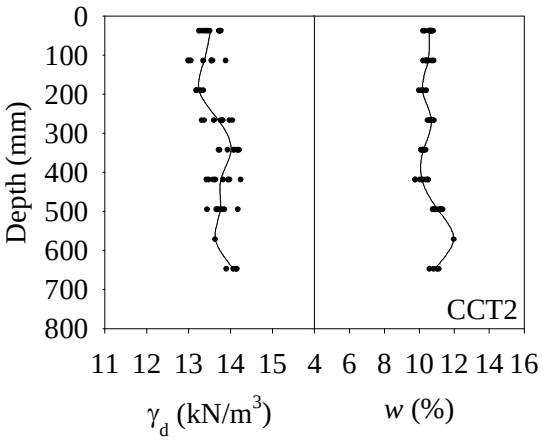

Figure B- 1: γ_d and *w* Distribution with Depth in Soil Bed CCT2

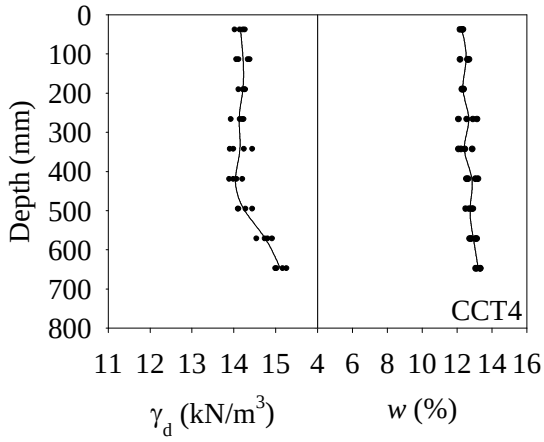

Figure B- 3: γ_d and *w* Distribution with Depth in Soil Bed CCT4

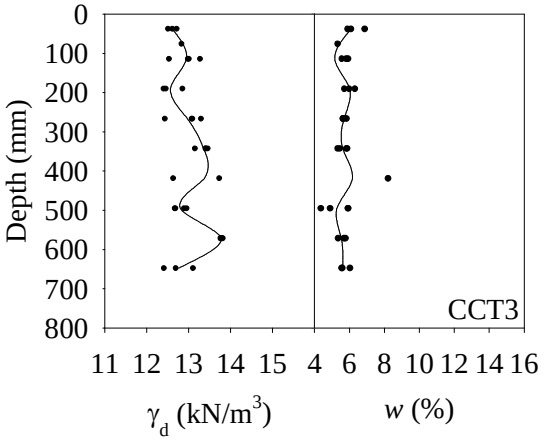

Figure B- 2: γ_d and *w* Distribution with Depth in Soil Bed CCT3

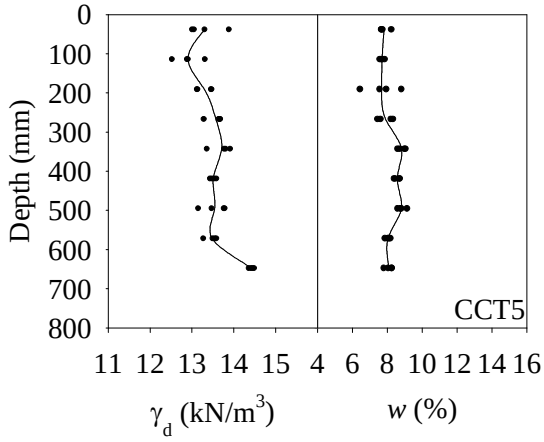

Figure B- 4: γ_d and *w* Distribution with Depth in Soil Bed CCT5

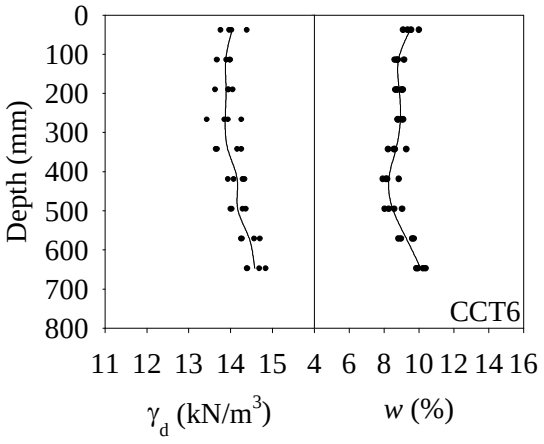

Figure B- 5: γ_d and *w* Distribution with Depth in Soil Bed CCT6

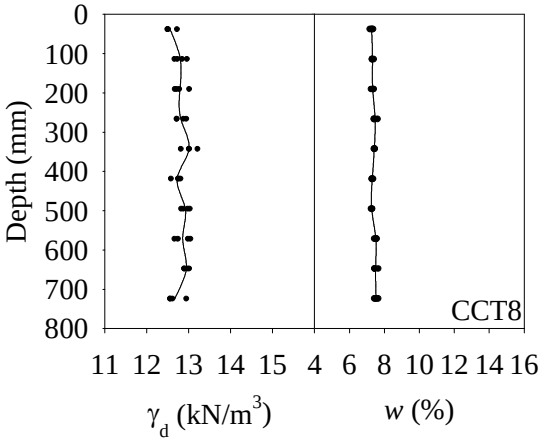

Figure B- 6: γ_d and *w* Distribution with Depth in Soil Bed CCT8

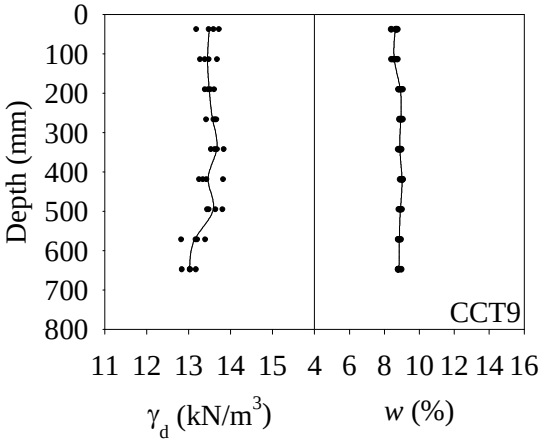

Figure B- 7: γ_d and *w* Distribution with Depth in Soil Bed CCT9

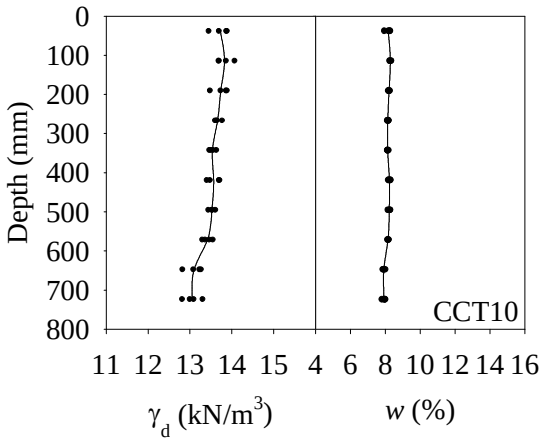

Figure B- 8: γ_d and *w* Distribution with Depth in Soil Bed CCT10

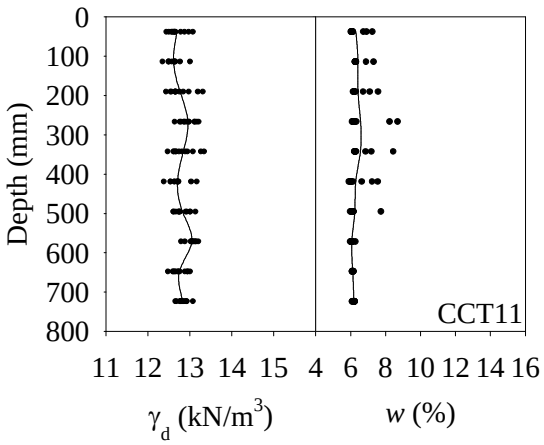

Figure B- 9: γ_d and *w* Distribution with Depth in Soil Bed CCT11

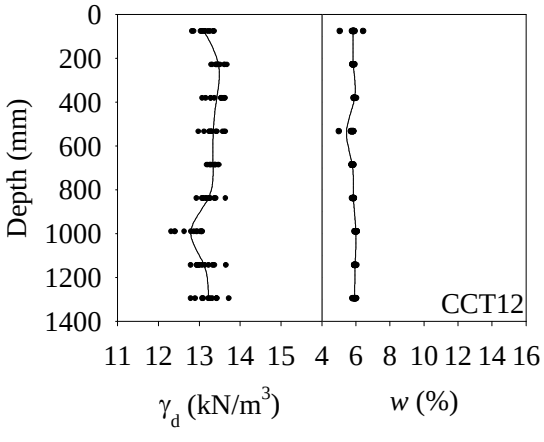

Figure B- 10: γ_d and *w* Distribution with Depth in Soil Bed CCT12

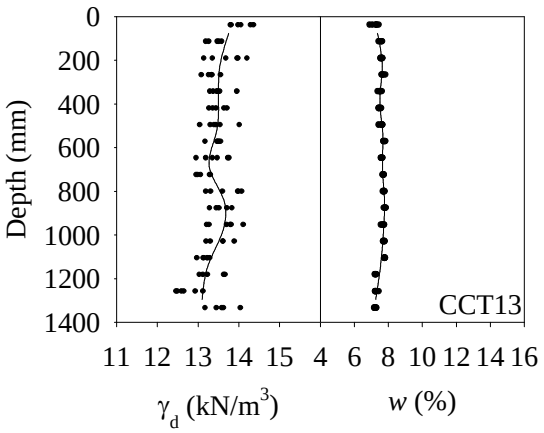

Figure B- 11: γ_d and *w* Distribution with Depth in Soil Bed CCT13

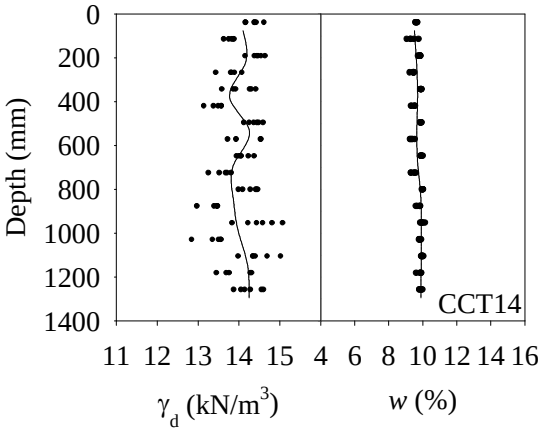

Figure B- 12: γ_d and *w* Distribution with Depth in Soil Bed CCT14

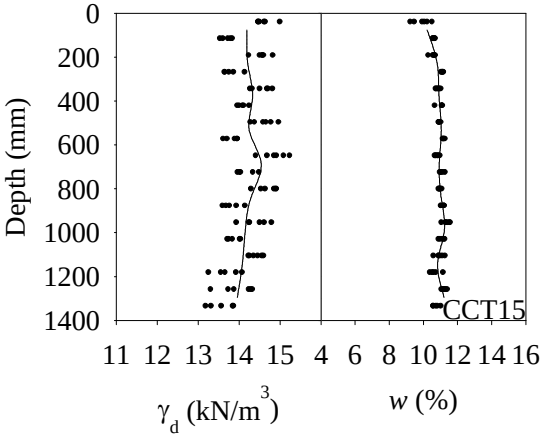

Figure B- 13: γ_d and *w* Distribution with Depth in Soil Bed CCT15

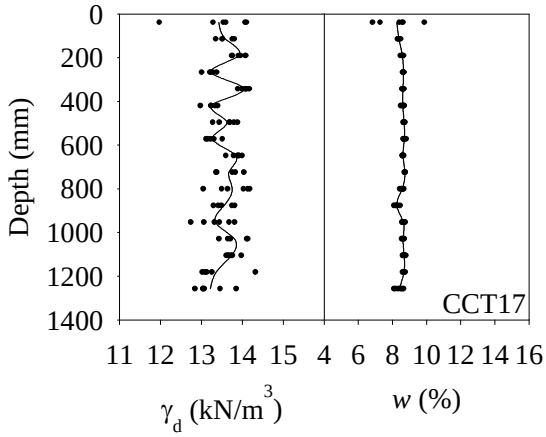

Figure B- 14: γ_d and *w* Distribution with Depth in Soil Bed CCT17

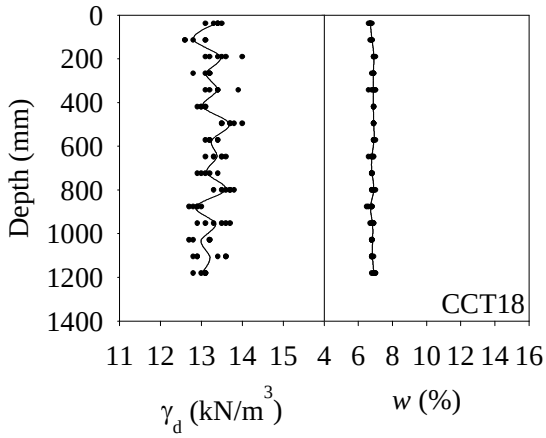

Figure B- 15: γ_d and *w* Distribution with Depth in Soil Bed CCT18

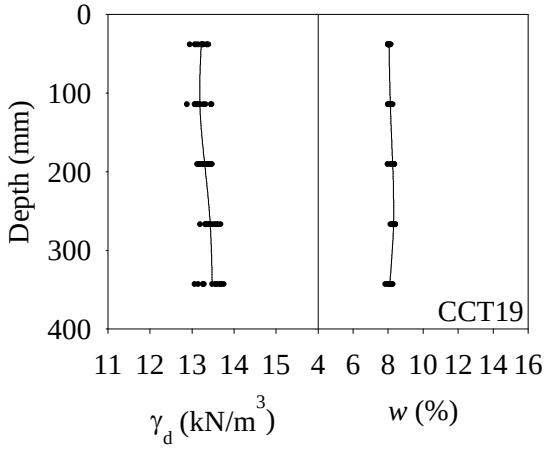

Figure B- 16: γ_d and *w* Distribution with Depth in Soil Bed CCT19

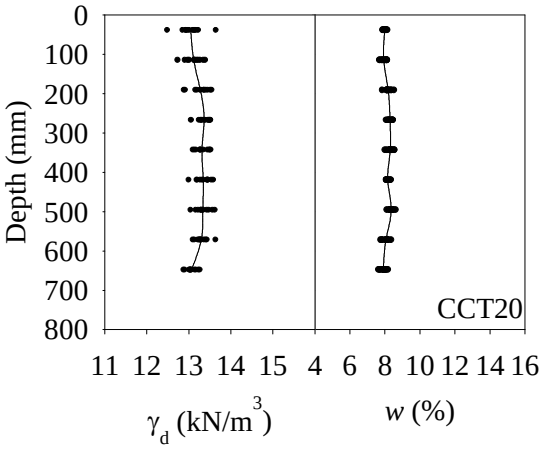

Figure B- 17: γ_d and *w* Distribution with Depth in Soil Bed CCT20

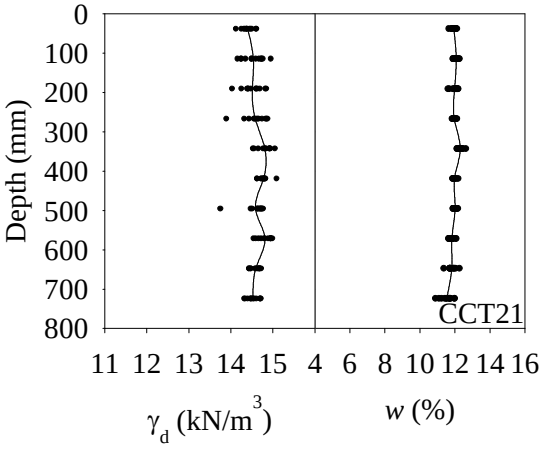

Figure B- 18: γ_d and *w* Distribution with Depth in Soil Bed CCT21

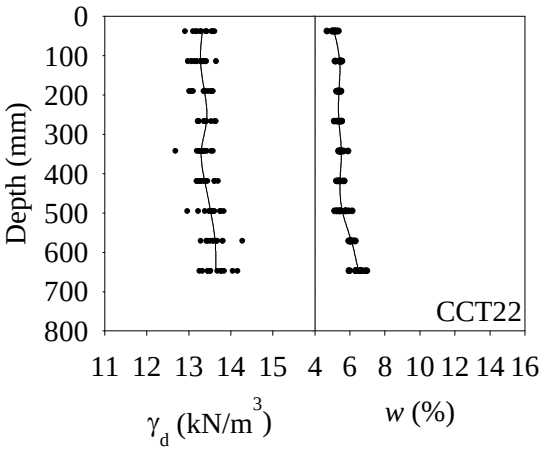

Figure B- 19: γ_d and *w* Distribution with Depth in Soil Bed CCT22

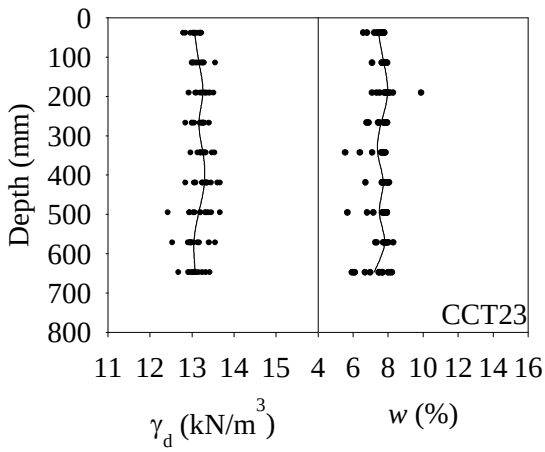

Figure B- 20: γ_d and *w* Distribution with Depth in Soil Bed CCT23

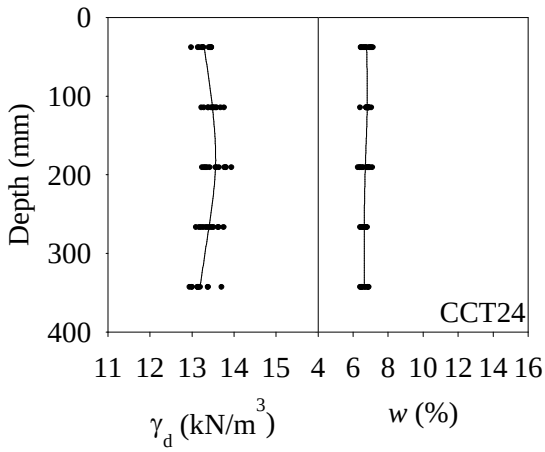

Figure B- 21: γ_d and *w* Distribution with Depth in Soil Bed CCT24

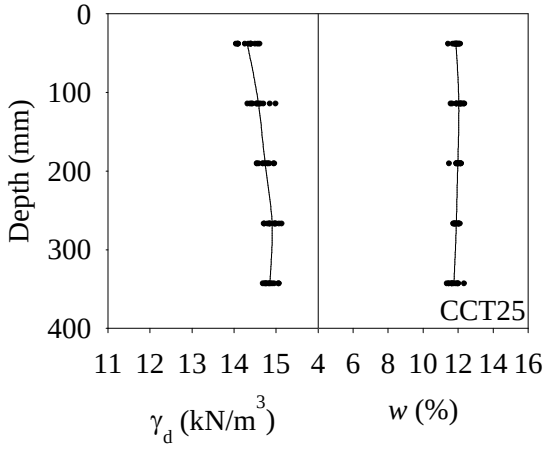

Figure B- 22: γ_d and *w* Distribution with Depth in Soil Bed CCT25

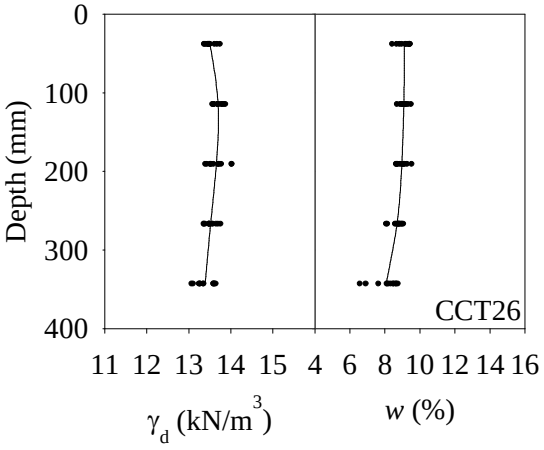

Figure B- 23: γ_d and *w* Distribution with Depth in Soil Bed CCT26

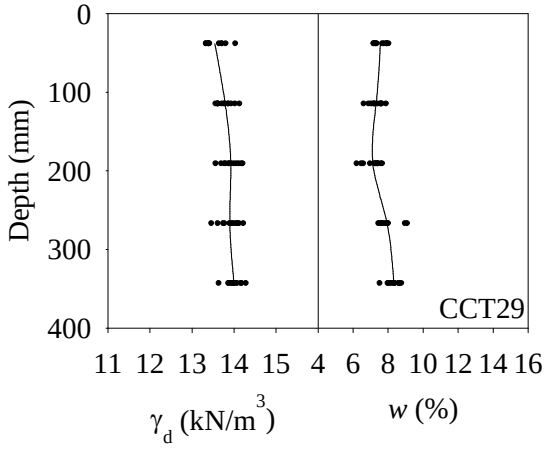

Figure B- 26: γ_d and *w* Distribution with Depth in Soil Bed CCT29

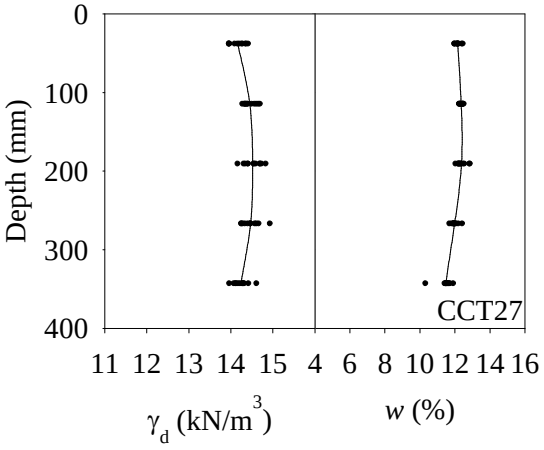

Figure B- 24: γ_d and *w* Distribution with Depth in Soil Bed CCT27

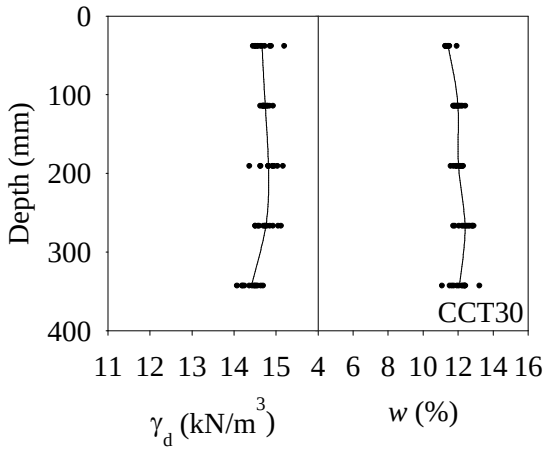

Figure B- 27: γ_d and *w* Distribution with Depth in Soil Bed CCT30

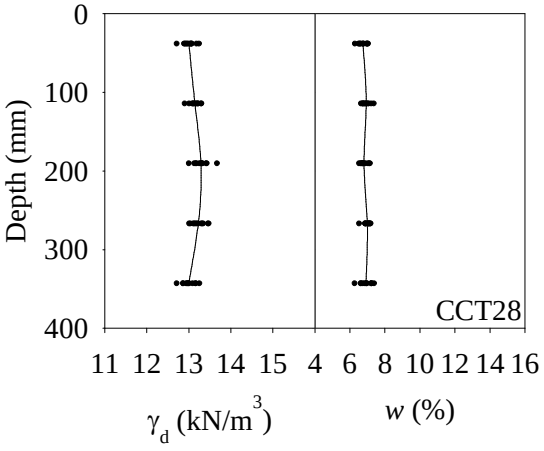

Figure B- 25: γ_d and *w* Distribution with Depth in Soil Bed CCT28

APPENDIX C: MPMT Pressure Expansion Curve

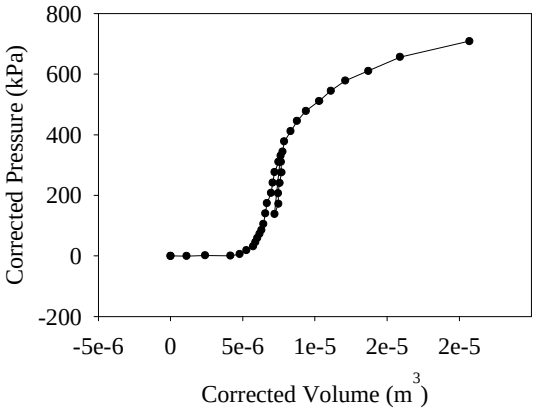

Figure C- 1: MPMT Pressure Expansion Curve (Test ID: 2A-1)

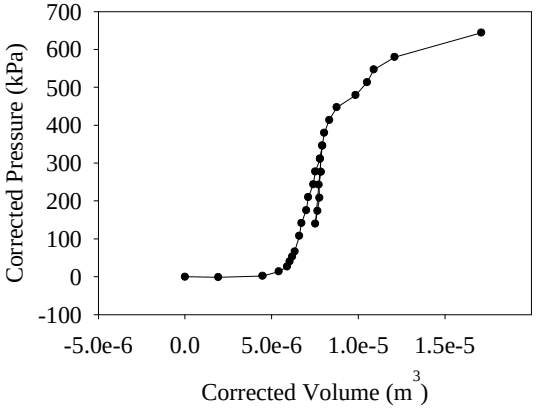

Figure C-2: MPMT Pressure Expansion Curve (Test ID: 2A-2)

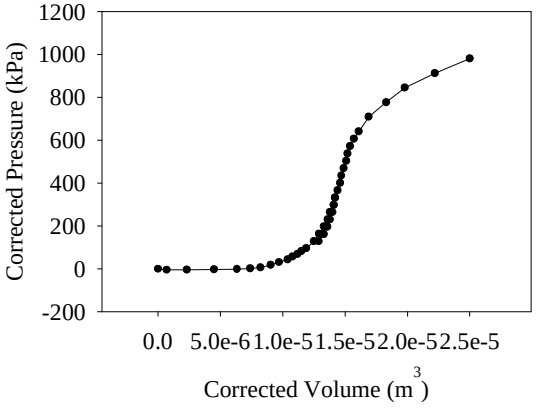

Figure C-3: MPMT Pressure Expansion Curve (Test ID: 3A-1)

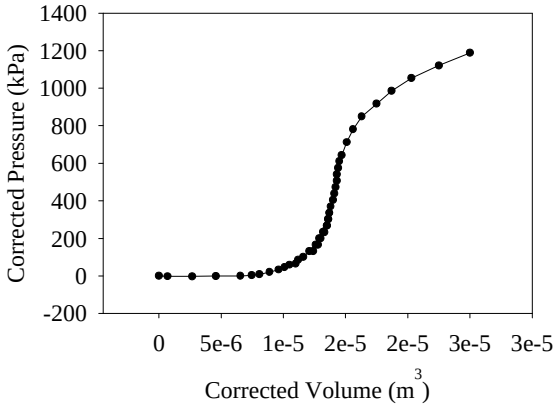

Figure C-4: MPMT Pressure Expansion Curve (Test ID: 3A-2)

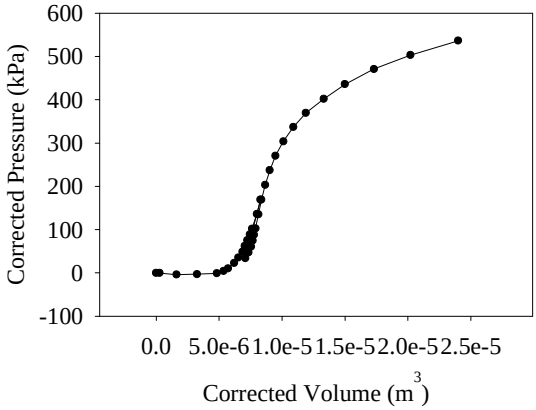

Figure C-5: MPMT Pressure Expansion Curve (Test ID: 4A-1)

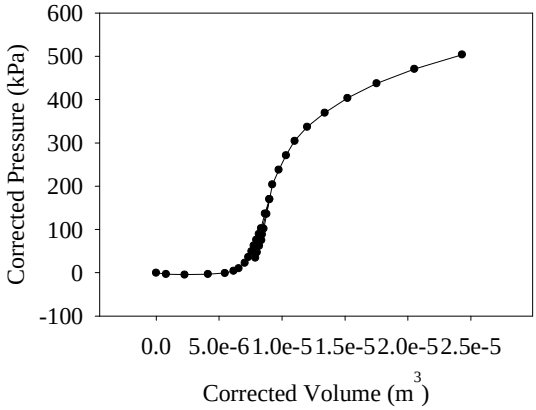

Figure C-6: MPMT Pressure Expansion Curve (Test ID: 4A-2)

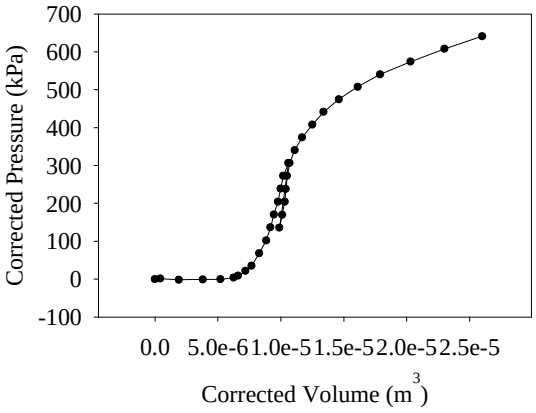

Figure C-7: MPMT Pressure Expansion Curve (Test ID: 5A-1)

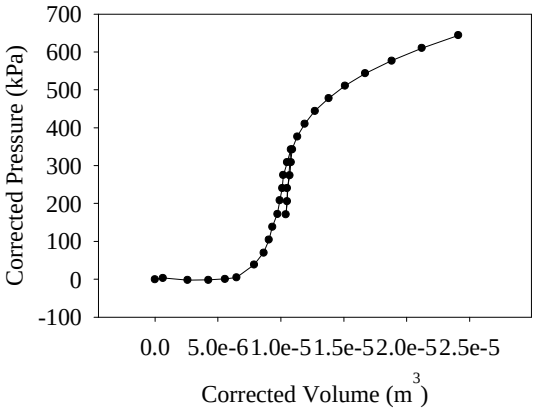

Figure C-8: MPMT Pressure Expansion Curve (Test ID: 5A-2)

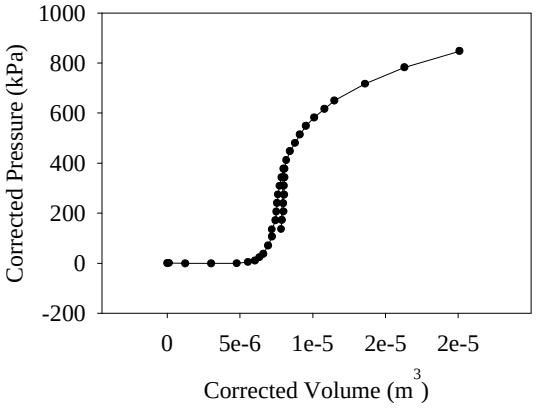

Figure C-9: MPMT Pressure Expansion Curve (Test ID: 6A-1)

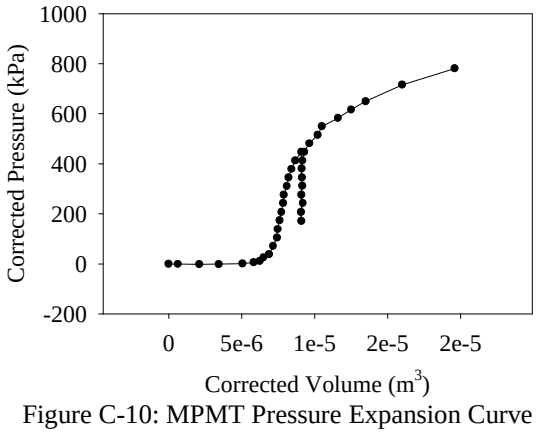

Figure C-10: MPMT Pressure Expansion Curve (Test ID: 6A-2)

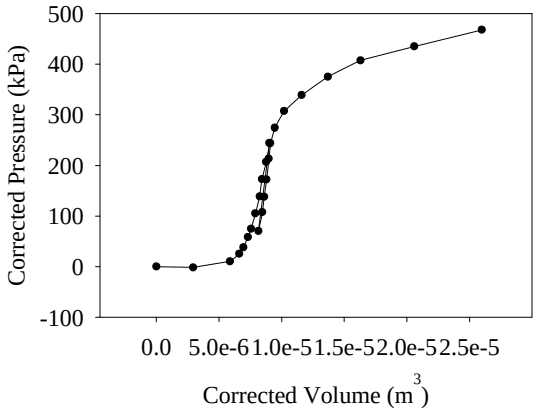

Figure C-11: MPMT Pressure Expansion Curve (Test ID: 8A-1)

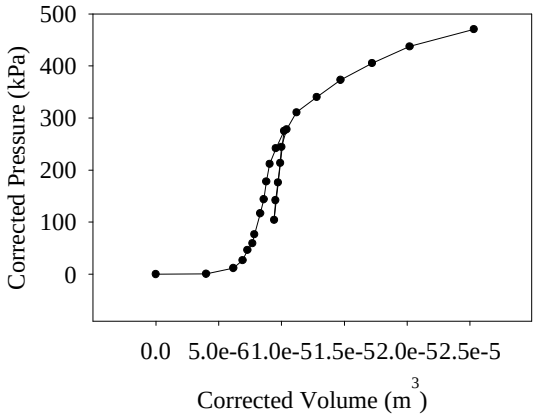

Figure C-12: MPMT Pressure Expansion Curve (Test ID: 8A-2)

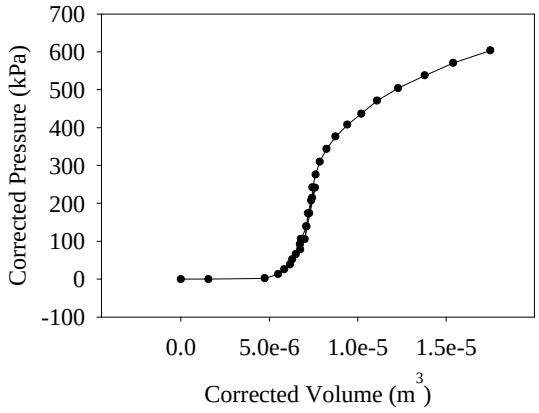

Figure C-13: MPMT Pressure Expansion Curve (Test ID: 9A-1)

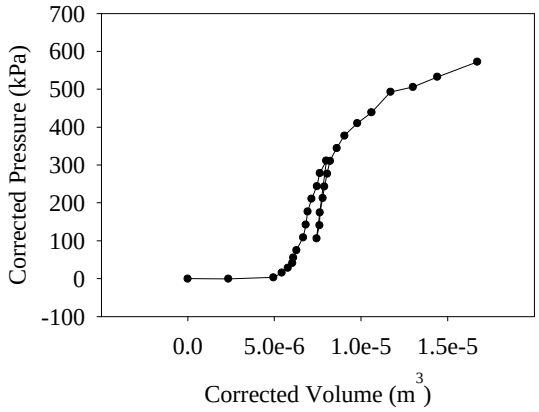

Figure C-14: MPMT Pressure Expansion Curve (Test ID: 9A-2)

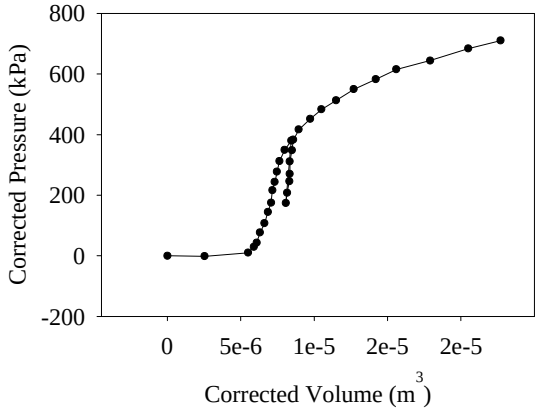

Figure C-15: MPMT Pressure Expansion Curve (Test ID: 10A-1)

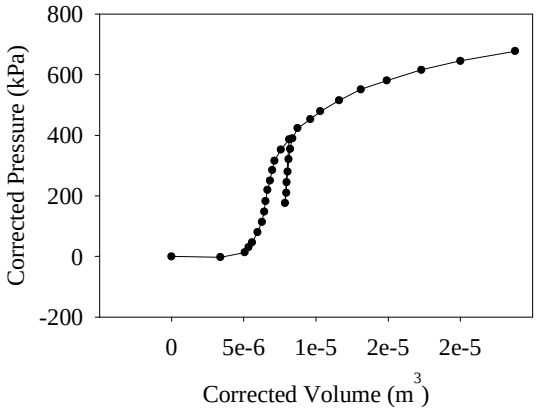

Figure C-16: MPMT Pressure Expansion Curve (Test ID: 10A-2)

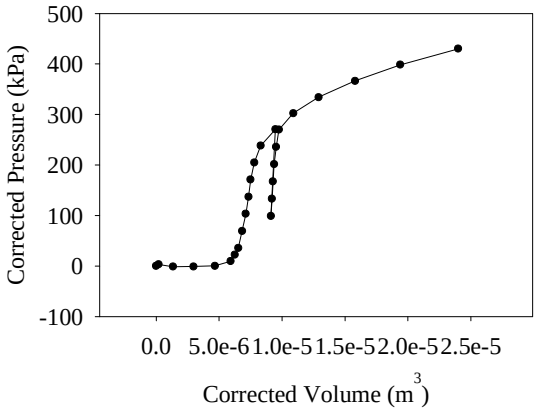

Figure C-17: MPMT Pressure Expansion Curve (Test ID: 11A-1)

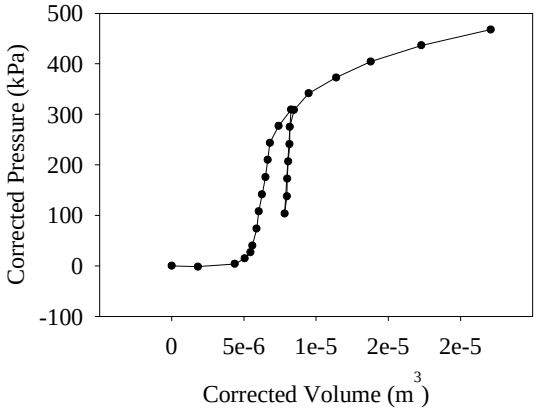

Figure C-18: MPMT Pressure Expansion Curve (Test ID: 11A-2)

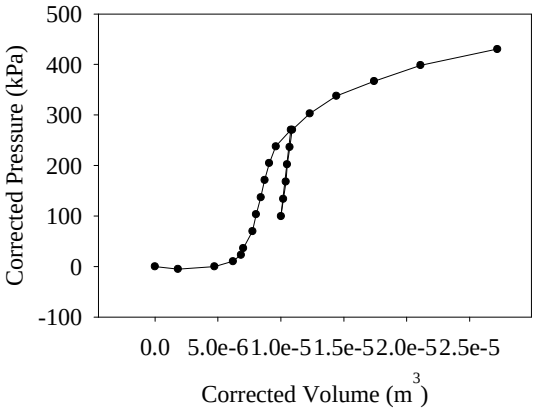

Figure C-19: MPMT Pressure Expansion Curve (Test ID: 11B-1)

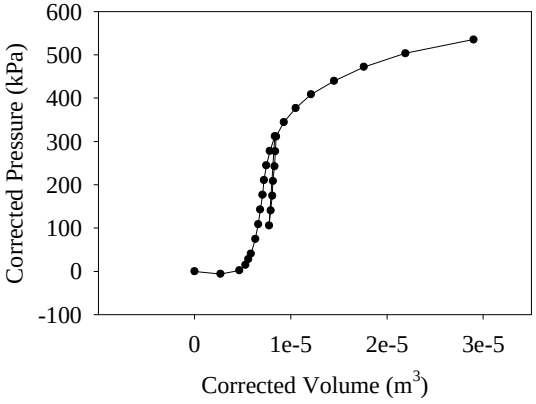

Figure C-20: MPMT Pressure Expansion Curve (Test ID: 11B-2)

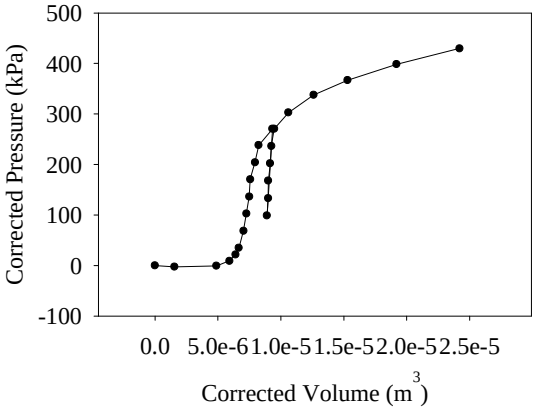

Figure C-21: MPMT Pressure Expansion Curve (Test ID: 11C-1)

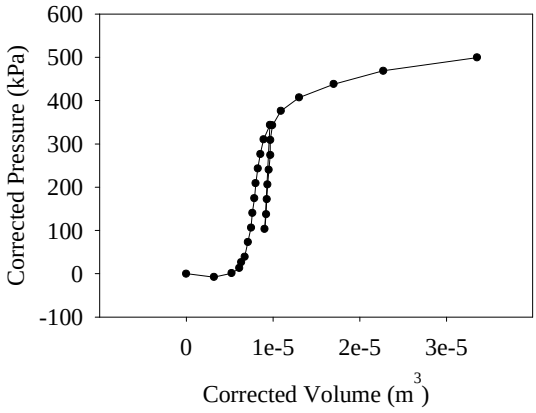

Figure C-22: MPMT Pressure Expansion Curve (Test ID: 11C-2)

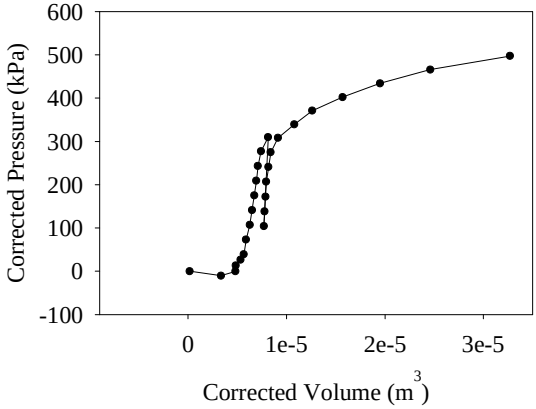

Figure C-23: MPMT Pressure Expansion Curve (Test ID: 11D-1)

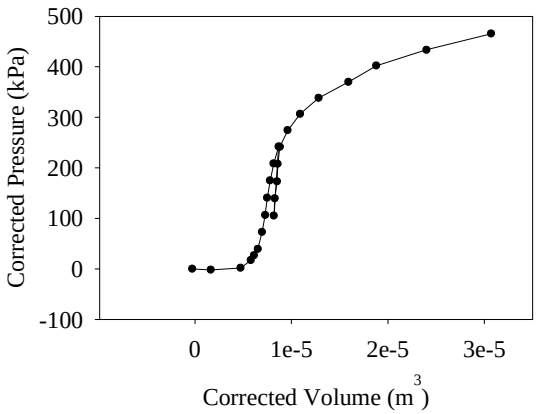

Figure C-24: MPMT Pressure Expansion Curve (Test ID: 11D-2)

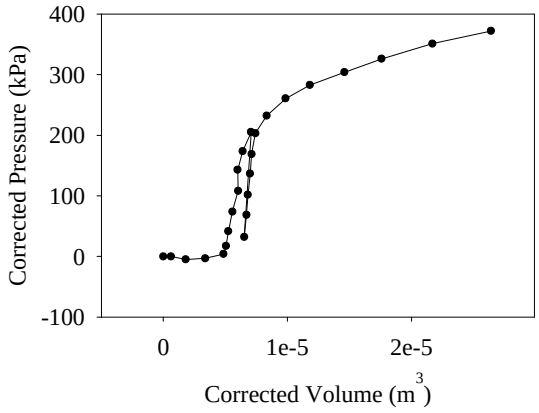

Figure C-25: MPMT Pressure Expansion Curve (Test ID: 19A-1)

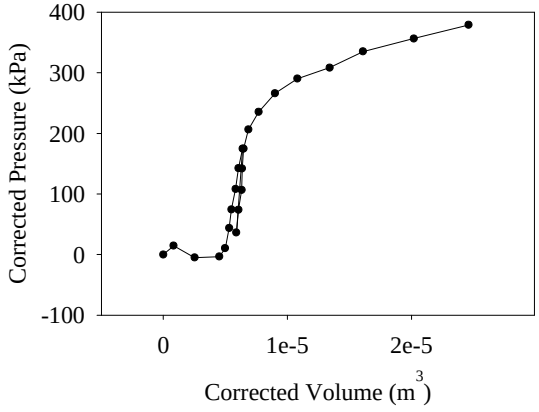

Figure C-:26: MPMT Pressure Expansion Curve (Test ID: 19B-1)

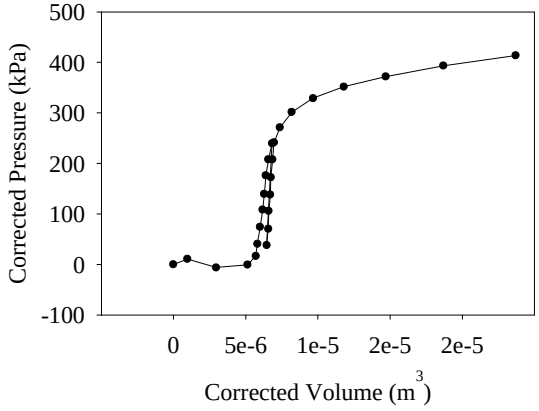

Figure C-27: MPMT Pressure Expansion Curve (Test ID: 19C-1)

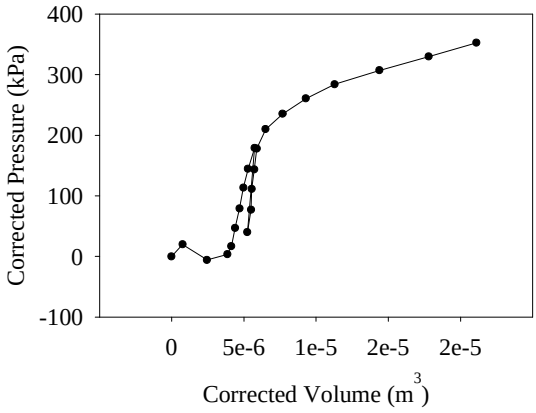

Figure C-28: MPMT Pressure Expansion Curve (Test ID: 19D-1)

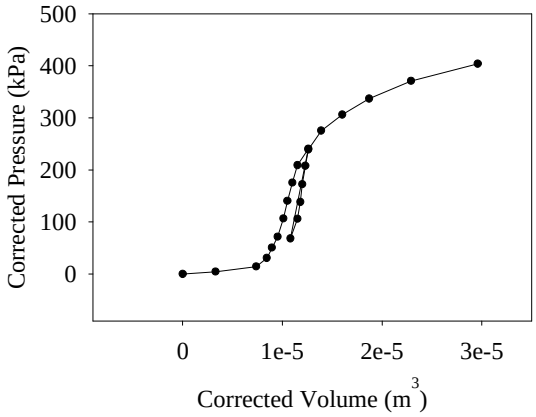

Figure C-:29: MPMT Pressure Expansion Curve (Test ID: 20A-1)

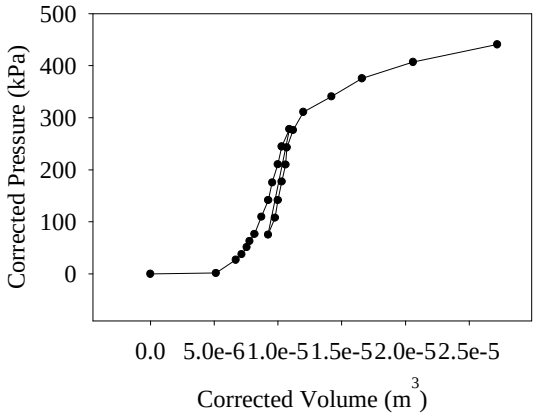

Figure C-30: MPMT Pressure Expansion Curve (Test ID: 20A-2)

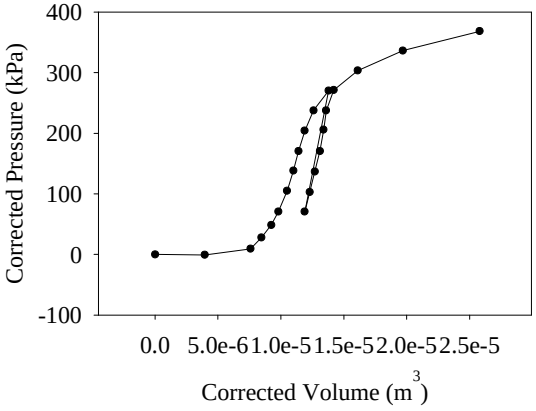

Figure C-31: MPMT Pressure Expansion Curve (Test ID: 20B-1)

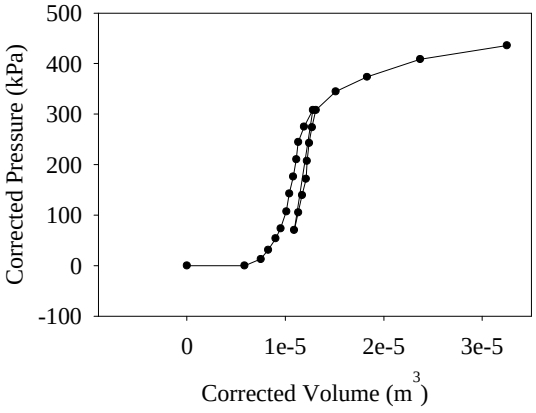

Figure C-:32: MPMT Pressure Expansion Curve (Test ID: 20B-2)

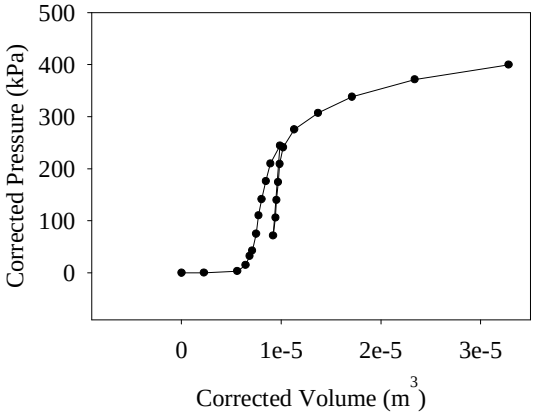

Figure C-33: MPMT Pressure Expansion Curve (Test ID: 21A-1)

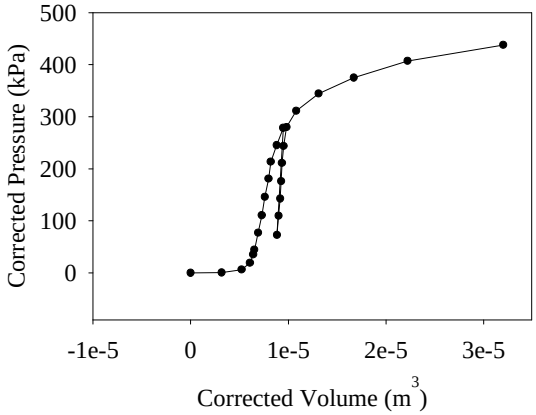

Figure C-34: MPMT Pressure Expansion Curve (Test ID: 21A-2)

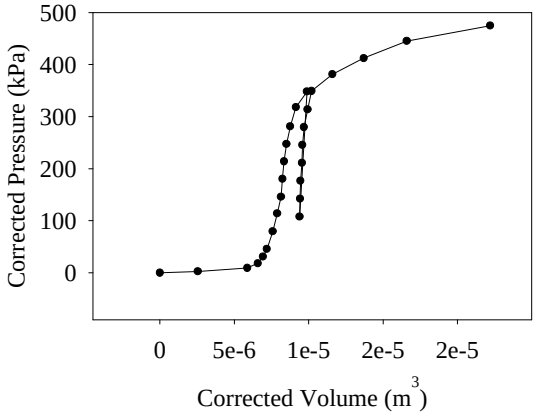

Figure C-:35: MPMT Pressure Expansion Curve (Test ID: 22A-1)

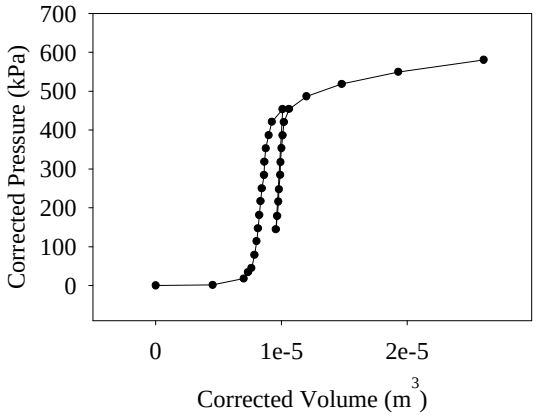

Figure C-36: MPMT Pressure Expansion Curve (Test ID: 22A-2)

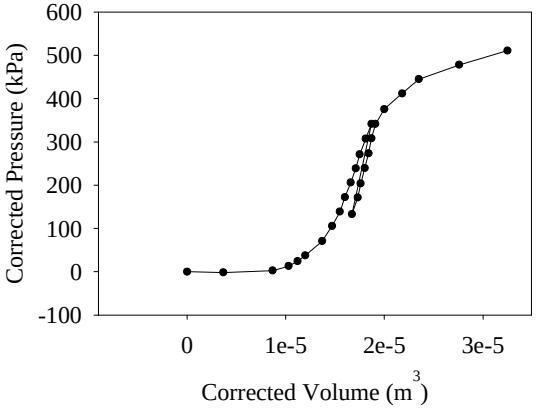

Figure C-37: MPMT Pressure Expansion Curve (Test ID: 23A-1)

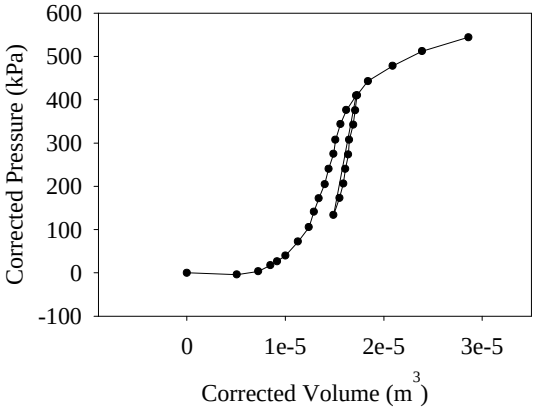

Figure C-:38: MPMT Pressure Expansion Curve (Test ID: 23A-2)

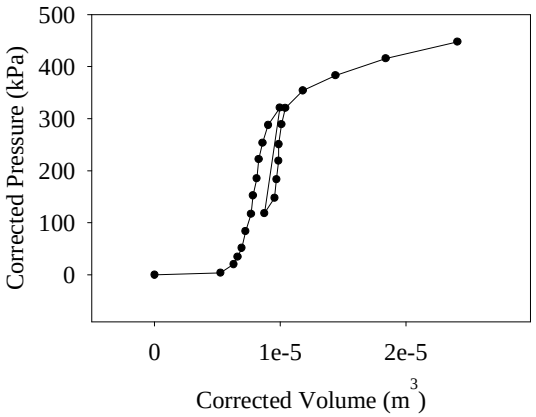

Figure C-39: MPMT Pressure Expansion Curve (Test ID: 24-15B)

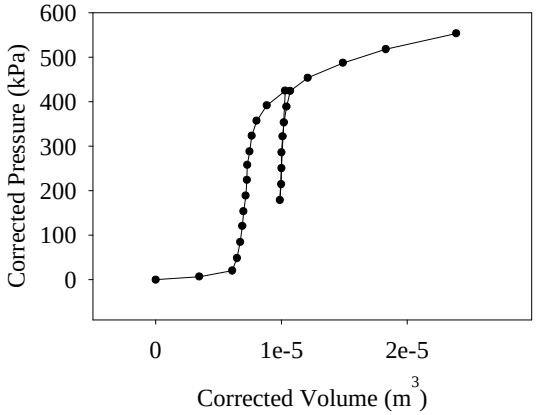

Figure C-40: MPMT Pressure Expansion Curve (Test ID: 24-22A)

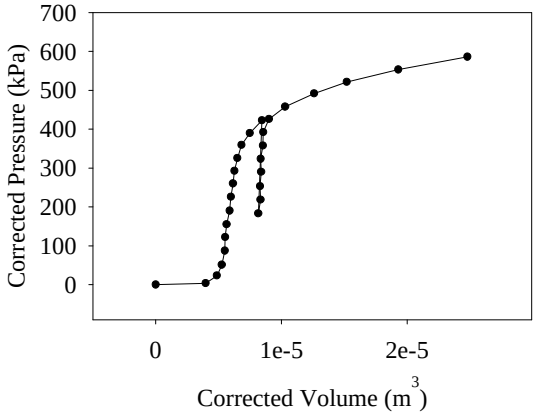

Figure C-41: MPMT Pressure Expansion Curve (Test ID: 24-22C)

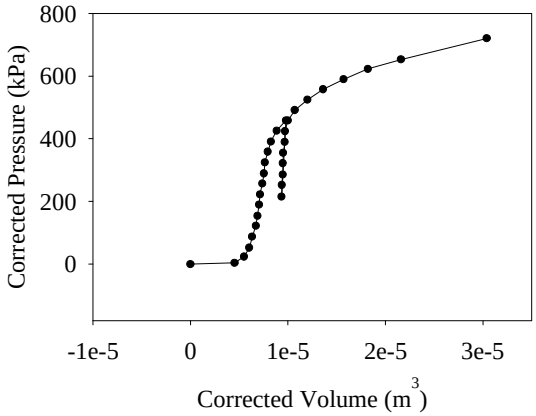

Figure C-42: MPMT Pressure Expansion Curve (Test ID: 24-30D)

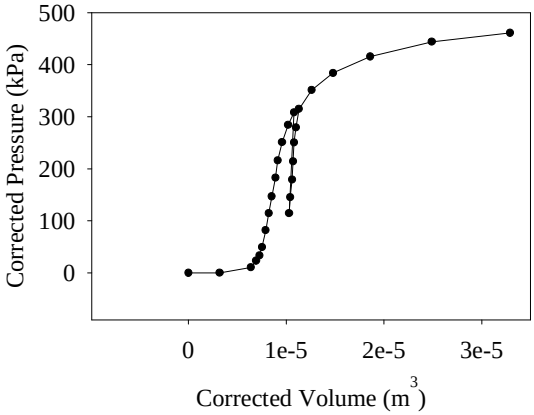

Figure C-43: MPMT Pressure Expansion Curve (Test ID: 25-15B)

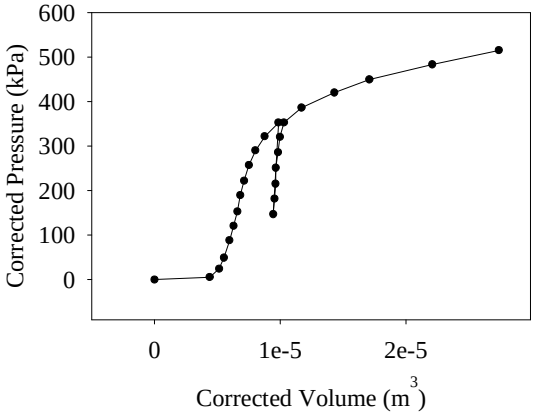

Figure C-44: MPMT Pressure Expansion Curve (Test ID: 25-22A)

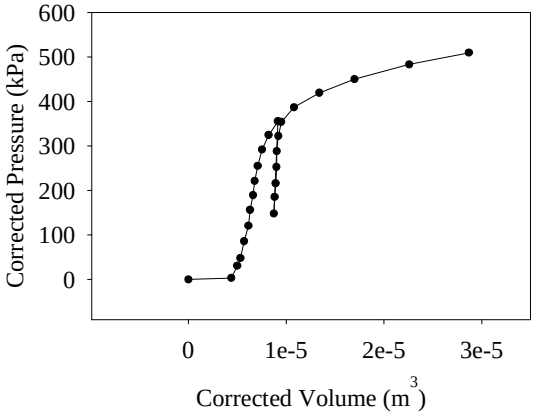

Figure C-45: MPMT Pressure Expansion Curve (Test ID: 25-22C)

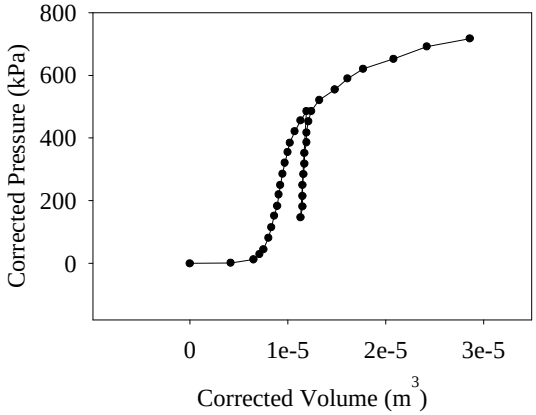

Figure C-46: MPMT Pressure Expansion Curve (Test ID: 25-30D)

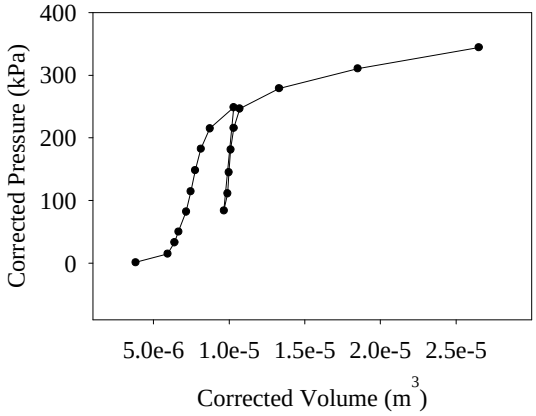

Figure C-47: MPMT Pressure Expansion Curve (Test ID: 26-15B)

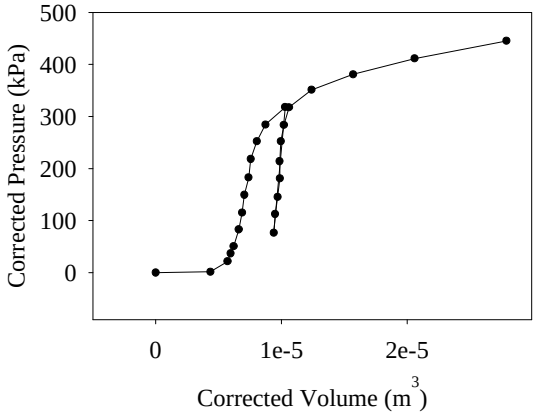

Figure C-48: MPMT Pressure Expansion Curve (Test ID: 26-22A)

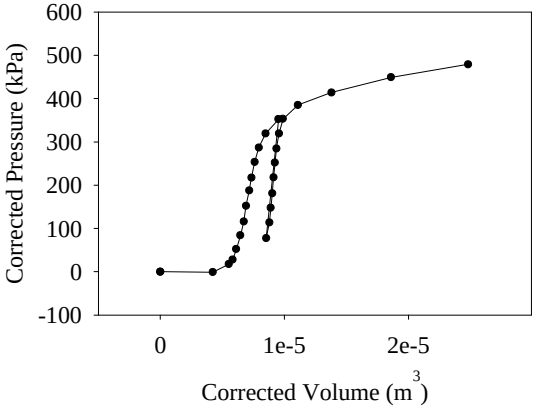

Figure C-49: MPMT Pressure Expansion Curve (Test ID: 26-22C)

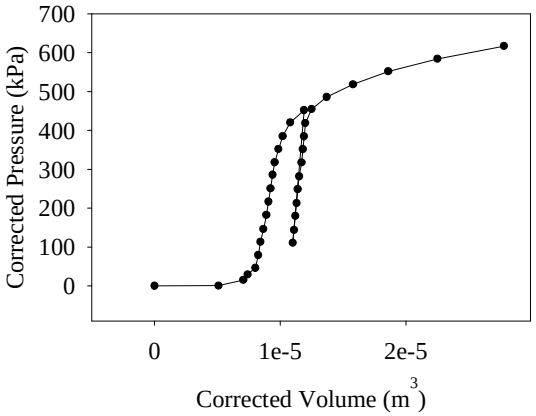

Figure C-50: MPMT Pressure Expansion Curve (Test ID: 26-30D)

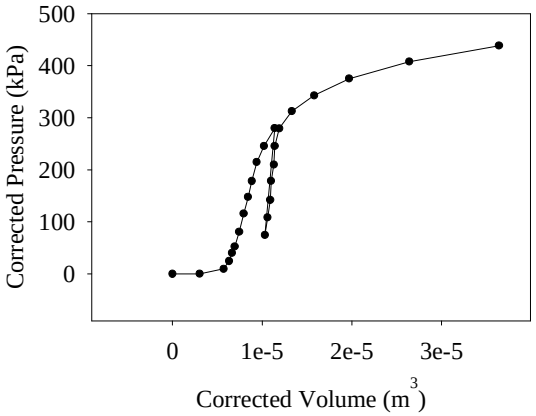

Figure C-51: MPMT Pressure Expansion Curve (Test ID: 27-15B)

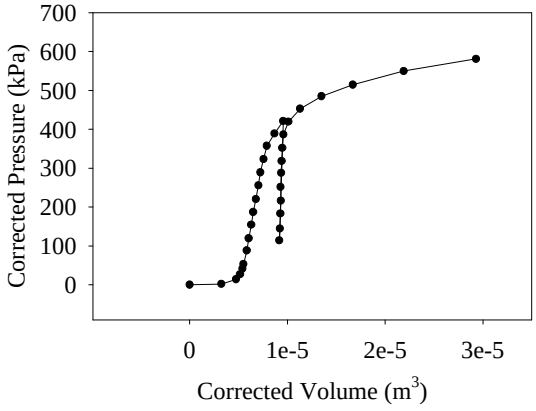

Figure C-52: MPMT Pressure Expansion Curve (Test ID: 27-22A)

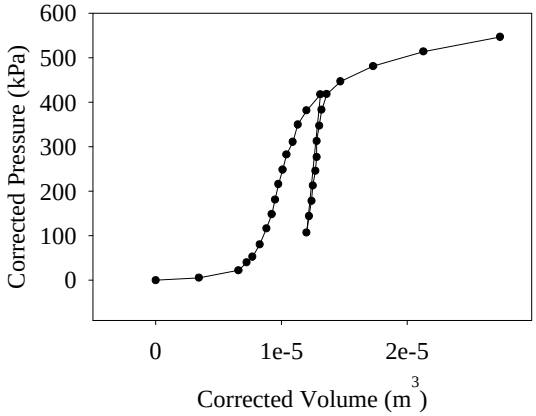

Figure C-53: MPMT Pressure Expansion Curve (Test ID: 27-22C)

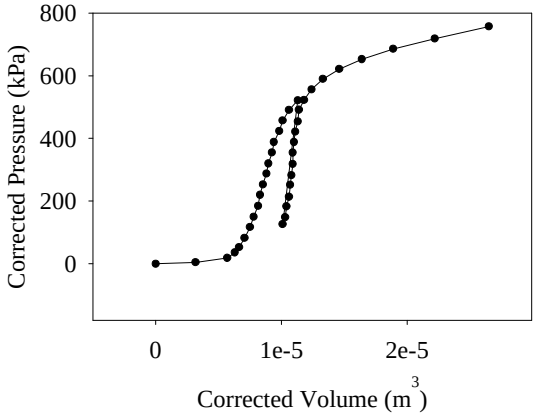

Figure C-54: MPMT Pressure Expansion Curve (Test ID: 27-30D)

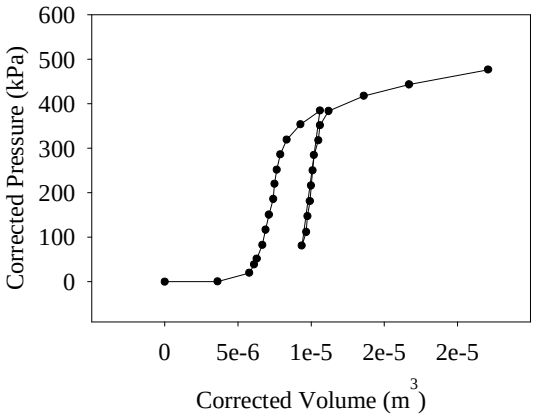

Figure C-55: MPMT Pressure Expansion Curve (Test ID: 28-15B)

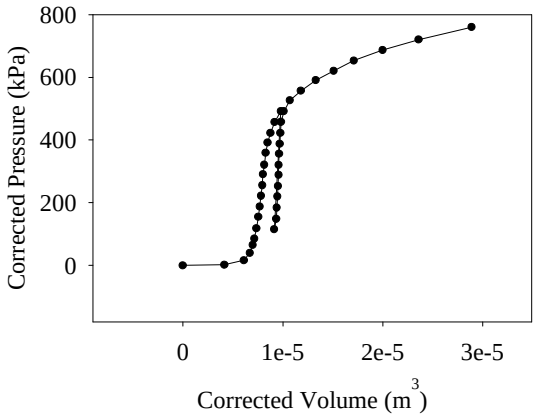

Figure C-58: MPMT Pressure Expansion Curve (Test ID: 28-30D)

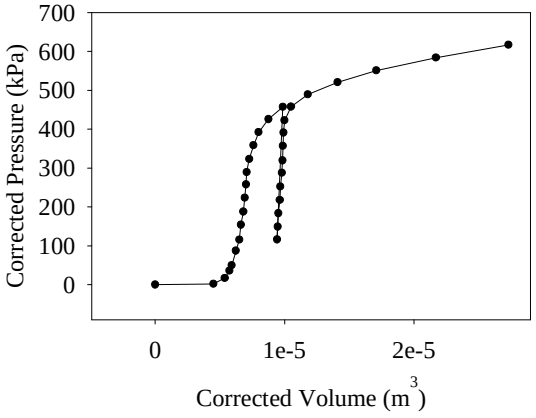

Figure C-56: MPMT Pressure Expansion Curve (Test ID: 28-22A)

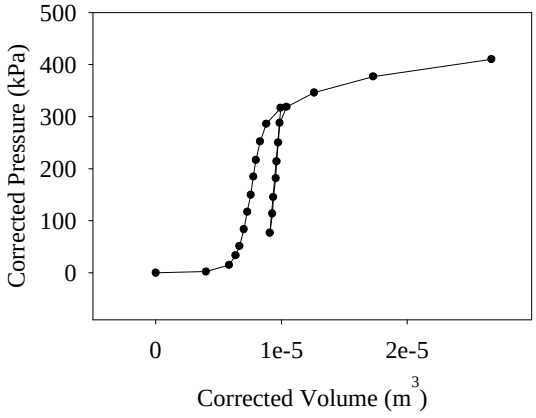

Figure C-59: MPMT Pressure Expansion Curve (Test ID: 29-15B)

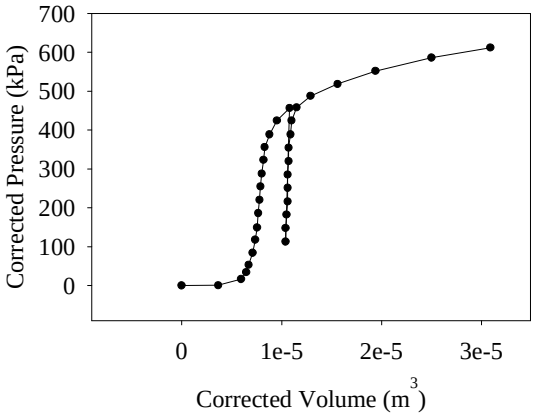

Figure C-57: MPMT Pressure Expansion Curve (Test ID: 28-22C)

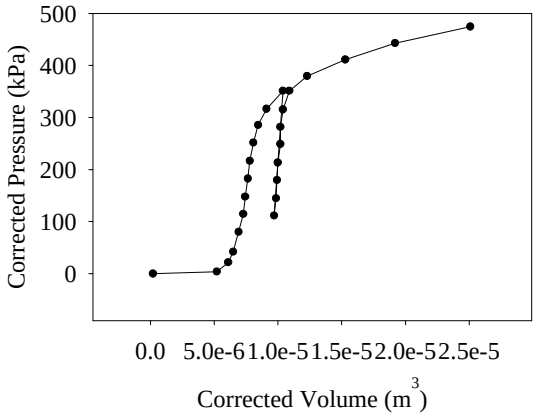

Figure C-60: MPMT Pressure Expansion Curve (Test ID: 29-22A)

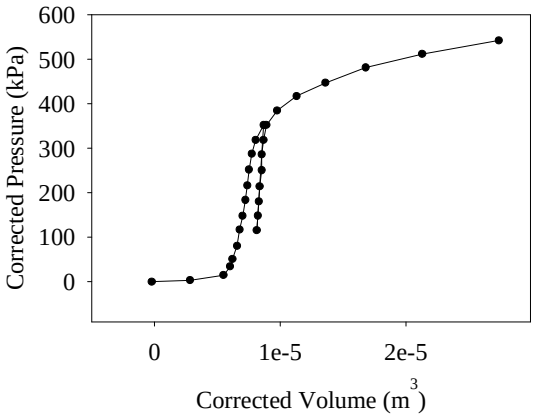

Figure C-61: MPMT Pressure Expansion Curve (Test ID: 29-22C)

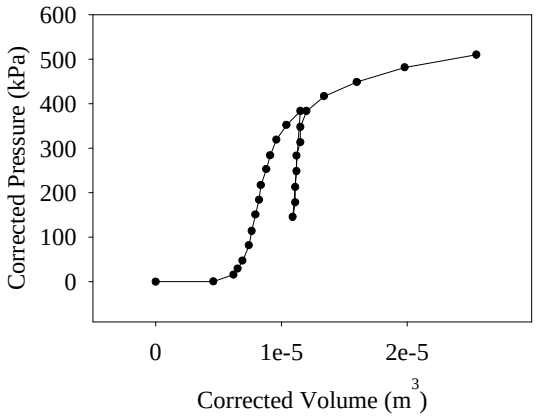

Figure C-64: MPMT Pressure Expansion Curve (Test ID: 30-22A)

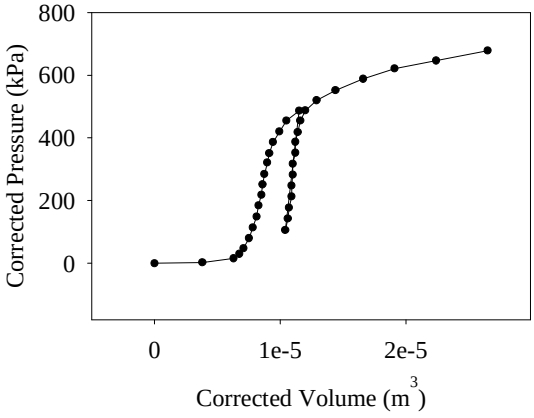

Figure C-62: MPMT Pressure Expansion Curve (Test ID: 29-30D)

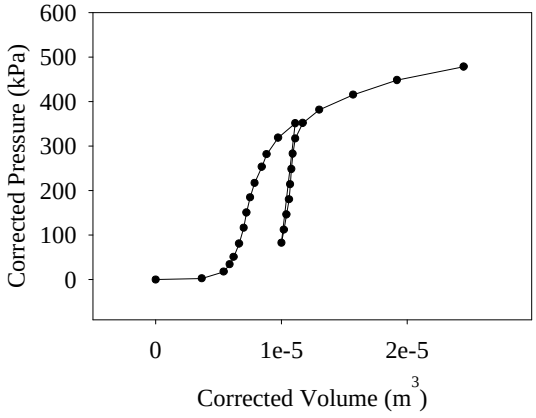

Figure C-65: MPMT Pressure Expansion Curve (Test ID: 30-22C)

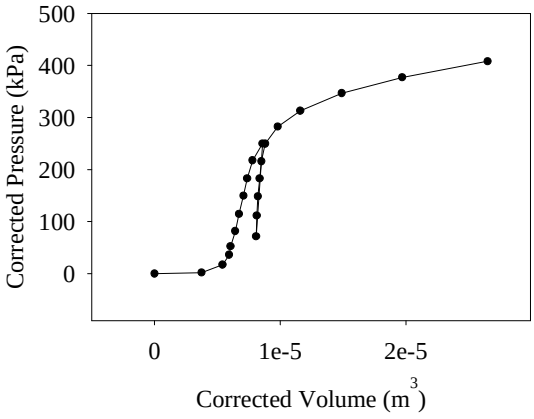

Figure C-63: MPMT Pressure Expansion Curve (Test ID: 30-15B)

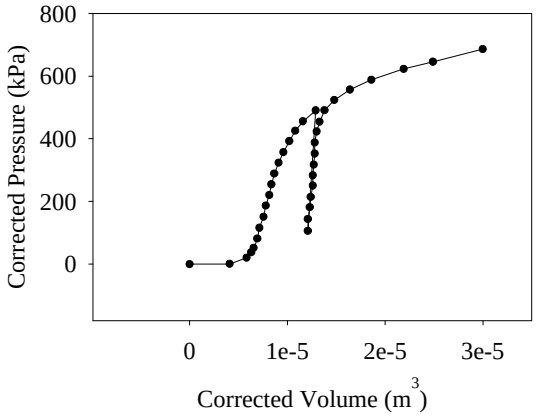

Figure C-66: MPMT Pressure Expansion Curve (Test ID: 30-30D)

APPENDIX D: MCPT Penetration Profile

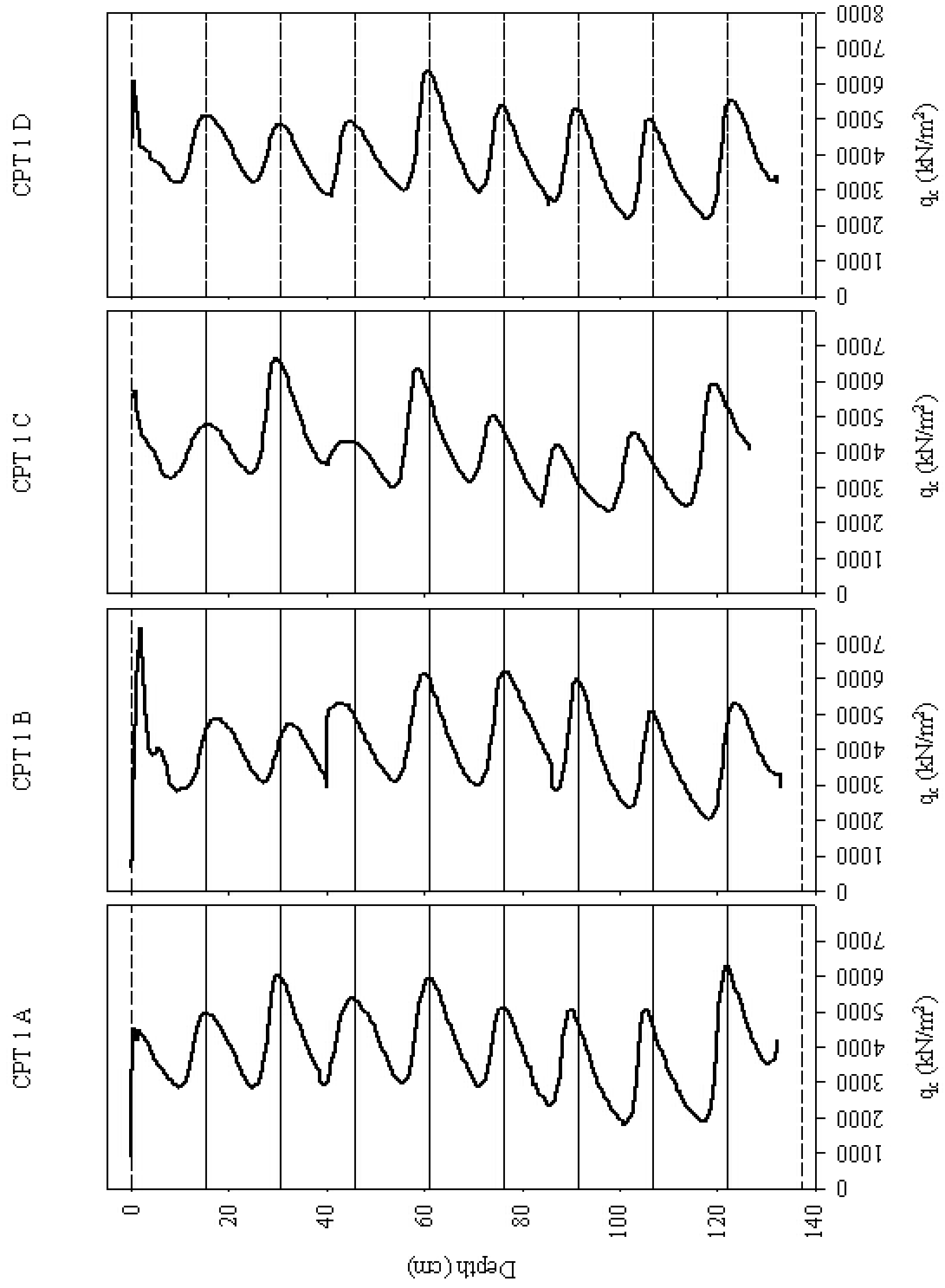

Figure D- 1: MCPT Penetration Profile (Test ID: CPT1)

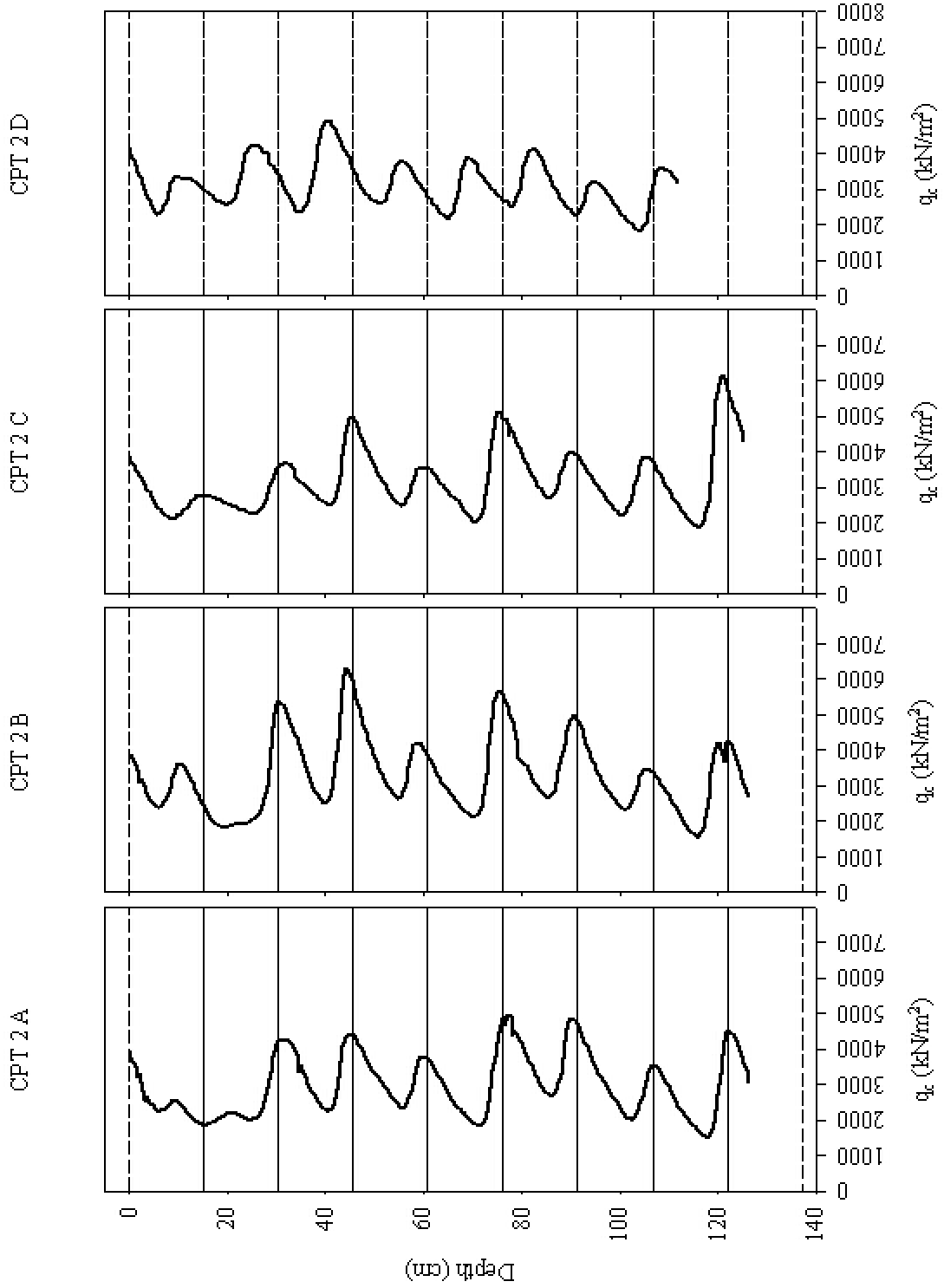

Figure D- 2: MCPT Penetration Profile (Test ID: CPT2)

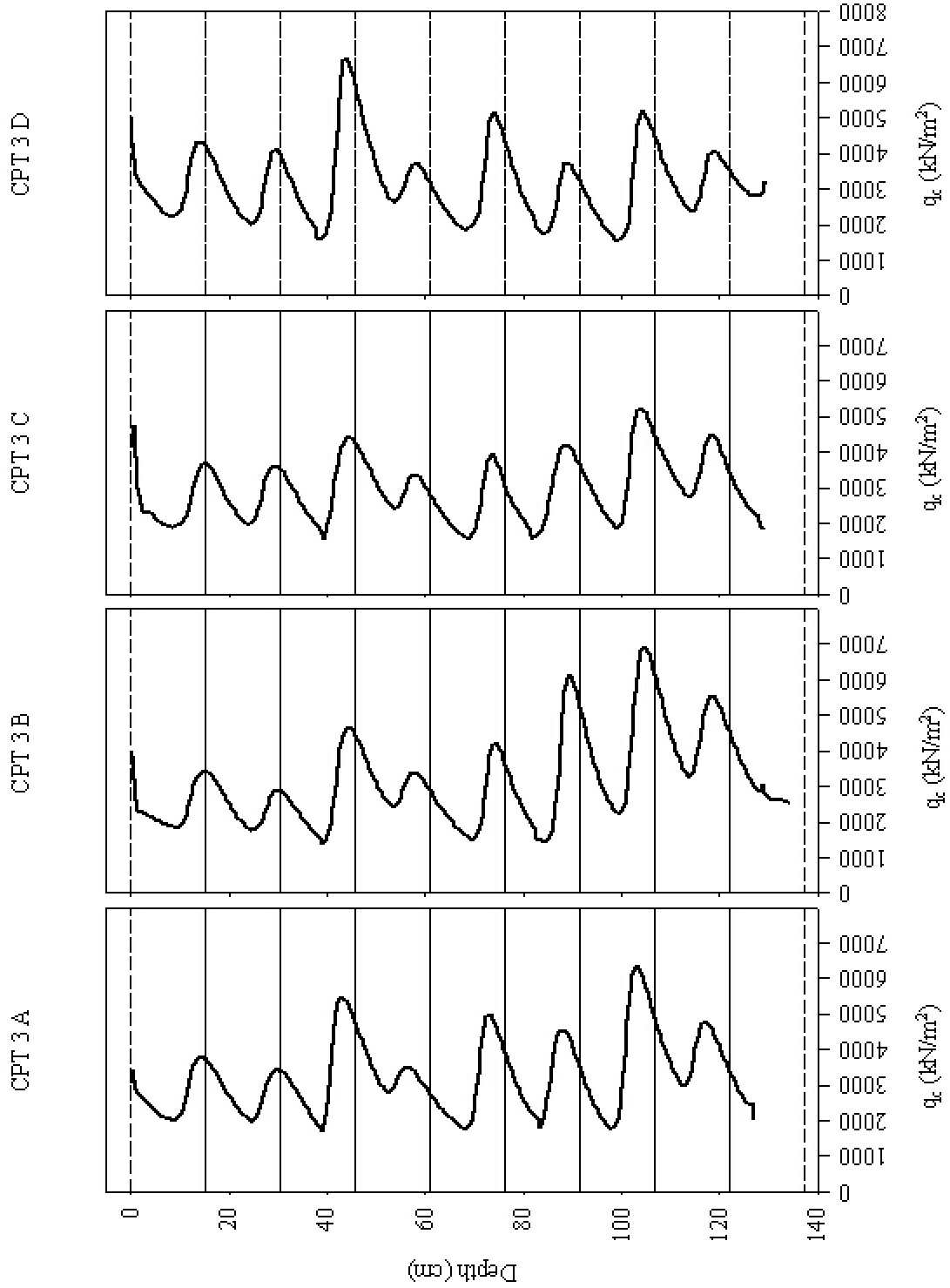

Figure D- 3: MCPT Penetration Profile (Test ID: CPT3)

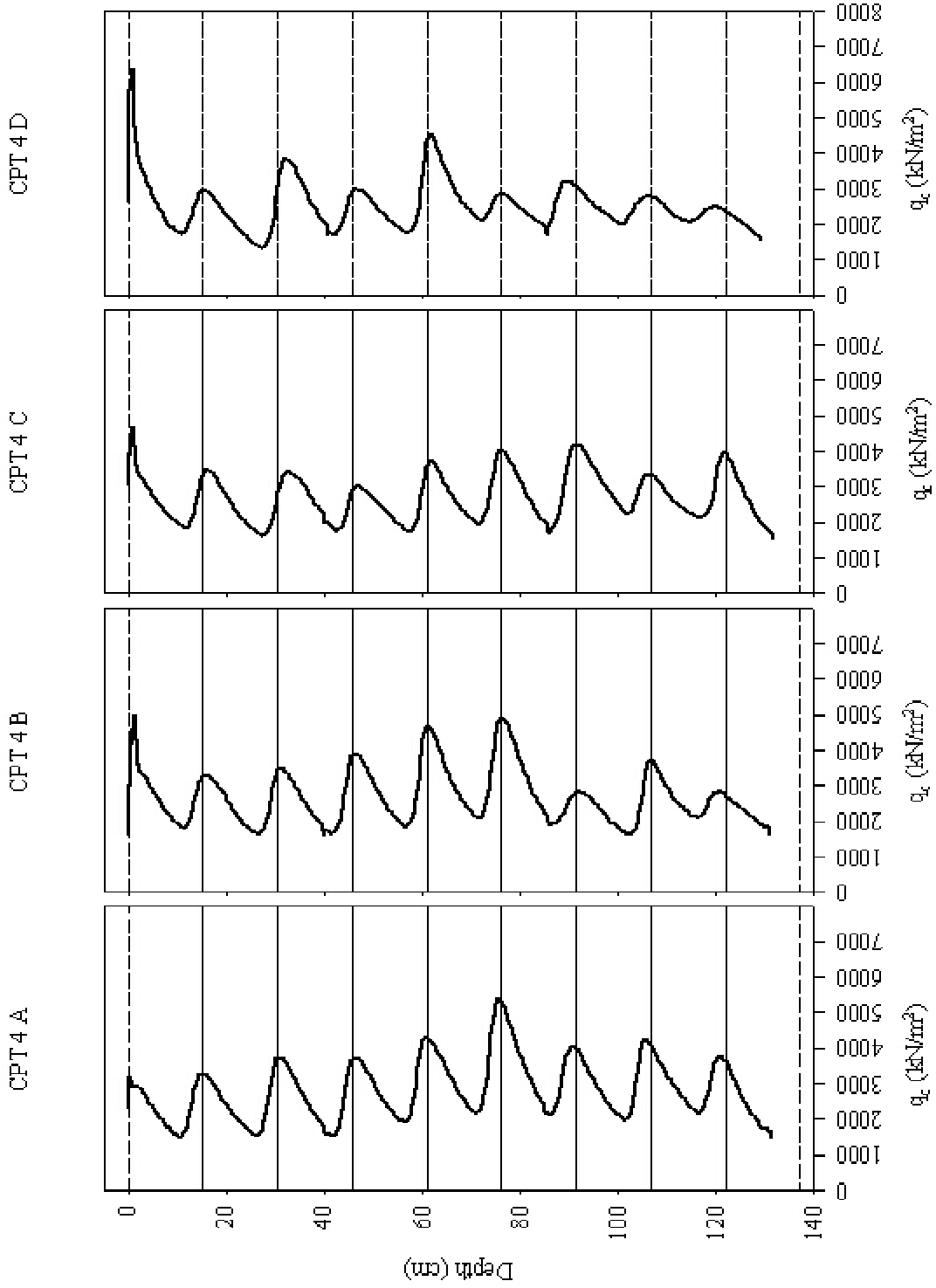

Figure D- 4: MCPT Penetration Profile (Test ID: CPT4)

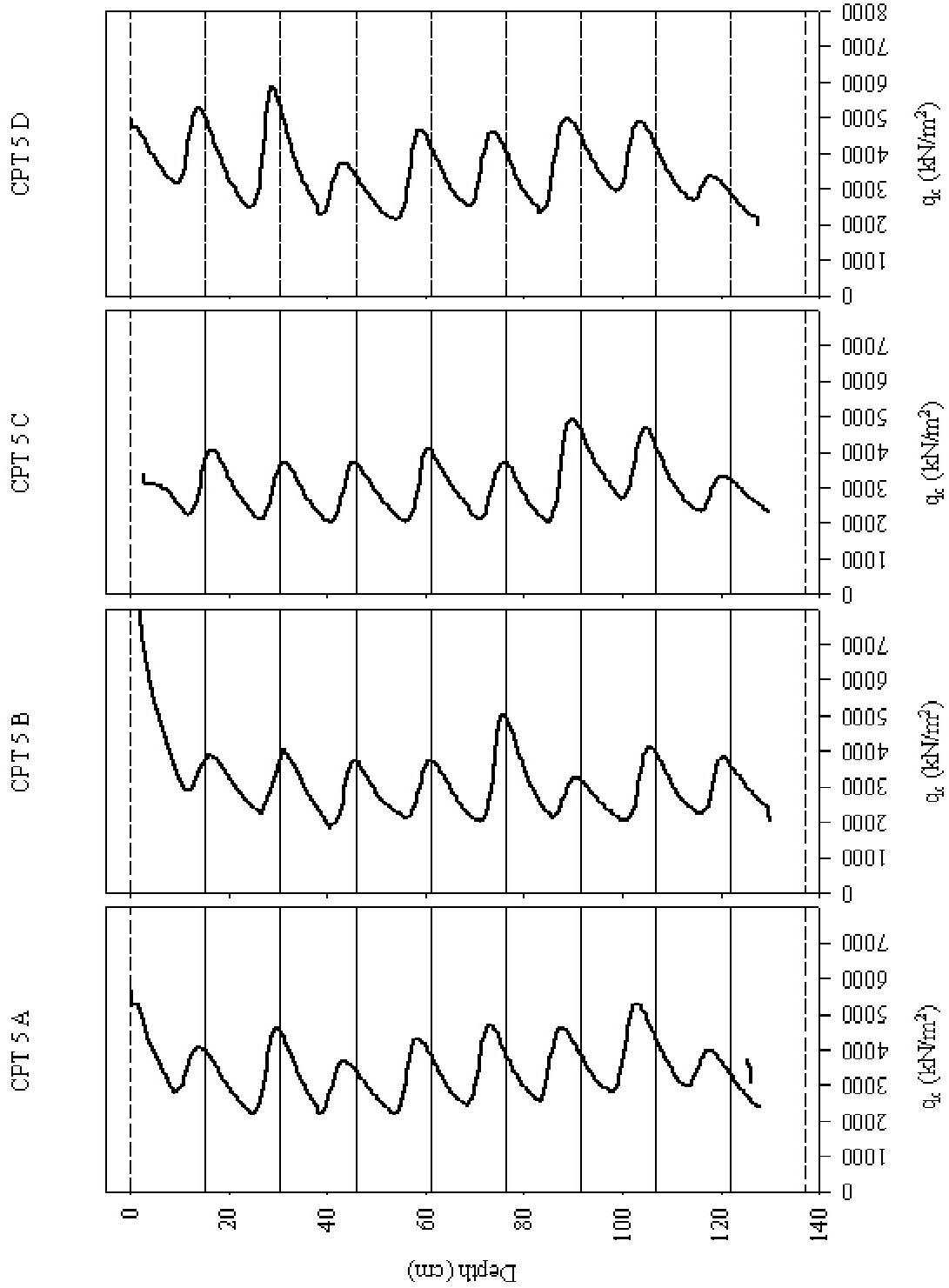

Figure D- 5: MCPT Penetration Profile (Test ID: CPT5)

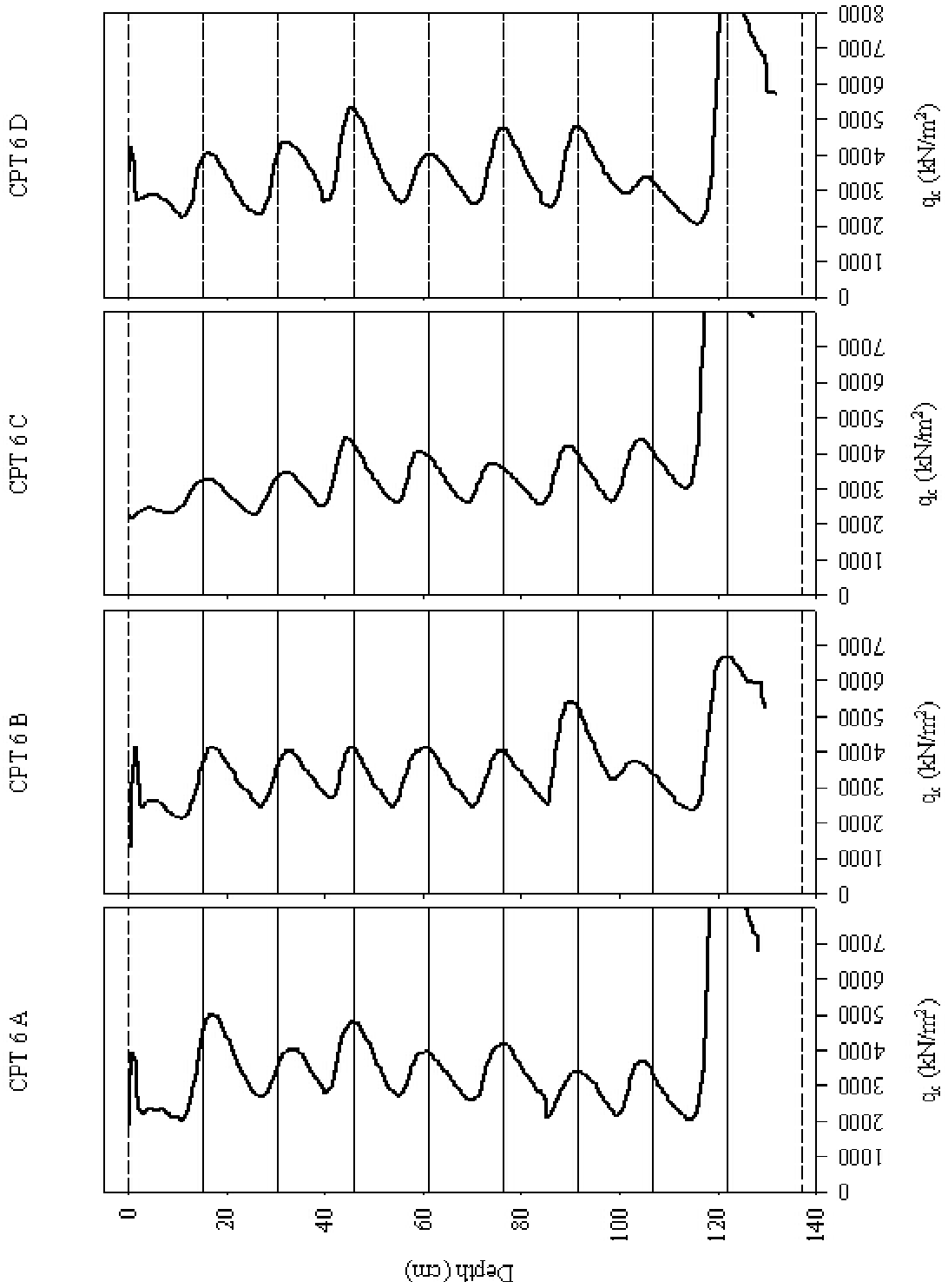

Figure D- 6: MCPT Penetration Profile (Test ID: CPT6)

APPENDIX E: SAS Procedure - MPMT Data

```
CARDS
103.4   606    7140     10674    12.8   14.3  13    0    1  0
103.4   635    7175     9417     12.5   14.2  13    0    1  0
103.4   765    14847    42962    11.0   13.7  17    0    1  0
103.4   793    15966    31324    8.1    13.5  32    0    1  0
103.4   863    15704    35418    8.0    13.5  33    0    1  0
103.4   782    10317    12100    7.8    13.5  35    0    1  0
103.4   1308   12919    18364    5.9    13.0  63    0    1  0
103.4   1578   20202    31058    5.4    13.3  74    0    1  0
103.4   776    18797    44293    8.2    13.5  32    0    1  0
103.4   833    16009    30400    10.1   13.7  20    0    1  0
103.4   774    16128    23054    8.8    13.5  28    0    1  0
103.4   741    14478    23368    8.7    13.5  28    0    1  0
103.4   1024   28950    92081    8.7    13.9  28    0    1  0
103.4   978    25457    262927   8.6    14.3  29    0    1  0
103.4   525    9798     15554    7.3    12.8  40    0    1  0
103.4   549    9564     13810    7.2    12.8  41    0    1  0
103.4   429    7935     18408    12.1   14.2  14    1    1  0
103.4   466    8720     21978    11.9   14.3  15    1    1  0
103.4   413    9123     18925    8.3    13.3  31    1    1  0
103.4   386    8383     16490    8.3    13.4  30    1    1  0
103.4   468    6308     11508    8.3    13.3  31    1    1  0
103.4   406    9112     19150    8.3    13.4  31    1    1  0
103.4   443    5559     9501     8.3    13.3  31    1    1  0
103.4   482    8606     10252    8.2    13.3  32    1    1  0
103.4   448    17268    32234    8.2    13.4  32    1    1  0
103.4   501    7454     13086    8.2    13.5  32    1    1  0
103.4   658    7448     13465    7.8    12.9  35    1    1  0
103.4   606    6331     9606     7.6    13.0  37    1    1  0
103.4   629    23271    38458    5.6    13.2  70    1    1  0
103.4   547    14485    50569    5.4    12.9  74    1    1  0
103.4   528    10870    20299    6.2    12.8  56    1    1  0
103.4   487    11663    26270    6.1    12.7  59    1    1  0
103.4   502    10847    23555    6.1    12.9  58    1    1  0
103.4   523    12116    24108    6.0    12.9  60    1    1  0
103.4   506    9453     18547    5.9    12.6  63    1    1  0
103.4   532    14764    41269    5.9    12.8  62    1    1  0
103.4   580    10930    23992    5.9    12.7  63    1    1  0
103.4   485    7798     17243    6.0    13.1  60    1    1  0
103.4   493    8674     21476    12.0   14.4  15    1    1  1
103.4   465    5608     14284    12.3   13.6  14    1    1  1
103.4   442    10087    23839    7.6    13.4  37    1    1  1
103.4   444    7684     20829    11.9   14.2  15    1    1  1
103.4   500    12671    22887    6.7    12.9  48    1    1  1
103.4   379    8596     22830    8.9    13.2  27    1    1  1
103.4   535    13659    23183    6.8    12.7  46    1    1  1
151.7   613    21156    48900    6.7    13.2  47    1    2  1
151.7   637    18843    44463    6.5    13.2  50    1    2  1
151.7   565    8891     21653    12.0   14.5  14    1    2  1
151.7   546    11439    23004    11.9   14.5  15    1    2  1
151.7   481    11525    22759    8.9    13.4  26    1    2  1
151.7   521    12054    20640    9.0    13.4  26    1    2  1
151.7   617    10590    29073    12.3   13.8  14    1    2  1
```

```
151.7   612    8564     22177    12.1   13.8  14    1    2  1
151.7   664    22299    46922    6.9    13.0  45    1    2  1
151.7   653    18714    47444    6.9    13.0  45    1    2  1
151.7   528    11212    28447    7.5    13.6  38    1    2  1
151.7   591    14477    26663    7.7    13.6  36    1    2  1
151.7   570    9304     20209    12.2   14.5  14    1    2  1
206.8   543    7708     19366    12.2   14.5  14    1    2  1
206.8   752    18004    54227    6.7    13.4  48    1    2  1
206.8   808    12443    35994    11.9   14.7  15    1    2  1
206.8   686    15697    28818    8.5    13.6  29    1    2  1
206.8   846    11193    28642    12.0   14.1  14    1    2  1
206.8   840    20423    44381    7.0    13.1  44    1    2  1
206.8   765    14578    31816    7.4    13.8  39    1    2  1
206.8   756    9361     33945    12.5   14.7  13    1    2  1
```

```
data Soil Processing Methods;
input NNS PL EP ER GWC D MS SPM M N;
IF M=1;
Cards;
Proc Print;
proc reg;
model PL EP ER = D MS SPM /P r CLI influence selection = stepwise;
run;
```

```
data CRUSHER D MS;
input NNS PL EP ER GWC D MS SPM M N;
IF SPM=0;
IF M=1;
Cards;

Proc Print;
proc reg;
model PL EP ER = D MS/P r CLI influence;
run;
```

```
data GRINDER1 D MS;
input NNS PL EP ER GWC D MS SPM M N;
if SPM=1;
IF M=1;
Cards;

Proc Print;
proc reg;
model PL EP ER = D MS/P r CLI influence;
run;
```

```
data GRINDER2 D MS;
input NNS PL EP ER GWC D MS SPM M N;
IF N=1;
Cards;
```

```
Proc Print;
proc reg;
model PL EP ER = D MS NNS/P r CLI influence;
run;
```

```
data C Normalized D;
input NNS PL EP ER GWC D MS SPM M N;
NPL=PL/MS;
NEP=EP/MS;
NER=ER/MS;
if SPM=0;
IF M=1;
Cards;
Proc Print;
proc reg;
model NPL NEP NER = D/P r CLI influence;
run;
```

```
data G2 Normalized D;
input NNS PL EP ER GWC D MS SPM M N;
NPL=PL/MS;
NEP=EP/MS;
NER=ER/MS;
if SPM=1;
IF M=1;
Cards;
Proc Print;
proc reg;
model NPL NEP NER = D/P r CLI influence;
run;
```

```
data G2 Normalized D NNS;
input NNS PL EP ER GWC D MS SPM M N;
NPL=PL/MS;
NEP=EP/MS;
NER=ER/MS;
IF N=1;
Cards;
Proc Print;
proc reg;
model NPL NEP NER = D NNS/P r CLI influence;
run;
```

```
data c Normalized VWC;
input NNS PL EP ER GWC D MS SPM M N;
VWC=GWC*D/9.81;
NPL=PL/MS;
NEP=EP/MS;
NER=ER/MS;
if SPM=0;
IF M=1;
Cards;
```

```
Proc Print;
proc reg;
model NPL NEP NER = VWC/P r CLI influence;
run;
```

```
data G1 Normalized VWC;
input NNS PL EP ER GWC D MS SPM M N;
VWC=GWC*D/9.81;
NPL=PL/MS;
NEP=EP/MS;
NER=ER/MS;
if SPM=1;
IF M=1;
Cards;
Proc Print;
proc reg;
model NPL NEP NER = VWC/P r CLI influence;
run;
```

```
data G2 Normalized VWC NNS;
input NNS PL EP ER GWC D MS SPM M N;
VWC=GWC*D/9.81;
NPL=PL/MS;
NEP=EP/MS;
NER=ER/MS;
if SPM=1;
IF N=1;
Cards;
Proc Print;
proc reg;
model NPL NEP NER = VWC NNS/P r CLI influence;
run;
```

APPENDIX F: SAS Procedure - MCPT Data

```
Cards;
5.7          13.3  59    15.7  3888
5.9          13.0  59    15.5  4055
5.9          13.2  59    15.9  4006
5.9          13.2  59    15.9  3918
7.6          13.5  43    21.7  2883
7.6          13.6  43    21.8  3208
7.6          13.3  44    20.8  2978
7.6          13.1  45    20.1  3101
9.6          13.8  27    28.4  2979
9.9          14.4  22    32.1  2779
9.9          14.2  23    31.2  2908
9.6          13.4  28    26.9  3035
11.0         14.0  18    33.8  2812
10.8         14.5  18    35.5  2507
10.9         14.5  18    36.0  2741
11.0         13.7  20    32.1  2450
8.6          13.6  34    24.6  3433
8.5          13.6  35    24.6  2896
8.6          13.7  34    25.1  2988
8.6          13.4  35    23.8  3471
6.9          13.0  53    17.9  3363
6.9          13.4  50    19.2  3439
6.8          13.4  51    19.1  3327
6.8          13.0  52    18.0  3455
```

```
data QC D MS;
input GWC D MS S QC;
Cards;
Proc Print;
proc reg;
model QC= D MS/P r CLI influence;
run;
```

```
data QC NORMALIZED D
input GWC D MS S QC;
NQC=QC/MS;
Cards;
Proc Print;
proc reg;
model NQC= D/P r CLI influence;
run;
```

```
data QC NORMALIZED VWC
input GWC D MS S QC;
VWC=GWC*D/9.81;
NQC=QC/MS;
Cards;
Proc Print;
proc reg;
```

```
model NQC= VWC/P r CLI influence;
run;
```